

**NATIONAL ACADEMIES OF SCIENCES AND ENGINEERING
NATIONAL RESEARCH COUNCIL
of the
UNITED STATES OF AMERICA**

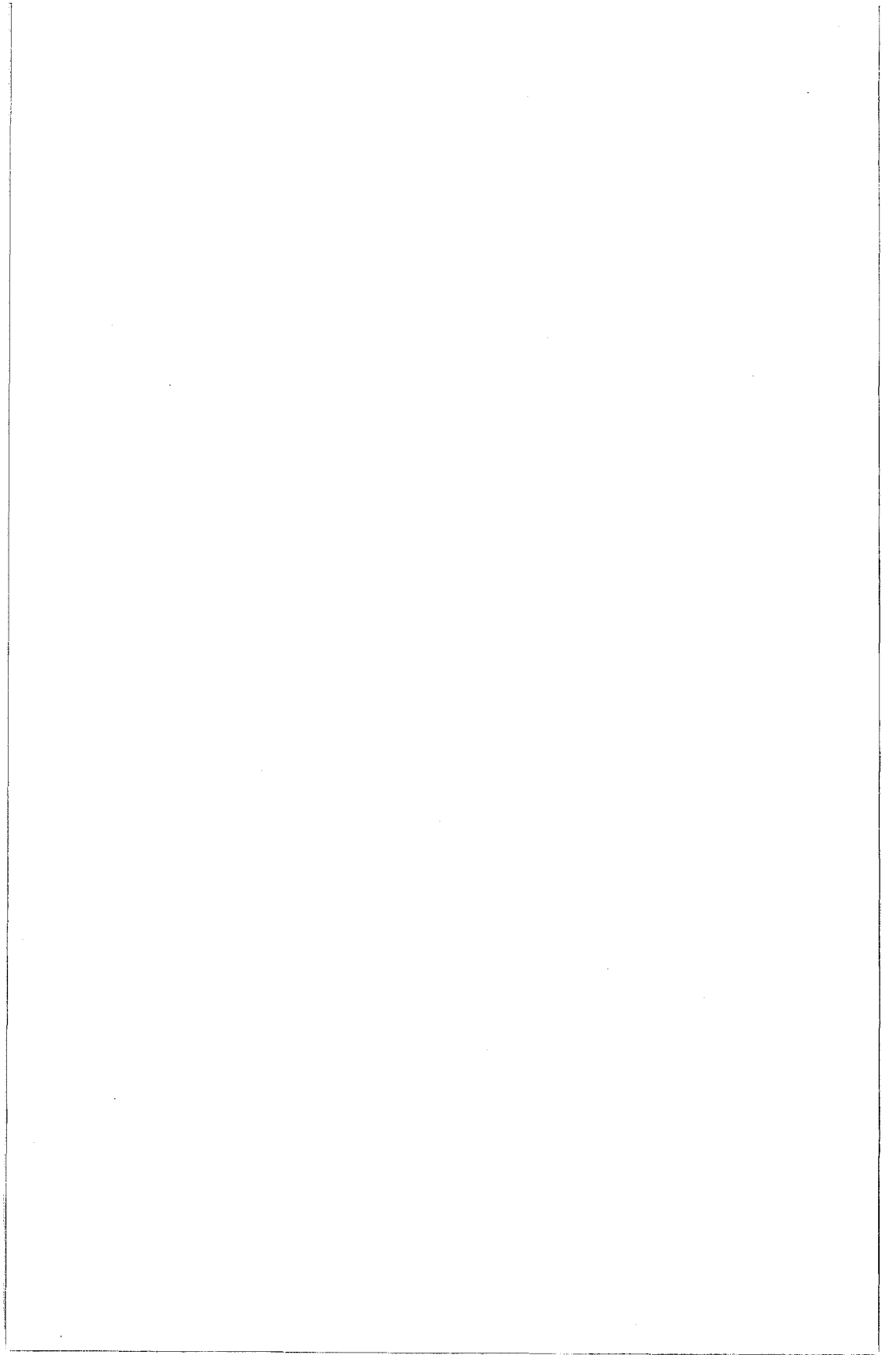
**UNITED STATES NATIONAL COMMITTEE
International Union of Radio Science**



National Radio Science Meeting
5 – 8 January 2005

Sponsored by USNC/URSI

University of Colorado at Boulder
Boulder, Colorado
USA



United States National Committee
International Union of Radio Science

ABSTRACTS

National Radio Science Meeting
5–8 January 2005

University of Colorado, Boulder

Sponsored by USNC/URSI

Table of Contents

Session	Page No.	Session	Page No.
Membership Information	iii	F/J1	207
Description of URSI	iv	G1	219
Plenary Session		G2	229
A1	1	G3	241
A2	13	G4	253
B1	19	H1	263
B2	29	H2	271
B3	39	H3	279
B4	49	H4	287
B5	57	H5	295
B6	65	H/G1	305
B7	73	H/G2	313
B8	83	H/G3	321
B9	97	H/G4	333
B/D1	107	H/G5	343
C1	113	H/G6	349
D1	119	H/G7	361
D2	127	H/G8	371
E1	135	H/G9	377
E2	143	J1	387
F1	151	J2	401
F2	163	J3	415
F3	171	J4	429
F4	179	J5	439
F5	187	K1	453
F6	195	Index	465

Membership

United States National Committee INTERNATIONAL UNION OF RADIO SCIENCE

Chair: Umran S. Inan*
Secretary & Chair-Elect: Piergiorgio L.E. Uslenghi*
Immediate Past Chair: Gary S. Brown*

Members Representing Societies, Groups, and Institutes:

American Astronomical Society: Thomas G. Phillips
American Geophysical Union: Donald T. Farley
American Meteorological Society: Dusan S. Zrnica
IEEE Antennas and Propagation Society: Linda P.B. Katehi
IEEE Geosciences and Remote Sensing Society: Roger Lang
IEEE Microwave Theory and Techniques Society: Arthur A. Oliner

Members-at-Large

Amalia Barrios
J. Richard Fisher
Anthony C. Frasier-Smith
Melinda Picket-May
Ronald Pogorzelski
Michael S. Shur
Yahya Rahmit-Samii
Richard Ziolkowski

Chairs of the USNC-URSI Commissions:

Commission A: William A. Davis
Commission B: Ronald Pogorzelski
Commission C: Jeffrey Krolik
Commission D: Samir M. El Ghazaly
Commission E: Ira Kohlberg
Commission F: Kenneth Anderson
Commission G: Anthea Coster
Commission H: Gurudas Ganguli
Commission J: John Carlstrom
Commission K: Om Gandhi

Officers, Chairs and Vice Chairs of Commissions of URSI residing in the United States

URSI Honorary President: William E. Gordon
Vice Chair, URSI: Chalmers Butler
Chair, Commission A: Quirino Balzano
Chair, Commission C: A. F. Molisch
Chair, Commission H: Umran S. Inan

*Member of USNC/URSI Executive Committee

Description of the International Union of Radio Science

The International Union of Radio Science is one of the world scientific unions organized under the International Council of Scientific Unions (ICSU). It is commonly designated as URSI from its French name, Union Radio Scientifique Internationale. Its aims are (1) to promote the scientific study of radio communications, (2) to aid and organize radio research requiring cooperation on an international scale and to encourage the discussion and publication of the results, (3) to facilitate agreement upon common methods of measurement and the standardization of measuring instruments, and (4) to stimulate and to coordinate studies of the scientific aspects of telecommunications using electromagnetic waves, guided and unguided. The International Union itself is an organizational framework to aid in promoting these objectives. The actual technical work is largely done by the National Committee in the various countries.

The officers of the International Union are:

President:	Kristian Schlegel (Germany)
Past President:	Hiroshi Matsumoto (Japan)
Vice Presidents:	Chalmers M. Butler (USA)
	François Lefeuve (France)
	("URSI Exposure" Officer)
	Andrzej W. Wernik (Poland)
	(Treasurer)
	Paul H. Wittke (Canada)
Secretary-General:	Paul Lagasse (Belgium)
Assistant Secretary-General:	Frank Olyslager (Belgium)
Assistant Secretary General (Publications):	W. Ross Stone (USA)
Administrative Assistant:	Inge Heleu (Belgium)

The Secretary-General's office and the headquarters of the organization are located at Avenue Albert Lancaster, 32, B-1180 Brussels, Belgium. The Union is supported by contributions (dues) from 38 member countries. Additional funds for symposia and other scientific activities of the Union are provided by ICSU from contributions received for this purpose from UNESCO.

The International Union, as of the XXVIth General Assembly held in Maastricht, Netherlands, August 2002, has ten bodies called Commissions for centralizing studies in principal fields.

Every three years the International Union holds a meeting called the General Assembly. The next is the XXVIIth, to be held in New Dehli, India, 23–29 October, 2005. The Secretariat prepares and distributes the Proceedings of the General Assemblies. The International Union arranges international symposia on specific subjects pertaining to the work of one or several Commissions and also cooperates with other Unions in international symposia on subjects of joint interest.

Radio is unique among the fields of scientific work in having a specific adaptability to large-scale international research programs, since many of the phenomena that must be studied are worldwide in extent and yet are in a measure subject to control by experimenters. Exploration of space and the extension of scientific observations to the space environment are dependent on radio for their research. One branch, radio astronomy, involves cosmic phenomena, URSI thus has a distinct field of usefulness in furnishing a meeting ground for the numerous workers in the manifold aspects of radio research; its meetings and committee activities furnish valuable means of promoting research through exchange of ideas.

Steering Committee:

P.L.E. Uslenghi, University of Illinois at Chicago

K. Grosland, CU Conference Services, University of Colorado

Julie Mckie, Cooperative Institute for Research in Environmental Sciences,
University of Colorado

Technical Program Committee:

U. Inan, Chair

P. Uslenghi, Secretary

S. Reising, Student Paper Competition

(A) W. Davis

(F) K. Anderson

(B) R. Pogorzelski

(G) A. Coster

(C) J. Krolik

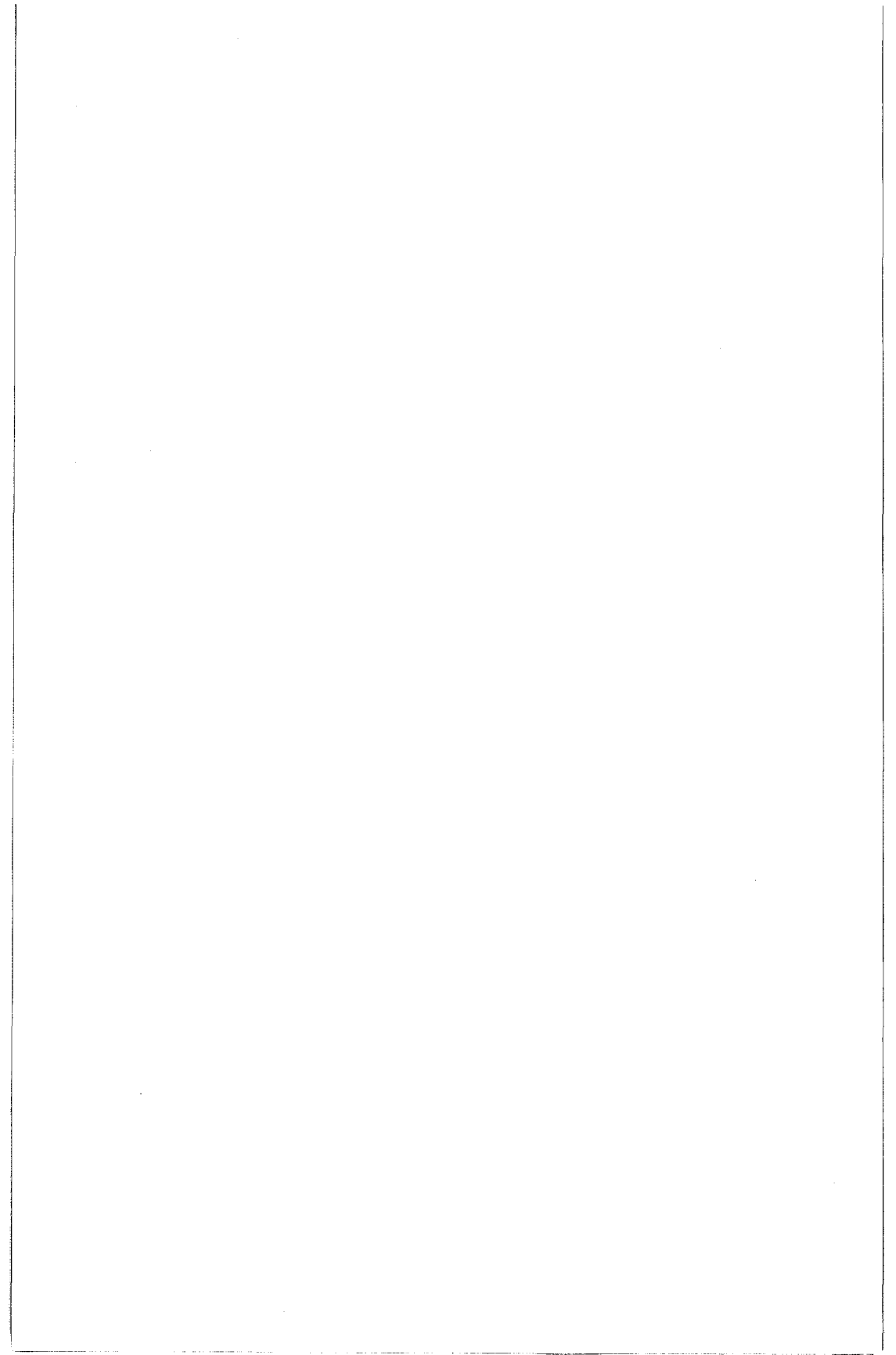
(H) G. Ganguli

(D) S. Ghazaly

(J) J. Carlstrom

(E) I. Kohlberg

(K) O. Gandhi



Plenary Session, 9:00-Thurs.

**APPLICATIONS OF MICROWAVES
IN MEDICINE**

M.A. Stuchly, N. Engheta

Plenary

APPLICATIONS OF MICROWAVES IN MEDICINE

Stuchly, M.A.

Electrical and Computer Engineering, University of Victoria, Victoria, BC, Canada

Applications of radiofrequency and microwave fields in medicine are not new, but recent advances in computer modeling, component fabrication and decrease in cost have resulted in new and old ideas coming to fruition. The non-ionizing nature of this part of the electromagnetic spectrum makes it particularly attractive for diagnostic applications. On the other hand, heating, the well-known interaction with biological tissues, enables some therapeutic uses. Because of the heterogeneous electrical properties of the human body and irregular shapes, the finite difference time domain (FDTD) is extensively employed to model interactions of fields with tissues and to design effective devices. The finite element method (FEM) is also used, although less popular, as most human body models consist of cubic voxels, and are thus directly compatible with FDTD.

One of the most promising diagnostic methods is the breast cancer detection. This application is based on differences in electrical properties between a healthy and diseased tissue. Two approaches have been explored, a classical tomography, and a wideband radar-based technique. Tomography provides complete maps of tissue properties and involves the solution of inverse scattering problems, which are not unique; furthermore, the wave penetration depth limits resolution. Despite these inherent difficulties, promising results have been reported and there is at least one system in clinical trials in the USA. The radar-based approach considers illumination of the breast with ultra-wideband pulses, typically from 0.5 to 15 GHz, from several antenna locations and observation of the scattered returns by the same antenna. The critical issues involve processing of the return signals to ensure coherent addition of these returns from the same tissue location for different antenna positions. In practical implementations of this approach, the system operates in the frequency domain with wide range of frequencies, and the data are converted into the time domain in post processing. Excellent results promising detection of sub-millimeter tumors have been reported by two research groups.

Several highly successful therapeutic applications have been reported. They include highly localized, as well as regional heating. Examples of localized heating include angioplasty, cardiac ablation to treat arrhythmias, esophageal ablation and cornea shaping. Regional heating has been achieved with implanted antennas, and surface arrays. What made a significant difference in efficiency of these treatments in recent years is the extensive modeling and simultaneous temperature evaluation, and thus control of the heating profile.

SEEING THE INVISIBLE: POLARIZATION VISION, ITS BIOPHYSICAL MECHANISM AND NON-INVASIVE IMAGING APPLICATIONS

Engheta, N.

Electrical and Systems Engineering, Univ. of Pennsylvania

Certain species of animals in nature have visual systems that are sensitive to lights polarization a capability that is lacking in the human eyes. Our eyes cannot effectively sense and utilize the polarization information without appropriate instruments. However, the species with polarization vision can sense and detect this characteristic of light and can extract its information. Polarization is obviously an important feature of electromagnetic waves, and it can be affected by surface shapes, materials, local curvature and features, and relative location of sources and objects, and thus it can provide useful information about the observed scene and objects.

What can we learn from this interesting ability of polarization sensing and detection in nature that has been evolved in certain biological visual systems? Of course, two types of questions may be asked about this ability. (1) How do these species detect and sense the lights polarization?, (2) Why do they have this ability? The first general question points to the biophysical mechanisms of polarization detection in such visual systems. This has been a subject of interest for biologists, zoologists, and recently neuroscientists, physicists, and engineers. (see e.g., R. Wehner, "Neurobiology of Polarization Vision," Trends in Neurosciences, vol. 12, pp. 353-359, 1989.) The second question aims at the functionality and advantages of this sensing mechanism in nature. Indeed this interest dates back to the discovery by Nobel laureates Karl von Frisch who investigated how honey bees can sense the polarization of skylight and use it for navigation. Beyond this navigational utility of polarization sensing, it has been understood that some species use polarization vision to enhance their ability to detect and classify targets – indeed to see otherwise transparent targets, and to recognize conspecifics.

Understanding the biophysical mechanism behind the polarization vision and reverse engineering its functionality leads to exciting novel methods and techniques in sensing and imaging with various applications. Motivated and inspired by the features of polarization vision, we have developed several non-invasive imaging methodologies that have shown marked advantages over the conventional imaging techniques. These techniques provide enhanced visibility, longer-range detection, adaptability to changing scenes and non-invasive surface-deformation sensing, to name a few.

In this talk, I will discuss several optical and electromagnetic aspects of this topic, review the biophysical mechanisms of polarization vision, and present sample results of our bio-inspired imaging techniques.

Session A1, 08:35 – Wed.

**MICROWAVE MEASUREMENTS AT
NIST AND ANTENNAS**

Co-Chairs: J. Jargon, D. DeGroot

MEASUREMENT SERVICES: SYSTEMS, TECHNIQUES AND UNCERTAINTY CONSIDERATIONS

Ronald A. Ginley

NIST, 325 Broadway, Boulder, CO 80305

This talk will describe the Microwave S-parameter and Power measurement services at NIST. These services cover a frequency range of 100 kHz to 110 GHz. The measurement systems as well as the standards used will be discussed. The general techniques for the measurements will be covered and general uncertainty considerations will be described. Future directions for both of the services will also be covered.

The S-parameter services cover a wide variety of connector types including 14 mm, 7 mm, Type N, 3.5 mm, 2.92 mm, 2.4 mm coaxial connectors and the WR 90, WR 62, WR 42, WR 28, WR 22, WR 15 and WR 10 waveguide sizes. The measurements are performed on NIST dual six-port systems or commercial vector network analyzers, these systems are calibrated using multi-line calibration techniques. Comparisons will be shown that detail the differences between the multi-line calibration technique and short, open, load, through technique. Also, the uncertainty sources connected with the air transmission line standards and connectors will be covered.

The Power measurement systems are based on the direct comparison method, using either six-port systems or specialized direct comparison systems. The 7 mm, Type N, 3.5 mm, 2.92 mm, 2.4 mm coaxial connectors and the WR 90, WR 62, WR 42, WR 28, WR 22, WR 15 and WR 10 waveguide sizes are covered. The measurement systems are calibrated with primary bolometric transfer standards that are calibrated in the NIST microcalorimeter. Two types of primary standards are used, thermistor based and thin-film construction. The major sources of uncertainty including the mismatch correction, adapter characterization and power meters will be described.

A STATISTICAL APPROACH TO RF VECTOR NETWORK ANALYZER CORRECTIONS

Donald C. DeGroot

NIST, Electromagnetics Division, Boulder, Colorado

We describe a statistical framework for correcting measurements of RF and microwave scattering parameters, focusing on the application of a new 16-term method to a wideband vector network analyzer (VNA). Before examining the details of this method, we will examine why statistical treatments of vector network analyzers are only now gaining some attention, and why the VNA user community has managed to perform calibrations at all when just taking a single measurement of a deterministic number of standards. A new class of wideband network analyzer is a major driver for the adoption of statistical analysis because of their increased noise level. These instruments are used to characterize nonlinear circuits and devices by measuring harmonically rich signals. The wideband VNA either downconverts a broadband harmonic series or modulated signals into a wide intermediate frequency (IF) channel. The IF bandwidth can be larger than 4 MHz, increasing the noise in the measured data by many orders of magnitude over traditional, one-tone-at-a-time VNAs. To work with the noisy data in nonlinear network analysis, a joint effort between NIST and the Vrije Universiteit Brussel produced a new method for estimating the 16-term VNA model. It applies a convenient nonlinear least-squares optimization process to multiple measurements (electrical and connector repeats) of transmission line and reflection standards, and gives estimates for both the VNA model parameters and the propagation constant for the transmission line standards. By comparing the distribution equation residuals at the end of the process to what one would expect for Gaussian noise in the measurements, the method estimates the modeling errors in comparison to the maximum likely-hood result. The talk gives quantitative statements regarding the quality of the parameters, showing parameter values and estimates of their Type A uncertainty. It also shows that the modeling errors are typically less than a factor of 6 smaller than the Type A uncertainty induced by the measurement noise. Finally we present extensive simulation results showing that the parameters are statistically unbiased.

MEASUREMENT
METHODS FOR THE BROADBAND CHARACTERIZATION
OF DIELECTRIC SUBSTRATES

Janezic, M.D., Baker-Jarvis J.
National Institute of Standards and Technology

The Electromagnetic Properties of Materials Project was established at the National Institute of Standards and Technology (NIST) in order to develop and evaluate measurement methods for characterizing the high-frequency electrical properties of dielectric and magnetic materials. Recently, this project has focused on evaluating techniques for measuring the relative permittivity and loss tangent of low-loss dielectric substrates such as printed-wiring boards, ceramic substrates, and other packaging materials as a function of frequency.

With the increasing interest in system performance and the advent of new applications over a wider frequency range, substrate manufacturers are developing new, high-performance substrate materials. In order to build microwave components, engineers must know the frequency-dependent electrical properties of these new materials. However, due to the many techniques available in the literature, selecting an appropriate measurement method can often be difficult.

In this presentation, we will overview four nondestructive techniques that are appropriate for measuring the relative permittivity and loss tangent of dielectric substrates over the frequency range of 1 to 60 GHz. For metal-clad substrates, we will overview the full-sheet resonance method. Next, we will discuss measurements of unclad substrates at microwave frequencies using split-cylinder and split-post resonators. Finally, we will consider the Fabry-Perot resonator for measurements of unclad substrates at millimeter frequencies. The frequency range, complexity of the theoretical model, sample geometry, orientation of the electric and magnetic fields, and overall measurement accuracy varies greatly between these four techniques. To understand the applicability of each method, we will discuss each of these variables and summarize the merits and limitations of the four measurement techniques.

AMPLIFIER AND TRANSISTOR NOISE-PARAMETER MEASUREMENT AT NIST

J. Randa

Electromagnetics Division, National Institute of Standards and Technology, Boulder, CO 80305

The Thermal Noise Metrology Project of the National Institute of Standards and Technology (NIST) develops methods and standards for very accurate measurements of thermal noise in electronic systems, and it provides support for such measurements in the communications and electronics industries, as well as for other government agencies. Work is currently in progress in three major areas. The first area is in the measurement of noise temperature of one-port noise sources, where we offer measurement services at 30 and 60 MHz and at all frequencies from 1 GHz to 65 GHz. The second general thrust of the Project is measurement of noise parameters of low-noise amplifiers and transistors, and the third major effort aims at improving methods for calibration and validation of microwave radiometers used for remote sensing. This talk will review activities and capabilities in the second area, noise-parameter measurements.

The Projects noise-parameter efforts comprise work both on packaged amplifiers and on transistors on a wafer. We have developed and are refining a measurement capability for packaged amplifiers for 1 GHz to 12.4 GHz, and we are collaborating to improve methods for measuring noise parameters of poorly matched transistors on a wafer in this same frequency range. Central to any such development are verification methods and uncertainty analysis. We have developed and implemented verification methods and a Monte Carlo uncertainty analysis for amplifier measurements and are currently extending the verification methods and uncertainty analysis to measurements of transistors on a wafer. Both the amplifier and the transistor work include measurement comparisons with other laboratories, and in the case of packaged amplifiers we intend to offer a measurement comparison service. Results of the amplifier noise-parameter work and current work on noise parameters of transistors on a wafer will be reviewed.

PRACTICAL IMPLEMENTATION OF PROBE-POSITION
CORRECTION IN PLANAR NEAR-FIELD MEASUREMENTS

Jeff Guerrieri, Katie MacReynolds, Ron Wittmann
, Mike Francis

National Institute of Standards and Technology, Electromagnetics
Division, Boulder, Colorado 80305

The Planar Near-field Technique is a widely used and relatively inexpensive method for characterizing large aperture, high frequency antennas. This technique requires taking amplitude and phase information at accurate and equal point spacing on a plane in the near-field of the antenna under test. The required position accuracy on this plane has been determined to be approximately one-fiftieth wavelength. As frequencies become higher, the accuracy in point spacing position on the planar grid becomes more difficult to achieve and can become a large contributor to the measurement uncertainty budget.

The National Institute of Standards and Technology (NIST) has developed algorithms to correct for position errors [1,2,3] providing the true coordinates of each data point on the measurement plane are known. While the position correction algorithms have been available for several years, methods for obtaining the position coordinates have been tedious and labor intensive. We recently integrated a laser tracking system into our planar near-field (PNF) measurement system that can provide this information. The laser tracker can simultaneously obtain position information in x, y, and z at each point where amplitude and phase data are acquired during a planar near-field antenna measurement. The position uncertainty for the tracker is specified to be 10m/m, which is .001cm at 5 meters. This could provide position correction for measurements up to 500 GHz.

This talk discusses the implementation of a laser-tracking device to provide position information in x, y, and z. Near-field and far-field pattern results are shown for a cassegrain reflector dish antenna at 16 GHz and a parabolic reflector dish at 35 GHz with and without using position correction algorithms.

NEAR FIELD MICROWAVE POWER IMAGING WITH MICROMACHINED CANTILEVERS

T. Mitch Wallis, John Moreland, Simone Lee , Pavel Kabos

National Institute of Standards and Technology, Boulder, CO 80305

We have developed techniques based on micromachined, bimaterial cantilevers for spatially-resolved measurements of microwave power emitted by microwave circuits in the 4 to 20 GHz frequency range. Patterned metal structures on the cantilevers absorb microwave power via induced eddy currents within the patterned structures. The power absorption by the cantilever leads to heating which causes a deflection of the bimaterial system. The deflection may be detected with a laser beam bounce technique similar to that employed in some atomic force microscopes. Custom structures may be lithographically patterned onto the cantilever to optimize eddy current induction and lateral spatial resolution. For example, we deposited a gold film on a silicon nitride / silicon oxide cantilever and patterned the film into a ring 10 μm in diameter.

If the metal structures on the cantilever are patterned from a ferromagnetic material such as permalloy, microwave power absorption may be enhanced by applying an appropriate external magnetic bias field and inducing ferromagnetic resonance (FMR) within the structure. Enhancement of the power absorption by FMR significantly improves the signal to noise ratio. However, where the eddy current effect is broadband, the FMR enhancement occurs only at the resonant frequency.

Images are generated by placing a cantilever in close proximity ($\sim 300 \mu\text{m}$) above a microwave circuit and measuring the cantilever deflection as a function of position. At present, the best lateral spatial resolution achievable with this technique is about 10 μm with prospects for sub- μm imaging in the near future. Circuits imaged with this technique to date include a microstrip resonator and the 60 μm center conductor of a coplanar waveguide.

SIMULTANEOUS MEASUREMENT OF ELECTRIC AND MAGNETIC FIELDS WITH A LOOP ANTENNA HAVING TWO RESISTIVELY LOADED GAPS

Keith D. Masteron¹, John Hamilton^{1,2}

¹National Institute of Standards and Technology, Electromagnetics Division, Boulder, CO USA

²University of Colorado, Dept. of Physics, Boulder, CO

Abstract. We describe a measurement system that uses a loop antenna with two resistively loaded gaps to simultaneously measure orthogonal components of the E and H fields. The technique is useful in near-field situations where a plane-wave approximation is not valid. Our system is based on earlier work by Kanda and uses optical fiber links for signal retrieval in order to eliminate field distortion caused by metallic cabling. Mach-Zehnder interferometric modulators inside the antenna loop are used for the signal transducers to measure the voltage drops across the resistors. Receivers in an electronics module convert the optical signals to electrical signals that are added and subtracted to give the E and H fields. Since the unit is intended for use in varied environments, active bias control of the modulators is required. This is accomplished via optical fiber up-links and photovoltaic (PV) cells. Traditional control algorithms that null the second harmonic content in a small dither signal were found to be unusable because of nonlinearities in the PV cell response. A control algorithm that circumvents this problem was developed. The algorithm and other system controls run on a digital signal processor and computer embedded in the electronics module. The antenna loop is 170 mm in diameter with a 17 mm tubular cross section. The system response covers frequencies from 50 kHz to 300 MHz in two measurement ranges, and field levels from below 50 V/m to 2 kV/m, also in two measurement ranges. We give a detailed description of the system and the results of recent measurements made for system characterization and calibration.

M. Kanda, IEEE Transactions on Electromagnetic Compatibility, Vol. EMC-26, No.3, 1984.

THE EXACT INVESTIGATION OF THE EFFECTS OF AIR GAP AND FINITE GROUND PLANE ON PERFORMANCE OF THE RECTANGULAR DIELECTRIC RESONATOR ANTENNAS

Reza Mohamadi Baghaee, Jalil Rashed-Mohassel
Univ. of Tehran , ECE Dept. , Faculty of Eng., Center of Excellence on Applied Electromagnetic Systems, North Kargar st., Tehran, Iran

Different arrangements can be used to excite the resonator such as coaxial probe, microstrip line, slot-coupled transmission line and co-planar waveguide. The probe fed dielectric resonator antenna is most suggested, while the resonator is situated on a metallic ground plane and fed by a coaxial probe extending above the ground plane along the edge of the resonator.

DRA's are normally used with the support of a ground plane. The radiation and impedance properties therefore depend not only on their physical dimensions and dielectric properties, but also on the mechanism of feeding such as size of the ground plane and the gap in the structure.

First, we obtain the Green function of the rectangular dielectric resonator antennas with fed-probe that has air gap between dielectric and ground plane and supported by the finite ground plane. Thus, the electric field in all regions will be found as a function of the frequency, the dimensions of dielectric resonator, the gap between dielectric and ground plane, the size of ground plane, length of the probe and the gap between probe and dielectric. Then, we find the electric field according to the distribution of current on the probe, and verify our solution with other one found by software package such as HFSS. This verification has shown a good agreement between these two types of solutions. After this hard work, we investigate the effects of each variables that stated above such as air gap and the size of finite ground plane on the radiation performance of the RDRA including resonance frequency, input impedance, pattern and side-lobe level. Also our results have a good agreement with the published experimental work.

OPTIMIZATION OF APERTURE SHAPE IN APERTURE-COUPLED MICROSTRIP ANTENNAS USING GENETIC ALGORITHM

Hadi Aliakbarian^{1,2}, Nasrin Hojjat^{1,2}, Jalil Rashed-Mohassel¹

¹Univ. of Tehran , ECE. Dept., Faculty of Eng., Center of Excellence on Applied Electromagnetic Systems, North Kargar st., Tehran, Iran

²Iran Telecommunication Research Centre (ITRC), North Kargar Ave, Tehran, Iran

One of the best promising structures for bandwidth requirements is microstrip aperture coupled antennas. It is declared that these kind of antennas can demonstrated impedance bandwidths ranging from 5 This improvement in bandwidth is primarily a result of the additional degrees of freedom offered by the stub length and coupling aperture size and shape.

The shape of the coupling aperture has a significant impact on the strength of coupling between the feed line and patch. Thin rectangular coupling slots have been used in the majority of aperture coupled microstrip antennas, as these give better coupling than round apertures. Slots with enlarged ends, such as dogbone, bow-tie, or H-shaped apertures can further improve coupling. In this paper the problem of finding an optimized aperture shape using the genetic algorithm is regarded.

The first step of solving this problem is to analyze the antenna accurately. Analysis of the aperture coupled microstrip element is complicated by the presence of two dielectric layers, and the microstrip line-to-slot transition. Adding up the advantages and disadvantages if some of the analysis methods, we chose the moment method. The detailed formulation about the slected method will be presented in full paper.

One of the key points in solving optimization problems using these algorithms is to evaluate each solution of the problem and score it by the means of an appropriate function named cost function. The fitness function for evaluation of each chromosome is considered as a weighted sum of S11 parameter in different frequencies. In order to find the best shape, which can be used as an aperture, the problem of optimization of bandwidth in a simple rectangular patch antenna is considered and optimized. It is obvious that for other variations of microstrip antenna such as dual band structure the similar problem can be used. The regarded area for aperture is divided to many squares and the algorithm will determine that which of them should be metal or not.

As it will be discussed in the main paper, very suitable results are obtained and some important results about the shape of the aperture are concluded. Some considerations on constructability of the obtained results are presented.

Session A2, 13:35 – Wed.

ANTENNAS AND TRANSIENTS

Co-Chairs: W.A. Davis, C.E. Baum

REDUCED ANTENNA MODELS AND PATTERN GENERATION

Licul, S., Davis, W.A.

Virginia Tech Antenna Group, Bradley Dept of Elec Comp Engr,
Blacksburg, VA 24061-0111

Simple models for antennas provide flexibility in the analysis and design of systems. They also offer a basic methodology for obtaining patterns over a wider range of frequencies. In a separate paper, the reduction of multipath in antenna measurements using time-domain modeling was presented. In this paper, the extension of the process to the full modeling of an antenna for pattern measurement is considered, and, as an aside, how the measurements may be included in a link response.

The measurement at each angle of a pattern may be measured as swept frequency data or as transient data. The initial measurements are made at boresight to determine the basic model for the antenna. As in the previous paper, the transient data (an IFFT of the frequency data) is windowed in time to start after the equivalent incident impulse has passed and end before any multipath appears. This data contains the basic response of the antenna based on the singularity expansion method (SEM) [Baum, Interaction Note 88, 1971]. The poles of the response are obtained using the matrix pencil method [Hua and Sarkar, 1989] and the residues for boresight obtained by standard Prony techniques. Observation of the residue amplitudes and pole locations can be further used to enhance the results of the matrix pencil method. Once the final poles are obtained, the revised residues are determined from the windowed data.

Since the boresight measurement generally contains all of the poles of interest (a check is worthwhile in case some asymmetric poles exist), these poles are used for the determination of the residues for all look angles of the antenna. This use of the same poles is based on the SEM observation that the poles of the antenna are independent of aspect angle. The end result is a set of poles that describe the antenna with residues at each pole that represent the pattern performance of the antenna.

Basic pole structures will be shown for selected antennas to demonstrate the potential data reduction for pattern estimation that may be obtained with this technique. The results of pattern measurements and pole-residue estimates of the pattern will then be compared for a Vivaldi antenna.

REDUCING MULTIPATH IN ANTENNA MEASUREMENTS

Davis, W.A., Licul, S.

Virginia Tech Antenna Group, Bradley Dept of Elec Comp Engr,
Blacksburg, VA 24061-0111

Many ranges are limited by the effects of multipath propagation due to reflection from adjacent structures. Such structures may include buildings, range walls, floors, ceilings. The classic methods of reducing these effects use diffraction fences and absorber. With modern processing capabilities, new methods can be incorporated to reduce the multipath effects. Actually the method of reduction is not new, but is the implementation of the older techniques of the singularity expansion method [Baum, Interaction Note 88, 1971] and the matrix pencil method [Hua and Sarkar, 1989].

This paper presents the results that push the limits of an outdoor range due to ground bounce. A 400MHz Uda-Yagi antenna was simulated in both free space and over a ground plane with a dipole transmit antenna. The configurations were swept in frequency from 50MHz to 2050 MHz, typical of an 801 point sweep on a network analyzer. The results are then inverse Fourier transformed (IFFT) to the time domain. Similar results may be obtained for direct time-domain measurements. The processing is basically done in the time-domain. Based on the range limits, the transient response is truncated to eliminate multipath. At higher frequencies, the truncation is sufficient to obtain the needed data and a forward FFT may be used to obtain the frequency response. Such a process would be repeated for each angle of interest.

In the case of interest, the truncation is well before the antenna response has settled. The matrix pencil method is then applied to the response to obtain a pole-residue model for the response. Care must be taken in the choice of the window, starting after the equivalent incident waveform has passed and ending before the multipath appears. The matrix pencil method can be enhanced by observing poles additional poles that have little contribution to the basic response, but represent noise in the system. From the pole structure, both the transient and frequency responses may be computed without the interference of multipath. The results for the boresight response of the 400MHz Yagi will be presented along with measured boresight responses of several antennas, including frequency-independent antennas, UWB antennas, and a monopole.

TRANSMISSION-LINE ANTENNAS FOR SPARSE DIELECTRIC AIRFOILS

Carl E. Baum

Air Force Research Laboratory/DEHP

Transmission-Line Antennas for Sparse Dielectric Airfoils

Carl E. Baum Air Force Research Laboratory Directed Energy Directorate. 3550 Aberdeen Ave SE Kirtland AFB, NM 87117-5776 USA

This paper considers the design of TEM-transmission-line antennas as pulse receptors/transmitters. Such are suitable for mounting on sparse dielectric airfoils. The placing of antennas on aircraft is a complicated matter, depending on frequencies and pulses of interest. This paper considers another type of antenna for reception/transmission of fast pulses. This utilizes dielectric airfoils as a suitable place to locate such antennas. The type of antenna considered is a length l of TEM transmission line. The conductors are mounted on or inside a sparse dielectric airfoil (sparse so as not to interfere significantly with the antenna performance). With the response in reception well understood, the reciprocity theorem is used to characterize its response in transmission, leading to an interesting general result. Then specific transmission-line geometries are considered. Consider adding conductors (wires, strips, etc.) to a mechanical dielectric structure of approximately two-dimensional shape such as an airfoil. Let this be sparse (for low weight) and let the average dielectric constant be near to (slightly greater than) 1.0 (free space, $\epsilon = \epsilon_0$) with permeability μ_0 . The added conductors can be quite light, such as foil, while giving two-dimensional cross sections of transmission line with characteristic impedance of nearly whatever one may wish. Somewhere near the center, or better position of maximum thickness h , place four strip conductors (foil, paint, etc.), two on the upper surface (inside or outside), and similarly two on the lower surface. To the degree practical try to locate them symmetrically with respect to an approximate symmetry plane as indicated. By appropriate connection of these strips in pairs these can be made to transmit/receive in both vertical and horizontal polarizations. Here the degree to which symmetry can be achieved will determine the degree to which polarization purity (orthogonality of the two polarizations) can be achieved. This paper now generalizes some previous results concerning TEM-transmission-line antennas. Using the reciprocity relationship a particularly simple form of the far field is found for the response to a current source driving two arbitrarily shaped parallel plates (perfectly conducting) on a plane (mathematical infinite) parallel to and between the two conducting plates. Specializing to TEM transmission lines (two-dimensional structures) the characteristic impedances are treated for certain symmetrical cases. Together with the length of the line and the impedance(s) at the antenna port(s) this characterizes the antenna(s) on boresight in both transmission and reception.

MITIGATING THE TRANSIENT CHIRP OF CONICAL LOG-
SPIRAL ANTENNAS

T. Yang, W. A. Davis

Virginia Tech Antenna Group, Blacksburg, VA 24061-0111

When an ultra-wideband pulse antenna is required, the conical log-spiral antenna is often considered at first because of its low-profile and frequency independent nature. However, it suffers from a strong chirp in time. Based on simulation, Thorsten W. Hertel, et al, [IEEE Transactions on antennas and propagation, Vol. 51, pp. 1426-1433, Jul. 2003] showed that the chirp can be removed by using an up-chirp input signal. However, if we need a very short-time pulse to cover ultra wideband, we need to be able to generate the incident pulse with a pulse duration of several nano seconds, which is not very feasible with contemporary technology. In this research, we propose the alternative methods to mitigate the chirp, though introducing other trade-offs.

For conical log-spiral antennas fed at the apex, the radiating signal travels backward along the structure from the apex to be radiated in the reverse direction toward the apex. The dispersion may be lowered if we reduce the height of conical structure or wrap the metal pattern more quickly with the same minimum and maximum diameters of the conical log-spiral antenna. In order to demonstrate this concept, we fabricated several sets of test antennas with the operational range of 3 - 9 GHz, different wrap rate of the arms, and different heights. In addition, a resistive-loaded case was also considered to lower the ringing phenomenon. Antenna tests were performed using two identical antennas with an HP 8510 network analyzer in the frequency-domain. Time-domain results were obtained by an inverse Fourier transform. The antennas were oriented in a co-polarized manner and separated by 101.6 cm (40") distance to be in the far field. The equivalent transient source is a Gaussian with a 50 pico second pulse width, corresponding to a 20 GHz frequency spectrum.

Experimental results showed that a conical log-spiral antenna with a fast rate of wrap has a significant reduction in chirp. The detail results will be presented and compared in terms of antenna input impedance, gain, radiation pattern, and impulse response. The results will also be compared in the time domain to other classic UWB antennas.

Session B1, 08:55 – Wed.

ELECTROMAGNETIC THEORY

Co-Chairs: W.A. Davis, P.L.E. Uslenghi

REVIEW OF FUNDAMENTAL LIMITS OF ANTENNAS AND
IDENTIFICATION OF THE TERMS MISSING IN RECENT
DEVELOPMENTS

Davis, W.A.

Virginia Tech Antenna Group, Bradley Dept of Elec Comp Engr,
Blacksburg, VA 24061-0111

Fundamental limits of antennas has received periodic consideration over the half century. The fundamental work of Chu has been debated by many has being approximate. For small antennas, the arguments are rather mundane since all of the techniques lead to the same result. However, as the size of the antenna, newer approaches (McLean and Grimes in particular) claim higher bounds on the minimum radiation quality factor Q .

For the minimum Q , all formulations restrict the discussion to the TM₀₁ mode, recognizing that higher-order spherical modes simply increase the Q . Chu developed his result from an equivalent circuit model for the wave impedance. McLean developed a new formulation based on the average electric-field energy of a equivalent infinitesimal dipole outside the ka sphere, a being the radius of the enclosing sphere of the antenna to be considered. He subtracted a term proportional to kr that represents the energy radiated to the far field and not reacting with the source. Grimes added a transient aspect to the development of McLean to compute the maximum stored energy in the system. If properly done, one would expect these results to provide the same result, since 2 times the average stored electric energy should equal the maximum stored energy in the system.

What went wrong? Both Grimes and McLean did not account for the energy delay in the radiation of energy. The energy does not travel outward at the speed of light, but has a slight delay as energy is stored locally on the way to the far-field. This can be seen from the Poynting vector of the field when separated into a radiated power and a stored energy transfer that should be orthogonal in phase. This term is small relative to the kr term that has already been deleted, but is sufficient to explain the differences in all of the methods. When this energy delay is incorporated into both McLean's and Grimes' formulations, the end result is again Chu's formulation for Q . The actual term that is missing will be presented and an observation about the derivative Chu made will suggest his formulation provides the correct result rather than being an approximation. Equivalent bandwidths will also be demonstrated to further emphasize the point.

AN ANALYSIS OF COUPLING BETWEEN A WHISPERING GALLERY MODE LASER AND THE DOMINANT MODE IN AN OPTICAL FIBER SURROUNDED BY IT

Reyhan Baktur*¹, L. W. Pearson¹, J. M. Ballato²

¹Holcombe Department of Electrical and Computer Engineering, Clemson University

²School of Material Science and Engineering, Clemson University

The problem of coupling a whispering gallery mode (WGM) laser into an optical fiber is considered. The whispering gallery mode laser is generated in a polymer microring formed coaxially on an optical fiber. The focus of this work is to determine factors that influence the coupling between the laser and the fiber around which it is formed.

The coupling mechanism is analyzed and as the result, there is no coupling between the WGM laser and fundamental mode in the fiber if both fiber and microring are rotationally symmetric. So, disturbing the orthogonality becomes the key issue in obtaining the coupling. Some structures with disturbed symmetry are studied and an elliptical microring on an elliptical fiber is found to be the most simple and practical geometry. Elliptic-cross-section fibers have been shown to preserve polarization and they are important in applications where polarization mode dispersion is a performance limiting effect. Beyond this, we are able to show that modes in an elliptical fiber are not orthogonal to each other across the different material regions, and consequentially we expect coupling of the laser into the fiber.

From the characteristics of Mathieu functions, in terms of which the fields in an elliptical dielectric waveguide are represented, we determine that the coupling between the laser and the dominant mode in the fiber can be controlled by the dimension of the microring, the eccentricity of the elliptical cross section, and the material contrast between fiber and microring.

The most convenient control is found to be the eccentricity of the ellipse. The more eccentric ellipse results in the stronger coupling, and this opens the promise of pumping fiber-optical devices, such as amplifying fiber, from an array of WGM lasers arrayed along the fiber.

*a.k.a. Rehanguli Gayiti

REVIEW OF FUNDAMENTAL LIMITS OF ANTENNAS AND
IDENTIFICATION OF THE TERMS MISSING IN RECENT
DEVELOPMENTS

Davis, W.A.

Virginia Tech Antenna Group, Bradley Dept of Elec Comp Engr,
Blacksburg, VA 24061-0111

Fundamental limits of antennas has received periodic consideration over the half century. The fundamental work of Chu has been debated by many as being approximate. For small antennas, the arguments are rather mundane since all of the techniques lead to the same result. However, as the size of the antenna, newer approaches (McLean and Grimes in particular) claim higher bounds on the minimum radiation quality factor Q .

For the minimum Q , all formulations restrict the discussion to the TM₀₁ mode, recognizing that higher-order spherical modes simply increase the Q . Chu developed his result from an equivalent circuit model for the wave impedance. McLean developed a new formulation based on the average electric-field energy of a equivalent infinitesimal dipole outside the ka sphere, a being the radius of the enclosing sphere of the antenna to be considered. He subtracted a term proportional to kr that represents the energy radiated to the far field and not reacting with the source. Grimes added a transient aspect to the development of McLean to compute the maximum stored energy in the system. If properly done, one would expect these results to provide the same result, since 2 times the average stored electric energy should equal the maximum stored energy in the system.

What went wrong? Both Grimes and McLean did not account for the energy delay in the radiation of energy. The energy does not travel outward at the speed of light, but has a slight delay as energy is stored locally on the way to the far-field. This can be seen from the Poynting vector of the field when separated into a radiated power and a stored energy transfer that should be orthogonal in phase. This term is small relative to the kr term that has already been deleted, but is sufficient to explain the differences in all of the methods. When this energy delay is incorporated into both McLean's and Grimes' formulations, the end result is again Chu's formulation for Q . The actual term that is missing will be presented and an observation about the derivative Chu made will suggest his formulation provides the correct result rather than being an approximation. Equivalent bandwidths will also be demonstrated to further emphasize the point.

GREEN'S FUNCTION ANALYSIS OF AN IDEAL HARD SURFACE RECTANGULAR WAVEGUIDE

Huang, W., Yakovlev, A.B., Kishk, A.A.,
, Glisson, A.W., Eshrah, I.A., Zhang, Y.
Department of Electrical Engineering, The University of Mississippi,
University, MS 38677-1848, USA

In this paper, we study a rectangular waveguide with an ideal hard surface boundary conditions, which is modeled by alternating longitudinal perfect electric conductor (PEC) and perfect magnetic conductor (PMC) strips with vanishing widths. Compared to PEC and PMC rectangular waveguides, which can support only TM and TE modes, the most important feature of this ideal hard surface rectangular waveguide is that it allows a propagation of the TEM mode with a zero-cutoff frequency, which can provide new applications for this type of guided-wave structure. Whereas the TM and TE modes see the waveguide as a PEC and PMC waveguide, respectively, the TEM mode sees the ideal hard surface waveguide as a combination of PEC and PMC waveguides modeled by alternating PEC/PMC strips with vanishing widths, and it satisfies the boundary conditions on the ideal hard surface partially contributed by PEC and PMC waveguides.

The purpose of the present paper is to develop an electric dyadic Greens function for the modal analysis of an ideal hard surface rectangular waveguide excited by an arbitrarily-oriented electric current source. A decomposition of the hard surface waveguide into PEC and PMC waveguides allows the representation of dyadic Greens function as a superposition of TM and TE waveguide modes, respectively. In addition, a term corresponding to the TEM mode is obtained analytically as the solution of vector Helmholtz equation in the zero-cutoff limit subject to the boundary conditions for the electric field on the ideal hard surface. The electric Greens dyadic of the ideal hard surface waveguide consists of solenoidal and irrotational parts, where the solenoidal part is obtained in the eigenmode expansion form in terms of TM, TE, and TEM modes of the hard surface waveguide and it is understood in the principal value sense. The irrotational part includes a depolarizing dyadic, which is associated with a slice-pillbox principal exclusion volume. The main singularity of the Greens function is contained in the solenoidal part and represents a source-plane singularity.

Numerical results for field distributions are demonstrated for the TEM mode and a few representative TM and TE modes propagating in a rectangular waveguide with ideal hard surface boundary conditions due to an arbitrarily-oriented electric dipole source. It is shown that the TEM mode of the ideal hard surface waveguide has uniform field distribution over the waveguide cross-section, and the polarization of the mode necessarily depends on the polarization of the electric dipole source.

EFFICIENT CALCULATION OF DIELECTRIC RESPONSE
OF TWO-DIMENSIONAL SCATTERERS USING ELEMENT
METHOD

Ari Sihvola, Jukka Venermo

Helsinki University of Technology, Electromagnetics Laboratory,
Finland

In this presentation we show an extremely efficient method to calculate the polarizability of two-dimensional inclusions. It is based on a special property of the polarizability of complementary inclusions: the polarizabilities of inclusions with permittivities ϵ_r and $1/\epsilon_r$ are very closely related. It turns out that the numerical errors in a finite element method to solve the complementary polarizabilities go into different directions, and the individual numerical results can be played against each other to compensate for the errors.

The special property can be appreciated from the following observation concerning the normalized polarizability of a circle (two-dimensional sphere) with permittivity ϵ_r :

$$\alpha_\epsilon = 2 \frac{\epsilon_r - 1}{\epsilon_r + 1} \quad (1)$$

Namely, the polarizability of a "complementary circle," in other words, a circle with permittivity $1/\epsilon_r$ is closely connected to (1): the numbers are the opposite:

$$\alpha_{1/\epsilon} = 2 \frac{1/\epsilon_r - 1}{1/\epsilon_r + 1} = -2 \frac{\epsilon_r - 1}{\epsilon_r + 1} = -\alpha_\epsilon \quad (2)$$

It seems that this property is not only limited to the circle but is more universal: for any isotropic homogeneous two-dimensional shape, the polarizabilities of complementary inclusions are opposite numbers to each other. The theorem by Keller (*Journal of Applied Physics*, Vol. 34, No. 4, Part I, pp. 991-993, April 1963), seems to be applicable to confirm this result.

The complementary result also applies to anisotropic two-dimensional scatterers. The presentation will show how this property can be exploited to boost the accuracy in the evaluation of the polarizability of scatterers.

Calculations were done with FEMLAB (an environment suitable for modeling and simulating problems obeying partial differential equations). All numerical calculations were performed using a PC machine equipped with AMD XP 1800+ processor and 768 Mbytes of RAM. We calculated the polarizability of an object and the complementary object with the same shape. Theoretically, the results should be connected. It turns out that the numerical method overestimates the absolute value of the polarizability of the object with permittivity $\epsilon > 1$, and underestimates the complementary problem. We show how the accuracy can be increased by even several orders of magnitude.

DISTRIBUTION OF ELECTROSTATIC CHARGE ON ROTATIONALLY SYMMETRIC CONDUCTORS

Uslenghi, P.L.E.

Department of Electrical and Computer Engineering, University of Illinois at Chicago

The distribution of electrostatic charges on the surface of a perfect electrical conductor has elicited recent, renewed interest (see, e.g., J. Van Bladel, *IEEE Antennas and Propagation Magazine*, vol. 45, no. 5, pp. 118-122, October 2003). In particular, for a metallic prolate spheroid, it was proven in the above paper that the electrostatic charge per unit length along the symmetry axis of the spheroid is constant. This result can be trivially verified for the particular case of a conducting sphere.

In a reply to the work of Van Bladel (P.L.E. Uslenghi, *IEEE Antennas and Propagation Magazine*, vol. 46, no. 2, pp. 146-148), it was proven that the constancy of electrostatic charge per unit length along the symmetry axis is valid also for the case of a conducting paraboloid of revolution. The fact that the charge per unit length is constant along the symmetry axis of two very different bodies such as a prolate spheroid and a paraboloid, independently of the fatness of the body, prompted the author of the present work to pose the question: could this result be valid for all bodies of revolution? In this paper, an attempt is made to answer that question.

The approach followed consists in introducing a local orthogonal coordinate system at and near the surface of the body of revolution, and in determining the functional form that the electrostatic field assumes in such a system. From the component of the electric field normal to the body's surface, the surface charge density is obtained, and the charge per unit length along the symmetry axis is determined. In so doing, some relationships introduced in the book by W. R. Smythe (*Static and Dynamic Electricity*, 2nd edition. New York: McGraw-Hill, 1950) are utilized.

CALCULATION OF MICROSTRIP FIELDS USING ELECTROMAGNETIC SCALAR POTENTIALS

Lahart, M.J.¹, Fazi, C¹, Kohlberg, I²¹U.S. Army Research Laboratory, Adelphi, MD 20783-1197²Kohlberg Associates, Inc, Alexandria, VA 22304

Propagation constants and electric and magnetic fields of the propagation modes of open microstrip are computed using a hybrid method of computation. Analytical expressions for the propagation modes of a dielectric covered ground plane describe fields far from the microstrip, and numerical computations enforcing boundary conditions for a conducting surface on the conducting strip are used to find fields close to it. The analytical expressions are assumed to describe the fields on a boundary between the two regions, and fields inside this boundary are computed numerically by using the values computed from the analytical expressions as boundary values. Separate computations are carried out for each mode of a dielectric covered ground plane. Linear combinations of these modes are sought for which the derivatives of the fields are continuous at the boundary. The continuity conditions of the derivatives of the fields along the boundary are taken as a measure of the accuracy of the hybrid procedure.

Propagation modes of a dielectric covered ground plane have been classified as proper modes, whose amplitude decreases in the direction normal to the dielectric interface, and improper modes, whose amplitude increases in this direction. Microstrip fields are shown to have the same properties because they are constructed from the modes of a dielectric covered ground plane.

Calculations are carried out in terms of electromagnetic scalar potentials. Pairs of scalar functions are defined such that all components of the electric and magnetic fields can be derived from them. It is shown that scalar potentials can describe the fields when the components of their gradients in each of two orthogonal directions obey the wave equation, and that the coordinate system of the microstrip can be defined so that this is the case. The use of scalar potentials simplifies the calculations greatly, while retaining the accuracy of full vector calculations. Computation of the electric and magnetic fields from these potentials is demonstrated.

INCIDENT FIELD EXCITATION OF A RANDOM MULTICONDUCTOR TRANSMISSION LINE IN A CORNER FORMED BY CONDUCTING WALLS

Pincenti, J.C., Uslenghi, P.L.E.
University of Illinois at Chicago

The problem of finding the response at the terminations of a random multiconductor transmission line, when the line is placed in a corner formed by conducting walls is considered. Often in practice, the exact orientation of a multiconductor transmission line (or cable bundle) is not known. The position of the wires may vary along the length of the line, which for the case of external field excitation will cause random orientations of the line with respect to the incident field. This will then cause the signals induced on the line to be random, and thus the response is studied using a probabilistic approach.

The particular problem of interest here, is the field excitation of a transmission line that is placed in a corner formed by conducting walls. Such a situation may be encountered by cables in the body of an aircraft where the external field may be due to the waves from a radar system. It is assumed that such a line will not be laid out in an exact manner, and is therefore random. This problem will be analyzed in the frequency domain using transmission line theory. In particular the line will be modeled as a non-uniform transmission line excited by an external field. The solution will be found by using the chain parameter matrix, which relates the currents and voltages on the line. The advantage of the chain parameter matrix is it provides a method for solving non-uniform lines. The non-uniformity will be modeled by dividing the line into small discrete uniform sections, finding the chain parameter for each section and then cascading the results together to approximate the overall line.

Using this model, a number of random cables will be generated and solved producing a statistical solution. For a given excitation frequency the response can be shown as either the cumulative distribution function (CDF) or the probability density function (PDF). From these, the probability that the response will be in a particular range can be determined.

Session B2, 13:35 – Wed.

**METAMATERIALS AND OTHER
COMPLEX MATERIALS FOR
RADIO FREQUENCY
APPLICATIONS**

Co-Chairs: G.V. Eleftheriades, J.L. Volakis

MORE ON TRANSPARENCY OF OBJECTS USING PLASMONIC METAMATERIALS

Alu, A.^{1,2}, Engheta, N.¹¹University of Pennsylvania, Department of Electrical and Systems Engineering, Philadelphia, Pennsylvania 19104, U.S.A.²Universita di Roma Tre, Department of Applied Electronics, Rome, Italy

In a recent presentation, we discussed the possibility of reducing the total scattering cross section of a small dielectric sphere or a thin cylinder by adding over it a layer of metamaterial with negative real parts for permittivity and/or permeability or metamaterial with low (positive) permittivity or permeability. (A. Alu and N. Engheta, Reducing Scattering from Cylinders and Spheres Using Metamaterials presented at the 2004 USNC/URSI National Radio Science Meeting, Monterey, CA, June 20-25, 2004, p. 231.) We pointed out how the addition of such a metamaterial layer over the object can nullify the scattering coefficient for a specific spherical (or cylindrical) scattering mode, and when such a scattering coefficient is the dominant term of scattering for the uncovered sphere, the nullification of this coefficient due to the presence of the layer can thus lead to reduction of the total scattering cross section of this object. As was mentioned then, this effect is essentially opposite to the resonance phenomenon that may be induced by properly covering a homogeneous dielectric sphere or cylinder with a concentric shell of metamaterials with negative effective constitutive parameters [A. Alu, N. Engheta, Proceedings of the ICEAA03 Meeting, Torino, Italy, Sept. 8-12, pp. 435-438].

In the present work, we extend our investigation to the case of spheres that are not necessarily small compared with the wavelength of operation. In such a scenario, the role of higher-order multipoles in scattering should also be taken into account. By adding the metamaterial layers with negative or low-positive permittivity, one can reduce the scattering coefficient due to the TM dipolar term, which is in general a dominant term, but one also needs to be aware of other scattering terms such as TE dipolar term, TM and TE quadrupolar terms, etc. It can be shown that by properly selecting the values for both permittivity and permeability of the cover layer (i.e., having negative or low-positive permittivity and permeability), one can significantly reduce both TM and TE dipolar scattering terms, leading to further reduction of the total scattering cross section of the object. It is also possible that by adding more metamaterial layers, one can increase the degrees of freedom that can be used to reduce higher order scattering coefficients and thus to decrease the total cross section even further.

In this talk, we will present some of our new findings on the field distributions and the Poynting vector variation in this problem, and we will provide physical insights and intuitive remarks into these results.

METAMATERIAL-BASED REALIZATIONS OF EFFICIENT
ELECTRICALLY SMALL ANTENNAS

Aycan Erentok, Richard W. Ziolkowski
ECE, University of Arizona

METAMATERIAL-BASED REALIZATIONS OF EFFICIENT ELEC-
TRICALLY SMALL ANTENNAS

Aycan Erentok* and Richard W. Ziolkowski

Department of Electrical and Computer Engineering The University of
Arizona 1230 E. Speedway Tucson, AZ 85721-0104 USA

Tel: (520) 621-6173 Fax: (520) 621-8076 E-mail:
erentoka@ece.arizona.edu, ziolkowski@ece.arizona.edu

The possibility of an efficient electrically small antenna (EESA) was predicted recently by Kipple and Ziolkowski [IEEE Trans. Antennas Propagat., vol. 51, pp. 2626-2640, October 2003]. It consisted of an electrically small dipole antenna surrounded by an electrically small double negative (DNG) metamaterial shell. The DNG metamaterial was lossless. Reciprocity between the proposed EESA geometry and resonant scattering from spheres with DNG coatings has also been demonstrated by Kipple and Ziolkowski [IEEE Antennas and Propagation Society International Symposium and USNC/URSI National Radio Science Meeting, Session 91, Monterey, CA, June 20-26, 2004]. Furthermore, it was demonstrated that the EESA could be realized with only an epsilon-negative (ENG) metamaterial shell.

We will report further results for the EESA geometry. Predictions of the EESA sizes and performances at 10GHz and at 400 MHz will be presented. These will include determining the power gain of the EESA in the presence of a lossy DNG metamaterial shell. It is found that losses decrease the amplitude and broaden the resonance. However, significant enhancements are still realized. Variations in the index of refraction of the DNG shells have also been explored. Analogous studies have also been performed for the lossy ENG shell based EESA with similar conclusions. The ENG shell based EESA has also been designed with ANSOFTs High Frequency Structure Simulation (HFSS) tools. Results for these simulations will also be presented. The HFSS simulations have allowed us to explore the near-field and far-field operating characteristics of an electrically small dipole antenna in the presence of an ENG shell.

We are also investigating how one could realize the DNG and ENG metamaterial shells. We are considering the use of lumped element based artificial electric and magnetic molecules to achieve the desired metamaterial effects. Preliminary results from these studies will also be given.

RECEIVING ANTENNAS EMBEDDED WITHIN NONRECIPROCAL MAGNETIC PHOTONIC CRYSTALS

Gokhan Mumcu, Kubilay Sertel, John L. Volakis
Electro Science Lab, ECE Dept., The Ohio State University, 1320
Kinnear Rd., Columbus, OH 43212 USA

A new class of magnetic photonic crystals (MPCs) constructed from periodic arrangements of readily available anisotropic layers was recently introduced (A. Figotin and I. Vitebsky, "Nonreciprocal magnetic photonic crystals," *Physical Review E*, vol. 63, pp. 117, May 2001). Initial analytical studies of these in a semi-infinite model demonstrated that they exhibit phenomena of drastic incoming wave slow-down and concurrent amplitude growth while maintaining a minimal reflection at the boundary (A. Figotin and I. Vitebsky, "Electromagnetic unidirectionality in magnetic photonic crystals," *Physical Review B*, vol. 67, pp. 120, Apr. 2003). These phenomena are a consequence of the frozen modes realized at specific frequencies where a stationary inflection point exists within the band diagram. In a recent presentation (Mumcu et al., "RF propagation in finite thickness nonreciprocal magnetic photonic crystals," *IEEE APS Symposium 2004*, vol. 2, pp. 1395-1398), we demonstrated a full wave characterization (amplitude growth, bandwidth, coupling and thickness required for maximum amplitude) of the phenomena for finite thickness MPCs. We demonstrated that for a practical MPC slab, the frozen mode phenomena can be indeed realized, and have promise in developing miniature antenna arrays embedded within the MPC.

In this paper, we consider the performance of a receiving antenna element within the MPC. We concentrate on the problem of a short dipole antenna placed within a finite thickness MPC. The current induced on the dipole due to an incident plane wave illumination is found via the spectral domain-method of moments (SP-MOM) approach. However, since the MPC consists of highly anisotropic dielectric and magnetically gyrotropic materials, the mathematics are rather complex. Our analysis specifically focuses on the frozen mode regime to investigate the effect of MPC on the receiving properties of the dipole antenna. Along with pattern shaping, the phenomenon of minimal reflection at the MPC boundary can be utilized for improving the gain.

We will present the analysis method along with representative results for radiating and receiving dipoles embedded within the crystal. We will also discuss the SD-MOM for anisotropic layered structure.

NEGATIVE REFRACTION AND FOCUSING USING CONTINUOUS METALLIC GRIDS OVER GROUND

Omar Siddiqui, Trevor Andrade, Anthony Grbic

, George V. Eleftheriades

Department of Electrical and Computer Engineering, University of Toronto, 10 King's College Road, Toronto, ON M5S 3G4, Canada

In the past 2-3 years a range of planar metamaterials has been demonstrated by loading a host transmission-line network with lumped-element inductors and capacitors (chip or printed). Normally the unit cell of these metamaterials is much smaller than the operating wavelength so that effective material parameters such as a negative permittivity or/and permeability, and a negative refractive index can be defined. Using this approach negative refraction and focusing effects have been demonstrated using isotropic [1] or anisotropic metamaterials [2].

In this paper we will demonstrate that simple continuous metallic grids over ground can be utilized to achieve negative refraction and focusing effects of electromagnetic waves at microwave frequencies. The periodicity of the unit cell in these grids is comparable to the operating wavelength; hence they cannot be described in terms of effective material parameters. Nevertheless, they are simple to fabricate since no lumped loading elements (chip or printed) or vias are needed. Moreover, they are inherently scalable from microwave to millimeter-wave frequencies. Both isotropic as well as anisotropic grids with hyperbolic dispersion characteristics can be implemented in this approach [3]. In fact, the isotropic grids can be arranged to grow evanescent waves. These concepts will be supported by analytical, simulation and experimental results between 5 GHz and 10 GHz.

[1]G. V. Eleftheriades, A. K. Iyer, P. C. Kremer, Planar negative refractive index media using periodically L-C loaded transmission lines, *IEEE Trans. on Microwave Theory and Tech.*, vol. 50, no. 12, pp. 2702-2712, Dec. 2002.

[2]K.G. Balmain, A.A.E. Lttgen, and P.C. Kremer, "Power flow for resonance cone phenomena in planar anisotropic metamaterials," *IEEE Trans. Antennas Propagat.*, Special Issue on Metamaterials , vol. 51, no. 10, pp. 2612-2618, Oct. 2003.

[3]O. Siddiqui and G.V. Eleftheriades, Resonance-cone focusing in a compensating bilayer of continuous hyperbolic microstrip grids, *Applied Physics Letters*, pp. 1292-1294, Aug. 16, 2004.

STUDY OF SLOW WAVE PROPAGATION IN A METAMATERIALS-BASED ELECTRONICALLY-CONTROLLED TRANSMISSION LINE

Lim, S.¹, Leong, K.M.K.H.¹, Caloz, C.², Itoh, T.¹

¹University of California, Los Angeles

²the Ecole Polytechnique of Montreal, Montreal

Recently, left-handed metamaterials (LHM's) have been spotlighted due to their interesting natures, such as negative refractive index and backward propagation. A backward propagation of fast wave can be used for antenna applications. We recently proposed a backfire-to-endfire leaky-wave (LW) antenna by using a composite right/left-handed (CRLH) concept, in which lower frequencies operate in the left-handed (LH) region and higher frequencies operate in right-handed (RH) region. Despite its full-space scanning capability, it had a limitation in practical applications since a scanning angle is a function of a frequency. For this reason, we developed an electronically-controlled transmission line (TL) which is an extension of CRLH TL. The CRLH TL is represented by a series capacitance/ shunt inductance and a physically unavoidable series inductance/ shunt capacitance. In that sense, since propagation constant becomes a function of capacitive and inductive parameters, we can manipulate propagation constant by introducing varactor diodes to change capacitances. Therefore, the proposed structure, as a LW antenna application, is able to radiate backward to forward through broadside, by varying the bias voltages at a fixed frequency. In addition, it provides a beamwidth control capability with non-uniform bias distribution.

Since LW antennas radiate only in the fast wave region ($|\beta| < k_0$), we were mainly interested in this radiation region. In this paper, we investigate the electronically-controlled TL in the slow wave region ($|\beta| > k_0$). It is previously reported that a phase in the LH region is advanced, while a phase in RH region is delayed. The slow wave factor (SWF, $|\beta|/k_0$) is plotted versus a frequency or a bias voltage, from the measured S-parameters at different bias voltages. The SWF in the LH region is typically higher than the SWF in the RH region and the phase slope can be adjusted with capacitive and inductive parameters. In the proposed electronically-controlled TL (in effect, a phase controller), the SWF in the LH region is varied from 1 to 6 by tuning the bias voltage at a fixed frequency. It is observed that the range of SWF in the LH region decreases, as a frequency is lower.

MEASURED AND SIMULATED FIELDS INSIDE NEGATIVE REFRACTIVE INDEX METAMATERIALS

Steven A. Cummer, Bodan-Ioan Popa

Electrical and Computer Engineering Department, Duke University

To date most measurements (both simulated and experimental) of the properties of negative refractive index metamaterials (NIMs) have relied on wave transmission and reflection measurements. These measurements at best exactly determine the material properties (as opposed to more robust overdetermination) and can in some cases be ambiguous and difficult to interpret. Moreover, they do not easily demonstrate the fundamental behavior of electromagnetic waves in these materials (for example, the antiparallel phase velocity and energy flow direction). We show, using HFSS simulations of a wire-SRR (split ring resonator) metamaterial that, although the field structure inside the metamaterial is complicated due to the metallic inclusions, there can be slices through the material where the total fields inside the metamaterial are surprisingly close to the wave fields expected if the medium were homogeneous. This supports the general finding that metamaterials behave like homogeneous materials even for surprisingly large inclusions (only a few per wavelength). This also suggests the possibility of robustly measuring the effective medium properties of the metamaterial (i.e., permittivity and permeability) by probing the spatial field dependence in a three slab (air/NIM/air) configuration.

To test this idea experimentally, we designed and constructed a wire-SRR medium with negative permittivity and permeability near 2.6 GHz and measured the spatial field distribution in a three slab configuration inside a rectangular waveguide. The phase gradient shows directly and unambiguously that inside the NIM, the phase velocity points towards the source while the energy flows away from the source. We also show how the measured three slab spatial field pattern determines the effective medium properties robustly and with minimum uncertainty.

DOMAIN DECOMPOSITION METHOD FOR MODELING METAMATERIALS IN ELECTROMAGNETICS

Vouvakis, M. N., Lee, S.-C., Lee, J.-F.

ElectroScience Laboratory, The Ohio State University

In recent years, there are significant interests in studying and investigating various types of metamaterials. For example, in (J. B. Pendry, A. J. Holden, D. J. Robbins, and W. J. Stewart, *IEEE Trans. Microwave Theory and Techniques*, **47**, 2075-2084, 1999) Pendry et al utilized an array of splitting-resonators (SRR) and proclaimed the physical realization of the negative index medium or left-handed media (LHM). Later, Eleftheriades et. al (G. Eleftheriades, A. K. Iyer, and P. C. Kremer, *IEEE Trans. Microwave Theory and Techniques*, **50**, 2702-2712, 2002) proposed the use of dual-transmission line, by inverting the L and C in conventional transmission line construction, to realize the LHM and subsequently demonstrate a perfect lens (A. Grbic, G. Eleftheriades, *IEEE Antennas and Wireless Propagation Letters*, **2**, 186-189, 2003) using such a structure. Also, another class of metamaterials is the magnetic photonic crystals recently proposed by Figotin and Vitebsky (A. Figotin and I. Vitebsky, *Physical Review*, **63**, 066609, 2001). It is shown that by proper spatial arrangement of magnetic and dielectric components, the MPC can produce the so-called frozen mode, which corresponds to a block wave with zero group velocity. It goes without saying that it is then becoming very crucial to have a reliable and efficient numerical simulation tool, which can solve the full-wave Maxwells equations in the presence of these exotic metamaterials. However, both the focusing effects exhibited in the NIM as well as the frozen mode phenomena described by A. Figotin require extremely fine resolution within certain regions in the numerical simulation. For example, an extremely non-uniform mesh is needed to efficiently simulate the dual-transmission line lenz proposed by Eleftheriades. The entire structure is electrically small (on the order of $1/2\lambda$), however, it took roughly 2 million $p=2$ higher order vector finite elements in order to provide the resolution needed. It would quickly become prohibitive to employ numerical simulation once more combination of materials and complexities are added into the structure. Fortunately, almost all of these metamaterials constructed/proposed are periodic in nature (though finite). Consequently, they are well-suited for the application of the advanced computational techniques such as domain decomposition method. In this presentation, we shall share our experiences and our findings in using a newly developed domain decomposition method described in (S. C. Lee, M. Vouvakis, and J. F. Lee, *Accepted for publication in J. Comp. Physics*) to solve for such electromagnetic problems with metamaterials.

RESOLUTION BOUNDS TO IMAGING WITH NEGATIVE-REFRACTIVE-INDEX TRANSMISSION-LINE LENSES

Anthony Grbic, George V. Eleftheriades

Dept. of Electrical and Computer Engineering, 10 King's College Road, University of Toronto, Toronto, ON M5S 3G4, Canada

The perfect lens concept proposed by John Pendry in 2000 has captured the imagination of the scientific and technical communities alike [1]. Since then, numerous questions were raised concerning the issue of how close one can approach the perfect lens concept in practice. In a recent experiment, a negative-refractive-index (NRI) transmission-line (TL) lens was used to demonstrate imaging beyond the diffraction limit at microwave frequencies [2]. This experimental device consisted of a NRI region comprising microstrip lines loaded with series capacitors and shunt inductors. The so created NRI region was sandwiched between two dense microstrip meshes acting as parallel-plate waveguides. Using this NRI-TL lens, a resolution of $\lambda/6$ was achieved as opposed to the diffraction-limited resolution which would have been $\lambda/2$ [2]. Although the achieved resolution beats the diffraction limit, it does not correspond to perfect imaging. In this paper, we will discuss the practical resolution bounds of the experimental lenses in [2] due to material and mismatch losses.

A key result of our analysis is that the resolution is logarithmically bounded by the losses on the loading series capacitors. Specifically, the maximum resolved transverse wavenumber k_x is determined by,

$$R = \frac{k_x}{k_o} = \frac{\ln(Q_c)}{k_o d}$$

where $k_o d$ is the electrical thickness of the lens in radians and Q_c is the quality factor of the loading series capacitors.

[1] J. B. Pendry, Negative refraction makes a perfect lens, *Phys. Rev. Lett.*, vol. 85, no. 18, pp. 3966-3969, Oct. 2000.

[2] A. Grbic and G.V. Eleftheriades, Overcoming the diffraction limit with a planar left-handed transmission-line lens. *Phys. Rev. Lett.*, vol. 92, no. 11, pp. 117403, March 19, 2004.

Session B3, 13:35 – Thurs.

**COMPUTATIONAL
ELECTROMAGNETICS**

Co-Chairs: D.R. Jackson, E. Topsakal

WELL-CONDITIONED INTEGRAL EQUATIONS FOR OPEN TARGETS

Robert J. Adams, Gang Wang

Electrical Computer Engineering, University of Kentucky

We outline a well-conditioned integral equation formulation of three-dimensional scalar wave scattering from open targets. The new formulation is well-conditioned in the presence of fairly general geometric singularities.

The three-dimensional surface integral equation for the Dirichlet problem is

$$0 = \Phi^i(S) - \int_S G(k|r-r'|) \frac{\partial \Phi}{\partial n'}(S') dS' \quad (1)$$

where S indicates the surface of the scatterer, $\Phi^i(S)$ indicates the impressed field on S , and $G(kR) = \exp(-jkR)/4\pi R$ with $R = |r-r'|$. The condition (1) follows from the Helmholtz equation $((\nabla^2 + k^2)\Phi(r) = 0)$ using Green's theorem and the Dirichlet surface boundary condition $\Phi(S) = 0$.

It is convenient to represent (1) using an operator notation,

$$0 = \Phi^i + Z\partial_n\Phi \quad (2)$$

where Z indicates the surface integral operator of (1). It is well-known that Z is a smoothing operator. Consequently, (2) is a first-kind integral equation.

A well-conditioned form of (2) is obtained as

$$= YD_Y\Phi^i + YD_YZD_Z\partial_n\Phi \quad (3)$$

where D_Y and D_Z are diagonal operators, and Y is the hypersingular dual of Z . The diagonal elements of matrices D_Y and D_Z are determined by solving the linear systems

$$Zd_Z = \psi_o \quad (4)$$

$$Yd_Y = \psi_o \quad (5)$$

for the vectors d_Z and d_Y . In (3) and (4), ψ_o is an appropriately defined function over S .

Numerical examples will be provided demonstrating that the formulation indicated by (2) is well-conditioned for open targets. The conditioning will also be shown to be stable with respect to refinements in the vicinity of geometric singularities. Finally, we will also demonstrate that, for a given mesh, equations (3) and (4) each need only be solved once in order to determine a formulation which is asymptotically well conditioned for all linearly independent excitations at all frequencies.

A BEAM TRANSFORM METHOD FOR PLANE WAVE RESPONSE MATRICES

Robert J. Adams¹, Francis Canning², Faisal Mev¹

¹Electrical Computer Engineering, University of Kentucky

²Simply Sparse Technologies, Morgantown, WV

Numerical solutions of surface integral equation formulations of time-harmonic electromagnetic radiation and scattering from perfectly conducting targets involve solving linear systems of the form

$$ZJ = M^i \quad (1)$$

where Z is the impedance matrix.

The use of surface integral equations to determine (1) usually leads to a full impedance matrix. As a result, the computational costs associated with standard solutions of (1) are often prohibitive for electrically large problems, and it is often necessary to solve (1) iteratively using compression algorithms for Z . However, the computational costs of fast iterative solvers can be significant when the impedance matrix is poorly conditioned, and when solutions are required for a large number of linearly independent excitations.

A general scheme for addressing the limitations associated with fast iterative solvers for electrically large problems should have two properties. First, it should provide a computationally efficient representation for the inverse of the impedance matrix, Z^{-1} . To be generally applicable, such a scheme should also provide an efficient procedure to determine the compressed representation of the inverse from more directly available information, such as that contained in (1).

In this paper we restrict our attention to the first of these requirements. Furthermore, instead of working directly with the inverse of the impedance matrix, we outline a compression algorithm for a related problem. The algorithm we report compresses the plane wave response matrix (P-matrix) which specifies the currents excited on the surface of a target by a spectrum of incident plane waves. The motivation for working with spectrally forced representations of the scattering problem instead of working directly with the spatial domain representation indicated by (1) follows from the physical characteristics of wave phenomena. In particular, for many electrically large scattering problems, with proper weighting, it is possible to group plane wave sources originating from a small spread of angular directions in order to form incident beams which excite surface currents that are nonzero over a small fraction of a large obstacle. Using this principle, we demonstrate that it is possible to determine a sequence of linear transformations in the domain of the P-matrix which yield sparse representations for electrically large problems.

ANALYSIS OF A PEC HEMISPHERE BACKED CIRCULAR APERTURE EXCITED BY AN AXIALLY DIRECTED DIPOLE

Bopp III, C. L., Butler, C. M.
Clemson University

A circular aperture in an infinite pec plane backed by a pec hemispherical cavity is excited by an axially-directed electric dipole located outside the cavity on the axis of symmetry of the hemisphere and hole. The materials in the region above the aperture and the region inside the hemisphere may be different but are homogeneous throughout the given region. The field in this structure and the currents induced on conducting surfaces by the dipole excitation are determined from an integral equation solution. A single integral equation for the unknown electric field in the circular hole, or for the equivalent surface magnetic current over the shorted aperture, is derived. The domain of the integral equation is the aperture bounded by the rim of the hole and its kernel includes a Greens function which enforces the boundary condition that the electric field tangential to the hemispherical surface be zero on that surface. Explicitly, the kernel is the sum of a free space Greens function and a cavity Greens function expressed in terms of spherical harmonics. The integral equation enforces the continuity of magnetic field tangential to the aperture plane along axially directed paths from within the cavity to the exterior region, and it embodies the radiation condition that must hold in the exterior region. The boundary condition of the electric field on the pec plane is also enforced by the integral equation. The integral equation is solved by a standard numerical method which is complicated slightly by the need to ensure convergence of the cavity Greens function. From the integral equation solution, field components inside and outside the cavity are determined. Also, the physical surface currents induced on the wall of the hemispherical cavity are derived from knowledge of the integral equation solution and this current is computed for numerous cases of interest.

COUPLING TO A LOADED THIN WIRE IN A CYLINDRICAL/COAXIAL CAVITY

Bopp III, C. L., Butler, C. M., Tesche, F. M.
Clemson University

The electromagnetic field coupling to a loaded thin wire in a cylindrical/coaxial cavity is investigated. There is an interest in understanding how electromagnetic fields couple to wires and tubes that may be present in an enclosed structure and in how to efficiently analyze this coupling as part of an overall system. The cavity may consist of multiple cascaded coaxial and circular cylindrical sections with sections coupled through apertures and conducting elements common to more than one section. The sections may have different axial and radial dimensions and may be filled with material having different magnetic and electric properties. The technique for analyzing the field in these cavities with the wire absent was presented at the 2003 APS-URSI Symposium in Columbus, OH. A loaded thin wire protrudes into a cavity section and is placed in close enough proximity to the outer wall of the section that transmission line approximations are valid. The coupling of the cavity field to the wire is accounted for via a distributed voltage source model similar to that outlined by Agrawal, Price, and Gurbaxani (IEEE Trans. on Elect. Comp, May 1980) for a transmission line in open space or a wire parallel and close to a conducting surface. A coupled integral equation method was presented at the 2004 APS/URSI Conference in Monterey. The characteristic impedance of the wire in the presence of the cavity wall is developed. A Greens function for the current and voltage along a loaded transmission line due to a set of distributed voltage sources is developed and used to calculate the voltage and current at points along the wire. For the purpose of demonstrating the accuracy of the procedure and numerical solutions obtained from this analysis, a cavity model is constructed and measurements made on the laboratory model are compared with computed results. The measured voltage and current at a port on the wire is compared with values obtained computationally at the port. The computed results from this analysis are also compared with results from the coupled integral equation method.

THE BEST CHOICE OF THE SPLITTING PARAMETER IN
THE EWALD METHOD

Oroskar, S. , Jackson, D. R., Wilton, D. R.
University of Houston

The Ewald method is a powerful means to efficiently evaluate the free-space periodic Green's function (FSPGF). In the Ewald method, the FSPGF is expressed as the sum of a "modified spectral" and a "modified spatial" series. Each series possesses Gaussian exponential decay and this leads to an overall series representation that exhibits very rapid convergence. The overall convergence is optimum when the asymptotic rate of convergence of each series is the same, and this occurs when using the "optimum" value of the Ewald splitting parameter E given by $E_{\text{opt}} = \sqrt{\pi/A}$, where A is the cross-sectional area of the periodic lattice cell.

However, one problem with the Ewald method is that at high frequency (when the period becomes large relative to a wavelength) the numerical accuracy degrades quickly. This is due to a loss of significant figures in the summation of the two series, since the two series converge to very large and nearly opposite values. This, in turn, is caused by the $(0,0)$ terms in each of the two series becoming very large. This fundamental observation was first noticed in (A. Kustepeli and A. Q. Martin, *IEEE Microwave and Guided Wave Letters*, **10**, 168-170, May 2000).

A method is proposed here for choosing the "best" value of E (denoted here as E_L) that gives the fastest convergence of the Ewald sum, while limiting the number of significant figures L that are lost to a specified level (e.g., $L = 3$). In particular, the method determines the value of E_L that is required to limit the size of the $(0,0)$ terms in each of the two series relative to the numerical value of the total Greens function, in order to limit the loss of significant figures to the specified level.

In order to limit the size of the $(0,0)$ term in the spatial series of the Ewald method, the parameter E should be larger than a particular value called E_{spat} , which can be approximated in closed form. Similarly, in order to limit the size of the $(0,0)$ term in the spectral series, the parameter E should be larger than a particular value called E_{spect} , which can also be approximated in closed form. The best value for the parameter E is then given by the formula

$$E_L = \max (E_{\text{opt}}, E_{\text{spect}}, E_{\text{spat}}) .$$

The loss of significant digits has been verified through numerical simulations for both planar and non-planar cases, and the results verify the accuracy of the above formula.

COMPUTING THE SHIELDING EFFECTIVENESS OF A
DOUBLY-PERIODIC CONDUCTING SCREEN OF APERTURES
USING A MODE-MATCHING TECHNIQUE

Love, D.C., Rothwell, E.J.

Michigan State University, 2120 Engineering Building, East Lansing,
MI 48824-1226

Prior efforts have investigated the use of mode-matching techniques to evaluate the transmission of electromagnetic waves through screens perforated with apertures. Typically, the focus has been on screens whose thickness is comparable to the aperture dimensions. The technique is now being extended to determine the shielding characteristics of doubly-periodic screens whose thickness is several times the size of the aperture. This paper investigates the impact of considering thicker screens with rectangular and hexagonal apertures over a broad range of frequencies. The rectangular case involves the use of standard expressions for the fields in the apertures and closed-form computations for integral expressions. The hexagonal case requires numerical techniques for evaluating the aperture fields and computing integrals. Numerical data for the rectangular case will be compared to results using the waveguide below cutoff formula. In addition, numerical results for each case will be compared to measured data for samples of aluminum honeycomb.

The screen is modeled as an array of cylindrical waveguides, where the cross-section of the waveguides is rectangular or hexagonal. The reflected field above the screen and the transmitted field below the screen are represented using Floquet waves. The fields within the screen are modeled using waveguide fields. After enforcing boundary conditions and building a system of linear equations, the system is then truncated to produce a matrix equation which is solved using standard techniques. The shielding effectiveness of the screen is determined by comparing the transmitted power to the incident power. It is clear that as the thickness of the screen increases, the transmitted power is greatly reduced at frequencies below the cutoff frequency of the dominant waveguide mode. However, increasing the thickness also attenuates the higher-order waveguide modes at a greater rate, leading to non-convergent solutions to the matrix equation. By selectively eliminating higher-order modes from consideration, meaningful solutions are found. Other results show the effect of increasing or decreasing the number of Floquet modes and changing the angle of incidence.

In comparing the mode-matching results to the waveguide below cutoff data, the two approaches are closely related when the thickness is about five times the aperture dimensions or greater. The measured data also supports the mode-matching approach at and below cutoff.

MULTI-RESOLUTION FINITE ELEMENT BOUNDARY INTEGRAL SIMULATION OF SHIELDING EFFECTIVENESS IN A SYMMETRIC TEM CELL

Erdem Topsakal, Tutku Karacolak
Mississippi State University

Many electromagnetic problems today involve the propagation of waves at microwave or optical frequencies through single or multilayered composite structures. Composite materials are mainly used for spacecraft and aircraft structures for their light weight, high strength and ease of fabrication. Electromagnetic properties of composite materials are completely different in nature than those of simple metals and dielectrics. Accurate shielding effectiveness (SE) modeling of these materials is crucial for an effective design which complies with electromagnetic interference (EMI) and electromagnetic compatibility (EMC) requirements.

A conventional symmetric TEM cell consists of two symmetric sections coupled through an aperture. In this study, we present a multi-resolution hybrid Finite Element-Boundary Integral (FE-BI) method for modeling SE in a symmetric TEM Cell. We apply the hierarchical mixed-order tetrahedral tangential vector finite elements (TVFEs) given in [1] to obtain a computational model which accurately predicts the overall field behavior within the TEM cell. Since the properties of hierarchical TVFEs allow for the simultaneous use of low and higher order TVFEs within the same computational domain, we use higher order TVFEs only in regions associated with highly varying field intensities. The lowest order TVFEs are employed elsewhere to achieve an accurate and efficient field solution.

To validate the computational TVFE model, sample materials were placed on the aperture of the TEM cell, and SE was measured using a network analyzer (HP8753D). Comparative results regarding simulations and measurements will be presented.

[1] L. S. Anderson and J. L. Volakis, "*Hierarchical tangential vector finite elements for tetrahedra*," IEEE Microwave and Guided Wave Letters, vol. 8, pp. 127-129, March 1998.

AN INVESTIGATION ON FDTD SOLUTIONS WITH NON-ABSORBING BOUNDARIES

Natzke, J.R.

George Fox University, 414 N. Meridian St., Newberg, OR 97132

For FDTD solutions of scattering structures in unbounded domains, an investigation has been carried out on the necessary radiative field conditions at the outer lattice boundary. Also of interest was a simple yet suitable treatment at the truncation point of enclosed waveguiding structures that are semi-infinite in extent. The intention was to replace the much more complex absorbing boundary conditions or perfectly matched layers in typical use, understanding the likely trade-off of coding efficiency with loss of some accuracy.

Instead of applying an absorbing boundary condition, the coupled curl equations are truncated and appropriate field values substituted for the edge grid points. These field values are based on the local field values from the prior time step. This technique is thus frequency and angle independent, and the boundaries do not need to be far removed from the sources or scatterers. In one dimensional transmission line models, a perfect match is obtained at the termination. Scattering and waveguiding structures have been tested in two dimensions. Plane wave reflections of two percent are typical, though a portion of this can be attributed to numerical dispersion. These tests were performed with a collocated, Cartesian grid, and several classes of edge treatments are developed.

Even if the limits of accuracy cannot be pushed much further beyond a few orders using this technique, it nevertheless provides insight into the radiation requirements at the boundaries, since Maxwell's equations are dealt with directly. The local radiating behavior of the coupled curl equations is analyzed and discussed.

As it stands, these straight forward edge treatments provide a quick turn-around from start to finish, which reduces code development and computation time tremendously. Such a solution is especially helpful for training the electromagnetics engineer on computational methods. Indeed, since the physical insights are directly accessible without advanced field theory, the resulting pedagogical advantage is very desirable, as discussed in (J. R. Natzke, *URSI Digest*, June 2004).

Session B4, 13:15 – Thurs.

**ANTENNAS FOR WIRELESS
APPLICATIONS**

Co-Chairs: D.S. Filipovic, J.T. Bernhard

OPTIMIZING THE PERFORMANCE PROPERTIES OF
SMALL ANTENNA ELEMENTS

Steven Best
AFRL/SNHA

As the size of wireless devices decrease, there is an increasing demand on the antenna engineer to design and develop antenna elements having reduced size without sacrificing their performance properties. In many instances, there may also be additional requirements to increase the number of operating bands to allow device connectivity with multiple wireless systems. In this presentation we will first examine the fundamental performance limitations of electric dipole and magnetic dipole (loop) elements as a function of decreasing size. Performance trade-offs that occur with size reduction will be described in terms of the antennas radiation resistance, efficiency and bandwidth. Techniques for optimizing the electrically small antennas input impedance, efficiency and bandwidth are discussed. Electrically small dipole element designs are presented that exhibit a 50 Ohm input impedance, high radiation efficiency and a quality factor that is within 1.5 times the lower bound on Q for a single resonant mode antenna. It is demonstrated that operating bandwidth is the fundamental performance limitation in the design of small electric and magnetic dipole elements. Next, the performance limitations associated with spacing a dipole element very close ($\approx 0.05\lambda$) to a PEC ground plane are considered. A simple feed technique for achieving an impedance match and high radiation efficiency for the closely spaced folded dipole element are described. The equivalence of the folded dipole element and a microstrip patch radiator is considered. Finally, this simple feed technique is used to reduce a 2.4-2.5 GHz patch antennas width by a factor of 2, while maintaining a low return loss and fixed operating bandwidth. This microstrip patch size reduction technique does not require an increase in either the patch height or substrate dielectric constant.

A COMPARATIVE STUDY OF DIVERSITY AND SPATIAL
COVERAGE: FIXED VS. RECONFIGURABLE ANTENNAS
FOR PORTABLE DEVICES

Roach, T. L., Huff, G. H. , Bernhard, J. T.

Univ. of Illinois at Urbana-Champaign, Urbana, IL, USA

Simple, single antennas deployed on portable wireless data devices are usually minimally functional and limit noise immunity, battery life, and, ultimately, data throughput. This kind of limited antenna functionality could have a significant impact on performance of high-speed communication links in the future. One approach to expand system capability to meet new challenges is to develop reconfigurable antennas for portable devices. Ideally, new communication systems can then leverage this broad antenna functionality to take advantage of emerging techniques in wideband microwave circuits, signal processing, and protocols, resulting in more efficient, secure, and cost-effective high performance communication and sensing systems. While the possibility of integrating phased arrays (as proposed in S. Bellofiore et al., Proc. IEEE Antennas and Propagation Int. Symp., 1, 2001, 26-29) may be remote, an alternative is to combine a small number of reconfigurable antennas to achieve diversity, direction-of-arrival capabilities, and limited beam-forming (without phase shifters) depending on the operating environment and desired throughput.

This study investigates the performance of planar fixed and pattern-reconfigurable antennas (G. H. Huff et al., IEEE Microw. Wireless Comp. Lett., 13, 57-59, Feb. 2003) on a cubic structure which is representative of a portable device. This geometry has been chosen based on previous studies which have demonstrated a high degree of radiation pattern versatility when integrated with pattern reconfigurable elements. In conjunction with this, previous work involving a laptop computer chassis has also demonstrated improvements in diversity gain and spatial coverage when using pattern reconfigurable antennas. In this work, the broad range of radiation pattern possibilities brought forward by conformally integrating reconfigurable elements onto a cubic structure is examined by exploring possible configurations that work to deliver diversity and/or beam-forming in accordance with the device chassis itself. Since the reconfigurable antennas implemented in this work are switched between a discrete set of states, antenna placement (relative to the chassis and to one another) determines the utility and uniqueness of operating states from each set of integration positions.

SMALL-APERTURE SMART ANTENNAS WITH BROAD-BAND OPTOELECTRONIC SIGNAL PROCESSING

Smith, P.¹, Erickson, K.¹, Baylor, M.²,
Popovic, Z.¹, Anderson, D.Z.²

¹Department of Electrical and Computer Engineering, University of Colorado at Boulder

²Department of Physics, University of Colorado at Boulder

This paper addresses the problem of adaptive reception of N unknown wireless signals with the smallest possible antenna aperture of N elements. In conventional smart antennas, in order to resolve spatially N sources, typically an array of $M \gg N$ elements is needed, with unfavorable square-law scaling. In this work we present a smart antenna array with analog processing that requires the theoretically minimal number of elements, $M=N$ to separate N sources. The sources can spatially be within an antenna beamwidth and a small-aperture array with high inter-element coupling can be used by virtue of adding processing gain to replace antenna gain.

In this paper, we present a multibeam lens array front end with a electrooptic processor that performs two-signal Principal Component Analysis (PCA), i.e. adaptively extracts the strongest component in the signal space. The experimental prototype receives signals modulated onto a 10-GHz carrier with a 130-MHz IF and demonstrates a 26dB/dB enhancement power ratio between two signals. The processor is based on dynamic holography and performs signal decorrelations in analog hardware with up to a 3-GHz signal bandwidth. All the components of the system will be discussed: the receiving antenna, microwave receiver, electrooptic multichannel modulator, analog processor and electronic output circuit.

The more general problem of separating unknown signals adaptively is referred to as Blind Source Separation (BSS), and one of the algorithms that can be used to perform BSS is known as Independent Component Analysis (ICA), which is an extension of PCA. The talk will present new developments at the University of Colorado at Boulder in extending the PCA hardware to the ICA problem for broadband RF wireless signals. Measurements on a 2-signal extractor with voice signals will be presented and compared with existing state-of-the art digital solutions.

MICROSTRIP-FED PRINTED LOTUS ANTENNA FOR WIDEBAND WIRELESS COMMUNICATION SYSTEMS

Abdelnasser A. Eldek, Atef Z. Elsherbeni, Charles E. Smith

The University of Mississippi, Electrical Engineering Department,
Center of Applied Electromagnetic Systems Research (CAESR)

Since modern communication systems require smaller size antennas with wideband characteristics, many researchers have investigated techniques to improve the antenna bandwidth and to reduce its size in order to fit in the new wireless tools like PDAs, cell phones, and computer PCMCIA cards. Printed microstrip antennas are therefore widely used in wireless communication systems as they exhibit a very low profile, small size, lightweight, low cost, and ease of installation. Furthermore, they are generally economical to produce since they are readily adaptable to integrated circuits fabrication techniques. Among the most widely used printed antennas in wireless communication systems are printed meander lines, dipoles, and quasi-Yagi antennas fed by microstrip or coplanar strip line (CPS).

In this paper, two new configurations of printed Lotus antenna, are designed and presented for wideband wireless communication systems. These antennas are designed to cover the two frequency ranges from 1.56 to 2.91 GHz and from 3.8 to 6.7 GHz, respectively. The return loss and far field radiation characteristics of these antennas are introduced. The simulation and analysis for the presented antennas are performed using the commercial computer software package, Ansoft HFSS. Verification for the computed return loss is performed using measurements and further computations using the commercial software Momentum of Agilent Technology Advanced Design System (ADS). The two printed Lotus antennas are characterized by a wide bandwidth of 60 and 55 percent, stable radiation patterns, cross polarization level less than -15 dB, wide beamwidth, and relatively high gain (5 dB). Fabrication tolerance analysis is also performed to predict the antenna performance sensitivity due to any small fabrication errors. The characteristics of these new designs are found to be insignificantly sensitive to fabrication errors up to 10 percent. The small profile of these antennas makes them suitable for a variety of modern wireless communication devices.

EFFECT OF ENVELOPE CORRELATION OF VECTOR ANTENNAS CONSISTING CO-LOCATED LOOPS AND DIPOLES ON MIMO CHANNEL CAPACITY

Konanur, A.S., Krishnamurthy, S.H., Hughes, B.L. , Lazzi, G.

NC State University, EGRC, 2410 Campus Shore Drive,, Raleigh, NC 27606, USA

Vector antennas are antennas realized by means of co-located and possibly co-polarized antennas, which have been shown to be capable of increasing the capacity of a wireless communication channel in proportion to the number of elements in the vector antenna itself. The capacity of systems employing these antennas is comparable to that of a spatially separated array with the same number of elements. Since the elements of the vector antenna are co-located, it is of interest to assess the actual orthogonality of the individual radiation patterns of the vector antenna elements as this can affect the power efficiency of the communication system and influence the actual power requirement at the transmitter for a given receiver power. In fact, capacity results will be affected by the coupling between vector antenna elements. The envelope correlation between the radiation patterns of the individual elements of the vector antenna is a measure of this orthogonality. In addition, it also allows for an estimation of the distortion of the individual element radiation patterns due to their proximity to other elements.

In this work, we use a method based on the measured S parameters of the antenna system to compute the envelope correlation between individual elements of three and four element vector antennas realized by means of two dipoles and a loop placed in a planar configuration and three orthogonal dipoles and a loop, respectively.

Preliminary results show that the pairwise envelope correlation is below 0.015 at the design frequency of 2.25 GHz for both the three and four element antenna systems, indicating that the radiation patterns of the elements of the considered vector antennas are actually orthogonal, thus ensuring negligible cross-coupling between elements. This indicates that the designed vector antennas can function efficiently in a MIMO communication system.

Session B5, 7:55 – Fri.

**ARRAYS AND PATTERN
SYNTHESIS**

Co-Chairs: R.J. Pogorzelski, S.R. Rengarajan

ANTENNA AND TOPOLOGY CHOICES FOR A LARGE N
ARRAY FOR LEO SATELLITE DOWNLINK

Barott, W.C., Steffes, P.G.

Georgia Institute of Technology, School of Electrical and Computer Engineering, Atlanta, GA

The ever increasing volume and importance of data provided by low earth orbiting (LEO) satellites necessitate developing downlink systems that are more cost efficient than those presently in use. A popular alternative is to replace the costly high-gain dish antennas with phased arrays of many wide-beam and inexpensive elements. A prototype array of this type is presently in development at the Georgia Institute of Technology. Some design choices and analyses will be presented in the areas of antenna design, volumetric array layout, and thinned linear array (TLA) optimization. Genetic algorithms have been used extensively in the design and optimization processes.

A design for a novel type of elementary antenna was explored, in which the beam pattern is matched to the inverse of the propagation loss of the satellite link. Using this antenna will significantly reduce the required number of elements as compared to other antenna choices. It is possible to construct this elementary antenna as a fixed array of simple antennas of varying position, size, and stimulation. Results will be presented for array-factor and method-of-moments simulations for active and parasitic designs.

It was found that an array based on the radials of a platonic solid has advantages in resolution, sidelobe, and optimization complexity when compared to the popular geodesic design. Sidelobes and pseudo-grating lobes of a platonic array can be reduced by optimizing a similar TLA. Although the optimization of TLAs has been a subject of previous research, novel applications and conditions have been explored and improvements have been made to the results of other methods. Results will be presented for arrays in which combinations of average spacing, minimum spacing, and quantized spacing are enforced.

A PHASED-ARRAY ANTENNA WITH MECHANICALLY CONTROLLABLE MICROWAVE PHASE SHIFTERS

Junho Cha , Yasuo Kuga²⁶ , Sangil Lee

¹University of Washington, Department of Electrical Engineering, Seattle, WA 98195-2500

²University of Washington, Department of Electrical Engineering, Seattle, WA 98195-2500

³Mokpo National University, Electronics Engineering Department, Chonnam, Korea

A low-cost steerable antenna will be essential for the wide adaptation of satellite-based communication systems. The most flexible satellite to ground/airplane communication systems are based on electronic phased-array antenna technology. However, the cost of a phased-array antenna is related to the number of active elements, and thus the present systems are often too expensive for many commercial and military applications. In this paper, we will discuss a new approach which uses a low-cost mechanically controllable microwave phase shifter. By conducting detailed numerical simulations (Ansoft HFSS), we will show that a movable dielectric slab placed close to a coplanar waveguide (CPW) can be used as a phase shifter for a current Milstar Satellite which is operating at 44 GHz for uplink and at 20 GHz for downlink. When the movable dielectric slab was inserted into the gap of a CPW, the effective dielectric constant was calculated as a function of the slab height and the characteristics. In addition, we have simulated the phase shifter using high-resistivity ($> 3000 \text{ ohm.cm}$) silicon wafers at 20, 40 and 60 GHz. The movable high-dielectric constant slab was added to the CPW. The effective dielectric constant and characteristic impedance was also calculated as a function of slab height. The advantage of silicon wafers as a substrate is that they are easy to integrate and fabricate. When the dielectric slab is added to the CPW, the characteristic impedance also changes which increases reflection. To minimize reflection due to the dielectric slab and obtain the desired phase shift, we need to set the dielectric constant of the slab to be a certain value. We will show that both impedance matching and desired phase shift can be achieved at the chosen frequencies.

A DEMONSTRATION OF THE USE OF COUPLED OSCILLATORS IN AN AGILE BEAM RECEIVER

Ronald J. Pogorzelski

Jet Propulsion Laboratory - Caltech, 4800 Oak Grove Drive,
Pasadena, CA 91109-8099

Agile beam phased array antennas in which the aperture phase distribution is derived from an array of mutually injection locked electronic oscillators were originally proposed and developed by York and his students. [R. A. York, *IEEE Trans., MTT-41*, pp.1799-1809, Oct. 1993] [P. Liao and R. A. York, *IEEE Trans., MTT-41*, pp. 1810-1815, Oct. 1993] More recently, considerable additional work has been reported. [R. Ispir, S. Nogi, M. Sanagi, and K. Fukui, *IECE Trans. Electron., E80-C*, 1211-1220, Sept. 1997] [R. J. Pogorzelski, *Microwave and Guided Wave Letters*, 10, pp. 478-480, Nov. 2000] [J. Shen and L. W. Pearson, *Nat. Radio Sci. Mtg, Boston, MA, July 2001*] These studies concern transmit-only arrays. A corresponding receive array concept was described and demonstrated by Cao and York in a five element linear array. [1995 *IEEE AP-S Symposium Digest*, 1311-1314] Here we report a laboratory demonstration of this concept in a fifteen element linear array of oscillators using a phase diagnostic system to monitor the phase distribution across the array.

The operation of such a receive array is based on the fact that, in a linear array of mutually injection locked oscillators, one may induce linear phase tapers across the aperture by anti-symmetrically detuning away from the ensemble frequency only the end oscillators of the array. Thus, if each oscillator output is mixed with the signal received by a corresponding element of the receive aperture, the linear phase taper due to the angle of incidence of the wave impinging on the aperture can be removed by the phase taper of the oscillator array effectively steering the receive beam. The experiment reported here involves an array of fifteen L-band (1.265 GHz) oscillators mutually injection locked via coupling of their tank circuits with transmission lines terminated in resistor networks. A set of on-axis incident wave induced element signals (at 1.950 GHz) is simulated by means of a signal generator and a fifteen-way power divider. Each of these element signals is then mixed with the corresponding oscillator output and the resulting intermediate frequency (685.2 MHz) signals are combined via a fifteen-way power combiner. The receive beam is characterized by steering it through this simulated normally incident wave and plotting the output of the power combiner versus the interoscillator phase difference. The results agree quite well with the theoretical prediction.

HIGHER ORDER MODE COUPLING BETWEEN COUPLING SLOTS IN A PLANAR SLOT ARRAY

Sembiam R. Rengarajan¹²¹Department of Electrical and Computer Engineering, California State University, Northridge, CA 91330-8346²Jet Propulsion Laboratory, California Institute of Technology, Pasadena, CA 91109

Waveguide-fed planar slot arrays generally consist of a feed waveguide for each sub-array. The feed waveguide excites a number of radiating waveguides stacked next to each other. Longitudinal offset slots are cut in the broadwall of radiating waveguides so as to obtain the desired radiation. The excitation of radiating waveguides is facilitated by centered-inclined coupling slots cut in the common broadwall between the feed waveguide and each radiating waveguide. In the design of slot arrays the coupling slots are modeled as series elements in equivalent transmission lines. In the prior literature it has been shown that ignoring the higher order mode coupling may result in significant errors in the excitations of radiating waveguides, especially when coupling slots have small values of tilt angles and/or the spacing between adjacent slots in the order of 0.6 free space wavelength (Rengarajan, *IEEE Trans. Microwave Theory Tech.*, vol. 39, 7, pp. 1219-1222, 1991). Presently there exists a technique that includes the higher order mode coupling between adjacent longitudinal slots in the radiating waveguides (Elliott and OLoughlin, *IEEE Trans. Antennas Prop.*, vol. 34, pp. 1149-1154, 1986).

In this paper we propose a method to account for the higher order mode coupling between adjacent coupling slots. Initially the design of the planar slot array is carried out without including the higher order mode coupling between coupling slots. In this design all the coupling slot tilts and lengths are such that they are resonant. Subsequently we account for the higher order mode coupling between adjacent coupling slots and perturb the values of the slot lengths and tilts so that they have the required resonant excitations. Using this perturbation procedure we are able to perform a fast optimization whereas an optimization technique employing a full wave moment method program would be extremely inefficient. The design algorithm is validated by a full wave moment method analysis.

COUPLING BETWEEN LOOP ANTENNAS

Li, S., Scharstein, R.W.
University of Alabama

An array of N thin, identical circular rings that are coaxial provides an analytically tractable model to study electromagnetic coupling effects in phased array antennas. The circular symmetry of the pertinent integrodifferential equation (Pocklington's equation for the loop) and the boundary conditions do not break the orthogonality of the azimuthal Fourier modes $\exp(in\phi)$. Therefore, physically realizable three-dimensional antenna elements can be characterized by a single complex number for each independent Fourier index n , without recourse to a 'single mode' approximation. Both plane wave (receive mode) and localized voltage sources (transmit mode) are considered.

Equivalent circuits are constructed from an electrostatic and magnetostatic analysis to model the low frequency coupling between a pair ($N = 2$) of rings and compared to the low frequency limit of the full electrodynamic equations-of-motion. Such lumped-circuit modeling of field problems requires the identification of self and mutual capacitance and inductance. Partial validation of the low frequency analysis applied to a single ring is obtained by comparison with appropriate limits of exact solutions to potential problems in toroidal coordinates.

At the other extreme, a large array ($N \gg 1$) offers another glimpse into the edge-effects in mutual coupling that have captivated antenna engineers for decades. Accurate calculations lead here to the usual observations of traveling wave behavior in the terminal currents and admittances for finite arrays. One goal is to better explain the physics of these effects, perhaps by exploiting a semi-infinite array approximation. The individual coupling terms involve Fourier coefficients of the thin-wire kernel, which are evaluated via a combination of numerics (FFT) and asymptotics.

NULL GENERATION USING FAR FIELD PARASITIC ELEMENT

Aliakbarian H., Akhavan M.

ECE Dept. , Faculty of Eng., Univ. of Tehran, P.O.Box: 14395-515

Generation of a null in patterns of antennas is a common problem in modern electromagnetic projects. Wireless communications and radars are two examples of such fields. In spite of the fact that almost all of researchers have paid attention to array antennas, we faced the problem of generating null in ordinary antennas.

A single antenna can be designed to produce a null in an arbitrary direction, when the null term is considered in the designing goal. Using the following method, the distance and angle in which a parasitic element should be placed to suppress the pattern of any antenna in an arbitrary direction can be determined. Expanded formulas can describe the theory for two or more nulls in two or three dimensional patterns using more parasitic elements. In this paper the problem of generating a null in a 2D pattern of predefined antenna using a parasitic element is considered.

In order to find the distance and direction which a parasitic element should be placed, the magnitude and phase of the radiated field in the null directions is forced to be zero. Thus two resulted equations for phase and magnitude are calculated and simplified and then should be solved simultaneously.

In order to check this theoretical equations, two-element dipole array antenna which is fed evenly is considered and a half wave rod is designed to generate a null in one direction of the active antenna. In addition, some observations in computer simulations is concluded. Simulation results are compared with analytical formulas and show suitable agreement.

Session B6, 10:15 – Fri.

COMPLEX MEDIA

Co-Chairs: E.F. Kuester, K. Sarabandi

CHARACTERIZATION OF NEGATIVE-REFRACTIVE-INDEX MATERIALS WITH MRTD

Nathan Bushyager, Manos Tentzeris

The Georgia Electronic Design Center, School of Electrical and Computer Engineering, The Georgia Institute of Technology

The Multiresolution Time Domain (MRTD) technique (M. Krumpholz and L. P. B. Katehi, *IEEE Trans. Microwave Theory Tech.*, **44**, 555-561, 1996) has been presented as an advanced technique that is advantageous when compared to other time-domain techniques because of its inherent time-and-space adaptive grid. This grid allows complex structures to be simulated in high resolution while surrounding and connecting areas are simulated in low resolution. Through the use of wavelet thresholding, the resolution can be varied automatically during simulation, in response to the transient field propagation. Recently, a composite-cell technique has been presented for Haar wavelets that allows the modeling of complex structures within a cell, including lumped elements (N. Bushyager and M. Tentzeris, *Proc. 2004 IEEE MTT-S*, June, 2004). This technique can be directly applied to the characterization of negative-refractive-index (NRI) materials.

NRI materials have recently been fabricated using lumped elements embedded in transmission lines (O. Siddiqui, M. Mojahedi, G. Eleftheriades, *IEEE Trans. On Antennas and Prop.*, **51.3**, 2619-2625, 2003). These materials can have unique properties such as simultaneous negative magnetic permeability and electric permittivity. Waves propagating in these materials also feature unique properties, such as negative phase and/or group velocity.

These materials can be efficiently modeled in MRTD using the composite cell MRTD technique. When compared to the FDTD technique, Haar-cells contain the equivalent of several FDTD cells, with resolution (the number of embedded cells) varying as a function of time and space. It is possible to represent the NRI unit cell (the transmission line with embedded lumped elements) as a single MRTD cell. This high resolution cell can be combined with low resolution connecting cells, as well as adaptive cells, to efficiently simulate the NRI structure over a wide band. The presentation will focus on the modeling of NRI materials in an adaptively gridded MRTD simulation, as well as the analysis of the output. Due to the time-domain nature of the simulation technique, properties of NRI materials such as negative group and phase velocity can be observed directly in the time domain output.

CONTROLLABLE
PLANE-WAVE REFLECTION AND TRANSMISSION FROM
A GYROTROPIC METAFILM

Kuester, E.F.¹, Holloway, C.L.², Kabos, P.²

¹Department of Electrical and Computer Engineering, University of Colorado, 425 UCB, Boulder, CO 80309, USA

²National Institute of Standards and Technology, 325 Broadway, Boulder, CO 80305, USA

In previous work (E. F. Kuester *et al.*, *IEEE Trans. Ant. Prop.*, **51**, 2641-2651, 2003) we introduced the idea of a *metafilm*: a distribution of polarizable scatterers on a surface whose response to an incident wave modifies the behavior of the overall field in some desired way. A metafilm is the surface analog of a metamaterial. The main result was an averaged boundary condition for the jumps of the tangential \mathbf{E} and \mathbf{H} fields across the metafilm. The coefficients of the boundary conditions involve the densities of the polarizabilities of the scatterers. In subsequent work (C. L. Holloway *et al.*, submitted to *IEEE Trans. Electromag. Compat.*, 2004), we proposed the use of resonant scatterers as a way of modifying the plane wave reflection and transmission properties of the surface. In particular, spherical magnetodielectric scatterers such as the ones proposed as an alternative to the split-ring scatterers widely used for obtaining negative-index metamaterials (C. L. Holloway *et al.*, *IEEE Trans. Ant. Prop.*, **51**, 2596-2603, 2003) were proposed as a means of obtaining substantial reflection from the metafilm.

In this paper, we suggest that this type of metafilm can be controlled via an externally applied DC magnetic bias field. If the spheres are made from a ferrite material, the material becomes magnetically gyrotropic, and the previously obtained boundary conditions no longer apply, since they assumed diagonal polarizability dyadics for the scatterers. Thus, we extend the theory to cover a gyrotropic metafilm by way of the following steps. First, the polarizabilities of magnetically gyrotropic spheres are derived in a Lorenz-Mie form, displaying various kinds of resonant behavior. Second, the previously obtained boundary conditions are generalized to be valid for gyrotropic scatterers. Third, the new boundary conditions are used to derive formulas for the plane wave reflection and transmission coefficients from a gyrotropic metafilm.

Numerical calculations of the reflection and transmission coefficients will be presented. The new theory will also be compared to experimental measurements in waveguide, simulating oblique incidence of plane waves. The measured results show promising correlation to the theory. The results of this study point to the possibility of controlled or "smart" surfaces made with metafilm techniques, enhancing the capabilities of communication systems through the use of nontraditional design methods.

MINIATURIZED EMBEDDED-CIRCUIT METAMATERIALS FOR ANTENNA ARRAYS DESIGN: CONCEPT AND CHARACTERIZATION

Mosallaei, H., Sarabandi, K.

University of Michigan, Ann Arbor, MI 48109

Patch antennas have found numerous applications in wireless systems for their simplicity in fabrication, compatibility with planar circuitry, low profile and planar structures, and unidirectional radiation capability. Despite many nice electrical and mechanical features of microstrip antennas, their use for a number of applications has been limited due to the limitation in bandwidth and/or size. The size of a patch antenna can be miniaturized by printing the antenna on a high dielectric substrate, however the high permittivity material increases the coupling between the antenna and its ground plane and reduces the antenna bandwidth. The bandwidth can be increased with the use of a thicker substrate, but the high dielectric-thick substrate generates surface wave that drastically degrades the antenna performance. This effect is more dominant when the patch is used as an element of a compact antenna array design.

To improve the bandwidth of patch array antennas without increasing the element size or array spacing an approach must be developed that should allow substrate thickness increase at the same time suppress the mode transition to surface waves. To accomplish this we propose using of resonant Embedded-Circuit Metamaterials (ECM) as the isolators printed between the array elements in order to remarkably suppress the surface waves. The resonant ECM are constructed of miniaturized loop circuits terminated to the loading capacitors. Above the resonance frequency of the loops the metamaterial shows a negative effective permeability which is responsible for determining the stop-band characteristic. Note that compared to the previously proposed structures for suppression the surface waves, designed based on the dielectric and metallo-dielectric band-gaps, the ECM has a much smaller size and one can use only one layer to significantly stop the surface waves.

A Finite Difference Time Domain (FDTD) technique with Periodic Boundary Conditions/Perfectly Matched Layers (PBC/PML) walls is applied to comprehensively characterize the ECM and highlight their superior advantages for the design of high performance antenna arrays.

MULTI-LAYER FREQUENCY SELECTIVE VOLUMES FOR THERMOPHOTOVOLTAIC FILTERS

Aaron Zach Hood, Erdem Topsakal
Mississippi State University

Compared to traditional photovoltaic (PV) converters which use the extreme heat of the sun to generate electricity, thermophotovoltaic (TPV) systems provide a method for the direct conversion of secondary thermal radiation from a heat source of relatively low temperature into electricity. A TPV consists of three basic components: a heat emitter, a spectral filter, and a sheet of PV cells. Maximum conversion efficiency occurs at the wavelength of the secondary radiation, but the heat from the emitter contains many frequency components other than that of the secondary radiation, which leads to poor overall performance. With a properly designed spectral filter, all undesirable frequencies may be reflected before reaching the PV cells to dramatically improve system performance. Frequency selective volumes (FSVs), screens that exhibit frequency selective properties, are good candidates for the band-pass, band-stop infrared filter required by TPV converters.

The overall efficiency of a TPV depends on the performance of the spectral filter. The filter should only allow those frequencies with the wavelength of the secondary radiation to pass while rejecting all others. The performance requirements of the spectral-control filter are high reflection ($> 90\%$) for $\lambda > 2.4\mu m$, high transmission ($> 90\%$) for $1 < \lambda < 2.4\mu m$, insensitivity to large $\Delta\theta$, insensitivity to polarization, and broadband operation ($1-10\mu m$).

In [1], several FSV geometries were explored including commensurate multi-layer designs; wire loop configurations were tested using both one and two layers. It was shown that single layer wire loop FSVs generally utilized approximately 89% of the desired spectrum while two layer configurations of equivalent depth only offered about 85% utilization. Our new results found that non-commensurate multi-layer designs may offer upwards of 90% spectral utilization with dimensions similar to the commensurate layouts of the previous work. In this paper, we present results regarding non-commensurate multi-layered FSV structures and compare those with the single layer configurations given in [1].

[1] E. Topsakal and A.Z. Hood, "A Near Infrared Optical Thermo-photovoltaic Filter Design Using Frequency Selective Volumes", IEEE Antennas and Propagation Society International Symposium, Monterey, California June 20-26, 2004.

THE IMPACT OF CHIRALITY ON THE MUELLER MATRIX
ELEMENTSBahar, E.University of Nebraska-Lincoln, EE Dept., Lincoln, NE 68588-
0511, USA

Electromagnetic waves propagating in free space over a half space with media possessing chiral properties satisfying the Drude-Born-Fedorov constitutive relations, are expressed in canonical form in terms of right and left circular polarized waves. However the elements of the Mueller Matrix are expressed in terms of scattering coefficients for linear vertical (parallel) and horizontal (perpendicular) polarized waves. Thus in order to explore the impact of chirality on the elements of the Mueller Matrix, it is initially necessary to determine the impact of chirality upon the reflection and transmission coefficient for right and left circular polarized waves that are incident from free space, upon a chiral half space. Since the degree of chirality in biological materials is much smaller than one, it is necessary to retain only first order terms in the chiral parameter in the expressions for the circularly polarized reflection and transmission coefficients. It is shown that while the circular like polarized reflection coefficients are proportional to the chiral parameters, the circular cross polarized terms depend on higher order terms in the chiral parameters. Through a series of transformations (that relate circular to linear polarized waves), the corresponding reflection coefficients for linear polarized waves are obtained. Consequently it is shown that the explicit expressions for the linear, like polarized reflection coefficients are insensitive to chirality and the linear cross polarized reflection coefficients are proportional to the chiral parameters. The explicit expressions for the reflection coefficients also depend upon the angle of incidence, frequency, and polarization (through the transmission coefficients associated with the permeability and the permittivity of the host medium). Thus chirality impacts only upon the eight off diagonal elements of the Mueller Matrix. The results satisfy the duality and reciprocity relations in electromagnetic theory. It is also shown that the results satisfy energy conservation for non-dissipative media.

Session B7, 13:35 – Fri.

MICROWAVE ELEMENTS

Co-Chairs: C.M. Butler, L.W. Pearson

FABRICATION OF MULTILAYERED WAVE INTEGRATED
CIRCUITS IN A POLYMER MATERIAL SYSTEM

Jabberia R. Miller*, Harriss, J. E., Pearson, L. W.

Holcombe Department of Electrical and Computer Engineering,
Clemson University, Clemson, SC 29634-0915

In recent years, workers at the University of Michigan have developed a multilayered technology for the fabrication of millimeter-wave integrated circuits (T. M. Weller, R. M. Henderson, K. J. Herrick, S. V. Robertson, R. T. Kihm, and L. P. B. Katechi, *IEEE Trans. Microwave Theory Tech.*, **48**(10), 1635-1642, 2001), (R. M. Henderson, K. J. Herrick, T. M. Weller, S. V. Robertson, R. T. Kihm, and L. P. B. Katechi, *loc. cit.*, pp. 1643-1651). This work employed extensive micromaching of silicon in the preparation of four-layered circuits.

A micromachining practice can be based on Epon[®] SU-8 photoresist manufactured by Shell Chemical. SU-8 supports micromachining of structures on substrates hundreds of microns thick. The material is a negative photoresist, polymerizing and becoming impervious to the original diluting solvent upon exposure to ultraviolet light. The exceptional optical clarity of SU-8 accommodates the formation of well defined walls in thick layers. All SU-8 patterning is conducted with UV and solvents, making it considerably easier and safer to process than micromachined silicon.

In this paper, we report progress in developing a practice for millimeter-wave circuit fabrication using SU-8 as the substrate material. Simply preparing "wafers" of precise thickness from SU-8 requires care. We have developed a molding process where the form comprises a silicon wafer and Teflon[®] sidewalls. Material near the mold edges is sacrificed, allowing consistent fabrication of 400 ± 15 micron rectangular wafers. We have developed circuits using coplanar transmission lines, thereby requiring a process for airbridge formation. Other components, including filters, electromagnetically coupled feedthroughs, and mounted semiconductor components. Available results for these will be presented.

INVESTIGATION OF THE DOUBLE-Y BALUN FOR FEED-
ING A RESISTIVE V-DIPOLEVenkatesan, J.¹, Scott, W. R. ²¹JPL, California Institute of Technology²Georgia Institute of Technology

Various versions of the double-Y balun have been studied in the past for use with balanced mixers. These baluns have been characterized via VSWR and insertion loss measurements. In this paper, the performance of a double-Y balun, implemented with coplanar waveguide (CPW) and coplanar strip (CPS) lines, is investigated for feeding a 200Ω resistively loaded V-dipole that is being studied for use in ground penetrating radar (GPR) applications. Attractive features of the double-Y balun, implemented with CPW and CPS lines, include: low metal content, ease in construction (can be manufactured precisely on a PCB), and reported broadband performance. These features make this double-Y balun attractive for use in ground penetrating radar (GPR) applications, where the antennas are often used in close proximity to a metal detector. In this work, the performance of the double-Y balun designed to feed a resistive V-dipole, is evaluated via VSWR, insertion loss, and antenna pattern measurements. To conduct the antenna pattern measurements, an automated measurement system employing an optical link, was constructed. Details of the automated antenna pattern measurement system are presented. Using the automated measurement system, amplitude patterns were measured for a 5 cm dipole and a resistively loaded V-dipole, fed with and without the double-Y balun. Loading the double-Y balun with the 5 cm dipole serves to model a stressful case for the balun because of the impedance mismatch between the dipole and the balun. The measured amplitude patterns illustrate the improvement in performance obtained for the dipole and the resistive V-dipole when fed with the double-Y balun.

EFFECTS OF SHIELD SLOTS ON INPUT IMPEDANCE OF SHIELDED COIL

Lockard, M. D., Butler, C. M.
Clemson University, Clemson, SC, USA

The inductance of a coil in the close proximity of a conducting surface is reduced from its inductance remote from the conductor due to the reduction in the rate of change of flux linkage caused by the current in the conductor. This effect causes the inductance of a shielded coil to be reduced when the shield is present. To lessen the reduction in inductance of a shielded coil, thin slots are cut in the shield to interrupt the induced shield current. On this basis, the effects of slots in the outer conductor of a shielded coil are investigated. A portion of the center conductor of a shorted coaxial cavity is removed and replaced with a ferrite-cored coil. The input impedance of the shielded load as "seen" from one end of the cavity is measured. Longitudinal slots are cut in the shield and the input impedance measurement is repeated. The experiment is repeated for various loads that differ in numbers of turns, core materials, and core radii. Several shields are constructed and the effects of the number of slots on the input impedance of the load structure are investigated.

A method is presented for accurate measurement of the input impedance of the shielded loads. The impedance of the shielded coil is measured by a network analyzer through an adapter. The input impedances of three different lengths of shorted coaxial cavities are measured through the adapter and these data are used to de-embed the impedance of the shielded coil from that of the adapter-shielded-coil structure.

The utility of slotted-shield coils in a loaded dipole over an infinite conducting plane is assessed. The shielded coils are deployed in a dipole antenna that has the same radius as the outer shield of the load. A circumferential slit is cut in the outer shield of the load to allow coupling between the current in the coil and the current on the surface of the dipole. The slit is placed far from the coil so that only the TEM component of the coupling field is relevant. The measured input impedance of the shielded coil is used in a hybrid integral equation/measurement method to determine the input impedance of the loaded dipole. It is assumed that the narrow slots do not significantly alter the current on the exterior surface of the dipole. The presence of the slots are accounted for in the physical measurements of the load and the input impedance of the dipole but are not represented in the model for the exterior region of the loaded dipole. Data for the input impedance of dipoles loaded with various shielded loads are presented and compared.

MICROMACHINED SI WAVEGUIDE FOR THz APPLICATIONS

Peter L. Kirby, John Papapolymerou
Georgia Institute of Technology, 85 5th St NW - Room 543, Atlanta GA 30332

There is increasing interest in using Terahertz (THz) frequencies for a variety of different applications. Since THz signals are non-ionizing and do not damage cells like X-rays, they offer great promise in the medical imaging field. THz signals have already been used for military applications such as scanning for land mines, space exploration and imaging. THz signals are generally conducted in a waveguide medium. Metallic waveguide is often difficult to machine for use at very high or THz frequencies, requiring the expert skills of an experienced machinist which can be very costly and generally not suitable for large unit production. For heterodyne imaging applications it is necessary to reduce cost of waveguide components in order to create large format arrays.

To realize a low cost approach, there must be a movement away from the metallic waveguide in to a different material. We propose to use a silicon substrate to form the waveguide. While this is not a new approach, the previous method of choice to form the waveguide has been done by wet etching. Although this is effective in forming simple waveguides, it can be limiting when choosing to form structures that are more complex. To this end we propose using a deep Reactive Ion Etching (RIE) as initial step toward using a more precise laser etching technique for frequencies greater than 600 GHz. In order to prove this approach to be valid we select to create design centered around 400 GHz (WR-2.5, 25 X 12.5 mils) for our initial step. This frequency allows for the challenges of very high frequency design, while keeping the dimension involved relatively large and manageable. For this phase we seek to construct and measure a straight section of 400 GHz waveguide and a 400 GHz bandpass filter.

We fabricate the complete waveguide by splitting the structure in the H-plane, forming two halves. Although this is not the preferred plane to split, it eases the fabrication of the bandpass filter. The waveguide and the die are etched using a deep RIE process and the two halves are mounted in a holder. The holder is assembled forming the complete waveguide with precision flange patterns on each face of the holder. The complete device is measured at Jet Propulsion Laboratories using an ABmm Network Analyzer.

DESIGN OF FOLDED OVERSIZED-WAVEGUIDE PARTITIONED BY METAL PLATE WITH FINITE THICKNESS FOR MILLIMETER-WAVE PLANAR ANTENNA

Futoshi Kuroki¹, Kouichi Yamaoka¹, Tsukasa Yoneyama²

¹Kure National College of Technology

²Tohoku Institute of Technology

Millimeter waves have attracted much attention for the construction of novel wireless systems such as automotive radars and high bit rate wireless communications. Actually, several types of millimeter wave front ends have been developed in many institutes, laboratories, and companies. A high performance millimeter-wave antenna which is compatible with integrated circuits is a key technology for developing such millimeter-wave systems, and several transmission lines such as a microstrip line and a slot line have been used as antenna feeders. These printed transmission lines are preferable for application at centimeter frequencies, but they suffer from large transmission loss at millimeter-wave frequencies.

Another candidate for use as antenna feeder is the NRD guide, which consists of dielectric strips inserted in a below cutoff parallel metal plate waveguide and features no radiation at curved sections and discontinuities. Indeed, this NRD guide has been investigated and applied in a radiator for the purpose of antenna applications at 35 GHz.

With this in mind we analyzed a folded oversized-waveguide to construct a compact planar antenna at 60 GHz. This oversized-waveguide, consisting of a double-layered structure, is partitioned by a metal plate with a finite thickness. A planar antenna is located at the upper layer with a height of 1 mm and a two-dimensional parabolic reflector fed by NRD guide radiator and NRD guide integrated circuits are installed in the lower layer with a height of 2.25 mm.

To efficiently introduce a guided mode from the lower layer to the upper layer, a unique matching technique was applied. A small transmission loss less than 0.5 dB and a good return loss larger than 20 dB were successfully performed at an operating frequency of 59 GHz.

A BAND-PASS FILTER WITH WIDE-BANDWIDTH AND SHARP SKIRT-CUTOFF AT IF-BAND IN MILLIMETER-WAVE MULTIPLE TV SIGNAL DISTRIBUTION SYSTEM

Futoshi Kuroki, Makoto Kimura
Kure National College of Technology

An IF-band band-pass filter was designed for a multiple TV signal distribution system using millimeter-wave frequencies. Main emphasis of developing the filter was placed on a broad-band performance in a pass-band and a sharp skirt cutoff nature in a rejection-band because the TV signals in the intermediate frequency of this system consist of more than 100 channels and because other applications exist in neighboring frequency-bands. We devised a band-pass filter in a centimeter-frequency band by assembling low-pass and high-pass filters.

At first we discussed a 5-stage high-pass filter with an elliptic function response, which consists of capacitors in series arms and series L-C resonators in parallel arms. The inductors have generally poor frequency responses in centimeter frequencies, so that they were replaced by short ended stubs, where this filter was made by a microstrip line circuit.

Next consideration was concerned with a 5-stage low-pass filter with an elliptic function response, which consists of inductors in series arms and series L-C resonators in parallel arms. To reduce the series inductors in the first stage and the final stage, the Kuroda's transformation was applied, and the inductor in the 3rd stage was replaced by a short and narrow line with high characteristic impedance.

By connecting the low-pass and high-pass filters, a band-pass filter was constructed, where this filter was designed so as to be a relative pass-bandwidth of 65% and attenuations more than 20dB in frequencies of 5 % apart from the low and high cutoff frequencies. The insertion and return losses of this filter were less than 1dB and larger than 10dB, respectively, in the pass band.

A remarkable point of this filter is a small size, because the circuit pattern was successfully contained in the area of $0.1 \lambda \times 0.2 \lambda$.

LOW-LOSS PRINTED BAND-PASS FILTER USING HIGHER MODE STRIP LINE FOR MILLIMETER WAVE INTEGRATED CIRCUITS

Futoshi Kuroki, Kazuya Miyamoto
Kure National College of Technology

Printed transmission lines such as a microstrip line and a coplanar waveguide are preferable for applications in centimeter-frequencies, and they are usually used in millimeter-wave regions due to good mass-productivity, though the printed transmission lines suffer from considerable transmission loss. To reduce such transmission loss, a higher order mode of the microstrip line has been studied, but it is problematic that such a mode easily emits unwanted radiation at curved sections and discontinuities.

To realize a low-loss printed transmission line at millimeter-wave frequencies, we propose the use of the first higher mode in a tri-plate strip line. This transmission line, termed higher mode strip line (HS line) in this paper, consists of metal strips inserted in a below cutoff parallel plate waveguide, and has no radiation at any discontinuities. A remarkable point of this transmission line is its small transmission loss, close to that of a rectangular waveguide, though it is a kind of printed transmission line. The transmission loss was measured to be 3 dB/m in a frequency range from 31 GHz to 35 GHz, and hence a novel type of printed transmission line with low-loss nature and mass-productivity can be developed.

Since the HS line has good advantage such as high unloaded Q factor, measured to be 1500, it is expected that a low-loss printed filter can be realized at millimeter-wave frequencies. A 3-pole, 0.1-dB Chebyshev ripple band-pass filter with a 2 % relative bandwidth was designed and fabricated at 32 GHz. The insertion loss was found to be 0.7 dB, and thus a low-loss printed band-pass filter was successfully developed. This type of filter is expected to play a key role in printed ICs in the millimeter-wave frequencies.

Session B8, 08:15 – Sat.

**SCATTERING, PROPAGATION
AND COUPLING**

Co-Chairs: A.Z. Elsherbeni and R.W. Scharstein

EDUCATIONAL SOFTWARE PACKAGE FOR ELECTRO-MAGNETIC SCATTERING FROM SIMPLE TWO AND THREE DIMENSIONAL OBJECTS

Mohamed Al Sharkawy, Veysel Demir, Atef Z. Elsherbeni

The University of Mississippi, Electrical Engineering Department,
Center of Applied Electromagnetic Systems Research (CAESR)

In electromagnetics education, the fundamentals of electromagnetic scattering theory are usually taught through solutions of scattering from canonical objects due to excitation by incident plane, cylindrical, or spherical waves. These solutions are in general available in closed mathematical forms that in many cases are hard to visualize and difficult to extract from them the physical characteristics of the scattering process. Therefore, it is important to have such canonical solutions programmed and arranged in an easy to use tool for the purpose of visualizing the physical phenomena of scattering from these scattering objects. Furthermore, such tools can be used as benchmarks for a wide range of researchers who are developing numerical electromagnetic techniques. Thus, the availability of programs that solve these types of canonical problems on the widely available personal computers and workstations provides students with a better understanding of electromagnetic scattering theories. Furthermore, researchers would be able to have immediate access to verification solutions to a variety of test cases. With this need in mind, a software package has been developed to compute and display the scattering from two and three-dimensional canonical objects based on exact boundary value solutions. In addition to canonical objects this developed package also includes simple non-canonical objects where the presented scattering parameters are based on simple approximations. Many objects are considered in this package such as, thin strip, circular cylinder, capped wedge, triangular and circular flat plates, sphere, and ellipsoid. The package is constructed to provide solutions for both dielectric and conductive materials whenever appropriate. It calculates the far and near field components due to excitation from a line source or a plane wave. In the two-dimensional problems the TE and TM cases are treated separately. Electromagnetic analysis software packages are judged not only by their computational efficiency and adaptability, but also by their ease of use and the friendliness of their user interfaces. Graphical user interface is developed for each object considered in order to supply the object parameters and excitation type and parameters and to display the computed near and/or far field results and any other appropriate parameters. Since the computations are considerably fast, the user interface is organized such that the user can interactively observe, in near real time, the effect of changing any of the physical or electrical parameters on the resulting far field patterns and parameters.

MEASUREMENTS AND THEORETICAL RESULTS FOR THE
SCATTERING BY A RIDGE ON A METAL PLANE

Sharmin Rahman, Badria Elnour, Danilo Erricolo
, Piergiorgio L.E. Uslenghi
Department of Electrical and Computer Engineering, University
of Illinois at Chicago, Chicago, IL 60607

The geometry of the problem is two-dimensional and it consists of an infinite planar boundary separating the perfect electric conducting half space $x < 0$ from the penetrable half space $x > 0$. The quadrant $x > 0, y > 0$ is filled with material with dielectric conductivity and magnetic permeability. The quadrant $x > 0, y < 0$ is filled with material with dielectric and magnetic parameters ϵ_1 and μ_1 , respectively. The media filling the two quadrant are isorefractive, i.e. $\epsilon_1\mu_1 = \epsilon_2\mu_2$. The metal plane $x = 0$ has a ridge represented by a semiellipse whose foci are located along the $y = 0$ axis and symmetrically positioned with respect to $x = 0$. The source is either a plane wave whose direction of propagation is perpendicular to the z axis or a line source parallel to the z axis. The solutions for the fields and induced currents are expressed using series expansions of Mathieu functions, where the unknown modal coefficients are determined by imposing the boundary conditions. Preliminary results for this problem were previously given in the case of E-polarization (D. Erricolo, F. Mioc, P.L.E. Uslenghi, "Exact scattering by a ridge on a metal plane with isorefractive quadrants", Digest of National Radio Science Meeting, p. 141, Salt Lake City, Utah, July 2000).

The new contributions consist in providing 1) analytical and numerical results for the H-polarization case and 2) measurement results when the penetrable media are free space ($\epsilon_1 = \epsilon_2 = \epsilon_0, \mu_1 = \mu_2 = \mu_0$). Measurements are carried out for the limiting case of the semiellipse that shrinks to the half-focal segment; hence this geometry corresponds to a strip perpendicular to a perfectly conducting ground. A high-frequency solution to the problem is also obtained for the case of the strip, and compared to both the exact solution and the measurement results. This research is important because it presents exact solutions to a new boundary value problem, thus enriching the list of geometries for known canonical solutions.

BISTATIC SCATTERING FROM A RESISTIVE SHEET USING A MODIFIED PO CURRENT

Dwyer, D.¹, Havrilla, M.¹, Hastriter, M.¹,
Terzuoli, A.¹, Rothwell, E.²

¹Air Force Institute of Technology, AFIT/ENG, 2950 Hobson Way,
WPAFB, OH 45433-7765

²Michigan State University, 2120 Engineering Building, East Lansing,
MI 48823

The physical optics (PO) current $\vec{J}_{PO} = 2\hat{n} \times \vec{H}^i$ (where \hat{n} is the surface normal and \vec{H}^i represents the incident magnetic field intensity) is frequently used to obtain a high-frequency approximation to the scattering from perfect electric conducting (PEC) objects. However, in certain applications, structures may be fabricated using imperfect conductors or resistive layers for the purpose of reducing certain scattering mechanisms. Under these conditions, the use of the above PEC physical optics current will lead to gross errors in the scattered-field calculation. In order to mitigate these errors, a non-PEC physical optics current expression must be developed. The purpose of this paper is to derive a physical optics current to accommodate a resistive layer and experimentally verify the analysis via bistatic radar cross section (RCS) measurements of a rectangular resistive strip under both horizontal and vertical polarizations.

The PO current of a resistive layer will be developed based upon a plane-wave analysis. The derivation will assume that the layer is an infinite non-magnetic planar slab having thickness d , permittivity ϵ and conductivity σ . A closed-form solution is found for the fields inside the layer for both horizontal and vertical polarizations. A Taylor-series analysis is then performed to obtain an approximate expression for the PO current \vec{J}_{RPO} in terms of the resistance $R_s = 1/\sigma d$ (Ω/\square) of the finitely-conducting sheet for both polarizations, namely

$$\vec{J}_{RPO} = \vec{J}_{PO} \left(1 + \frac{2R_s}{Z_0} \right)^{-1}$$

where $Z_0 = \eta_0 \cos \theta_i$ for horizontal polarization, $Z_0 = \eta_0 / \cos \theta_i$ for vertical polarization and θ_i is measured relative to the surface normal. It should be noted that, in the high-frequency limit, this condition will also be approximately valid in a non-planar environment so long as any curvature is large compared to wavelength.

The RCS of several resistive strips of various thicknesses will be experimentally measured and compared to bistatic RCS calculations based on the above analysis for theoretical verification. In addition, a Method-of-Moments integral equation solution based upon a resistive boundary condition will be formulated and compared to the above results to validate \vec{J}_{RPO} .

¹The views of the co-authors expressed in this article do not reflect the official policy of the U.S. Air Force, Department of Defense, or the U.S. Government.

RESONANT TRAVELING WAVES INDUCED ON A RING SCATTERER

Li, S., Scharstein, R.W.
University of Alabama

An integro-differential equation for the current induced by a plane wave incident upon a thin circular conducting loop is solved using a combination of numerics and high frequency asymptotics. The thin-wire kernel approximation is used. Fourier coefficients of the ring current are evaluated using the FFT algorithm applied to the kernel function. The self-convergence of the numerical results plus agreement with published data by King and Smith indicate that the numerical implementation is accurate. Asymptotic formulae are derived for the Fourier coefficients of the thin wire kernel in the integral equation and checked against the FFT results. The total current induced on the ring by a plane electromagnetic wave is approximated by a modified physical optics term proportional to the incident field, plus resonant terms of lossy circulating waves. Numerical evaluation of the dominant poles and residues of the ring transfer function provides the amplitudes and complex propagation constants of these natural modes.

The real part of the dominant poles (in complex Fourier index n) is always close to ka . The Fourier coefficients of the excitation are roughly $J_n(ka \sin \theta_0)$, which demonstrates the increasing importance of the resonant currents for angles of incidence approaching grazing ($\theta_0 \rightarrow \pi/2$).

The phase velocity of the eigenwaves of the ring is therefore close to c ; both faster and slower wave components are possible. The attenuation constant (imaginary part of the pole of the transfer function) must account for radiation damping by circulating charges. No meaningful purely analytic expressions have been found for these physically important parameters that are numerically extracted from the complex transfer function of the ring scatterer.

This conference paper is an oral presentation of research reported in:

Shaohua Li and R.W. Scharstein
High Frequency Scattering by a Conducting Ring
IEEE Trans. Antennas Propagat. (in review)

SCATTERING CROSS-SECTION FROM RANDOMLY ORIENTED PARTICLES

Voronovich, A.G.¹, Gasiewski A.J.¹, Irisov V.G.²¹NOAA/Environmental Technology Laboratory, 325 Broadway, Boulder, CO, 80305-3328²Zel Technologies, LLC, 325 Broadway R/ETL-O, Boulder, CO, 80305-3328

Scattering cross section from a cloud of identical, arbitrarily oriented particles is often of interest in practical applications. If multiple scattering between particles can be neglected, the problem reduces to averaging of appropriate scattering cross-section over particle orientation. This problem is easily solved in the case of Rayleigh scattering. It seems that the other limiting case of geometric optics (GO) was overlooked in the literature. It is demonstrated in this talk that within limits of the GO approximation orientation-averaged scattering cross-section from a convex dielectric particle at a given angle is proportional to the product of a square modulus of the Fresnel reflection coefficient and a total area of the particle surface. For in-plane and orthogonal-to-plane scattering the Fresnel reflection coefficient corresponds to p- and s-polarization, correspondingly (cross-polarization scattering cross-section in the GO limit turns to zero). The proof is based on Gauss mapping and is very similar to the proof of the Gauss-Bonnet formulae. Simple treatment of the Rayleigh scattering case will be also presented in the talk.

The results obtained could be used for particle remote sensing applications. In the low-frequency (Rayleigh) limit orientation-averaged scattering cross-section depends on three parameters: a volume of a particle and two form-factors which depend on particle shape, and has both isotropic and dipole components. Thus, to determine those parameters one has to make one absolute and two relative measurements using different angles and/or polarizations. In the high-frequency (GO) limit for convex particles orientation-averaged scattering cross-section depends on dielectric constant of the particle and is directly proportional to the total area of the particle surface. Angular dependency of the scattering cross-section coincides with the corresponding angular dependency of the appropriate Fresnel reflection coefficient. Thus, for perfect conductor scattering is isotropic.

STATISTICS OF TRAVEL TIMES AND INTENSITIES OF THE
EARLIEST ARRIVED SHORT PULSES BACKSCATTERED
BY A ROUGH SURFACE

Fuks, I.M.¹, Charnotskii, M. I.¹, Godin, O.A.²

¹Zel Technologies, LLC and NOAA/Environmental Technology
Laboratory, Boulder, CO

²CIRES, University of Colorado and NOAA/Environmental Tech-
nology Laboratory, Boulder, CO

Precise measurements of the travel times of backscattered waves, and especially the travel times of the first (i.e., earliest) arrivals, underlie a number of geophysical remote sensing techniques. In this paper, statistical properties of the travel time and intensity of pulses backscattered by a two-dimensional rough surface are investigated within the geometric optics approximation by adopting a method originally developed in the theory of excursions of a stochastic process.

Two specific cases are investigated: a sufficiently wide collimated incident beam with plane wave front, and a spherical wave front. Signals from the rough surface return to the source location earlier than from the mean plane by $O(2\sigma/c)$, where c is the velocity of wave propagation, and σ is an r.m.s. of surface roughness. We assume a wave source located sufficiently far from a rough surface with a Gaussian statistics, and show that the probability distribution functions of the deviation of the travel time of the first and second backscattered pulses from the travel time in the absence of roughness, normalized by $2\sigma/c$, are functions of a single dimensionless parameter, $T = \gamma_0^2 H / (2\pi\sigma)$, where γ_0^2 is the variance of the rough surface slope, and H is the source altitude. On average, the travel times of the first and second arrivals decrease as parameter T increases, with the travel time shift being proportional to $\sqrt{\ln T}$. The time delay between the first and the second arrivals is inversely proportional to $\sqrt{\ln T}$.

The joint probability density functions (PDF) of the travel times and the intensities of the first two backscattered pulses are derived. This allows us to obtain the travel time PDF for signals exceeding the given intensity threshold. It is shown that travel time and the intensity are strongly correlated: on average, earlier arrivals have smaller amplitudes.

NUMERICAL STUDY OF ANGULAR AND FREQUENCY
CORRELATION FUNCTION OF SEA ICE AT VHF: ONE-
DIMENSIONAL CASE WITH THE FINITE-DIFFERENCE
TIME-DOMAIN METHOD

Pak, K.¹, Hussein, Z. A.¹, McDonald, K¹

, Holt, B.¹, Lee, S. W.², Kuga, Y.²

, Ishimaru, A.², Jaruwatanadilok, S.²

¹Jet Propulsion Laboratory, California Institute of Technology,
Pasadena, CA 91109

²University of Washington, Department of Electrical Engineering,
Seattle, WA 98195

Angular and frequency correlation function (ACF/FCF) of the electromagnetic wave scattered from sea-ice in the VHF band is studied using the finite-difference time-domain method (FDTD). The problem is modeled as four-layered medium with air, snow, sea-ice, and ocean. The medium interfaces are modeled as one-dimensional random rough surfaces (two-dimensional in scattering). Snow and ocean medium are assumed homogenous with the appropriate bulk permittivities at VHF. The sea-ice consists of homogeneous host ice medium with random distribution of scatterers to represent the effects of brine and air pockets. The accuracy of the FDTD model is tested with the first-order small perturbation, integral equation, and finite element models for a single rough surface interface. Also, the FDTD results are compared with that of a theoretical multi-layer model to further validate the FDTD model. Next, the ACF/FCF are calculated by taking the correlation between the backscattering fields at two different set of incidence angles and frequencies ($\alpha_1 = 30$ degrees, $f_1 = 137$ MHz ; $\alpha_2 = 25$ degrees $f_2 = 162$ MHz) for varying snow and sea-ice thickness for sensitivity analysis. Backscattering angles are selected based on where the ACF/FCF of the surface is much larger than the volume to minimize the volume scattering contribution. The snow and sea-ice parameters for these cases are chosen to represent a typical young sea-ice type with dry snow cover and smooth ice-ocean interface. Results show that the backscattered power contributions from the snow layer are typically less than -20 dB below that of the ice-ocean interface and the phase of the AFC/FCF changes linearly with increasing sea-ice thickness. The linear relationship between the AFC/FCF phase and sea-ice thickness is lost for sea-ice thickness greater than 3 meters due to significant signal attenuation and smooth ice-ocean interface used in this simulation. The ACF/FCF phase is most sensitive to the ice-thickness, but it is also sensitive to snow thickness and bulk permittivity. Therefore, accurate sea-ice thickness retrieval will require a priori information about the snow parameters. Nevertheless, this study shows that the sea-ice thickness can be estimated from the ACF/FCF phase information where the scattering contribution from the ice-ocean interface is dominant.

ULTRA-WIDEBAND EMI SPECTROSCOPY FOR DETECTION OF UXO: A METHOD OF INVERSION FOR ESTIMATION OF PHYSICAL DIMENSIONS AND PROPERTIES OF METALLIC OBJECTS FROM WIDE-BAND ELECTROMAGNETIC INDUCTION MEASUREMENTS

Haider, Shah A.¹, O'Neill, Kevin²

¹College of Engineering and Technology, Old Dominion University, Norfolk, VA 23529

²Cold Region Research and Engineering Laboratory, U. S. Army Corp of Engineers, Hanover, NH 03755

The UXO objects are highly conducting and permeable and therefore, almost indistinguishable from non-UXO metallic litters at ground penetrating radar frequency range since metallic objects in general behave as PEC. It is therefore highly desirable to develop UXO detection method that uses highly sophisticated discrimination criteria so that underground unexploded explosive cleanup to be cost effective. In this presentation it is shown that ultra-wide band (1Hz to 300kHz) EMI spectroscopic measurement data obtained from the buried metallic objects representing UXO's can be inverted to estimate physical dimensions and certain material properties of the object. There are two specific advantages using low frequency excitation. First, the ground is almost transparent to both the incident primary and scattered secondary fields at this low frequency range. Second, low frequency fields are capable of penetrating highly conducting magnetic or non-magnetic objects giving rise to in-phase and quadrature components of secondary fields; this is known as the EMI response of the object. In phase component is due to induced surface currents where as Gaussian shaped quadrature component is due to induced volume currents. Measured EMI response data contain wealth of information waiting to be extracted. Extensively studying the EMI responses due to canonical objects both solid and shell structures under axial and transverse excitation several characteristics parametric features have been identified: peak value, peak frequency, peak width, zero-crossing frequency etc. etc. These crucial parameters contain all the information about the physical dimension of and material properties the object. First step is to extract these parameter values from the measured spectroscopic EMI response data. In order to match each of these measured parameter values using analytical expressions for canonical objects we can generate for example all possible outer diameters and shell thicknesses that correspond to a specific parameter value. Next, each of these parameter values graphically plotted as a function of all possible diameters and shell thicknesses. The intersection of various parameter curves reveal the estimated diameter and thickness of the object. A number of inversion (estimated diameter and thickness) examples are presented using experimentally measured EMI response data and compared with actual dimensions. Inverted diameters and thicknesses are realistically accurate.

THE IMPACT OF DIFFRACTED FIELD ON INDOOR WIDE-BAND PROPAGATION MODELING

Wang, H., Rappaport, T. S.

The University of Texas at Austin, Department of Electrical and Computer Engineering, Wireless Networking and Communications Group

Diffraction is one of the main mechanisms required in accurate ray-tracing based propagation prediction modeling. Particularly when line-of-sight ray path is not available, diffraction models the radio signal into shadowed regions and contributes significantly to the receiver power delay profile. Thus appropriate yet simple diffraction modeling is important for accurate wave propagation prediction in wideband multipath environments.

In our study, we use our previously developed parametric formulation to model the building edge diffracted field. In this construction, the UTD-like diffraction coefficient consists of four terms, each of which has a complex multiplying factor to be determined. As the vertical edges of building walls can be modeled as right-angle dielectric wedges, the multiplying factors are functions of incidence angle, diffraction angle, and relative permittivity. A least-square constrained polynomial fitting method is applied to determine the four factors. It is shown that the parametric formulation of the diffraction coefficient yields significant improvement over the existing heuristic formulations in accurate prediction of the diffracted field in the shadowed region.

The influence of diffraction on indoor wideband propagation modeling is investigated through ray-tracing predictions and validated with measurements in several buildings on the campus of Virginia Tech. The transmitters operate at 1.3 GHz and 4.0 GHz and are located in corridors. The effects of diffraction on receiver power delay profiles are presented. It is observed that diffracted rays form important multipath components in the case of obstructed propagation scenarios such as L-shape corridors. Good agreement is shown between the ray-tracing predictions with proposed diffraction modeling and the wideband measurements.

TIME-DOMAIN COUPLING TO A DEVICE ON A PRINTED
CIRCUIT BOARD INSIDE A CAVITY

Lertsirimit, C.¹, Jackson, D. R.¹, Wilton, D. R.¹
, Erricolo, Danilo²

¹University of Houston

²University of Illinois at Chicago

A time-domain electromagnetic pulse that impinges on a cavity (metallic enclosure) with an aperture may cause significant interference for a device on a printed circuit board (PCB) that is inside the cavity. The interference may be particularly large when an exterior cable or wire passes through the aperture and makes contact with a conducting trace on the PCB that leads to the device. If the interference is large enough an upset to the device may occur, and the device may even be damaged. Clearly, a calculation of the signal level at the input of the device due to an incident time-domain electromagnetic signal is an important problem.

This investigation focuses on calculating the signal level at the input port of the device on a PCB. The incident electromagnetic field is assumed to be a time-domain plane wave in the form of a pulse, and two pulse shapes are studied. One is a sinusoidal carrier modulated by a Gaussian envelope centered at time zero. The other is a damped sinusoid, i.e., a sinusoidal signal starting at time zero, which is modulated by a decaying exponential envelope.

The time-domain response at the input to the device is calculated by first determining the frequency-domain response for time-harmonic incident plane waves, and then using the Fourier transform. The frequency-domain response is obtained by using an efficient hybrid method, as discussed in (C. Lertsirimit, D. R. Jackson, D. R. Wilton, D. Erricolo, and D. H. Y. Yang, *IEEE AP-S Intl. Symp. Digest*, Monterey, CA, June, 2004).

Results show how different incident pulse characteristics produce different types of signals at the input to the device. The results can be explained by the nature of the frequency-domain cavity response.

The time-harmonic results from the hybrid method are validated by comparing with a rigorous moment-method solution. The time-domain results are validated by comparing with simple expressions based on the resonant frequencies and Q of the cavity.

ANALYSIS OF HIGH-POWER RF INTERFERENCE ON DIGITAL CIRCUITS

H.Y. David Yang, Ronald Kollman²
U. of Illinois at Chicago

Recently, there is significant interest in understanding and mitigating the effects of high power electromagnetic (EM) source on electrical systems and equipment. Most of the focus of EMI investigation has been for interference between circuit components and the interference is well below GHz. There are many research efforts in trying to determine the susceptibility of the systems experimentally coupled with a statistical approach. Most of the theoretical analysis is for large-scale electromagnetic analysis to determine the conducting or radiating EMI at the digital system input due to coupling of high-power microwave sources through cavities with apertures. The detail analysis of the external EMI at the input pins coupling into digital circuit causing spurious waveforms has not been available. The main reason is that typical digital circuitry includes hundreds or thousands of components and complete circuit analysis to determine the cause of distortion is too complicated and impractical. This paper describes the analysis of intentional high-power RF interference on digital circuits. The interference is modelled as a noise in the form of single-frequency sinusoid and is superposed to the pulse trains of the digital signals. Spice simulations for a CMOS inverter and a 4-bit adder are performed to determine the threshold of the state change (error bits) under various interference frequencies and voltage levels. Propagation effect of error bits through the circuits is investigated. It is found that in general the digital circuits will reduce the error bit rates as signals propagate through and EMI effect is smaller when the noise and signal frequencies are farther apart. The phase difference between noise and signal is an important factor to determine the bit error rates. Inverter BER is further related to the external microwave source for the case of a wire penetrating a cavity aperture.

Session B9, 13:35 – Sat.

**ANTENNA DESIGN AND
MEASUREMENT**

Co-Chairs: J. Huang, Y. Rahmat-Samii

BROADBAND OFFSET FED CYLINDRICAL DIPOLE ANTENNA

McDonald, J.L., Lalezari, F.

First RF Corp., 4865 Sterling Drive, Ste. 100, Boulder, CO 80301

A novel broadband offset fed cylindrical dipole antenna has been designed. This dipole is fed using a biconical feeding structure to improve return loss over the band of interest. The antenna has been designed to operate over a 15:1 bandwidth, from 150 MHz to 2.5 GHz. The antenna shows a traditional dipole response but over a much larger bandwidth than found in a standard offset fed cylindrical dipole. Comparisons have been made to this antenna and a traditional dipole. This antenna can be used in a variety of communication applications.

The antenna has return loss less than 10 dB over the specified band. For a 10730; degree field of view at broadside this antenna exhibits excellent pattern stability over the specified band. The broadside directivity varies from 2 dBi to -4 dBi over the specified band.

Several measured results have been used to design an infinite twin lead balun to feed the antenna. Measured results have been used to verify a model that has been simulated using Ansoft's High Frequency Structure Simulator (HFSS). Simulations have been run to extract impedance data, pattern data, and the current distribution along the antenna.

Parametric studies have been done to see the effects that changing antenna dimensions have on the broadside gain, impedance, and the current distribution. The antenna dimensions that have been analyzed are dipole diameter, feed location, and total antenna length.

Simulations have been performed to optimize feed location, dipole diameter, and total antenna length to provide maximum broadside directivity while maintaining pattern stability and return loss over the specified band.

PARTICLE SWARM OPTIMIZATION AND FINITE DIFFERENCE TIME DOMAIN (PSO/FDTD) FOR PATCH ANTENNA DESIGN: SIMULATION AND MEASUREMENT

Nanbo Jin, Yahya Rahmat-Samii

Department of Electrical Engineering, University of California, Los Angeles

The optimization of a multi-function patch antenna geometry is a challenging antenna engineering problem. In most cases the antenna configuration can be selected based on the desired antenna performance; however, the specific values of the geometrical parameters are left to be determined by the designer. Since the electromagnetic functionality of each parameter is hard to be investigated quantitatively due to the complexity of antenna structure, the conventional design process usually relies on the computationally intensive methodologies such as trial and error, and generally fails in obtaining the design that best fits the requirement.

In this paper a novel global optimization methodology is introduced into patch antenna design to solve the problem stated above. The optimization kernel is constructed using the technique of Particle Swarm Optimization (PSO), and Finite Difference Time Domain (FDTD) is exploited in the algorithm for fitness evaluation. With a predefined basic antenna structure, the PSO/FDTD optimizer is able to effectively select an optimum combination of the geometrical parameters within the solution space. The optimized antenna structure leads to the best design for specific antenna performance. Several algorithmic modifications to the conventional PSO kernel, such as the utilization of invisible boundary condition and repeated position checking, along with parallel computation were applied in the optimization system to reduce the computational cost caused by full wave analysis.

In this paper the PSO/FDTD algorithm is utilized to solve two representative design problems: initially a rectangular patch antenna is designed to test the algorithm functionality, and to demonstrate that the optimizer provides different designs by using different fitness functions. Next, to further validate the accuracy and resolution of the optimizer in higher dimensional cases, it is used to design wideband and dual-frequency E-shaped patch antennas. The optimized antennas are also analyzed, fabricated and measured. A 30.5% bandwidth from 1.79GHz to 2.43GHz (for wideband antenna) and two resonant frequencies at 1.8GHz/2.4GHz with return loss less than -18dB (for dual-frequency antenna) were observed from the measurement result, which confirms the potential application of the PSO/FDTD algorithm in antenna engineering and modern wireless communications.

A NEW UNI-PLANAR COMPACT CPW FED SURFACE WAVE LAUNCHER FOR LEAKY WAVE ANTENNA APPLICATIONS

Bekheit, M.Z.I¹, Freundorfer, A.P.¹, Antar, Y.M.M²

¹Electrical and Computer Engineering Dept., Queens University, Kingston, Ontario, Canada

²Electrical and Computer Engineering Dept., Royal Military College of Canada, Kingston, Ontario, Canada

Recently there has been a growing interest in developing new leaky wave antennas with new properties like scanning capability, conformability, ease of integration with planar active circuits and low cost for applications in communications and automotive radars. Periodic leaky wave antennas have been realized recently at millimeter wave frequencies by means of periodic dielectric gratings (Hammad, H.F.; Antar, Y.M.M.; Freundorfer, A.P, Sayer, M., IEEE Transactions on Antennas and Propagation, 52, 36-44, 2004) where scanning was achieved by varying the frequency.

Currently we are investigating a new uni-planar periodic leaky wave antenna that uses a new scanning technique. An important component is the antenna feed. In this paper we report a new CPW-fed surface wave launcher that has some important practical properties. The developed launcher is more compact and flexible in design than the previously reported ones (Hammad, H.F.; Antar, Y.M.M.; Freundorfer, Mahmoud S.F., IEEE Transactions on Microwave Theory and techniques, 1234-1240, 51, 2003) and this makes it suitable to be integrated with the scanning antenna. The main components of the launcher are two resonant slots in the ground plane of a dielectric slab wave-guide; one of them is a folded slot and referred to as the primary slot and the other one is inductively coupled to the input CPW line and referred to as the secondary slot. The coupling and the distance between the slots can be optimized to achieve the best performance.

Two different full wave EM simulation tools were used; IE3D from Zealand and HFSS from Ansoft and promising and consistent results have been achieved. A return loss better than 15 dB has been achieved over a bandwidth of 10.6%, which outperforms previous Yagi-Uda based designs. Also a directivity of 14.5 dB was achieved. A critical parameter of the launcher is the modal purity, which is defined as the ratio of TM₀ to TE₁ power excited. The proposed launcher was designed to operate above the cutoff of the TE₁ mode and therefore it is important to investigate the excitation level of higher order modes. Further investigation into the modes structure revealed that the excited TE₁ mode is 40 dB below than that of the TM₀ fundamental mode. The launcher is currently being fabricated and the measured results and other aspects of the configuration will be reported.

A MODIFIED BOW-TIE ANTENNA FOR SINGLE AND DUAL POLARIZED WIDEBAND PHASED ARRAY APPLICATIONS

Abdelnasser A. Eldek, Atef Z. Elsherbeni, Charles E. Smith

The University of Mississippi, Electrical Engineering Department,
Center of Applied Electromagnetic Systems Research (CAESR)

Radar systems that operate in the C and X-bands are normally designed as separate systems. Since it is becoming more and more important to use such systems in one setting, it is desirable to design a system that operates in both frequency bands. This, in turn, requires a wideband antenna that covers the two bands. In addition, many applications require end fire patterns, which can be produced by different types of antenna elements. Printed microstrip antennas are widely used in phased array radar systems. They exhibit a low profile, small size, light weight, low cost, high efficiency, and ease of fabrication and installation. This paper introduces a modified printed bow-tie antenna that exhibits a wide impedance bandwidth with good radiation characteristics. The antenna consists of two identical printed bows, one printed on the top side and the other printed on the bottom side of the substrate material. The top and bottom bows are connected to a microstrip feed line and the ground plane through a stub and mitered transition to match the bow-tie with the 50 Ohms feeding network. The return loss, VSWR and far field radiation characteristics of this antenna are analyzed using the commercial computer software package HFSS and verification for the computed return loss is performed using measurements. This new design provides over 90 percent impedance bandwidth that covers the entire C and X bands and part of the Ku band. The single element antenna provides more than 95 degrees beamwidth, low cross polarization level (less than 18 dB), and relatively high gain in the frequency range between 5.3 and 10 GHz in addition to the endfire radiation pattern with a good front-to-back ratio that exceeds 12 dB. A stable radiation pattern and a wide bandwidth are also obtained using a modified two-element array configuration. Two of this two-element array configuration are snapped perpendicular to each other to form antenna unit providing circular, vertical, or horizontal polarization based on the feeding arrangements of the ports of the four individual antenna elements. The new antenna design is found to be a good candidate for wideband phased array systems with single linear, dual linear or circular polarization.

A WIDE-BAND DUAL-POL VHF MICROSTRIP ANTENNA FOR SEA-ICE THICKNESS MEASUREMENT

Huang, J, Hussein, Z. A.

Jet Propulsion Laboratory, California Institute of Technology,
Pasadena, CA 91109

Presented in this paper are the design, characterization and test results of a dual-polarized and broadband multi-layer VHF (127-172 MHz) microstrip antenna. The antenna with 30% bandwidth has been developed for an aircraft (Twin Otter) field experimental system (FES) to measure the sea ice thickness. This FES is equipped with a new instrument technology: a combined spatial- and frequency-domain interferometer providing angular and frequency correlation functions (ACF/FCF) between two radar waves with different frequencies (in the VHF band), incidence angles and observation angles. The FES system requires two separate measurements from different altitudes (1.0 Km and 1.2 Km), with each measurement being at separate frequencies. The nominal central frequencies for each measurement are 137 MHz and 162 MHz with 20 MHz bandwidth each.

A lightweight antenna is required for placement outside a Twin Otter Aircraft passenger door. The antenna gain is required to be greater than 8 dB so that the FES system is sensitive to the weak backscatter return of the sea-ice sea water interface. The cross-polarization is required to be below 20 dB from the peak of the co-pol. A four capacitive feeding approach (instead of two orthogonal probes- one for each polarization) for the antenna with 180-degree hybrid connecting the two opposing probes is used to suppress the higher order modes presented in the thick multi-layer antenna substrate (total thickness is 29 cm). This approach allows for simultaneously reducing the antenna cross-polarization level below 20 dB, and the mutual coupling between probes. These four capacitive feeds are attached to the lower resonant (137 MHz) patch layer. The top layer resonates at 162 MHz, and is fed through the energy coupling from the bottom patch layer. A wide antenna bandwidth is achieved (127 MHz to 172 MHz) with antenna gain greater than 8 dB for both polarizations. The antenna has dimensions of 117 cm x 117 cm x 29 cm. A breadboard antenna element has been fabricated and tested. Excellent agreement is shown between theoretical and measured results.

DEVELOPMENT OF A TWIN-HORN FEED FOR DBS REFLECTOR ANTENNAS

Lee, S. W.¹, Schmieder, L.¹, Fathy, A. E.¹
 , El-Ghazaly, S. M.¹, Rodeffer, G.², Zihlman, B.²

¹Department of Electrical and Computer Engineering, University of Tennessee, Knoxville, TN 37996, USA

²Winegard Company, Burlington, IA 52601

We developed a compact dual linear/circular; dual beam feed for the 11.7-12.7 GHz DBS applications. The feed is composed of a twin horn antenna designed for feeding a 60 cm size dish to produce dual beams of 4.5 degree separation. First, horns were designed for equal E & H planes radiation patterns [1] with minimal side lobe levels, 14 dB gain, and an axial ratio less than 1 dB over the band. Fabricated horns demonstrated excellent match, very high isolation and outstanding similarity between measured and radiation patterns. Second, center-to-center spacing distance between the two horns was designed to provide a two-beam separation in space of 4.5 degrees. Where each horn center was mounted off-centered slightly from the parabolic dish focus. The center-to-center distance was estimated based on experimentally validated GTD calculations [2,3] and compared to other approximate expressions [4]. The two horns were connected by a surface with novel hard boundaries to efficiently impede the surface wave propagation. The presence of these hard boundaries led to over 35 dB isolation and no pronounced degradation in match or radiation patterns. The hard boundaries were used here also to sustain very similar E & H patterns. Finally, the performance of a 60 cm dish fed with the developed twin feed was both predicted and measured. At 12.2 GHz, the measured overall gain of the 60 cm dish is 35dB, and the dual beam separation is approximately 4.5 degrees in agreement with our design. The measured decoupling between the horns; in the presence of the reflector dish is roughly a 20 dB- consistent with theoretical expectations. Detailed experimental and theoretical evaluations of the feed structure for both the 60-cm and 76-cm dishes will be presented in this paper.

References : [1] Rodeffer et al., "Conical Corrugated Microwave Feed Horn," US Patent 5486839, Jan. 23, 1996.[2] J. L. Volakis, "SABOR: a fast analysis tool for horn and reflector antennas," IEEE Antennas and Propagation Magazine, vol. 40, Issue 3, pp. 104-108, June 1998. [3] T. H. Lee and R. C. Rudduck, "Numerical Electromagnetic Code -Reflector Antenna Code, NEC-REF (Version 3),"The Ohio State University ElectroScience Laboratory, Feb. 1994. [4] Y. T. Lo and S. W. Lee (ed), "Antenna Handbook Vol. II: Antenna Theory," Van Nostrand Reinhold, New York, NY, 1993.

This development work was carried out sponsored by a Generous Grant from Winegard Company, Burlington, Iowa.

SPACEBORNE MEMBRANE REFLECTOR ANTENNAS
WITH PERIODIC AND APERIODIC DISTORTIONS

Keyvan Bahadori, Yahya Rahmat-Samii
University of California, Los Angeles

The 21st century space science mission visionaries have been considering membrane structures for light weight and deployable large reflector antennas. For these reflectors, performance critically depends on the manufacturing accuracy of their surfaces. Structural inaccuracies may cause different types of surface distortions. In particular, since these reflector surfaces are very thin, (typically 5 to 10 mils) they are susceptible to various types of periodic and aperiodic distortion caused by gravitational effects or torsions from antennas attachment mechanism to the supporting structure. In particular, these distortions could become very important during 1-g ground testing of the antenna.

The focus of this paper is to characterize the effects of periodic and aperiodic surface distortions on the performance of membrane reflector antennas. The particular antenna dimensions used for this study are similar to the specifications for the JPL/UCLA half scale model of second generation precipitation radar (PR-2) mission reflector. Analytical expressions are introduced to model periodic and aperiodic surfaces and based on these models the effects of distortions on the radiation performance of the antenna are simulated. Aperiodic distortions are more realistic cases of distortions due to the fact that the period of the distortions is not constant through out the reflector surface. For each case, far-field patterns of the reflector are simulated and it is shown that closed-form expressions can then be derived which result in a very efficient computational method to predict some of the unique features of these patterns including location and level of observed grating lobes.

The simulation and calculation results reveal that the locations of these grating lobes are determined by the number of ripples on the reflector surface. The level of the grating lobe depends, in general, on the rms of the reflector surface and number of ripples. To calculate the gain loss, an expression is derived to relate the distortion peak level to rms of the surface. Furthermore, based on spatial Fourier analysis of the surface distortion, it is shown that deviation from periodicity in the distortions of reflector surface results in lowering these grating lobes. For the reflectors with no dominant spatial frequency, the energy will be radiated in a broad angular region. In the limit, the far-field pattern of a distorted reflector with spread spatial spectrum will approach to the average power pattern of the reflector with random surface errors. Parametric studies have been performed to provide design guidelines for acceptable surface behavior. This is an important consideration for evaluation the performance of large deployable membrane reflector antennas for future spaceborne missions.

ANTENNA FACTOR DETERMINATION FOR ANTENNAS IN THE NEAR FIELD OF A LARGE RADIATING APERTURE

Nicholas DeMinco

U.S. Department of Commerce, National Telecommunication and Information Administration, Institute for Telecommunication Sciences

ANTENNA FACTOR DETERMINATION FOR ANTENNAS IN THE NEAR FIELD OF A LARGE RADIATING APERTURE

Nicholas DeMinco, Author Institute for Telecommunication Sciences 325 Broadway Boulder, Colorado 80305-3328, USA

This paper will present the results of an analysis for determination of antenna factors in an environment over real ground in the near field of a large radiating aperture for some commonly used measurement antennas. The large radiating aperture that was simulated as a source was a medium-voltage electric utility power line 340 meters in length carrying HF and low VHF radio frequency signals. The probe antennas that were used to measure the electric and magnetic fields were at separation distances that were well within the near field of this power line. The probe antennas were also at separation distances that were both in the near and far field of the probe antennas. It was necessary to have antenna factors that better represented this scenario over a real ground. These antenna factors were significantly different than those supplied by the antenna manufacturers. Some measured data was also available to compare to analysis results. The antenna factor is a quantity by which one multiplies the output voltage of a receiving antenna to obtain either the incident electric or magnetic field. The antenna factor generally includes losses and mismatches in the antenna which could account for a balun, matching transformer, or other device incorporated into the antenna. The antenna factor is very dependent on what impedance is used to load the antenna in the process of measuring the antenna output voltage. Since the probe antennas used to measure the electric and magnetic fields of the large aperture were in the near field of the large aperture and in the near fields of the probe antennas themselves, the mutual impedance between the antennas must also be taken into consideration when determining the antenna factors of the probe antennas. Manufacturer's data usually include an antenna factor calibration for a measurement scenario that is quite unlike the scenario in which the antenna will actually be used. Usually this will be a free-space antenna factor measured in an anechoic chamber or some other scenario. The separation distances for the manufacturer's measurement of antenna factor may be unspecified. A more precise antenna factor in a scenario that better represents the actual antenna environment will permit a more confident determination of the electric and magnetic fields in close proximity to the power lines.

Session B/D1, 10:15 – Fri.

**RECONFIGURABLE/HIGHLY
INTEGRATED RF SYSTEMS AND
MODULES**

Co-Chairs: V. Nair, M.M. Tentzeris

ANALYSIS OF SPATIAL MULTIPLEXING OF LOCAL ELEMENT DIGITAL BEAMFORMING SMART ANTENNA RECEIVERS

Goshi, D.S., Wang, Y., Itoh, T.

University of California, Los Angeles, Dept. of Electrical Engineering

The Spatial Multiplexing of Local Elements (SMILE) technique has been introduced as a means to reduce the costly front end RF hardware in digital beamforming (DBF) smart antenna receiver systems. This highly integrated modular scheme reduces the necessary amount of RF hardware such as mixers and low-noise amplifiers, thus offering a reduction of overall size and power consumption while maintaining the same functionality of conventional DBF antenna arrays. This reduction can be as much as N-fold for an N-element array. Measured beamforming results validate this structure as a possible asset in practical DBF systems.

The SMILE architecture consists of an N-element antenna array, a multiplexing network, a single RF channel, a demultiplexer, A-to-D converters, and a digital beamformer. The main challenge in the operation of this structure is the multiplexing network, which uses a sequential switching technique to multiplex the received signals from N individual channels to one. This time-multiplexing process therefore places the greatest importance on the performance of the switching element.

The SMILE principle has been demonstrated with two architectures of different type of antenna elements, and different type of switching elements. The first uses quasi-yagi antenna elements with PIN diode switching elements, and the second has patch antenna elements and employs FET type switches in a low-noise amplifier configuration.

This paper will discuss and compare the two types of SMILE arrays. For application in the SMILE scheme, it is determined that choice of the switching configuration and antenna element can greatly influence performance. The switching aspect for both cases will be compared and evaluated by its effects on system performance.

A RADIATION AND FREQUENCY RECONFIGURABLE
CPW-FED DUAL SLOT ANTENNA FOR CPW RF MEMSHuff, G. H.¹, Reeder, M.², Bernhard, J. T.¹¹Univ. of Illinois at Urbana-Champaign, Urbana, IL, USA²Rose-Hulman Inst. of Technology, Terre-Haute, IN, USA

The demand for highly functional and multi-purpose devices will likely increase as a result of improved CPW-based circuit topologies and more reliable RF MEMS switches. In turn, this will open the doors for many new possibilities of component integration, and improve the ability of a single system to operate in a multitude of communication scenarios. An important example of this involves the integration of RF MEMS switching technologies and antenna designs into single elements and arrays. While the majority of RF MEMS are currently developed in a CPW topology, this is not the case for most antennas. Therefore, the creative use of antenna designs in the same CPW based environments should also be considered for hosting these emerging technologies. In doing so, allowing the radiating element to take full advantage of switching technologies whose primary current uses are limited to switching circuit elements such as delay lines and I/O devices.

As an example of an antenna utilizing these new technologies, this work develops a pattern and frequency reconfigurable co-planar waveguide fed dual slot antenna. Specifically, this antenna has the ability to switch the main beam direction in the longitudinal plane of the slot while maintaining a 2:1 VWSR impedance bandwidth. In addition to this, the antenna can also reconfigure its frequency while maintaining its radiation characteristics. To provide the added functionality and improve the applicability of this antenna, the CPW based design has been modified for integration and fabrication with CPW-based RF MEMS and other CPW based components. To demonstrate the pattern and frequency characteristics of this type of geometry, a 5.8 GHz version of this antenna has been designed. Measured and simulated performance of this design will be provided during the presentation. In addition, several other modifications to the overall antenna design will be examined, such as finite (small) CPW grounds, addition of a lower ground plane, switch biasing, and methods of excitation for the slot geometry.

NO ABSTRACT SUBMITTED

EFFICIENCY-OPTIMIZED MICROWAVE TRANSMITTER
POWER AMPLIFIERS WITH DYNAMIC BIASING

Wang, N., Youzefzadeh, V., Bell, P.
, Pajic, S., Maksimovic, D., Popovic, Z.
ECE, University of Colorado, Boulder

Advanced intelligent RF front ends require adaptive control of frequency, mode of operation, power etc. This paper focuses on high-efficiency power amplifiers with dynamic biasing that allows adaptive power variation and enables a degree of linearization. The single or dual-stage switched-mode high efficiency power amplifier (PA) is operated in switched mode which is inherently operated deep in saturation and is inherently nonlinear. If the input and/or output signals from the PA are sampled using a self-assessment circuit, the bias to the PA can be controlled to maintain high efficiency averaged over time. We will show how fast dynamic digitally-controlled biasing (through an FPGA) can linearize the PA to some degree. In addition, we show how tuning networks can be added to the PA to change the mode of operation from A to E depending on the demands on linearity, and as determined by the input signal. All the experiments are conducted at 10GHz with a signal bandwidth of a few MHz. Simulations using Agilent ADS with pre-measured PA AM-PM and AM-AM characteristics agree well with measured results and will be discussed. Finally, when adding intelligence to any component, complexity necessarily increases and usually the power consumption increases. The goal of this work is to show that the power consumption can be decreased, while increasing functionality of a component. For example, while varying the output power over 5-10dB, with bias dynamically adjusted to maintain efficiency, the average efficiency is increased from 40 to over 60 percent for a uniform power probability distribution function. The optimal PA efficiency is reduced by only a few percent when adding the intelligent circuitry (feedback loop with digitally-controlled DC-DC converter). The necessary trade-off in circuit size and complexity will be discussed.

Session C1, 08:55 – Wed.

SIGNALS AND SYSTEMS

Chair: J. Krolik

OPEN-LOOP TRACKING DURING CRITICAL MISSION PHASES

Sami Asmar, Douglas Johnston

Jet Propulsion Laboratory, 4800 Oak Grove Dr, Pasadena, CA 91109

Planetary probes can encounter a mission scenario where the communication is not favorable during critical maneuvers or emergencies. These can include launch, initial acquisition, landing, trajectory corrections, spacecraft safing, etc. Communication challenges can include sub-optimum pointing of the probes' antenna, sub-optimum transmission power, solar plasma interference, atmospheric and ring particle interference, spacecraft spin, and highly dynamic interactions with planets during encounters; all of which prevent locking on the signal using closed loop receivers, and subsequent extraction of telemetry. Recent examples of these scenarios with spacecraft included the loss of Mars Observer, the characterization of the early nutation of Ulysses, the Mars Pathfinder and Mars Exploration Rovers Entry, Descent, and Landing, and the Cassini Saturn Orbit Insertion.

Since the loss of Mars Observer and Mars Climate Orbiter, NASA has mandated that unless precluded by solar system obstacles, a spacecraft should be configured to allow real time telemetry during critical events. Utilizing the open loop Radio Science Receivers of the Deep Space Network has enabled missions to receive valuable information during these critical times when normal telemetry modes are not feasible. Several sets of specialized software have been developed to help track spacecrafts in these conditions. Real-time detection of signals as weak as -3dB was possible during the Cassini Saturn Orbit Insertion, while unmodeled frequency changes with accelerations over 20 Hz/s^2 were tracked during the MER landings.

This paper will describe the capabilities of the current open-loop tracking mechanisms used, and highlight interesting cases, as examples, such as the critical communications for the Mars rovers and Saturn Orbit Insertion and describe the ongoing preparation for radio tracking of the Huygens probe at (non-DSN) radio telescopes.

BLIND DEMODULATION OF CONTINUOUS-PHASE MINIMUM-SHIFT-KEYED SIGNALS IN THE VERY LOW FREQUENCY (3-30 KHZ) BAND

Robert C. Moore, Umran S. Inan
STAR Laboratory, Stanford University, Stanford, California, USA

It is well-known that electromagnetic waves in the Very Low Frequency (VLF, 3-30 kHz) band can propagate to large distances around the globe in the Earth-ionosphere waveguide suffering low attenuation rates (1 dB/Mm). For this reason, navies around the world employ high-powered 200-baud MSK-modulated VLF transmitters for the purposes of communications with submarines and surface ships. These VLF signals are sensitive to conductivity changes in the lower ionosphere and upper mesosphere, caused by both natural (e.g. electron precipitation) and man-made (e.g. HF heating) events. Changes to localized regions of ionospheric conductivity between transmitter and receiver can scatter the subionospherically-propagating wave and produce measurable deviations in both the amplitude and the phase of the signal as it is measured at the receiver.

Stanford University operates 20 VLF receivers world-wide that acquire amplitude and phase data, tracking at least 6 narrowband VLF transmitters at once, and transfer the data back to Stanford over the Internet on a nightly basis. Even in the VLF frequency range retrieval of the wideband waveform of the signal is not feasible due to Internet bandwidth limitations, and it is thus desirable to demodulate the 200-baud MSK-modulated signals in near-real-time, and extract both the amplitude and phase. Extraction of signal amplitude can be achieved with simple digital filtering. However, while the MSK modulation is seen, in this context, as a linear advance or retreat in phase by 90 over a 5 millisecond period, the ionospheric phase is seen as the true phase of the transmitted signal in the absence of the MSK modulation. For this reason, it is necessary to first estimate the imposed phase trellis, subtract it from the received phase signal, and average the resultant phase to the desired output data rate.

In order to extract ionospheric phase data from the MSK-modulated signal, a new real-time MSK-demodulation algorithm has been developed. In this paper, we describe this new algorithm and analyze its effectiveness under different signal-to-noise ratio conditions. One of the challenges in this type of analysis is the fact that the ambient noise in the VLF band is highly impulsive, and cannot be modeled as Gaussian. For our purposes, we use a noise model based on measured spectral and statistical properties of the VLF band.

SIMULATION OF PCS TRAFFIC LOADING AND INTERFERENCE DUE TO CELL DAMAGE OR FAILURE

Riley, T.J., Rusyn, T. L.

US Department of Commerce, National Telecommunications and Information Administration, Institute for Telecommunication Sciences

While cellular systems offer an attractive and necessary form of data and voice communications following a natural or man-made disaster, the system itself is not immune to damage. As base stations are removed from service, the traffic load patterns are altered and the resultant system performance and availability is negatively affected. In addition to the loss of base stations, as the availability of the existing land-line infrastructure declines, more users migrate to wireless communications. As is the nature of any emergency, the need for communication increases beyond levels experienced during non-emergency periods. Using a self-interference model developed at the Institute for Telecommunication Sciences (ITS), the effects of system damage, load shifting, and increased traffic, can be studied, allowing emergency service providers to anticipate system availability and the need for supplemental emergency communications equipment.

The model consists of an hexagonal array of circular cells with a base station positioned in the center of each cell and a random number of mobile stations randomly positioned throughout each cell. As base stations are removed from operation, the mobile stations are picked up by the remaining base stations. Additional mobile users may be added and their locations can be changed to reflect the nature of the emergency. The change in the aggregate air-interface spectrum is monitored and the resultant signal to interference (C/I) values are used to determine the change in service quality and the probability of service availability. Any number of scenarios can be developed, depending on the configuration of the system under study and the level of detail desired.

Since the model produces a cumulative baseband signal for both the forward and reverse directions, it can be used in both hardware and software simulations. Predicted C/I values can be used in software-based network models to anticipate system limitations, traffic bottlenecks, and the probability of overall system failure. The baseband signal produced can be used to generate a simulated traffic signal for the testing and evaluation of commercial equipment.

1.1 1.3 GHZ , FRACTIONAL DELTA-SIGMA SYNTHESIZER USING FPGA

Yousefi, L.¹, Banai, A.²

¹Electrical Engineer, Department of EE , Sharif University of Technology , Tehran , Iran

²Assistant Professor, Department of EE , Sharif University of Technology , Tehran , Iran

This paper introduces a new method for implementation of Fractional-N Delta-Sigma synthesizers. In this method, the delta-sigma modulator has been implemented in a FPGA IC. FPGA ICs have programmable hardware ,so they can easily be used to implement and compare various structures .

First, the phase noise of a fractional-N synthesizer using n-order Delta-Sigma modulator to control the divide ratio is calculated and it is shown theoretically that as the order of modulator increases the low frequency phase noise decreases. Then three different structures of Delta-Sigma modulators including 1st order , 2nd order and Mash 1-1-1 are implemented in a 1.1-1.3 GHz fractional synthesizer. The channel spacing is selected as 250 KHz but any smaller value can be implemented easily. Measurements verify the theoretical concepts about the influence of the order of the structure on the synthesizer phase noise.

The experimental results are exhibited and summarized and these results confirm the theoretical results too. These practical measurements show, the use of high order modulators in fractional-N synthesizer can decrease low frequency phase noise down to 90 dBc/Hz in the offset frequency of 100 Hz from the carrier.

One advantage of this design is that structures that can be implemented and measured on this board are not limited to the above structures. Any kind of structure being used to control the divide ratio in a fractional synthesizer can be implemented and tested by this board, so one of the most important use of this board is to test new designed structures before implementing them in an IC package.

Another advantage of this design, if used as a common fractional synthesizer in a system, is its possibility to be updated to any new structure that may be introduced for fractional synthesizers in the future thanks to the on board programming of FPGA IC.

Session D1, 13:35 – Thurs.

**TERAHERTZ TECHNOLOGY:
SOURCES, IMAGES AND
APPLICATIONS**

Co-Chairs: A. Fathy, J. Papapolymerou

SUBMILLIMETER WAVE OSCILLATOR

Alexeff, I

Department of Electrical and Computer Engineering, University of Tennessee, Knoxville, TN 37996, USA

We have developed an electrostatic analog [1,2], to the Gyrotron maser that has operated at one THz [3]. Our device, the Orbitron, operates by placing electrons in orbit around a positively - charged wire. The basic advantage of this device over the Gyrotron maser is that the electric fields can produce much higher orbital frequencies than the maser using conventional magnetic fields can produce. In addition, the electrostatic orbits are intrinsically unstable to the negative - mass instability, while the gyrotron must rely on relativistic effects (very - high voltage electrons) to operate. The device has been patented [4]. The basic advantages of this device over the Gyrotron Maser are :

1. No high magnetic field with superconducting magnet required. No magnet!
2. No high voltages and relativistic electrons required to achieve oscillation.
3. Higher frequencies intrinsically available due to the electric field configuration.

Operates at 1 THz.

The device apparently is quite efficient. A q - spoiled model had the central wire become incandescent when the RF emission was stopped. When the microwaves were being emitted, the wire became cold. Recent experiments overseas have confirmed the high efficiency [5].

References : [1] Victor Ganatstein and Igor Alexeff, "High - Power Microwave Sources", Artech House, 685 Canton Street, Norwood, MA 02062, 1987, Chapters 7, 8.[2] Igor Alexeff and Fred Dyer, "Millimeter Microwave Emission from a maser by use of plasma - produced electrons orbiting a positively - charged wire", Phys. Rev. Letters vol. 45, pp. 351 - 354, 1980.[3] Igor Alexeff et. al., "Orbitron operation at 1 THz", International Journal of Infrared and Millimeter Waves, Vol. 6, No. 7, pp. 481-482, 1985.[4] USA Patent 4 459 511.[5] Private communication, J. Felsteiner, Technion, Israel.

MICROFABRICATED TRAVELING WAVE TUBES FOR THZ REGIME RADIATION SOURCES

Welter, J.D.¹, Booske, J.H.¹, Bhattacharjee, S.¹,
Limbach, S.¹, Jiang, H.¹, Genack, M.¹,
van der Weide, D.W.¹, Sengele, S.¹, Kory, C.L.²,
Ives, R.L.², Read, M.E.²

¹Electrical and Computer Engineering, University of Wisconsin,
Madison, WI 53706

²Calabazas Creek Research, Inc., 20937 Comer Drive, Saratoga,
CA 95070

The Terahertz (THz) and sub-THz regions of the electromagnetic spectrum (approximately 100 to 3000 GHz in frequency or 0.1 to 3.0 mm free space wavelength) have enormous potential for advanced communications, radar, imaging, spectroscopy, trace chemical detection, surveillance, medical imaging and space and biological research. The critical barrier to full exploitation of this frequency band is a lack of compact, powerful (1 to 1000 mW) coherent radiation sources. Suitable solutions should be efficient, frequency agile ($\geq 1\%$ instantaneous bandwidth), compact, and relatively inexpensive. Efficient generation of significant power at these frequencies is a serious challenge for solid state electronics, due to charge carrier mobility limitations. In principle, slow wave vacuum devices (e.g., traveling wave tubes or klystrons) should provide attractive opportunities. For example, the mobility of collisionless electrons in a vacuum is extremely high. However, conventional fabrication methods can not reliably manufacture the small circuit dimensions required at these high frequencies.

We are investigating the prospects for adopting MEMS technologies to fabricate THz regime vacuum traveling wave tubes (TWTs). TWTs offer a much-needed amplifier technology with considerable bandwidth, they are more tolerant of circuit ohmic losses than klystrons, and they can be operated as both oscillators and amplifiers. The folded waveguide (FWG) slow wave circuit has been selected as one which offers attractive electronic characteristics (significant bandwidth and interaction impedance) while remaining readily compatible with planar microfabrication techniques. Recent achievements will be discussed including computational evaluation of THz TWT oscillators and amplifier conceptual designs. A novel adaptation of the conventional FWG circuit in which a waveguide gap replaces the conventional "beam tunnel" has been shown to be a viable, easily-fabricated means to allow for passage of the electron beam. We have also completed preliminary experimental evaluation of several microfabrication technologies, including x-ray LIGA, UV LIGA, and silicon deep reactive ion etching (DRIE). Of these three, DRIE offers the greatest appeal in terms of ease, speed, and precision of fabrication.

IMAGING IN THE THZ: TECHNOLOGY AND APPLICATIONS

Rosker, M. J.

DARPA/MTO, 3701 N. Fairfax Drive, Arlington, VA 22203-1714

"Since we have become accustomed to think of waves of electrical energy and light waves as forming component parts of a common spectrum, the attempt has often been made to extend our knowledge over the wide region which has separated the two phenomena and to bring the them closer together." [Rubens, H. Nichols, E. F., Phys. Rev. 4 (1897) 314-323]. More than a century after these words were written, the THz frequency band still remains the most immature and underutilized part of the electromagnetic spectrum. Recently, however, there has been considerable interest and renewed effort to close this so-called "THz Gap." This talk will discuss some of the potential applications for which the THz might be most useful and describes some of the key component developments which must be made in order to exploit the THz for commercial and government applications.

In particular, in my presentation the concept of THz imaging for remote sensing will be considered. Despite its generally limited atmospheric propagation, the THz spectrum has the potential to provide sensor information in IR-blind conditions (e.g., fog, rain, dust, smoke). Furthermore, THz imaging could offer clear advantages over conventional (i.e., MMW) all-weather imaging approaches. A current DARPA program, Terahertz Imaging Focal Plane Array Technology (TIFT), is focused on the development of such a class of sensors. Component technologies that are being addressed include high power sources, very sensitive detectors with wide dynamic range, antennas, and integration technologies. Such technologies stand not only to revolutionize THz imaging, but will also find wide applicability to other emerging THz applications.

TERAHERTZ PHOTONICS FOR IMAGING AND REMOTE SENSING

Herczfeld, P. R. , Li, Yifei

Center for Microwave-lightwave Engineering, Center for
Microwave-lightwave Engineering

The detection of concealed weapons and explosive hidden under clothing carried by terrorists is one of the most daunting problems facing the military and the civilian law enforcement personnel. Terahertz (THz) imaging, by virtue of its ability to penetrate materials and short wavelength (high resolution) is the most promising approach to address this problem. Terahertz frequencies fall in between the optical and millimeter wave domains of the electromagnetic spectrum, and there are no readily available techniques to generate low noise, frequency agile signals as required for imaging. To exploit the inherent advantages of THz imaging significant scientific and engineering breakthroughs are needed for the generation of THz signals. The extension of microwave photonics offers an ideal avenue for THz system development. This presentation concerns the design and related research for the development of optically generated THz sources for active illumination and for local oscillator applications, including a low loss optical distribution network. The fundamental approach of the evolving THz micro-system is comprised of three critical components; an efficient, high fidelity electro-optic microchip laser, a low loss fiberoptic/integrated optic distribution network and an optical to THz (O/THz) conversion module that includes 25 radiating elements on a chip. Each O/THz module is designed to radiate 50 mW of average (CW) power at .8 THz with an overall DC to THz efficiency of 2%. The micro-system is compact, lightweight, robust and scalable. The illuminator will be able to operate either in coherent or non-coherent mode. The frequency agility of the system is designed to be 10% of the carrier (THz) signal. The phase noise of the THz signal is designed to be -90dBc/Hz or lower, which is significant for coherent detection schemes. Finally, the micro-system is flexible and can be tailored to different applications. This approach has three significantly novel elements representing scientific and technological breakthroughs. These are: i. the imaging subsystem, that provides for high performance, flexibility and future improvements, ii. the high power, single mode microchip laser that generates the tunable, clean, low noise optical signals, and iii. the traveling photodetector that converts very efficiently the photons into electrons and millimeter waves, full details of the structure will be presented at the conference.

THZ TECHNOLOGY FOR OUTER AND 'INNER' SPACE

Peter H. Siegel^{1,2}¹California Institute of Technology, Division of Biology²Jet Propulsion Laboratory, Submm. Wave Adv. Tech. (SWAT)

After more than 30 years of niche applications in the space sciences area, the field of Terahertz Technology is entering a true Renaissance. While major strides continue to be made in submillimeter wave astronomy and spectroscopy, the past few years have seen an unprecedented expansion of terahertz applications, components and instruments. Broad popular interest in this unique frequency domain has emerged for the first time, spanning applications as diverse as biohazard detection and tumor recognition. Already there are groups around the world who have applied specialized Terahertz techniques to disease diagnostics [1], recognition of protein structural states [2], monitoring of receptor binding [3], performing label-free DNA sequencing [4] and visualizing contrast in otherwise uniform tissue [5]. A commercial terahertz imaging system has recently started tests in a hospital environment [1] and new high sensitivity imagers with much deeper penetration into tissue have begun to emerge [6]. Solicitations for more sophisticated instruments and enabling terahertz components have filtered into US agency proposal calls from DoD and NASA, to NSF and NIH, and many new research groups have sprung up, both in this country and in Europe and Asia. This talk will broadly survey terahertz technology from its cradle applications in space science and spectroscopy to more recent biomedical and chemical uses.

References: [1] R.M. Woodward, V.P. Wallace, R.J. Pye, B.E. Cole, D.D. Arnone, E.H. Linfield and M. Pepper, "Terahertz Pulse Imaging of ex vivo Basal Cell Carcinoma," *J. of Inv. Dermatology*, vol. 120, no. 1, Jan. 2003, pp. 72-78. [2] A. Markelz, S. Whitmore, J. Hillebrecht and R. Birge, "THz time domain spectroscopy of bimolecular conformational modes," *Physics in Medicine and Biology*, vol. 47, no. 21, 7 Nov. 2002, pp.3797-3805. [3] S.P. Micken, A. Menikhu, H. Liu, C.A. Mannella, R. MacColl, D. Abbott, J. Munch and X-C Zhang, "Label-free bioaffinity detection using terahertz technology," *Physics in Medicine and Biology*, vol. 47, no. 21, 7 Nov. 2002, pp.3789-3795. [4] P. Haring Bolivar, M. Brucherseifer, M. Nagel, H. Kurz, A. Bosserhoff and R. Buttner, "Label-free probing of genes by time domain terahertz sensing," *Physics in Medicine and Biology*, vol. 47, no. 21, 7 Nov. 2002, pp.3815-3821. [5] K.J. Seibert, T. Loffler, H. Quast, M. Thomson, T. Bauer, R. Leonhardt, S. Czasch and H.G. Roskos, "All-optoelectronic continuous wave THz imaging for biomedical applications," *Physics in Medicine and Biology*, vol. 47, no. 21, 7 Nov. 2002, pp.3743-3748. [6] P.H. Siegel and R.J. Dengler, "Terahertz Heterodyne Imager for Biomedical Applications," *SPIE Conf. on THz and GHz Electronics and Photonics III*, vol. 5354, San Jose, CA, Jan 25-26, 2004.

DEVELOPMENT OF SUBMILLIMETER-WAVE REFLECTOMETERS FOR TERAHERTZ COMPONENTS AND SYSTEMS

Weikle, II, R.M.¹, Liu, Z.¹, Crowe, T.W.¹,
Lichtenberger, A.W.¹, Ulker, S.²

¹Department of Electrical and Comp. Eng., University of Virginia,
Charlottesville. VA 22904

²Girne American University, P.O. Box 5 Karmi Campus,
Karaoglanoglu, Kyrenia/North Cyprus

Scattering parameter measurements based on vector network analysis have played a critical role in the development of modern microwave and millimeter-wave components. Unfortunately, commercial network analyzers are typically available only up to W-band (75 to 110 GHz), with extensions to higher frequencies being both expensive and cumbersome. Over the past several years, a number of investigators have explored alternatives to the traditional four-port network analyzer based on the vector voltmeter. Much of this work has been motivated by the need to characterize new devices and components that are capable of operating far beyond W-band as well as to measure the properties of materials in the submillimeter-wave range.

This paper focuses on research at the University of Virginia aimed at developing six-port reflectometers for scattering parameter measurements in the submillimeter-wave band. The six-port architecture is attractive because it requires only a passive, linear network and four power detectors. The primary drawback of this approach, however, is the requirement for an additional calibration step and a more complex data processing algorithm. In this work, the passive network is realized with a single section of waveguide that is coupled to Schottky diode detectors through an ensemble of E-plane waveguide probes. In essence, the probes sample the standing wave amplitude in the guide and the complex reflection coefficient is calculated through a series of bilinear transforms. The Schottky detectors used in this work are discrete, planar GaAs devices that are flip-chip mounted to quartz probe circuits. These circuits include a broadband waveguide probe, low-pass stepped-impedance filter, and dc return-to-ground. Calibration of the reflectometer is done using a custom-fabricated sliding load and a series of offset waveguide short-circuits. The design and performance of two prototype reflectometers operating in the WR-10 band (75 to 110 GHz) and WR-4 band (270 to 340 GHz) are described and compared to results obtained from commercially available instruments. In addition, current efforts to integrate the reflectometer, apply it to two-port measurements, and extend the operating frequency further into the submillimeter-wave region will be discussed.

Session D2, 08:15 – Fri.

**TRENDS IN OPTICS AND ULTRA-
WIDEBAND TECHNOLOGY**

Co-Chairs: P. Herczfeld, L.W. Pearson

OPTIMUM PULSE ENERGY IN AN ULTRAWIDEBAND COMMUNICATIONS SYSTEM SUBJECT TO PART 15 LIMITS

Venkatesh Seetharam*, L. W. Pearson, Carl W. Baum
Holcombe Department of Electrical and Computer Engineering,
Clemson University, Clemson, SC 29634-0915

The FCCs recent approval of UWB underlay communications systems subject to Part 15 radiation limitations poses a new point of view for transmitter design. Traditionally, transmitter power limitations are defined in terms of average power delivered to the input port of the antenna through which the system radiates. In contrast, Part 15 specifies the total power in the radiated field. Thus, the new situation requires one who wishes to optimize the power radiated by an UWB transmitter to take into account the frequency response of the transmit antenna as well as the pulse source. One would adjust the spectral distribution of the source to act in concert with the antenna to provide a flat radiated spectrum that fits snugly within the bounds of the Part 15 template.

We present a design approach for a UWB transmitter, taking into account the radiated field limit as the FCC defines it. Specifically, we employ a fast impulse generator to produce a quasi-Gaussian pulse in the transmitter. A transversal filter follows the pulse source, and the output of the filter is delivered to the transmitting antenna. The filter allows the coloration of the impulse source so that the *radiated* spectrum is nearly flat over the operating bandwidth. The powers are quite low in such a system, and there is no need to be unduly concerned about losses internal to the pulser and filter. Indeed, at least one attenuator is likely to be present to set the final output power in such a system.

We have implemented such a filter using microstrip fabrication. We have operated it with an off-the-shelf instrumentation pulser and delivered power to an electrically short monopole antenna, which is known to act as a differentiator. We obtain sensibly flat frequency response over a frequency range from 5.1 to 8.3 GHz. The Part 15 template specifies -41.3 dBm/MHz maximum EIRP over this band. Thus we are able to radiate .23 mW average power, while remaining within the template. The filter design employed limits the ratio of upper to lower frequency to a value of 1.63. This filter design consequently could yield a filter between 6.5 and 10.6 GHz. Such a filter would provide radiated power of .30 mW average power. We report the design and detailed results in this presentation.

DEVELOPMENTS OF A HIGH RESOLUTION SHORT RANGE SEE THROUGH WALLS UWB RADARS

Yang, Y., Fathy, A., Abidi, M.

the Electrical and Computer Engineering Department, University of Tennessee, Knoxville, TN 37996

Today's Army and the future Army must be prepared to fight in a new war zone with the overmatching operational capability that it has brought to the mobile battlefield. The challenge is to design and field advance system concepts using the latest technologies that will give soldiers an advantage in this new battlefield: the urban terrain. One such area is C4ISR technology. Successful tactical operations in MOUT (Military Operations on Urban Terrain) conditions will require a significant extension of C4ISR capabilities to provide commanders with instantaneous, precise information (measured in feet, not meters) on the 3D location and disposition of friendly, threat, and noncombatant personnel. In urban warfare scenario, door-to-door searches with possible enemy engagement are inevitable. It is desired to provide a new and enhanced situation awareness capability that would allow soldiers to know if and where people are located inside a building before entering, therefore potentially preventing death and injury.

The DoDs in most of the civilized nations have funded significant number of high tech solutions for problems facing their military forces. Many of these solutions have been effective for long-range mass destruction but have not been applicable for close-in combat operations in the streets. Our goal is to convert high-tech capabilities into cost effective tools to help soldiers do their jobs better and safer. Surveillance systems presently used by army make extensive use of television, infrared and other line-of-sight-surveillance hardware. However, these systems cannot tell what is happening on the other side of a wall, behind bushes, or around the corner. Our objective is to develop a new sensor (radar), technology developed by the DoD for missile warhead fusing. This small, lightweight, low power radar is based upon the fact that microwave frequencies can be optimized to penetrate non-metallic materials. This new capability can provide information about what is in a ceiling or floor or on the other side of a wall.

What is needed is a means to generate high quality images through walls to identify potential threat. This mandates the development of a special type of radar with the ability to detect targets through relatively high-density materials such as reinforced concrete, concrete block, sheetrock, brick, wood, plastic, tile, and fiberglass. A very promising and novel approach to address this concern is to use short-range impulse radar technology that utilizes time domain, and ultra-wide band signals. In this paper, we will present our latest results of our program to develop the basic building blocks of the see-through-walls radars.

DESIGN OF A LOW-POWER WIDE-LOCKING-RANGE VOLTAGE-CONTROLLED OSCILLATOR FOR COUPLED OSCILLATOR ARRAYS

Tompkins, C. M.¹, Pearson, L. W.¹, Pogorzelski, R. J.²

¹Holcombe Department of Electrical and Computer Engineering, Clemson University, Clemson, SC 29634-0915

²Jet Propulsion Laboratory, California Institute of Technology, Pasadena, CA 91109

Coupled oscillator arrays (COAs) have been introduced as a low cost method to achieve the appropriate phase shift for phased array applications. For many applications, including space deployment, power limitations are an important criterion. For good COA performance, it is important to fabricate individual oscillator cells with wide locking range. The design objective was to fabricate a three-element COA with S-band oscillators operating at 10mW input power and a $\pm 5\%$ inter-element locking range.

The design process involved choosing an appropriate transistor and oscillator structure, optimizing the design for wide locking range, and verifying the requirements on tuning. In conventional oscillator design, it is desired in oscillator designs to have high-Q resonant structures to minimize the phase noise, but high-Q structures have a relatively small locking range. To achieve a large locking range, an oscillator requires a low-Q resonant structure. In the design process, this was accomplished by performing an optimization to minimize the slope of the phase of the oscillator open-loop gain.

The oscillator design included a varactor to achieve the desired tuning of the voltage controlled oscillator. After one iteration of the design, the value of capacitance was varied over the necessary range, and the oscillation frequency and phase slope were analyzed to verify that the oscillator still operated as desired. If the phase slope changed too drastically upon tuning, then the optimization was performed again with a new starting point.

After the circuit design met the desired specifications, a three-element array was fabricated. Each oscillator operated at a bias of 1.5V and about 5-6mA, which corresponds to 7.5-9.0mW of input power. Each oscillator also required a tuning voltage of 2-15V with current on the order of a few μ A. The oscillators operated from 2.0-2.3GHz with an inter-element locking range measured as high as 5.2%.

CORRELATION OF LASER DIODE TWO AND ONE-TONE TESTS TO MULTICHANNEL COMPOSITE TESTS

Ernest M. Kim^{1,2}, Mikaya L. D. Lumori¹, Li Wei³

¹University of San Diego, San Diego, CA 92110

²Lightwave Solutions, Inc., San Diego, CA 92126

³Wilfrid Laurier University, Ontario, Canada N2L 3C5

Cable Television transmission has migrated to the use of highly linear fiber optic transmitters and receivers for transporting broadband video and data signals to customer neighborhoods. In order to test the Carrier-to-Noise Ratio (CNR), Composite Second Order Distortion, and Composite Third Order Distortion, a multichannel signal generator (such as the one manufactured by Matrix Corporation) is used. The multichannel signal generator allows testing with 79 channels and can be used to characterize laser diode linearity performance for transmitter designs. Unfortunately, multichannel signal generators are very expensive to have as standard test equipment in the manufacturing environment.

In order to reduce the equipment cost for laser linearity tests, two-tone and one-tone testing schemes have been applied to determine second-order distortions and compared to standard multi channel composite distortion results. Results show that second order distortions tested by both two-tone and one-tone tests correlate with result composite distortions measured with the use of a multichannel signal generator. Fifteen lasers were tested with the methods outlined.

Proper equivalent Optical Modulation Indices (OMIs) must be used when comparing the approximately 3.5

Second order distortions tested by both two-tone and one-tone were shown to have very good correlation with the multichannel signal generator method. The maximum difference between multichannel signal generator method and the two-tone or one-tone was 3.5dB. The average difference was about 1 dB.

OBTAINING THE UNKNOWN INDEX OF OPTICAL WAVEGUIDE BY USING GENETIC ALGORITHM BASED ON FINITE DIFFERENCE BEAM PROPAGATION METHOD

Reza Mohammadi-Baghaee, Hadi Aliakbarian, Reza Faraji-Dana, Nasrin Hojjat

University of Tehran, ECE Dept., Faculty of Eng., Center of Excellence on Applied Electromagnetic Systems, North Kargar st., Tehran, Iran

In this paper we use FD-BPM to propagate a given incident field that launched in to geometry along the structure that is z-invariant. This wave can be expanded in the mode of this structure. We use only the dominant mode of structure. But the indexes of any regions in the optical waveguide are unknown. It means that we have unknown package. For defining the index of the structure we use genetic algorithm (GA) and finite difference beam propagation method (FD-BPM). At first, a given incident field are measured completely. After this measurement of initial field we propagate it a long the waveguide. Then, the field is reached to the end of waveguide. By detecting the final field and evaluate this field, we determine the number of regions and estimate the index of any regions. By using this initial assumption the GA will start to generate the indexes in any regions. In any generation of indexes, the once initial field launched in to a structure and is propagated along the structure by using FD-BPM. After detecting at the end of waveguide, it compares with the first one that stated above. After comparison and define the error between them, this process will be continued to define the index in any regions. We use this method for defining the distribution of index at the cross section of the waveguide. But in this manner the estimation of index distribution has been occurred at the first step. Comparison between final fields in any steps with the one at first helps to define the quantity of index distribution in any points. Thus, using this method helps to define the parameters of the unknown optical structure only by knowing the initial field as input of the system and the final field as out put of the system. Finally, we examine our solution for indexes of the structure with original one, and a good agreement has been found.

Session E1, 13:35 – Wed.

**HIGH-POWER
ELECTROMAGNETICS**

Co-Chairs: C. Ropiak, D. Erricolo

RECIPROCITY, ENERGY, AND NORMS FRO PROPAGA-
TION ON NONUNIFORM MULTICONDUCTOR TRANSMIS-
SION LINES

Carl E. Baum

Air Force Research Laboratory/DEHP

Reciprocity, Energy, and Norms for Propagation on Nonuniform Multi-
conductor Transmission Lines

Carl E. Baum Air Force Research Laboratory Directed Energy Direc-
torate 3550 Aberdeen Ave SE Kirtland AFB, NM 87117-5776 USA

The general solution of propagation on nonuniform multiconductor transmission lines is described by product integrals which may be difficult to evaluate except in numerical form. However, the conservation laws of electromagnetics concerning reciprocity and energy can be used to determine some of the analytic properties of these product integrals. Special results occur when the transmission lines are lossless. An N -conductor (plus reference) nonuniform multiconductor line (NMTL) is characterized by the telegrapher equations. The vectors have N components and the matrices are $N \times N$. These can in turn be combined into a single first-order differential equations with $2N \times 2N$ matrices (supermatrices) in various equivalent forms. Substituting a $2N \times 2N$ matrix (the supermatrizant) for the voltage/current vectors (with sources neglected) defines a first order homogeneous supermatrizant differential equation. This equation has a solution in terms of the product integral [J.D. Dollard and C.N. Friedman, Product Integration with Application to Differential Equations, Addison-Wesley, 1979.] First we consider reciprocity between two solutions on the NMTL, leading to a concept of differential reciprocity, applicable at every cross section. Applying reciprocity to the product integral we find various constraints on the blocks of the supermatrizant. Considering next energy and power in both time and frequency domains we find results strikingly similar to those for electromagnetic fields. For the practical interesting case of lossless NMTLs there are special constraints on the supermatrizant blocks. For $s = j\omega$ no real power enters or leaves the NMTL (a form of Foster's theorem). Noting the relation of power to the 2-norm, we next obtain bounds on the blocks of the supermatrizant. Considering a previous paper [C.E. Baum, Electromagnetic Reciprocity and Energy Theorems for Free Space Including Sources Generalized to Numerous Theorems, to Combined Fields, and to Complex Frequency Domain, Mathematics Note 33, December 1973.], there are various reciprocity and energy theorems applicable to electromagnetic fields and sources in free space (or a lossless uniform isotropic medium). The present paper considers the application of such concepts to NMTLs, with various results found. Perhaps the list of such results can be extended.

A PROTOTYPE HIGH-VOLTAGE UWB TRANSMITTER

Everett G. Farr¹, Leland H. Bowen¹, Lanney M. Atchley¹
, Larry L. Altgilbers²

¹Farr Research, Inc., 614 Paseo Del Mar, NE, Albuquerque, NM,
87123

²U.S. Army / SMDC, 106 Wynn Dr., Huntsville, AL 35805

We describe here the early development of a high-voltage Ultra-Wideband (UWB) transmitter that combines a portable high-gain antenna and a fast-risetime triggered source. The device, which is currently in the early stages of development, integrates a compact triggered wave-erection Marx generator into the center support of a Collapsible Impulse Radiating Antenna (CIRA). The current version of the antenna (TX-1) must be deployed manually; however, a spring mechanism can be added to open the antenna automatically as it emerges from a housing. The Marx generator is a bipolar device with two outputs specifically designed for use on an Impulse Radiating Antenna (IRA).

For this project, we wanted an integrated UWB source and antenna that could be stored in as small a space as possible, and that could be deployed automatically. So a collapsible antenna similar to our CIRA-2 seemed appropriate. However, feeding such an antenna is a particular challenge. Normally an IRA includes a splitter balun that splits the signal from a 50-ohm source into two parallel 100-ohm cables, which are then connected in series at the feed point to drive the 200-ohm antenna. But such an arrangement is not practical in devices operating at high voltage within limited space, so we explored two options for avoiding the balun, a bipolar Marx generator and an unbalanced feed.

The first option for avoiding the balun was a bipolar Marx generator. This is just two identical Marx banks charged with equal and opposite polarities, timed to fire simultaneously, resulting in two equal and opposite outputs. We investigated this by building a prototype Bipolar Marx Generator that could demonstrate the principle. Our measurements showed a jitter of around 100 ps, which was a relatively small fraction of the risetime, so the device performed about as expected.

The second option for avoiding the balun was simply to use a single 50-ohm cable to drive the balanced 200-ohm antenna, resulting in an impedance mismatch, which we hoped would not be too severe. To test the theory, we built a scale model 46 cm (18 in) in diameter. This was a version of the standard IRA-2 without the splitter balun feed, driven with a single 50-ohm cable connected across the feed point. The results show that even with the mismatch at the feed point, the performance of the antenna was only modestly degraded at frequencies below about 12 GHz.

HIGH-POWER SCANNING WAVEGUIDE ARRAY

Carl E. Baum

Air Force Research Laboratory/DEHP

High-Power Scanning Waveguide Array

Carl E. Baum Air Force Research Laboratory Directed Energy Directorate 3550 Aberdeen Ave SE Kirtland AFB, NM 87117-5776 USA

Microwave antennas for hypoband (narrow band) operations are a well-established subject. For high-power application, with electric fields approaching breakdown in various media of interest, the subject is less well established. However, some basic techniques for radiating high-power microwaves (HPM) have been published in several papers. These have been summarized in a book [C. D. Taylor and D. V. Giri, High-Power Microwave Systems and Effects, Taylor Francis, 1994.] Among other things, these give techniques and canonical designs for HPM antenna systems (including waveguides) for pyramidal-horn fed reflector antennas with both high power and high gain. While these are quite appropriate HPM radiators, it is useful to consider other possible types for their potential advantages/disadvantages. Array antennas, while more complex, have the advantage of having less depth (and hence less volume) for the same total antenna aperture, and hence similar potential antenna gain. A common form of an array is formed by a set of slots in one or more rectangular waveguides. (However, small holes are not appropriate for high-power transmission through them.) Using the dispersive character of the lowest order waveguide mode (H_{1,0}) one can steer the antenna beam by changing the microwave frequency. Other types of guiding structures (e.g., dielectrics) have also been used for this purpose. However, for frequencies around a GHz the large size of the waveguides suggests that for low mass a hollow metal pipe has certain advantage. In [C.E. Baum, Some Features of Waveguide/Horn Design, Sensor and Simulation Note 314, November 1988.] I have discussed the division of a rectangular waveguide into a set of subguides by insertion of metal sheets parallel to the broad wall (and perpendicular to the electric field of the H_{1,0} mode) inside the waveguide and connecting to the side (narrow) walls. There, among other things, I suggested that this technique could be used to divide the power in the waveguide into N subguides which could be used to feed N array elements. This present paper expands on this in one form of such an array. So here we have a scanning waveguide array based on traditional principles, but extended into the high-power regime. When operated at a single frequency such an array merely compresses the antenna depth toward an aperture plane as compared to a standard horn-fed paraboloidal reflector. However, the array is a more complex structure. When operated with a frequency-agile source this array becomes an antenna with a beam which scans in one coordinate. The scanning rate depends on how fast the frequency can be shifted.

A HIGH-VOLTAGE UWB COUPLED-LINE DIRECTIONAL COUPLER

Farr, Everett G.¹, Atchley, Lanney M.¹, Lawry, Dean I.²
, Baum, Carl E.²

¹Farr Research, Inc., 614 Paseo Del Mar, NE, Albuquerque, NM,
87123

²AFRL / DE, 3550 Aberdeen Ave. SE, , Kirtland AFB, NM
87117-5776

Most UWB radar systems currently use two separate antennas for transmit and receive. If a single antenna could be used for both functions, a more compact and convenient radar system could be realized. We report here on the development of such a directional coupler.

The directional coupler developed here is based on two coupled parallel transmission lines. The four ports of the directional coupler are designated the Source, Through, Coupled, and Isolated Ports. When the Source Port is driven by a pulser, the Isolated Port sees, in theory, no signal until the backscattered signal returns. In practice, there is always leakage, so one goal of this design is to minimize the leakage from the Source Port to the Isolated Port. The signal at the Coupled Port is, in theory, a faithful replication of the returned signal for the round-trip transit time of the coupled lines.

The bandwidth of the coupler is determined by two factors. At the high end, the bandwidth is determined by the diameter of the coupled lines. At the low end, the bandwidth is determined by the length of the coupled lines.

We begin by providing the time domain equations that describe the circuit. We then demonstrate how to optimize the design to obtain the largest voltage into the scope.

We then built and tested two prototype designs that should be able to handle a short transient signal of 50 kV. We tested these two devices at low voltage, and found that they operated about as expected. The leakage signal at the Isolated Port was down by about 20 dB from the source signal driving the Source Port. In future designs we would hope to reduce the leakage signal to 40 dB down from the source signal.

We then used these one of these couplers in a radar measurement, using a fast low-voltage pulser, an IRA-3 antenna, and a fast sampling oscilloscope. We found that the field scattered from a corner reflector was readily apparent in the received signal.

TIME-DEPENDENT THREE-DIMENSIONAL ELEC-
TROMAGNETIC FIELDS GENERATED BY A REFLECTOR
IRA

Ira Kohlberg¹ , Isaac Chappell² , Hardev Singh³
, Harry Moore⁴

¹Institute for Defense Analyses, 4850 Mark Center Drive, Alexandria, VA 22311-1882

²Institute for Defense Analyses, 4850 Mark Center Drive, Alexandria, VA 22311-1882

³ARDEC, AMSTA-AR-CCL-D, Picatinny Arsenal, NJ 07806-5000

⁴ARDEC, AMSTA-AR-CCL-D, Picatinny Arsenal, NJ 07806-5000

TIME-DEPENDENT THREE-DIMENSIONAL
ELECTROMAGNETIC FIELDS GENERATED BY A REFLECTOR IRA

Ira Kohlberg and Isaac Chappell, Institute for Defense Analyses Hardev Singh and Harry Moore, Picatinny Arsenal

Abstract The reflector Impulse Radiating Antenna (IRA) produces an extremely large impulse radiated electric field on bore-sight at distances of the order of kilometers when the driving voltage source has a finite but extremely short risetime. For the ideal step function source a delta function radiated electric field is produced on axis. The radiated component varies as $(1/r)$ while the induction and electrostatic components vary inversely as the radius squared and cubed respectively. There are also other components of a reflector IRA that exist (e.g., the pre-pulse), but these are not considered in this paper. Users of an IRA need to be concerned with collateral effects at distances to the antenna where the induction and electrostatic components could be important. There is indeed a paucity of information in this arena in understanding how these fields affect systems. We have taken the first step in assessing collateral effects by deriving time dependent equations for the components of electric field in powers of $(1/r)$. We have developed explicit expressions for the fields as a function of polar angles, time, antenna dish size and source voltage waveform. From these results we can assess the ranges where unwanted collateral effects are important. For specified values of coordinates the electric field will be a function of time, and during the course of the transient will have a maximum value. From these results we develop three dimensional contours of range versus peak field. Parametric results as a function of risetime of the source voltage are presented.

Session E2, 15:15 – Wed.

ELECTROMAGNETIC EFFECTS

Co-Chairs: C.E. Baum, E.G. Farr

EVALUATION OF RISK OF IEMI FROM HPEM TO TELECOMMUNICATION NETWORKS

Boksiner, J, Chrysanthou, C

Network EMC, Safety, and Spectrum Management, Telcordia Technologies, Inc.

There is growing concern that High Power Electromagnetic (HPEM) sources can be used to create Intentional Electromagnetic Interference (IEMI) to electronic systems and equipment. See W.A. Radasky, C.E. Baum, M.W. Wik, *IEEE Transactions on Electromagnetic Compatibility*, **46**, 314-321, Aug. 2004 and companion articles for a recent review of research and standardization efforts in this area.

We are primarily concerned with the risk of disruption or damage from HPEM to the Public Telecommunications Network (wireline and wireless), and to ground-based assets of satellite telecommunication infrastructure. In general, interference to a single network element may not cause significant disruption of a telecommunication network. In order to cause significant disruption the ability to cause interference to multiple network elements, that are either collocated or geographically disbursed, may be required. In this context, a risk approach takes into consideration the fundamental physical constraints on the threat parameters such as size and directivity of the source as well as the location and purpose of the network elements.

Our overall approach of the risk evaluation is to work the problem backwards. Rather than analyzing an impact of a specific weapon, we work out the minimum combination of threat parameters needed to exceed equipment susceptibility thresholds. We consider the following threat parameters: Emitter size, gain, and directivity; Emitter power and frequency; Distance between weapon and target(s), intervening terrain and clutter; and Equipment installation and protection practices common in the telecommunication network.

In the US telecommunication network, the equipment generally has to meet stringent EMC requirements of Telcordia GR-1089-CORE. We estimate minimum levels of susceptibility of network equipment by analysis of EMC requirements, such as Telcordia GR-1089-CORE, and review of published HPEM test results. Similarly, we estimate the susceptibility of the ground-based satellite equipment by analysis of FCC and ITU-R Radio Regulations, manufacturer's specifications, and published test results.

The result of this analysis is the risk evaluation model that provides minimum combination of threat parameters needed to exceed equipment susceptibility thresholds for a selected set of network elements. This type of model can help network operators allocate the level of risk to the network from the HPEM threat.

THE PERFORMANCE OF RF DIGITAL CIRCUITS IN THE PRESENCE OF NOISE AND RF INTERFERENCE

Christian Fazi, Michael S Patterson
Army Research Laboratory, Adelphi, Md 20783

The Performance of RF Digital Circuits in the Presence of Noise and RF Interference

The progress made in silicon-germanium (SiGe) processing has led to a mini revolution in new high speed digital circuits. Some of these circuits are supporting GHz analog to digital conversion (ADC) functions which are getting closer to the rf input. Examples are 1.8 GHz cell phones with integrated GPS, GPS navigation receivers and time-frequency domain measurements. The newer generation of mobile communications relies on digital signal processing to increase receiver versatility and functionality. The key strategy of this software radio concept is the use of high speed analog to digital processing located as close to the rf input as possible, thereby replacing the mixing stages and baseband signal processing, eliminating further signal degradation due to losses in analog stages. For the first time since rf mixers were invented some 80 years ago, we are now seeing rf-front ends without mixers. Such a radical change would have been unheard of just a few years ago. The concern now is whether the new rf digital front-ends are inferior or superior to the conventional rf analog ones. The most important qualities of a superior radio are the signal to noise/distortion ratios and its dynamic range. The dynamic range is the useful operating range between the noise floor and the level of rf interference causing intermodulation distortion products (IMDs) to exceed the noise. In this paper we review the rf front-end parameters and infer the likely dynamic range values associated with digital rf front-ends as compared to conventional mixers. If rf mixers have been shown to have the highest dynamic range among rf circuits, is it realistic to assume that ADCs can equal or exceed this level of performance? This issue will likely be debated for some time and will bring back memories of similar questions raised in the past, are solid state devices better than vacuum tubes?

DOD ELECTROMAGNETIC ENVIRONMENTAL EFFECTS AND SPECTRUM MANAGEMENT TESTING POLICY

Golliday, C. L., Satyapal, S.

Institute for Defense Analyses, 4850 Mark Center Drive, Alexandria, VA 22311-1882

Emphasis in the US Department of Defense (DoD) on Net Centric Warfare (NCW) involves greater reliance on the use of the Electromagnetic Spectrum (EM) spectrum at a time when market forces are steering national policy makers to reallocate exclusive government/military portions of the EM spectrum to private use. Increased use of shrinking available spectrum presents Spectrum Management (SM) challenges and potential Electromagnetic Environmental Effects (E3) problems. Joint military operations could potentially have thousands of Communications-Electronics (C-E) systems operating in a confined geographic area presenting both SM and E3 challenges. Platforms are employing increasing amounts of onboard C-E equipment with increased equipment density, increased power levels, and increased bandwidths all contributing to the potential for E3 problems. Trends toward the use of Very High Scale Integrated Circuitry (VHSIC) and nanotechnology using lower threshold voltages and currents and toward the use of composite building materials with loss of conductive shielding effects also increase the potential for E3 problems. US and coalition security forces with their systems being deployed in more regions across the globe present SM challenges. Within the DoD, the Director of Operational Testing and Evaluation (DOTE) is working to increase the awareness of this problem and to ensure that DoD policy, regulations, and testing procedures concerning E3 and SM are up to date and adequately enforced. A significant challenge in the DoD systems acquisition and operational communities is ensuring that program managers and operational commanders are aware of the impacts of E3 and international spectrum regulations on their acquisition programs and fielded systems. Another challenge is anticipating advances in electro-technology, understanding their E3 and SM impacts, and ensuring that policies, regulations, testing procedures are kept current with respect to these advances. This paper presents the view of E3 and SM from within the DoD, how the DoD is organized to address E3 and SM issues including the role of testing, and challenges facing the DoD in these areas.

NONLINEAR DYNAMICS AND RADIOFREQUENCY INTERFERENCE

Christopher B. Wallace

Northrop Grumman Mission Systems

Wireless technologies are ubiquitous in modern life. As demand grows, the electromagnetic spectrum becomes more crowded thereby stimulating production of new waveforms and information transmission schemes to maximally employ allotted bandwidth, provide basic communication security with reliability, and, hopefully, minimize unwanted interference. Unfortunately, more sophisticated waveforms may come with an unintended price new physical, nonlinear dynamics that can corrupt desired electronic information flow.

The fundamental driven nonlinear element we are concerned with in any particular RF interference phenomena is the semiconductor p/n junction. Associated with it are resistances, inductances, self-capacitance, and external capacitances associated with other elements of the circuit or device of which it is a part. Physical insight comes from understanding effective junction current and voltage behavior and the self-consistent change in boundary conditions associated with the externally imposed RF interaction. Electromagnetic interference response results from voltage sources driving semiconductor devices interacting with complex impedances. The nonlinear semiconductor component response is the basic mechanism by which system level effects are induced.

The purpose of the present paper is to provide an overview, with examples (experimental, computational) of interesting nonlinear behavior introduced by various simple and complex waveforms in electronic components and circuits. This includes periodic, quasiperiodic, and chaotic responses. Measurement and diagnostic capabilities provided by modern commercial instrumentation are exploited to capture both pulsed and continuous induced electronic responses. Data analysis techniques that permit key metrics to be extracted from data will also be described and illustrated, while the robust interplay now possible between theory and numerical simulation provides meaningful explanation of the observed behavior.

EXPERIMENTAL AND THEORETICAL STUDY OF DIGITAL CIRCUITS SUBJECT TO ELECTROMAGNETIC INTERFERENCE

Bayram, Y., Khan, Z.A., Volakis, J.L.

The Ohio State University, ElectroScience Laboratory, 1320 Kinnear Road, Columbus, OH,43212,USA

This work will present experimental and theoretical study of digital circuits exposed to Electromagnetic Interference. We will particularly study an inverter subject to RF interference. The primary goal of this study is to experimentally observe the effects of electromagnetic interference on time delay and logic characteristics of an inverter operating near GHz range. Besides, we will also validate the measurements with the existing theoretical approaches in the literature.

The typical approach to represent the ambient field coupling to interconnects is to employ distributed voltage and current sources along the interconnects derived via quasi-static analysis. In this work, we replace external field coupling with an equivalent voltage source channel adjacent to the inverter input and output signal traces. This configuration also accounts for the signal integrity effects due to the on-board cross coupling.

Numerical validation of the measurement requires either time-domain analysis with SPICE or mixed time-frequency domain analysis via harmonic balance method to tackle the non-linearity of the inverter. In this analysis, we break the whole problem into two parts: EM structure and Circuit structure. The former consists of the whole PCB structure including interconnects while the latter only contains the sources and the inverter. To analyze the EM structure, we employ multi-port approach. In other words, we represent the EM section with an N-port broadband S-parameter network. Then, the resulting S-parameter model is used in SPICE in conjunction with inverter SPICE model for time-domain analysis.

The S-parameter characterization of the circuit board is done with both PEEC (Partial Element Equivalent Circuit) via PCBMod (Simlab Product) and full wave analysis. The former does not include retardation effects; thus leading to less reliable characterization at higher frequencies. However, the latter produces well accurate results at the frequency range of interest.

As an alternative to S-parameter port modeling, we will also validate the measurements via harmonic balance method. To do so, we solve the EM-structure in frequency domain at the harmonics of the input signal while the circuit part is handled in time-domain via SPICE analysis. The results will be shown and a comparative study of the existing techniques will be presented.

COMPLEXITY REDUCTION VIA CONVERGENCE OF THE SUM-PRODUCT ALGORITHM FOR LDPC UNDER FADING CHANNELS

John, S.¹², Kwon, H.M.¹³

¹Wichita State University, 1845 Fairmount, Wichita, KS-67208

²Indian Institute of Technology of Kanpur, Kanpur, India.

³Senior Member IEEE

LDPC codes are proved to approach near-Shannon limit of channel capacity when the length is long enough. It is desirable to have very long block length when the coding efficiency is concerned. Also thanks to the inherent interleaver effect, long codes are less likely to be completely corrupted in deep fades and can thus avoid serious performance degradation. However, the practical block length is confined by the implementation complexity of LDPC decoder, which increases significantly with block length. In this paper we show that for short length, less sparse parity matrices the decoding complexity is almost independent of noise statistics and number of iterations, (i.e. convergence is faster for the short length Low Density Parity Check Codes under the different fading channels as compare to the long length Low Density Parity Check Codes). Simulation results show that after certain number of iterations the decoding complexity becomes constant and the bit decision can be made under both, AWGN and Rayleigh fading channels. In this paper we reveal some efficient techniques to reduce the complexity of the Sum-Product algorithm for the Low Density Parity Check Code under the AWGN and Rayleigh Fading Channels to achieve approximately same bit error rate as proposed by the Belief Propagation Algorithm. Decoder convergence is utilized to reduce the processing time for the decoding of the bit under the AWGN and Rayleigh Fading channels. We also propose that how the complex computation can be confined to overcome the overflow and underflow at the message passing points, i.e. Bit node to Check node and Check node to Bit node propagation paths, via decomposing the complex matrix to the real matrix. The simulation results also reveal the convergence of likelihood surfaces at the Bit Node to Check Node and Check Node to Bit Node and how the extrinsic information is passed to decode the bit. We observe the three types of error that occur at the different SNRs and the decoder behavior is changing as the SNR changes, We also propose that these errors can also be corrected by simple procedures, and hence Maximum likelihood rule for decoding the bit can also be supported to reduce the error in bits according to the SNR values and the convergence graph of the respective bit. This algorithm can be implemented in chip designing with less complexity and via the structured programming.

Session F1, 13:15 – Wed.

**ATMOSPHERIC EFFECTS ON
SIGNAL PROPAGATION**

Co-Chairs: L.T. Rogers, S.A. Fast

THE MARINE ATMOSPHERIC BOUNDARY LAYER EN-
TRAINMENT ZONE: A BREEDING GROUND FOR SURFACE
BASED RADIO FREQUENCY DUCTS

Marshall, R. E.¹, Burgess, E. H.¹, Rottier, J. R.²

¹NSWCDD, Dhalgren, VA

²Johns Hopkins University/Applied Physics Laboratory, Laurel,
MD

Well-mixed marine atmospheric boundary layers are separated from the free atmosphere by a typically stably stratified entrainment zone. The water vapor in the free atmosphere is typically less than that in the mixed layer below leading to a negative gradient of the water vapor mixing ratio in the entrainment zone. This combination of thermal and humidity gradients tends to produce negative gradients of modified refractivity in the entrainment zone. If the thermodynamic gradients are large enough, the entrainment zone negative modified refractivity gradient will be larger in magnitude than the positive gradient in the well-mixed surface layer leading to formation of a surface based duct.

This paper will present the results of an application of a parameterization for normalized entrainment zone thickness to an equation for the gradient of modified refractivity in terms of potential temperature (q) and water vapor mixing ratio (w).

It is shown that the gradient of modified radio refractivity (M) is approximately equal to 0.128 km^{-1} in the well-mixed layer. This leads to a simple relationship for the maximum duct height (D) possible for the existence of a surface based duct as a function of the difference in temperature and humidity across the entrainment zone.

Similarly it is shown that for the duct strength to increase in terms of M below the surface value (M_{sv}) for the same entrainment zone thermodynamic gradients, the duct height must decrease.

The implications of entrainment zone thickness on duct height, trapping frequency, critical elevation angle and skip zone dimensions are analyzed employing highly resolved marine atmospheric boundary layer profiles from the Persian Gulf and the California coast.

ESTIMATION OF RADIO REFRACTIVITY FROM RADAR
CLUTTER USING BAYESIAN MONTE CARLO ANALYSIS

Yardim, C., Gerstoft, P., Hodgkiss, W.S.

Marine Physical Laboratory, University of California, San Diego,
USA

In sea-borne radar applications the radio refractivity can vary considerably with both height and range, heavily affecting the propagation characteristics. One of the most extreme examples is the formation of an electromagnetic duct, where a horizontal or near-horizontal signal sent from a surface or low altitude source will end up being totally trapped within the duct. In such cases, the precise knowledge of the radio refractivity is essential in interpreting the returned radar signal.

This paper describes a Markov Chain Monte Carlo sampling approach for the estimation of not only the radio refractivity profiles from radar clutter but also the uncertainties in these estimates. Similar to the previous papers that worked on the Refractivity From Clutter (RFC) problem, it is based on the Bayesian formulation. The difference is that, instead of treating the problem as a global optimization problem, it uses unbiased Markov Chain Monte Carlo (MCMC) sampling techniques, like Metropolis and Gibbs sampling algorithms, to gather more accurate information about the uncertainties. Application of these techniques using an electromagnetic split-step fast fourier transform parabolic equation propagation model within a Bayesian framework can provide the true unbiased values of means, variances and posterior probability distributions of the estimated parameters. They are computed by taking multi-dimensional integrals of the posterior probability density (PPD), which can easily be accomplished by a MCMC sampling method. MCMC is selected because it provides unbiased sampling of the PPD, unlike global optimizers like genetic algorithm, which usually over-sample the peaks of the PPD and introduce a bias. Estimated parameters and their uncertainties are compared not only with the exhaustive search results but also with genetic algorithm results and helicopter refractivity profile measurements. Although MCMC is slower than global optimizers, the probability densities obtained by this method are closer to the true distributions.

SYNOPTIC, MESOSCALE AND DIURNAL IMPACTS ON EM TRAPPING CONDITIONS

Haack, T., Burk, S.D.

Naval Research Laboratory, Marine Meteorology Division, Monterey, CA, USA

Ducting of electromagnetic (EM) energy is often associated with abrupt gradients that tend to occur in temperature and moisture at the top of the marine atmospheric boundary layer (MABL). We utilize the Navys globally re-locatable mesoscale model *COAMPSTM₁* to obtain the atmospheric forecasts necessary to analyze trends in EM ducting parameters for a variety of forcing regimes. In this study, the model has been setup over Wallops Island, Virginia and run for a continuous 6 weeks beginning 1 April 2000. High horizontal ($\delta x = 3$ km inner grid) and vertical ($\delta z = 43$ m in the MABL) resolutions are implemented to adequately represent details within a complex coastal environment. The forecasts encompass the time frame that data was collected for the Wallops 2000 MPME (Microwave Propagation Measurement Experiment) by fixed buoy, boat, radiosonde, rocketsonde and helicopter profiles. The buoy observations provide time series of the environmental variables used in the NPS Operational Evaporation Duct Model to give estimates of the evaporation duct height (EDH) based upon TOGA-COARE surface flux scaling parameters. These values are compared with the EDH predicted by COAMPS on a high-resolution ($\delta z = 1$ m) vertical grid using Monin-Obukhov similarity theory.

Statistics showing model-observed EDH bias and RMS error provide confidence in the model forecasts. At the buoy site, we examine time periods when the EDH reached the lower limit of 0 m or upper limit threshold of 40 m. Values within this range occurs 70% of the time and lie between 2-13 m in agreement with estimates given by Paulus (1984) for the thermally unstable regime (R.A. Paulus, Tech. Rep 966, NOSC prepared for NASC, Code 330). Eight periods (10%) are identified where the EDH reaches 40 m, which typically results from thermally stable conditions and low relative humidity. EDH values near 0 m occur the remaining 20% of the time as southeasterly flow advects warm, moist air into the area, tending to eliminate surface ducting and create subrefractive conditions. The 2D model-computed EDH fields are temporally averaged for the duration of the 6-week study period to elucidate regions of preferred ducting and subrefraction. These results will be shown at the conference.

¹ COAMPS is a trademark of the Naval Research Laboratory

FUSING OBSERVATIONS OF ATMOSPHERIC REFRACTIVITY WITH BACKGROUND FIELDS FROM A NUMERICAL WEATHER PREDICTION MODEL

Jablecki, M. C.¹, Rogers, L. T.¹, Hobbs, S. L.²

¹SPAWAR Systems Center 2858, San Diego, CA 92152-7385

²SPAWAR Systems Center 2711, San Diego, CA 92152-6193

The authors present a new approach for fusing observed modified refractivity, $M(z)$ where z is the height, with a background refractivity diagnosed from a numerical weather prediction (NWP) model. A key aspect of the approach is implementing a non-linear observation operator for handling differences between observed and modeled refractivity that are explained by vertical displacement as well as differences that can be characterized using linear methods.

The observation operator relies on a two-stage mapping. Let z be an array of height values. A Markov process is used to generate an array of perturbed heights z' . Thus $M(z')$ possesses random displacements with respect to $M(z)$. A second mapping takes the form of $M'(z') = M(z') + \epsilon$ where ϵ is too created via a Markov process. The random mappings $M(z) \rightarrow M'(z')$ can be generated *ad nauseum* and because of their Markov origins, an *a priori* probability (p_a) can be associated with each one. Out of an ensemble of these mappings, we choose the subset that provide "good" fits to the observed data when the background field at the location of the observation is mapped through them; all subset members are assumed to have identical experimental probabilities (p_e 's) that sum to 1. All other mappings (those outside of the subset) have $p_e = 0$. Assuming the *a posteriori* probability p_p is the product $p_p = p_a p_e$, it is clear that the mapping having the highest *a priori* probability that is in the subset of good fits is the MAP estimator.

The non-linear observation operator is inserted in the (otherwise) familiar minimum variance optimal interpolation (MVOI) data assimilation scheme. Inserting the non-linear operator in this manner results in a sub-optimal estimation scheme but one that is quite practical. Real data are used to show that: (a) the scheme improves the handling of mismatches where vertical displacements of features are major factors, and (b) that the cost of the sub-optimality is not necessarily excessive.

REFRACTIVITY INVERSION CALIBRATION

Rogers, L. T.¹, Jablecki, M. C.¹, Gerstoft, P.²¹SPAWAR Systems Center, San Diego, CA 92152-7385²Scripps Institution of Oceanography, La Jolla, CA 92093-0238

Algorithms for making inferences about atmospheric refractivity from observations of radar clutter have been described in the literature (e.g. Gerstoft *et al.*, *Radio Science*, **38** no. 3, MAR18-1-22, 2003). Most of this work has focused on developing a maximum likelihood (ML) or maximum *a posteriori* (MAP) estimate. We now focus our attention on an ultimate goal of having our algorithms generate a correctly adjusted *a posteriori* distribution. For the present time, we will settle for our *a posteriori* distributions having one property of a correctly adjusted distribution: that over an ensemble of inversion runs, the true value of our parameter of interest u (for “usage” variable) falls in the 0 to 20th percentile 20% of the time, in the 20th to 40th 20% of the time, and so on. This talk describes a simulation-based method for achieving *a posteriori* distributions with this property.

The method is implemented as follows:

1. We define the usage variable u to be a scalar statistic that is strongly related to vector quantity that we are trying to estimate in the first place.
2. Synthetic environments are used generate the true value of u and to generate a noise-corrupted clutter observation \mathbf{d}^o , from \mathbf{m}_{real} .
3. The noise-corrupted synthetic clutter observation is fed into the inversion algorithm which returns a sample representation of the *a posteriori* distribution of the environments. These are mapped into a posterior distribution of u .
4. The value of $u(\mathbf{m}_{\text{real}})$ is ranked within the values of u generated from the inversion algorithm results.
5. This process is repeated 1000 times and the ensemble behavior of the *a posteriori* distribution is examined to assess whether it satisfies the ensemble behavior described above.

The above procedure is used to tune the inversion algorithm to generate correctly adjusted posterior distributions.

TIME DELAY RANGE BIAS ESTIMATION USING THE PARABOLIC EQUATION

Gelman, J.Z., Dockery, G.D., Kochhar, A.K.
Johns Hopkins University Applied Physics Lab

Time-delay radar range measurements in the lower atmosphere are biased by time lags due to atmospheric bending and a non-vacuum propagation speed. The resultant errors are often appreciable for long-range, high-resolution radars. One can correct for standard atmosphere biases using classical range/angle/height lookup tables, however more complicated environments are not easily characterized.

The Fourier split-step solution to the Parabolic Equation (PE) is a popular method for modeling radar propagation in the lower atmosphere (J.R.Kuttler G.D.Dockery, *Radio Science*, **26:2**, 381-393, 1991). One feature that makes this approach quite powerful is the ability to accommodate both height- and range-varying atmospheric refractivity. Another advantage is that the PE provides full forward-wave solutions. This presentation concerns the feasibility of using the phase of the full forward-wave solution to predict time-delay range errors in an arbitrary atmosphere.

The Tropospheric Electromagnetic Parabolic Equation Routine, a PE solver developed by the Johns Hopkins Applied Physics Lab, is used to generate complex field solutions as a function of range and height for both a measured atmosphere and a reference atmosphere. The relative phase between these two fields is then computed. Ambiguities in the relative phase are resolved using a simple 2-D phase unwrapping algorithm (H.Lim, *IGARSS Proc.*, **1**, 196-198, 1995). The result is a range/height map of range errors incurred if one were to transmit radar energy in the measured atmosphere, while assuming a time delay commensurate with the reference atmosphere. In this way we can, for example, compute the residual errors experienced by a system using standard atmosphere lookup tables for time-lag corrections. This procedure shows promise for PE-based range error prediction. Potential complications, such as surface reflections and multi-mode ducts, are discussed.

JHU/APL NEAR-SURFACE ATMOSPHERIC PROFILER,
PART I: INSTRUMENTATION AND VERTICAL DATA PRO-
FILES

Elwood Green III¹, J. Ross Rottier², Charles R. Etheridge III²
, Charles R. Etheridge IV²

¹Morgan State University, Baltimore, MD

²Johns Hopkins University, Applied Physics Laboratory, Laurel,
MD

The Johns Hopkins University Applied Physics Laboratory developed and fielded an 8-meter atmospheric profiler, mounted on a catamaran, which collected temperature and humidity profiles from near the ocean surface to 7.3 meters in height. A chain drive system is used to move a sensor carriage up and down a sailboat mast. The height limits are adjustable to allow options for profiling. The profiler sensor housing is aspirated by a fan to minimize solar heating effects. The floatation is designed for minimum cross sectional area, to minimize atmospheric drag and atmospheric wake effects. The catamaran was tethered to a research boat, R/V Chessie with direct data links. An RF wireless data link is an option. The initial profiler configuration measured a vertical profile once every 7 minutes, but the rate of traverse is adjustable. A faster rate may be used in an unstable atmosphere, for example. The design of the profiler and vertical profiles of atmospheric parameters will be presented for a data set collected on the Wallops Island test range during December 2003. Atmospheric conditions were stable during the test, which makes a good first test of the profiling method compared to the more variable conditions expected during an unstable, convective marine atmosphere. A time series of vertical profiles of temperature indicate repeatable positive gradients with gradual heating throughout a 4-hour period that encompasses local noon. Positive gradients in temperature and vapor pressure produced subrefractive gradients in the vertical profiles of radar modified refractivity. Part II of this series of papers addresses comparisons of boundary layer model predictions to the profiler observations.

JHU/APL NEAR-SURFACE ATMOSPHERIC PROFILER,
PART II: COMPARISONS OF BOUNDARY LAYER MODEL
PREDICTIONS OF MODIFIED REFRACTIVITY TO OBSER-
VATIONS

J. Ross Rottier¹, Elwood Green III², Charles R. Etheridge III¹

¹Johns Hopkins University Applied Physics Laboratory

²Morgan State University

The Johns Hopkins University Applied Physics Laboratory developed and fielded an 8-meter atmospheric profiler, mounted on a catamaran, which collected temperature and humidity profiles from near the ocean surface to 7.3 meters in height. Part I of this series of papers addresses the instrumentation design and the first set of vertical data profiles. Vertical profiles of radar modified refractivity and virtual potential temperature were calculated from the raw data profiles. Boundary layer model results are compared to observations from a data set collected on the Wallops Island test range during December 2003. In particular the Naval Postgraduate School (NPS) version of the LKB boundary layer model was used to generate predictions of radar modified refractivity from coincident fixed sensor averages taken from mast-mounted meteorological boxes on the R/V Chessie. The NPS-LKB model first predicts profiles of temperature and humidity from bulk inputs, and then calculates profiles of radar modified refractivity from profiles of temperature and humidity. When evaporation ducts are present, NPS-LKB determines evaporation duct height from the minimum of modified refractivity as a function of height in the profile. No evaporation ducts were observed in the December 2003 data set. Atmospheric conditions were stable during the test, which is an area where the models are generally lacking in field validation. The NPS-LKB results are sensitive to the input sea surface temperature boundary condition. Bulk sea surface temperature from a thermistor at a depth of 2-cm and from APL downward-looking Infrared sea temperature sensor were used. Errors are reduced using the IR sensor, which provides sea surface skin temperature rather than a bulk sea temperature from the immersed thermistor. Initial comparisons of model predictions to field observations are promising.

WORLDWIDE CLIMATOLOGY TO SUPPORT RF PROPAGATION

Fast, S. A., Saunders, K. E., Valentine, C. G.
Remcom, Inc.

The long term climatology of ducted radio waves by atmospheric anomalies has long interested researchers and communications system and RADAR users. Several global climatology data sets have been investigated for use in the Electromagnetic Integrated Resource Environment (EMPIRE). The climatology data sets investigated produced sufficient data but did not contain all the required climate data needed to extract a duct profile or refractive index for RF propagation predictions. For example, the Historical Electromagnetic Propagation Conditions (HEPC) climatology data set that is a product of the Oceanographic and Atmospheric Master Library (OAML) contains acceptable data with climate data available for every 2 x 2 degree marsden square for night and day for each month. However, there are several caveats when estimating a ducting profile or refractive index for RF propagation predictions. In addition, the HEPC data only contains data over water. While ducting does not often occur over land, in certain strategically located areas, nocturnal ducting is prevalent. The National Oceanographic and Atmospheric Administration (NOAA) Cooperative Institute for Environmental Sciences (CIRES) together with the National Center for Environmental Protection (NCEP) and the National Center for Atmospheric Research (NCAR) conducted reanalysis using all weather measurements taken since 1948. This NCEP/NCAR reanalysis data contains all required data to produce atmospheric profiles for RF propagation predictions by supplementing surface and vertical level reanalysis data with Monin-Obukhov theory.

The NCEP/NCAR reanalysis project uses the latest weather forecast models and all historical measured data taken since January 1, 1948 to generate a global weather data set every 6 hours since 1948. The NCEP/NCAR reanalysis data consists of 2 meter air temperature, 2 meter specific humidity, surface pressure, surface roughness, 10 meter U and V wind at 10 m, latent and sensible heat net flux, and temperatures and specific humidity at 28 sigma levels. Monin-Obukhov theory can be applied to this data to derive atmospheric profiles for use in EMPIRE. Therefore, by applying statistical analysis techniques using the NCEP/NCAR reanalysis data, climate data can be generated for multiple sigma levels along with supporting surface data yielding high quality climate data with excellent resolution. Further, the integration of NCEP/NCAR reanalysis derived climate data was a straightforward extension of EMPIREs Monin-Obukhov based MetOc functionality. Thus by using the NCEP/NCAR reanalysis data, a reliable physically based climate data set was derived to support RF propagation loss predictions.

A STATISTICAL STUDY OF THE COMPARISON OF WATER VAPOR AND POTENTIAL TEMPERATURE TERMS FOR THE MODIFIED REFRACTIVITY GRADIENT EQUATION IN ADVECTION DUCTS

Burgess, E. H.¹, Marshall, R. E.¹, Rottier, J. R.²

¹NSWCDD, Dahlgren, VA

²Johns Hopkins University/Applied Physics Laboratory, Laurel, MD

Efforts to study the effects of pressure, temperature, and relative humidity on the refractive nature of the marine atmospheric boundary layer has led to a derivation of the modified refractivity (M) gradient equation in terms of the gradients of potential temperature (q) and water vapor mixing ratio (w).

The mean structure of stably stratified internal boundary layers (IBL) resulting when air heated over a land surface advects over a colder ocean has mostly been described in terms of the gradient of q (Rotheram, 1983, Smedman et al, 1997, Skyllingstad, 2004). In IBLs where thermal stability suppresses turbulence and the vertical mixing of water vapor, the gradient of M has the potential to be less than zero. It has also been demonstrated that the height of the IBL and the degree of mixing of q and w increase with offshore distance

This paper will present statistical results showing the relative influence of the mixing ratio gradient term to the potential temperature gradient term for three days of advection duct activity during the Wallops 2000 Microwave Propagation Measurement Experiment (MPME). During the multi-agency Wallops 2000 MPME, a wealth of sea surface and upper air meteorological observations were collected by helicopter, rocketsonde, and boat in order to document the spatial and temporal structure of the coastal atmospheric boundary layer near the Virginia Eastern Shore.

Preliminary results indicate that the mixing ratio term can be as much as three times as influential as the potential temperature term. Statistics of the ratio of the two terms will be binned by temporal location in the diurnal heating and synoptic meteorological cycles. Statistics will also be binned by spatial location in the offshore flow.

Session F2, 13:15 – Thurs.

**RECENT ADVANCES IN
PROPAGATION CHANNEL
MODELING**

Co-Chairs: E. Marengo, K. Sarabandi

A STATISTICAL MACROMODEL FOR THE REFLECTION COEFFICIENT OF SIMPLE MASONRY WALLS WITH WINDOWS

Casciato, M.D.¹, Thiel, M.¹, Thiel, W.¹, Sarabandi, K.²

¹EMAG Technologies, 1340 Eisenhower Place, Ann Arbor, MI 48108

²The University of Michigan, 1301 Beal Ave., Ann Arbor, MI 48109-2122

Current ray-tracing algorithms for urban propagation, model building faces as flat dielectric or impedance surfaces, which is an acceptable approximation at low frequencies. At shorter wavelengths any surface irregularities significantly effect the scattering of radio waves, and as the effect is cumulative, across each building surface that the ray encounters, significant error will result in the calculation of the received fields. These irregularities can include surface grooves, indentations, recessed windows, etc, and can also include impedance changes across the surface, such as from concrete to windows. The large size of the building structure precludes the brute force application of more exact numerical techniques, and high frequency techniques, such as ray-tracing, are inaccurate when these perturbations in the building surface are on the order of a wavelength. While ray-tracing methods are of acceptable accuracy as the electrical dimensions of the surface irregularities increase, the ray density necessary to capture the fineness of the structural details, makes the problem computationally intractable.

With these inherent limitations in current ray tracing techniques, a method is applied to accurately model the reflection coefficients from building surfaces. An FDTD simulation is applied to locally model an irregular building surface. A tapered incident beam is used to eliminate edge effects, and the beam position varied statistically, in a Monte Carlo simulation, across the wall section. Due to the robustness of the FDTD algorithm, the method can be applied to any building configuration, and is limited in principle, only by the maximum size of the building wall section which can be simulated.

In order to begin the development of the described macromodels for irregular building surfaces, a simple masonry wall, with inset windows will be simulated. The windows are assumed to have a periodic spacing, and therefore for this beginning analysis the inclusion of periodicity assumes a building wall that is infinite in extent. This assumption is valid for large buildings, or for cases where the major component of the incident power is concentrated in the center of the building wall. The goal of this work is to derive, from the statistical data gained, an algebraic, statistical, macromodel for the mean reflection coefficient, as a function of window density, window depth, incidence angle, and reflection coefficients of both window and wall sections.

WAVE PROPAGATION MODELING FOR COMMUNICATION BETWEEN MOVING VEHICLES

Knoerzer, S., Maurer, J., Fuegen, T. , Wiesbeck, W.
Institut fuer Hoechstfrequenztechnik und Elektronik, Universitaet
Karlsruhe (TH), Germany

In recent years the road traffic density has been increasing drastically and it seems that this trend has not yet come to an end. The large number of vehicles on the streets leads to congestion and many accidents. A necessary step to solve the problem is to provide the driver with specific information, i.e. any driver will be able to get just the information he needs, depending on his individual driving route. This includes mobility-relevant information (e.g. online information about the actual traffic conditions on the whole route) as well as safety-relevant information (e.g. detailed information about the road and traffic conditions in the vicinity of the vehicle). Thereby, the primary goal is to improve the traffic flow, avoid accidents and shorten journey lengths. Beyond this, the increasing demand for mobile computing will have the future automobiles being equipped with high data rate access to the internet. Various multimedia applications, such as video on demand, games, email, etc. will be available. To provide automobiles with the large amount of information, inter-vehicle communications (IVC) will be a necessary tool.

It is expected that in the future all vehicles on a road are able to communicate with each other and to share data. As the number of participants in such a dynamic communication scenario is fluctuating rapidly, IVC will be organised in an ad-hoc network manner.

A detailed knowledge about the inter-vehicle transmission channel is necessary for the design and optimisation of IVC systems. Basis for these investigations are typical high resolution time series of impulse responses (IRs) of the physical radio channel between automobiles. A new IVC-channel model is therefore developed, which is able to provide realistic time series of IRs in a quasi-continuous manner. The model can be divided in three major parts consisting of a realistic model for the dynamic road traffic, a comprehensive approach to model the environment adjacent to the road, and an accurate model to calculate the multi-path wave propagation between the transmit and receive vehicle. As wave propagation model, a ray-optical approach is implemented. The resulting IRs incorporate the complete channel information and can be directly used for system simulations.

The three different parts of the model will be presented. Finally, comparisons with measurements of typical traffic environments at 5.2 GHz are presented showing a good agreement.

RECENT ADVANCES IN FDTD MODELING OF ULF/
ELF PROPAGATION WITHIN THE GLOBAL EARTH-
IONOSPHERE WAVEGUIDE

Jamesina J. Simpson, Allen Taflove
Northwestern University

In a recent publication (Simpson and Taflove, IEEE Trans. Ant. Prop., vol. 52, pp. 443-451, Feb. 2004), we reported a novel, finite-difference time-domain (FDTD) algorithm suitable for highly detailed three-dimensional (3-D) modeling of extremely low-frequency (ELF) propagation within the entire Earth-ionosphere waveguide. The algorithm incorporates a latitude-longitude FDTD space lattice which wraps around the complete Earth-sphere. Our technique permits an efficient, direct time-domain calculation of impulsive, round-the-world ELF propagation accounting for arbitrary horizontal as well as vertical geometrical and electrical inhomogeneities / anisotropies of the excitation, ionosphere, lithosphere, and oceans.

While the above latitude-longitude gridding technique has shown promise for whole-Earth models of ELF propagation, it still requires the use of a large parallel computer to model fine-grained details of the lithosphere that may be important for simulations of earthquake precursors and remote sensing of mineral deposits. Therefore, we have pursued alternative whole-Earth meshes that have the potential for improved efficiency. In this spirit, we are constructing a new, 3-D spherical geodesic FDTD grid model for the Earth-sphere (Simpson and Taflove, IEEE Ant. and Prop. Lett., in press) that is considerably superior to our previously reported latitude-longitude grid. This geodesic grid is based on the work of Dr. David Randall and Dr. Ross Heikes at Colorado State University.

Our current work is geared towards applying the latitude/longitude and geodesic FDTD grids summarized above to study the response of the inhomogeneous global Earth-ionosphere waveguide to potential seismically-induced sources in the lithosphere. Specifically, we have calculated what amounts to be the Greens function of the global Earth-ionosphere waveguide for impulsive electrokinetic current sources located at various depths below the Earth's surface in the vicinity of the epicenter of the 1989 Loma Prieta earthquake near San Francisco. More generally, we are exploring the possibility of the global ELF electromagnetic environment being perturbed by localized transient currents within the lithosphere generated by several mechanisms resulting from accumulating stress. Our ultimate goal is to provide as rigorous as possible a physics basis for proposed earthquake prediction schemes employing either land-based or satellite-based detectors of ELF anomalies.

APPLICATION OF MOVING WINDOW FDTD TO MODELING THE PROPAGATION OF RADIO SIGNAL FROM ANTENNAS LOCATED NEAR THE GROUND

Wu, K., Schuster, J. W., Luebbers, R. J.
Remcom Inc., State College, PA 16801, USA

Recently, there has been a great deal of interest in unattended ground sensors (UGS) for remote monitoring applications. These UGS are deployed in a variety of outdoor environment, and are equipped with wireless communication systems to transmit sensor data back to a remote operator. Because the UGS are required to be physically small, their antennas must operate at heights very near to the ground. Therefore, to support the design of UGS, accurate model of the propagation of RF signal very near to the ground is needed.

Because the antennas are located near the ground, interaction between the RF signal and the terrain can significantly affect the propagation of the signal. Some of these effects include scattering and back scattering from the roughness of the terrain surface, blockage of the signal by obstructions (rocks, shrubs, etc.) on the propagation path, and coupling to ground wave modes. In addition, the ground can also significantly affect the radiation pattern of the antenna. Because of these effects, many of the standard propagation models, such as TIREM and geometric optics methods, are inapplicable. Instead, a full-wave method is needed.

We have applied the moving window Finite difference time domain (MWFDTD) method to study near-the-surface propagation. The MWFDTD model is based on the full-wave finite difference time domain (FDTD) method. It takes advantage of the fact that when a pulsed radio wave propagates over the terrain, the significant pulse energy exists only over a small part of the propagation path at any instant of time. Therefore only a relatively small FDTD mesh on the order of the width of the pulse needs to be used. As the pulse propagates along the terrain, the computational grid moves along with the pulse.

Since MWFDTD solves Maxwell's equation directly, effects such as rough surfaces, ground waves, and the interaction of the antenna with the ground can all be included in a straight forward manner. In this talk we demonstrate the utility of MWFDTD for modeling the propagation of RF signals from very-near-the-ground antennas located in complex environments.

COHERENT MULTIPLE SIGNAL CLASSIFICATION FOR TARGET LOCATION USING ANTENNA ARRAYS

Marengo, E.A.

Department of Electrical and Computer Engineering
Northeastern University, Boston, MA 02115

It has been shown in a number of recent papers (Gruber et. al., *J. Acoust. Soc. Am.*, **115**, 3042-3047, 2004; T. Miwa and I. Arai, *IEEE Trans. Antenn. Propagat.*, **52**, 220-229, 2004) how multiple signal classification (MUSIC) can be employed in the problem of estimating the locations of M scattering material inhomogeneities or targets that are small in the scale of the relevant wavelength from knowledge of the scattering matrix K , henceforth to be referred to as 'the multistatic response matrix (MRM) K ', of the system of targets, as measured by an array of $N > M$ same-transmit, same receive electromagnetic antennas or acoustic transducers (transceivers) actively probing the targets. This method enables the super-resolved location of very closely spaced targets beyond the diffraction limit and remains valid even if there is significant multiple scattering between the targets.

In the form of MUSIC for target location with active arrays available in the literature the so-called time-reversal matrix $T = K^\dagger K$, where \dagger denotes the adjoint, plays a central role, which is analogous to that of the autocorrelation matrix of the signals received by a passive array in the familiar MUSIC algorithm for direction-of-arrival estimation. For time-harmonic signals with a suppressed $e^{-i\omega t}$ time-dependence where ω is the angular oscillation frequency, the corresponding $(N - M)$ -dimensional noise subspace W appearing in the calculation of the MUSIC pseudospectrum is the orthogonal complement of the signal subspace S spanned by $M < N$ linearly independent Green function vectors or 'propagators' associated with the different target locations, so that $S \oplus W = \mathcal{C}^N$ where \mathcal{C}^N is the N -dimensional space of complex signals measured by the array. This method is useful only if the number of targets $M < N$ so that it can be used to locate up to only $N - 1$ targets. The central aim of this presentation is to show that actually one can do much better and that, in particular, theoretically one can locate up to $N(N + 1)/2 - 1$ targets embedded in a given linear and reciprocal but otherwise arbitrary background medium from knowledge of the entire MRM K . Two forms of MUSIC are considered: 1) A variant of the usual incoherent MUSIC method adapted to active scattering data instead of passive data only, for cases when many scattering measurements (random realizations) are available, as well as 2) a new form of purely coherent MUSIC for cases when a single data set (realization) is available. The new coherent MUSIC uses a pseudospectrum steering vector that steers in a single step in the entire parameter space of all target locations. These findings establish a fundamental bound on the information about target locations that is contained in a scattering data set.

Session F3, 15:15 – Thurs.

RADIOMETRY AND

REMOTE SENSING

Co-Chairs: E.R. Westwater, E.M. Klopf

RESULTS FROM THE 2004 NSA/AAO ARCTIC WINTER RADIOMETER EXPERIMENT

Westwater, Ed. R.^{1,2}, Cimini, D.^{1,2}, Mattioli, V.³,
Gasiewski, A. J.², Klein, M.^{1,2}, Leuski, V.^{1,2}

¹CIRES, University of Colorado

²NOAA, Environmental Technology Laboratory

³DIE, University of Perugia

Moisture and clouds in the cold, dry polar regions play key roles in climatic feedback. Also, the development of accurate radiative transfer models requires accurate measurement of water vapor. However, the measurement of water vapor during cold arctic conditions has been particularly problematic. Radiosonde soundings of humidity, especially those using Carbon Hygristor (CH) humidity elements, have been suspect. In addition, the standard measurements of total columnar vapor by either Microwave Radiometers (MWR) or Global Positioning Systems (GPS) lack sensitivity for column amounts less than about 3 mm. To determine the ability of Millimeter Wavelength Radiometry to measure small amounts of both vapor and cloud liquid, the Arctic Winter Radiometric Experiment was conducted at the Department of Energy's Atmospheric Radiation Measurement (ARM) Program North Slope of Alaska site near Barrow, Alaska, from March 9 to April 9, 2004. Instruments that were operated included the NOAA Environmental Technology Laboratory's Ground-based Scanning Radiometer, the dual-frequency MWR and Multi-channel Microwave Profiler, developed by Radiometrics Corporation and operated by ARM, and a GPS water vapor instrument. Moreover, active and passive microwave and infrared instruments are run operationally at the site by ARM, such as the Millimeter-wave Cloud Radar, the Micropulse Lidar and the Atmospheric Emitted Radiance Interferometer. Brightness Temperatures (T_b) over the frequency range 22.235 to 400 GHz were measured. In addition, as many as five simultaneous radiosondes were launched that used CH, Vaisala RS90, or Chilled Mirror humidity elements. In this presentation, we compare forward model calculations of T_b based on five contemporary absorption models, humidity soundings of the various radiosonde types, and selected derived meteorological products.

OBSERVATION OF ARCTIC CLOUD PROPERTIES WITH A
SUBMILLIMETER-WAVE RADIOMETER

Dowlatshahi, S.G.¹, Gasiewski, A.J.², Klein, M.³
, Cimini, D.³, Westwater, E.³

¹Science and Technology Corpo.

²NOAA ETL

³CIRES/University of Colorado

Radiometric brightness temperatures around 20 and 31 GHz have been used for several years to retrieve operationally integrated vapor water path and cloud liquid water path. Studies of moisture and clouds in the cold, dry Polar regions play significant roles in climate feedback. Theoretical studies indicate that radiometric brightness temperatures at 340 GHz may be sensitive to ice in clouds, yielding the possibility of integrated ice water path retrievals. During the recent experiment Arctic Winter Water Vapor Intensive Operating Period 2004 (WVIOP04), from March 9 April 9, the Ground-based Scanning Radiometer (GSR) of NOAA/Environmental Technology Laboratory was deployed in Barrow, Alaska. The GSR is a multi-frequency scanning spectrometer operating at radiometric bands ranging from 50 to 380 GHz, with eleven channels in the 50-56 GHz oxygen band, dual linearly polarized channels at 89 and 340 GHz, seven channels around the 183.31 GHz water vapor absorption line, and three channels around the 380.20 GHz water vapor line. The main goal of the WVIOP04 experiment was to demonstrate the capability of millimeter wavelength radiometers to improve water vapor observations during the arctic winter. One of the secondary goals included evaluation of the sensitivity of millimeter-wave window channels to arctic clouds. The 340 GHz radiometer was the primary radiometer used for the study of arctic ice clouds. Based on active remote sensing data from a cloud radar and lidar, case studies of the GSR vertically pointing brightness temperatures as well as the polarization difference at 340 GHz are being analyzed over the periods when mixed-phase clouds and ice clouds were present. By using estimates of IWP from 20-31 GHz radiometer retrievals and radar and lidar data, the possibility of radiometric ice water path retrievals are investigated.

DESIGN AND PERFORMANCE OF A MINIATURIZED CLOUD LIQUID WATER RADIOMETER TO AUGMENT A MINIATURIZED WATER VAPOR PROFILING RADIOMETER

Klopf, E. K.¹, Iturbide-Sanchez, F.², Reising, S. C.¹

¹Microwave Systems Laboratory, Colorado State University, Fort Collins, CO 80523-1373

²Microwave Remote Sensing Laboratory, University of Massachusetts, Amherst, MA 01003

A Miniaturized Water Vapor Radiometer (MWVR) was recently developed at the University of Massachusetts and Colorado State University. This microwave radiometer measures atmospheric emission at four K-band frequencies to enable inversion of vertical profiles of tropospheric humidity. An additional Ka-band MMIC radiometer is needed to augment this system in order to distinguish between precipitable water vapor and cloud liquid water.

This paper focuses on the design, specifications and capabilities of a 31 GHz miniaturized cloud liquid water radiometer to complement the existing K-band MWVR. The additional radiometer will have a separate antenna and receiver, while sharing data acquisition, temperature control, and power supply subsystems with the existing MWVR. The Ka-band radiometer will utilize commercial MMIC technology to minimize construction cost.

The relatively low cost of fabrication of MMIC-based radiometers makes possible the deployment of small networks of these radiometers. The objective of the long-term project is to deploy a four-node network of dual-frequency radiometers to demonstrate the retrieval of the 3-D water vapor and cloud liquid water fields. Retrievals of water vapor and liquid water from measured brightness temperatures will be validated with NWS radiosonde measurements. Remote measurements of the water vapor and liquid water fields are needed, along with high-resolution temperature and wind fields, to initialize numerical weather forecasting models.

In this paper, we will present an analysis of horizontal and vertical resolution for a scanning Ka-band radiometer. The resolution of a four-station network of these radiometers will be analyzed in terms of node topology and beam scanning. The results of this analysis will be compared to similar simulations for the K-band MWVR in order to determine an optimal configuration for the dual-frequency, four-station network.

CALIBRATION OF THE GROUND-BASED SCANNING RADIOMETER DURING THE ARCTIC WINTER RADIOMETRIC EXPERIMENT 2004

Cimini, D.^{1,3}, Dowlatshahi, S.^{2,3}, Gasiewski, A. J.³, Klein, M.^{1,3}, Leusky, V.^{1,3}, Westwater, E. R.^{1,3}

¹CIRES/University of Colorado

²Science and Technology Corporation

³NOAA/Environmental Technology Laboratory

The Arctic atmosphere is extremely important for the climate of our planet, because water vapor and clouds in the Arctic play a key role in the earth's energy budget. Thus, continuous and accurate monitoring of the Arctic atmosphere is needed to improve the understanding of its radiative properties. In contrast, there is lack of continuous measurements due to the extreme and remote conditions. For these reasons, the Environmental Technology Laboratory (ETL) of the National Oceanic and Atmospheric Administration (NOAA) has designed and developed a multi-channel polarimetric microwave radiometer, called the Ground-based Scanning Radiometer (GSR), for continuous and unattended observations of the Arctic atmosphere. The GSR is provided with twenty-five channels in the micro- and millimeter-wave spectrum (from 50 to 380 GHz), plus one infrared channel (10 μ m). The set of frequencies has been selected for the simultaneous retrieval of atmospheric temperature profile, water vapor content, cloud liquid path, and cloud depolarization ratio. Particularly, the millimeter-wave channels are very sensitive to low water vapor content and allow for accurate observations even in the extremely dry and cold conditions typical of the Arctic. The design of the instrument allows for three stages of the calibration process, suggesting a high level of expected accuracy. Internal calibration is achieved with fast switching between two reference loads. External hot and cold targets are observed every two minutes, accounting for system thermal drift and providing absolute calibration. Finally, tip-curve up to 3.5 air masses provides the third level of calibration. The GSR has been deployed for the first time during the Arctic Winter Radiometric Experiment held from March 10 to April 9, 2004, at the Department of Energy Atmospheric Radiation Measurement Program site in Barrow, Alaska. The different stages of the calibration process will be discussed and comparisons of GSR data with measurements from other in situ and remote sensors will be presented.

AN INTERFERENCE MITIGATION TECHNIQUE FOR PASSIVE REMOTE SENSING OF SOIL MOISTURE

McIntyre, E. M.¹, Gasiewski, A. J.², Leuski, V.³
, Klien, M.³, Weber B. L.¹, Irisov, V.⁴

¹Science and Technology Corporation, Boulder, Colorado

²NOAA Environmental Technology Laboratory, Boulder, Colorado

³CIRES University of Colorado, Boulder, Colorado

⁴Zel Technologies, Boulder, Colorado

As the cost of microwave hardware declines, an increasing amount of microwave communication equipment is in use on a global scale. As a result, interference from anthropogenic emissions has begun to noticeably influence the accuracy of passive remote sensing of soil moisture using C-band radiometry. Interference has been observed in both the NOAA Environmental Technology Laboratorys (ETL) PSR/CX airborne imaging instrument, as well as the JAXA AMSR-E instrument on the NASA EOS Aqua satellite. Both the PSR/CX and AMSR-E instruments detect C-band emissions at fixed frequencies of approximately 200 to 300 MHz bandwidth. Simultaneous observations using multiple subbands, incorporated into the PSR/CX instrument, have provided one means of interference mitigation that is useful under moderately contaminated conditions. To extend the mitigation capabilities of PSR/CX, ETL has developed a C-band spectrometer for use within the PSR/CX instrument. The spectrometer observes emissions within relatively narrower bandwidths of 10 and 100 MHz, and is tunable from 5.8 to 7.5 GHz. Because anthropogenic emissions currently have relatively narrow bandwidths, the ETL spectrometer is capable of accurately sampling microwave emission within any 10 or 100 MHz band that is found to be free of such interference, thereby reducing the interference at the expense of radiance sensitivity, and (because the instrument has to be tuned) at the expense of observation time. This paper will discuss the design and anticipated modes of operation for the spectrometer, the results of its use in the Department of Agriculture's SMEX-04 experiment, and its potential for use in future airborne and satellite programs.

Session F4, 08:15 – Fri.

**ADVANCES IN RADAR SENSING
OF PRECIPITATION**

Co-Chairs: N. Chandra, R.H. Lang

BACKSCATTER ALGORITHM DEVELOPMENT AND TESTING USING THE NASA MICROWAVE LINK

M. Kurum¹, R. F. Rincon², R H Lang¹ , R. Meneghini²

¹Dept. of Electrical Computer Eng., The George Washington University, Washington, DC 20052

²NASA Goddard Space Flight Center, Greenbelt, MD 20771

Backscattering measurements using the NASA 2.3 km microwave LINK will be used to test existing algorithms for rainfall retrieval. The LINK backscatter measurements will be compared to measurements from a ground-based network of disdrometers and rain gauges located under the LINK propagation path. By using this comparison technique single-frequency and dual-frequency radar retrieval algorithms for the drop size distribution (DSD) can be tested and improved. The algorithm development is particularly relevant to the ongoing TRMM and up coming GPM missions. The measurement system allows researchers to test algorithms under ideal conditions. When these algorithms are employed on satellite radars, ground truth is difficult if not impossible to obtain.

The backscatter measurements are obtained by using a stepped frequency radar in place of the LINK transmitter. The step frequency radar is being implemented by using a network analyzer in conjunction with transmit and receive amplifiers. The radar is operated at the two LINK frequencies of 25 and 37 GHz. The LINK receiving antenna is configured as a passive reflector by terminating the antenna in a short circuit. With the receiving antenna acting as a passive reflector, the radar receiver will measure backscatter from rain, as well as, path integrated attenuation (PIA). In this configuration, algorithms which require the PIA such as the forward and backward recursion algorithms can be checked in varying weather conditions. Algorithms which do not require the PIA such as the Hitschfeld-Bordan, the modified Hitschfeld-Bordan and the Self-Consistent Method can also be validated.

A brief account on algorithms will be given. Sources of error will be discussed. Finally modifications yielding smaller errors will be presented along with a discussion of their effects on the estimation of DSD parameters.

OBSERVATIONS OF THE MICROSCALE VARIABILITY OF
PRECIPITATION USING AN IMAGING RADAR

Palmer, R. D.¹, Cheong, B. L.², Hoffman, M. W.²
, Frasier, S. J.³, Lopez-Dekker, F. J.³

¹School of Meteorology, University of Oklahoma, Norman, Oklahoma

²Department of Electrical Engineering, University of Nebraska, Lincoln, Nebraska

³Department of Electrical and Computer Engineering, University of Massachusetts, Amherst, Massachusetts

For many years, spatial and temporal inhomogeneities in precipitation fields have been studied using scanning radars, cloud radars, and distrometers, for example. Each measurement technique has its own advantages and disadvantages. In the present study, an imaging boundary layer radar is used to investigate the effects of turbulence on the formation of rain. Conventional profiling radars point vertically and collect data while the atmosphere advects across the field of view. Invoking Taylor's frozen turbulence hypothesis, it is possible to construct time-history data which are used to study the structure and dynamics of the atmosphere. Of course, the data obtained in this fashion are located on the two-dimensional plane aligned with the horizontal wind. A true three-dimensional view of the atmosphere can be obtained from imaging radars, such as the Turbulent Eddy Profiler (TEP), which was developed by the University of Massachusetts (Mead et al., *J. Atmos. Oceanic Technol.*, **15**, 849-859, 1998). This unique 915-MHz radar has up to 64 spatially separated receive elements, each with an independent receiver. As such, it is possible to use this radar to implement sophisticated imaging/beamforming algorithms with high angular resolution and clutter rejection capabilities (Palmer et al., *Radio Sci.*, **33**, 1585-1598, 1998). Using data from the TEP radar collected in June 2003, it will be shown that boundary layer turbulence can have either a constructive or destructive effect on the formation of precipitation. Evidence will also be provided which shows that this effect can be enhanced by updrafts in the wind field.

EXPERIMENTAL INVESTIGATION OF AN X-BAND POLARIMETRIC ALGORITHM FOR ATTENUATION CORRECTION AND MICROPHYSICAL RETRIEVAL

Anagnostou, M.N.¹, Anagnostou, E.N.¹, Vivekanandan, J.²

¹Department of Civil and Environmental Engineering, University of Connecticut, Storrs, CT 06250

²National Center for Atmospheric Research, 3450 Mitchell Lane, Building 2, Boulder, Colorado 80303

This paper investigates attenuation correction for X-band dual-polarization radar (XPOL) observations. In addition, an algorithm is developed for estimating raindrop size distribution (DSD) model parameters on the basis of attenuation corrected XPOL reflectivity and differential reflectivity data. The DSD model is assumed to be a three-parameter normalized gamma distribution. Relationships are derived for determining specific and differential attenuation from horizontal/vertical polarization reflectivity and propagation phase shift data along a ray, while simultaneously retrieving variations of the normalized intercept DSD parameter (N_w) and mean drop diameter (D_0). Using a constrained relation between the shape and slope parameters of Gamma DSD model along with the retrieved normalized intercept parameter value and mean raindrop diameter we estimate all three parameters of Gamma DSD for discrete space intervals along a radar ray. Closely matched XPOL radar rays with longer wavelength (S-band) dual-polarization radar measurements (SPOL), taken during the International H₂O Experiment (IHOP), are used to assess the proposed XPOL algorithms. The study explores the dependence of attenuation correction on the selection of oblateness-size relation (or axial ratio) and the maximum diameter limit and evaluates its error characteristics for different total path-integration attenuation cases. Variations in the assumed form of the raindrop axial ratio may result in significant biases in attenuation and rain estimation. In addition, at this wavelength, resonance occurs for sizes larger than about 4 mm, and therefore several polarimetric variables exhibit non-monotone dependence on the drop diameter. This poorly documented region of raindrop sizes can consequently have a significant effect on some polarimetric variables. The XPOL estimated DSD parameters are evaluated against DSD retrievals derived from two existing SPOL algorithms.

CRITICAL EVALUA-
TION OF DUAL-POLARIZATION RADAR MEASUREMENTS
IN HYBRID MODE FOR MEASURING PRECIPITATION

Wang, Y, Chandrasekar, V.

Colorado State University, Fort Collins, CO 80523-1373

Polarimetric radar measurement in hybrid mode is realized by simultaneously transmitting and receiving horizontally (H) and vertically (V) polarized waves. When the eigen-polarization of precipitation aligns along the Horizontal and Vertical linear states, the co-polar polarimetric covariance variables of precipitation, defined in the linear H/V basis can be obtained. The standard variables in the H/V polarization basis under consideration are reflectivity (Z), differential reflectivity (Z_{dr}), Differential propagation phase (Φ_{dp}), linear depolarization ratio (L_{DR}) and copolar correlation coefficient. In contrast to the operation in the eigen-polarization mode of operation (H/V mode) the benefit of the hybrid mode is the simplification of transmission chain, though some of the variables are not measured, specifically the cross polar measurements namely LDR and cross polar correlation. However, if the eigen-polarization drifts away from H/V polarization, inherent biases will be introduced to the radar parameter estimates. In this paper, the hybrid polarization mode is evaluated in the context of precipitation measurement. A theoretical model for the scattering and propagation through precipitation medium will be used to analyze the inherent polarimetric errors specially at X band.

The cross polar components of backscattering is studied in a variety of precipitation types, as well as antenna polarization errors. The errors are evaluated for both quantitative applications such as rainfall estimation and qualitative applications such as hydrometeor classification. Extensive data from CSU-CHILL radar is analyzed to evaluate the performance of hybrid mode. For radar observation of rain, it is shown that, the antenna polarization purity and alignment are critical. Data collected from convective rain showers using both alternate mode (or eigen polarization state) and hybrid polarization mode are compared.

VALIDATION OF ATTENUATION CORRECTION AT X-BAND FREQUENCIES USING DUAL-POLARIZATION

Liu, Y, Bringi, V.N., Chandrasekar, V.

Colorado State University, Fort Collins CO 80523-1373

Attenuation correction is of great importance to quantitative rainfall estimation and retrieval of raindrop size distribution parameters (DSD), especially at C-band and X-band frequencies. Recent papers (Bringi et al. 2001; Le Bouar et al. 2001; Testud et al. 2000) evaluated the attenuation at C-band radars and proposed several attenuation correction algorithms conceptually based on differential propagation phase (Φ_{dp}) constraint. However, limited results are available done at X-band frequencies. The "self-consistent method with constraints" suggested by Bringi et al. (2001) is adopted for X-band frequencies here, and evaluated during the Global Precipitation Mission (GPM) pilot experiment. During this experiment, the X-band radar (NOAA X-pol) and CSU-CHILL radar observed common areas, also sampled by ground disdrometers. Reflectivity (Z_h) and differential reflectivity (Z_{dr}) are corrected for rain attenuation. To validate the correction algorithm, the corrected reflectivity (Z_h^c) and the corrected differential reflectivity (Z_{dr}^c) are compared to the values computed from the disdrometers. The rainfall estimated from a R(Z) relation are also compared against those derived from K_{dp} . A composite algorithm to estimate the rainfall rate from K_{dp} and Z_h^c is also evaluated.

[References]

Bringi V.N., T. D. Keenan, and V. Chandrasekar, 2001: Correcting C-band radar reflectivity and differential reflectivity data for rain attenuation: A self-consistent method with constraints. IEEE Trans. Geosci. Remote Sens., 39, 1906-1915.

Le Bouar, E., J. Testud, and T. D. Keenan, 2001: Validation of the rain profiling algorithm ZPHI from the C-band polarimetric weather radar in Darwin. J. Atmos. Oceanic Technol., 18, 1819-1837.

Testud, J., E. Le Bouar, E. Obligis, and M. Ali-Mehenni, 2000: The rain profiling algorithm applied to polarimetric weather radar. J. Atmos. Oceanic Technol., 17, 332-356.

Session F5, 10:15 – Fri.

SURFACE SCATTERING

Co-Chairs: K. Anderson, G. S. Brown

A SIMULATION MODEL FOR DIFFERENT COMPLEX WALL
STRUCTURES IN SUBWAYS OF URBAN MICROCELLS AT
MILLIMETER WAVE FREQUENCY 35GHZ

Goyal,A., Kwon,H.M.

Wichita State University, 1845 Fairmount, Wichita,KS-67260

A new simulation approach is used to examine wide estimation of signal coverage and other important factors in urban subway environments. In this model a simple computer simulation technique is used to observe effects of different complex wall structures and different surface materials. It is observed that the structure, roughness and material of a wall impart a major role in predictions at the receiver. The direct ray, the ground reflected ray, the multiple wall reflected ray, and the diffracted-multiple reflected ray component effects are simulated to achieve more practical situation predictions in subway environments(F.M.Pallars, F. J. Ponce Juan, Analysis of Path Loss and Delay Spread at 900 MHz and 2.1 GHz While Entering Tunnels, IEEE Transactions on Vehicular Technology, Vol.50,No.3,May 2001.). This study is emphasized on how the power delay profile, peak rms delay spread, fast and slow fading envelopes, and the slope of loss curves for power law calculations are changed for different wall structures like walls with multiple surface materials, wood, concrete, glass, and tile etc; walls having windows, and doors etc. Results show that a very high decay of signal power with high delay spread occurs near the entrance of subway and as the receiver moves away from the transmitter, the multiple reflected ray component, and the diffracted-multiple reflected ray component acts dominant causes decrease in the delay spread values. The fast fading and slow fading gives a good idea of the specific locations where the signal is highly distorted. The slope of loss curves gives the variation of received signal power law w.r.t the transmitter-receiver separation. Another study is performed to analyse interferece with the another transmitter placed in the microcellular street and a beamwidth optimization technique as used in(T.Tagar, and T.Tanaka,"Delay Spread Reduction Effect of Beam Antenna and Adaptively Controlled Beam Facing Access System in Urban Line-of-Sight Street Microcells", IEEE Transaction on Vehicular Technology, Vol.52,No.4, July 2003.) is proposed to reduce the effect of co-channel interference. Although authors do not claim high degree of accurate predictions for all the subway conditions, however the results can be utilized in analysis of specific propagation characteristics.

NEAR-EARTH WAVE PROPAGATION CHARACTERISTICS
OF ELECTRIC DIPOLE IN PRESENCE OF VEGETATION OR
SNOW LAYER

DaHan Liao, Kamal Sarabandi

Radiation Laboratory, Department of Electrical Engineering and
Computer Science, The University of Michigan

The unrelenting quest for ever more robust communication networks has not only prompted the innovation of novel communication devices and signal processing algorithms but also has underscored the need for a more complete understanding of electromagnetic wave propagation in different environments. In this study emphasis is given to propagation in a setting defined by natural surface features and obstacles such as terrain roughness (large and small scale undulations), hills, rivers, and vegetations and snow layers. Such a setting is of significant interest in the design of unattended ground sensor networks. Since the heights of the transmitters and receivers in the network are low, there is a number of challenging problems in the propagation model that must be addressed and resolved through either analytical or numerical means or a hybrid combination of both.

In the current phase of the study, the radiation characteristics of an infinitesimal, arbitrarily-oriented electric dipole in the presence of a dielectrically-covered terrain is investigated with the use of a two-layer half-space model in which the middle layer represents vegetation or snow. In the near field region of the dipole, the field components can be calculated using numerical integration; however, due to the complexity of the integrand, calculations in the far field must be carried out analytically. Many studies have demonstrated the relevancy of the lateral wave for the case when both the transmitter and receiver are located within the dielectric medium and are separated by large distances. Unfortunately, for other configurations in which the transmitter or receiver (or both) is located above the dielectric layer, far field analytical expressions for all the electric field components do not exist; although generalized expressions can be found in literature, those expressions (often in terms of the scalar potential) are applicable only for a one-layer medium and have not been explicitly evaluated for a dipole source. In view of the aforementioned limitations, in this study a complete asymptotic evaluation for the electric fields of the electric dipole for arbitrary source and observation point locations is carried out through the method of steepest descents. Although the transmitter has been restricted to an electric dipole throughout the study, extension to an arbitrary antenna can be made by noting that the asymptotic form of the Greens function is related to the derived expressions for the field components by a simple constant. Therefore, the far field radiation of an arbitrary source can be easily computed numerically once its current distribution is known.

SCATTERING PROPERTIES OF THE OCEAN SURFACE:
MILLER-BROWN MODEL REVISITED

Hristov, T. S.¹, Anderson, K. D.²

¹Department of Earth and Planetary Sciences, Johns Hopkins University, Baltimore, MD 21218 USA

²SSC-San Diego, 2858, 53560 Hull St., San Diego, CA 92152

Describing the propagation of electromagnetic signals in refractive ducts over the ocean requires to account for the scattering from the water surface. Although available, the exact formulation of the scattering problem is commonly replaced by approximations for computational efficiency. Miller-Brown's result for the scattering crosssection of the sea surface (A. R. Miller, R. M. Brown, and E. Vegh, *IEE Proceedings, Part H*, **131**(2), 114-116, 1984) has been broadly accepted and has been employed in models for electromagnetic propagation over the ocean.

Miller-Brown model is built on two essential elements: the Kirchhoff approximation and the assumption about the probability distribution of the ocean surface elevations. Using the analytic signal representation of the surface waves $\eta(\mathbf{x}, t) = A(\mathbf{x}, t) \exp[i\phi(\mathbf{x}, t)]$, the Miller-Brown model prescribes that wave amplitudes $A(\mathbf{x}, t)$ follow a Gaussian distribution and the wave phases $\phi(\mathbf{x}, t)$ have an uniform distribution. Consequently, the surface elevations maintain the distribution $P(\eta) = \pi^{-3/2} \sigma^{-1} \exp[-\eta^2/(8\sigma^2)] K_0[\eta^2/(8\sigma^2)]$, $K_0(\cdot)$ being a modified Bessel function of the second kind and $\sigma^2 = \langle \eta^2 \rangle$. While the Kirchhoff approximation has known strengths and limitations, the prescribed statistical distribution of the sea surface needs to be reviewed in the light of today's understanding of the surface wave dynamics (M. S. Longuet-Higgins, *Phil. Trans. R. Soc. Lond.*, **249**, 321-387, 1957) and experimental data on scattering (Y. Karasawa and T. Shiokawa, *IEEE Trans. Comm.*, **36**, 1098-1104, 1988).

We reconcile the Miller-Brown model with the surface wave dynamics by using the Kirchhoff approximation with realistic statistics for wave elevation. The nonlinear interaction of the surface waves can lead to smoother troughs and sharper crests, i.e. to asymmetry in the probability distribution of the ocean surface (M. S. Longuet-Higgins, *J. Fluid Mech.*, **17**, 459-480, 1963). Such asymmetry produces a complex-valued scattering coefficient. Both coherent and diffusive scattering can be treated within this approach.

THE DIFFERENTIAL REFLECTION COEFFICIENT FOR A SURFACE WAVE PROPAGATING OVER A GENTLY UNDULATING ROUGH SURFACE

Brown, G. S.

ElectoMagnetic Interactions Laboratory, Bradley Department of Electrical and Computer Engineering, Virginia Polytechnic Institute and State University, Blacksburg, VA 24061-0111

Propagation of the Norton surface wave over a flat, lossy, half-space, interface has been studied rather extensively for its importance to many practical problems. The effects of surface roughness have not received as much attention due to the complicating nature of the roughness. Recently, Ishimaru, Rockwell, et.al. have presented a numerical approach to this problem that deals with the case of small amplitude surface roughness whose spectral content is concentrated in the high frequency region, i.e., about the electromagnetic wavenumber. For this class of roughness, the primary effect is that of incoherent scattering and attenuation of the mean or average surface wave field. More recently, Brown has considered the case of a gently undulating rough surface which has a large radius of curvature everywhere in the direction of propagation of the surface wave. The large radius of curvature constraint eliminates the possibility of radiation or scattering from those parts of the surface with a varying radius of curvature. Brown obtained a simple expression for the mean or average surface wave propagating along the surface that clearly demonstrated the interplay between the roughness mean square height and slope.

The purpose of this paper is to present a relatively simple derivation of the differential reflection coefficient of the surface wave as it travels along the gently undulating rough surface. It can be shown that the dominant surface wave field components launched by a vertical electric dipole located on a lossy surface are (E_z, H_o) with E_p also existing but of lesser amplitude. As the surface wave propagates from a flat to a gently undulating surface, (E_z, E_p) must transition to field components that are normal to (n) and tangential (t) to the surface while H_o does not change its direction. On a flat surface, it can be shown that $E_z/H_o = Z_o$, the characteristic impedance of free space. On the rough surface, the impedance changes to $E_n/H_o = Z_{rs}$, the local impedance seen by the surface wave propagating along the rough surface. We derive an expression for Z_{rs} and then calculate the differential reflection coefficient per unit length using the change in the reflection coefficient along the surface. The results of this calculation exhibit a dependence on the local surface slope, curvature, and relative dielectric constant of the subsurface material. We discuss the significance of these results and their limitations.

MODELING AND SIMULATION OF WAVE SCATTERING FROM MULTI-SCALE SURFACES

Kuo, N. C., Fung, A. K.

Wave Scattering Research Center, Department of Electrical Engineering, University of Texas at Arlington, Arlington, TX 76019

It is apparent that most naturally occurring surfaces, land or sea, contain more than one scale of roughness. On the other hand, modeling studies of backscattering from these surfaces rarely deal with more than two scales of roughness. The purpose of this study is to investigate how the different scales of roughness in multi-scale randomly rough surfaces respond to backscattering at different frequencies and look angles.

This study is carried out through both numerical simulation and analytical modeling on Gaussian-distributed and Gaussian-correlated, two-scale and three-scale, randomly rough surfaces. In the numerical simulation, the method of moments (MoM), also known as moment method, is applied. In the analytical modeling, the integral equation surface-scattering model (IEM) is applied. The numerical simulation results are shown to compare well with surface model predictions. To provide points of reference, single-scale calculations of each individual scale of roughness are also provided.

It is observed from these studies that (1) at low frequencies, the total backscattering is similar to, but is at a higher level than that based on the large scale alone in a multi-scale rough surface; (2) at intermediate frequencies, the backscattering at small angles of incidence tends to follow that of the large-scale roughness, and at large angles of incidence, it tends to follow that of the small-scale roughness. The two different angular trends due to the difference in roughness scales are less obvious for a three-scale than a two-scale surface, and (3) at high frequencies (except for near normal incidence), backscattering is dominated and can be explained by the backscattering from the small-scale roughness.

Session F6, 13:35 – Fri.

**REMOTE SENSING OF THE
ATMOSPHERE**

Co-Chairs: S. Reising, A. Webster

ELECTROMAGNETIC WAVE PROPAGATION THROUGH A
2-D INHOMOGENEOUS ATMOSPHEREYe, X.¹, Dvorak, S.L.¹, Herman, B.²¹Department of Electrical and Computer Engineering²Department of Atmospheric Sciences and Institute of Atmospheric Physics, University of Arizona, Tucson, AZ 85721

Radio occultation methods are gaining increasing importance for sounding planetary atmospheres. For the Earth's atmosphere, Global Positioning System (GPS) satellites serve as the signal sources for the radio occultation measurements. By studying the signal that passes through the inhomogeneous atmosphere, and is received by a Low Earth Orbit (LEO) satellite, useful information about the atmosphere can be obtained, such as the refractivity, temperature at altitudes where water vapor is negligible, and with additional data, temperature and water vapor at levels where water vapor is significant. Multiple-phase-screen techniques are often used as an efficient computational method for solving the problem of wave propagation through an inhomogeneous atmosphere. In multiple-phase-screen techniques, the atmosphere is first divided up into a finite set of regions that are separated by parallel phase screens. The inhomogeneities in the vertical gradient of the atmosphere's refractive index that occur between two successive phase screens are then treated as a phase correction factor on the phase screens. Fast Fourier Transform (FFT) techniques are then used to propagate the field between the phase screens.

In previous studies, the incident GPS signal was treated as a plane wave and the phase screens were defined as parallel planes in the rectangular coordinate system. However, because of the finite distance between the GPS satellite and the Earth, the incident plane wave approximation is not suitable. If the finite distance to the GPS satellite is accounted for, then the incident wave will exhibit a rapidly varying phase on the first planar phase screen. In order to overcome this problem, we have developed a new method to model the forward EM wave propagation through an inhomogeneous atmosphere, in which the waves emanate from a 2-D line source and the propagation is studied in the cylindrical coordinate system. In this method, a 2-D line source that is placed at the origin of a cylindrical coordinate system is used to represent the GPS satellite. Phase screens are then defined at constant radial distances, thereby providing cylindrical phase screens. Since the cylindrical phase screens are centered about the origin, the phase will be constant, instead of varying rapidly as is the case for a planar phase screen. This new cylindrical, 2-D approach better matches the physical phenomenology of the cylindrical waves that are produced by a 2-D source that is located at a finite distance from the Earth, thereby leading to improvements in the accuracy and efficiency for this 2-D propagation problem.

PROPAGATION MODELLING ON AN EXPERIMENTAL MICROWAVE LINK

Akbarpour, R., Webster, A.R.

Dept. of Electrical and Computer Engineering, The University of Western Ontario, London, ON, N6A5B9. CANADA

Experimental measurements were made for a number of years on a 51 km tropospheric microwave link. The system used consisted of a 16-element vertical receiving array designed to determine the amplitude and angle-of-arrival of individual components in a multipath situation. The system operated at a frequency of 16.65GHz and accumulated such data at 1 second interval on a continuous basis over the summer fading season. Results indicated that signal fading often could be ascribed to the presence of either ground-based or elevated layers with distinctive characteristics.

Tropospheric refractivity profiles in the study of line-of-sight microwave links are often modeled as a piece-wise linear or a smooth function with no variation along the entire microwave link path. Observations using acoustic sounders at each end of the above microwave link suggest that in reality the tropospheric layers along the link are characterized by fluctuations in height of up to several tens of meters.

An attempt is made here to model statistically the behaviour of such rough layers and the effects on the propagation from transmitter to receiver. In this, use is made of a parabolic equation description of microwave propagation to calculate received signal amplitude and AOA. A split-step Fourier method has been selected to numerically implement the PE method. This approach is capable of accurate results and is implementable on a high-end personal computer in a reasonable time-frame. Interaction with the ground is well accommodated and an available detailed digital ground profile has been used in allowing for the effects of ground reflections. The results of this exercise are compared to the experimentally observed effects.

WAVEFORM DESIGN FOR SAR USING CRAMER-RAO THEORY

Robert Linnehan¹, John Schindler², Leonid Perlovsky¹
, David Brady³, Murlidhar Rangaswamy¹

¹Air Force Research Lab

²Anteon Corporation

³Northeastern University

The Cramér-Rao Bound (CRB) establishes a lower bound on the error variance of an unbiased parameter estimate. In this paper CRBs are derived for target parameter estimates using synthetic aperture radar (SAR). The design of efficient radar waveforms must account for the phenomenology of targets and clutter. Since radar waveforms are usually designed for specific algorithms, the designer faces a problem when the method of processing is not specified. The CRB offers an approach for resolving the difficulty. The CRB can be used to establish optimal waveform-dependent performance bounds independently from signal processing algorithms.

In a simple case of a flat, horizontal area, a SAR image can be regarded as the estimation of complex scattering coefficients at fixed, equally spaced points on the ground. We first consider the CRB for target reflectivity with the assumption that the sensor position is exactly known with respect to all scatterers on the ground, the only source of random error being measurement noise. Two methods in this case are presented. The first method assumes simultaneous estimation of all scatterers in the SAR field of view. The second method assumes estimation of only the scatterer of interest (the target) and treats all other scatterers as noise with known moments. By allowing random positioning of the scatterers in azimuth, range and height we explore the consequences of diversity in the radar aperture with respect to the CRB.

The CRB development is extended to a parameter of greater interest: target height. In this case scatterer positions are considered known only in the azimuth dimension, and height is assumed to be estimated jointly with ground range for a limited field of scatterers. Here we show that height can in fact be estimated by including vertical excursion in the aperture.

Motivation for this theoretical study is to aid the SAR research and development community. Solving lower error bounds on SAR parameters provides a measure to ensure efficient and effective algorithms or systems, prior to their development. Furthermore, Cramér-Rao theory can be used as a reference to analyze the performance of algorithms and systems already in existence.

COHERENCE EFFECTS IN PASSIVE MICROWAVE REMOTE SENSING

C. Utku, R. H. Lang

Dept. of Electrical and Computer Engineering, George Washington University, Washington, DC 20052

This work addresses the question of the importance of coherence effects in passive microwave remote sensing of vegetation. In the past, coherence effects in remote sensing of random media have attracted much attention especially over the last two decades. Some of these coherence effects exist irrespective of the statistics of the random medium, like the backscattering enhancement. Backscattering enhancement is attributed to particle-particle or particle-ground wave interactions in the backscattering direction. Some other coherence effects may also manifest themselves by modifying the extinction rate in the random medium and by enhancing return signals. There is also work in the literature where some of these enhancement effects are incorporated into the incoherent transport theory. The modified transport theory, for example, extends the classical transport theory by including the cyclical interaction terms to account for backscattering enhancement.

Most work regarding coherence in random media is considered for active remote sensing. For passive problems it is known that the emissivity of a layered medium is different when obtained by coherent wave theory and by transport theory. This is due to the coherent interactions of the reflections at layer interfaces. However, coherent interactions of particles and ground have not been considered in detail. It is known that passive problems can be related to active ones through reciprocity and energy conservation. This also implies the existence of similar coherence effects in passive remote sensing.

Specifically, a layer of randomly distributed particles over a flat ground is considered in this work. The Fluctuation Dissipation theorem is used to compute the field emitted from the layer with reference to sources of enhancement effects due to coherent wave interactions between the particles and the ground. Some relations between the magnitude of the enhancements, wavelength, layer depth and receiver bandwidth are established. Finally a brief discussion will be given regarding the relation between these enhancement effects and their counterparts in similar active problems.

BISTATIC RADAR SYSTEM DESIGN FOR CLEAR-AIR WIND MEASUREMENTS

Zeynep C. Tulu, Stephen J. Frasier
Microwave Remote Sensing Laboratory, University of Massachusetts, Amherst

BISTATIC RADAR SYSTEM DESIGN FOR CLEAR-AIR WIND MEASUREMENTS

Zeynep C. Tulu, Stephen J. Frasier Microwave Remote Sensing Laboratory University of Massachusetts, Amherst 113 Knowles Engineering Building Amherst, MA 01003

Bistatic radar systems for measurement of clear-air winds are considered. The proposed systems exploit bistatic Bragg scattering from refractive index turbulence which is visible to short wavelength radars (e.g. C-band and higher frequencies) for particular scattering geometries. These systems might be designed with continuous-wave (CW) radars or with pulsed radars. We first look into the theory, and study the signal-to-noise ratio (SNR) for bistatic radar systems. Then, the differences between monostatic- and bistatic radar SNR as well as the differences between CW and pulsed bistatic radar systems are pointed out. We consider both beam-limited resolution volume and pulsed-limited volume for these systems. We compare the relative influences of Bragg scattering and Rayleigh scattering from particulate tracers on the bistatic radar reflectivity, along with their influences on retrieved wind estimates. The system design constraints are considered. We show that there are limitations on the forward scatter angle, hence on the system design caused by measurement uncertainty and Bragg scattering mechanism. There are also limitations on the sampling time in turn sampling rate and bandwidth of the receiver as a result of measurement errors. We then design bistatic radar systems to sense high C_n^2 (refractive index structure parameter, e.g. $10^{16} \text{ m}^2/3$) quantities and show that, systems with relatively low power (e.g. hundreds of watts) are feasible where atmospheric turbulence occurs. Also, we demonstrate that we need to dwell at different times at different places to have small measurement errors for all the places scanned by the radars. Finally, we compare systems with different operating frequencies.

RAY TRACING TECHNIQUES APPLIED TO SKY WAVE OBSERVATIONS OF LIGHTNING-INDUCED IONOSPHERIC EFFECTS ON SHORT RANGE VLF PATHS

Cotts, B.¹, Pasko, V.², Inan, U. S.¹

¹Department of Electrical Engineering, Space, Telecommunications, and Radioscience Laboratory (STARLab), Stanford University, Stanford, CA 94305

²Department of Electrical Engineering, Communications and Space Sciences Laboratory (CSSL), Pennsylvania State University, University Park, PA 16802-2706

At locations close (100-km) to a VLF transmitter, observation of the sky wave signal from the transmitter is possible by aligning a proximate magnetic loop antenna to null the ground signal. Previous observations using this arrangement [e.g., Rodriguez et al. 1992], and [Pasko et al., 2002] show a very high degree of temporal variability in received signal amplitude. Consideration of Early/Fast and Lightning-induced Electron Precipitation (LEP) events under these constraints show an unusual number of remarkably large events. For example, we have observed Early/Fast events with positive amplitude changes up to 8 dB and negative amplitude changes as high as 19 dB. In addition we have observed possible LEP events with positive amplitude changes of 5 dB and onset duration of 15 seconds. The recovery signatures of these events are also very unusual, often with non-exponential recovery, or no recovery at all.

Combining the data from previous campaigns with a recent data set (August 2004) of observations at Arecibo, Puerto Rico we analyze four separate instances in which a magnetic loop antenna is deployed with the intent of observing the sky wave. Because the disturbed region must necessarily be nearly overhead the receiver and/or transmitter we can assume the received signal to be in the near and can employ simple ray tracing techniques to determine the evolution of the scattered field from the ionospheric disturbance over time. From these results we can determine whether the anomalous nature of these extraordinarily large events are primarily due to the high inherent variability of the observed amplitude signal or the close proximity of the receiver to the disturbed ionospheric region.

EXPERIMENTAL VALIDATION OF PHASED ARRAY DESIGN FOR BIOLOGICAL CLUTTER REJECTION

Cheong, B. L.¹, Hoffman, M. W.¹, Palmer, R. D.²,
Frasier, S. J.³, Lopez-Dekker, F. J.³

¹Department of Electrical Engineering, University of Nebraska, Lincoln, Nebraska

²School of Meteorology, University of Oklahoma, Norman, Oklahoma

³Department of Electrical and Computer Engineering, University of Massachusetts, Amherst, Massachusetts

This paper highlights recent results obtained with the Turbulent Eddy Profiler (TEP) which was developed by the University of Massachusetts (Mead et al., *J. Atmos. Oceanic Technol.*, **15**, 849-859, 1998). This unique 915-MHz radar has up to 64 spatially separated receive elements, each with an independent receiver. The calibrated data provided by this array can be processed using sophisticated imaging algorithms. TEP is capable of producing three-dimensional images of echo power, radial velocity and spectral width. From these, it is possible to estimate the three-dimensional wind above the radar with high horizontal and vertical resolution. Given the flexibility of the TEP system, various array configurations are possible. In the present work we attempt to exploit the flexibility of TEP to enhance the rejection of clutter from unwanted biological targets. Most cases of biological clutter occur from targets in the sidelobes or grating lobes of the receive antenna array. Since the TEP array minimum receiver separation exceeds the spatial Nyquist sampling requirement, substantial possibilities for grating lobe clutter exist and are observed in actual array data. When imaging over the transmit beam volume, the receive array main lobe is scanned over a ± 12.5 degree region. This scanning also sweeps the grating lobes over a wide angular region, greatly increasing the likelihood that a biological scatterer appears somewhere in the imaged volume. With a subtle change to the standard TEP array configuration, it is shown via both simulations and actual experimental observations (collected in June 2003) that *adaptive* beamforming methods can be used to significantly suppress the effects of biological targets on the wind field estimates. It should be noted that this same array configuration does not have this beneficial effect using standard Fourier beamforming.

CAPABILITIES OF A MICROWAVE RADIOMETER NETWORK FOR TOMOGRAPHIC RETRIEVAL OF THE 3D-WATER VAPOR FIELD

Flavio Iturbide-Sanchez¹, Steven C. Reising², Robert W. Jackson³

¹Microwave Remote Sensing Laboratory, University of Massachusetts, Amherst, MA 01003

²Microwave Systems Laboratory, Colorado State University, Fort Collins, CO 80523-1373

³Laboratory for Microwave and Millimeter-wave Devices and Applications, University of Massachusetts, Amherst, MA 01003

Recently, the maturation of MMIC technology has provided potential reductions in the volume, weight and cost of microwave and millimeter-wave radiometers for Earth remote sensing. Small and low-cost radiometers make feasible the implementation of two and three-dimensional (2-D and 3-D) arrays of sensors because they can be designed and produced in relatively large quantities. An example of the reductions afforded by MMIC technology is the prototype Miniaturized Water Vapor profiling Radiometer (MWVR), developed at the University of Massachusetts and recently moved to Colorado State University.

By mathematically combining information sensed at different times and from array elements at different positions, it is possible to produce an estimate of the object observed in both space and time. Although numerous mathematical methods are capable of retrieving the source field, 3-D emission tomographic methods are selected to retrieve the water vapor density in the atmosphere as a function of both altitude and horizontal position from measurements using a 2-D array of water vapor profiling microwave radiometers. 3-D emission tomography takes as input a set of emission measurements at discrete viewing angles and positions and provides an optimal solution to the inverse problem; i.e., the spatial structure and density of the source of the emission. When a time series of measurements is available, the 3-D tomographic solution is in reality a 4-D solution, using time as the fourth dimension.

Measurements from a small, 2-D network of ground-based radiometers can be combined using 3-D emission tomography to retrieve the 3-D water vapor field in the troposphere. In this paper, the choice of both a receiver topology and a scanning strategy are examined, based on both logistical constraints and calculated expectations of retrieval errors. The retrieval accuracy depends not only on the accuracy of the tomographic techniques and the positions/viewing angles of the radiometers, but also on single-sensor considerations such as the altitude resolution of radiometric sounding and the beamwidth of each radiometer.

CHARACTERIZATION OF THE AZIMUTHAL DEPENDENCE OF THE MICROWAVE EMISSION FROM FOAM GENERATED BY BREAKING WAVES

Padmanabhan, S¹, Reising, S. C.¹, Klopff, E. M.¹, Asher, W. E.², Rose, L. A.³

¹Microwave Systems Laboratory, Colorado State University, Fort Collins, CO 80523

²Applied Physics Laboratory, Univ. of Washington, Seattle, WA 98105

³Naval Research Laboratory, Washington, DC 20375

Wind speed has been retrieved reliably from SSM/I radiometric measurements since 1990 with a precision of better than ± 2 m/s. However, the dependence of brightness temperature on the azimuth angle of observation with respect to the wind direction is at most 2-3 K peak-to-peak, much smaller than the dependence of brightness temperature on wind speed. Both WindSat, now on orbit, and the NPOESS Conical Microwave Imager/Sounder (CMIS), planned for launch in 2009, have as a primary objective the retrieval of the ocean surface wind vector. Since foam substantially increases the brightness temperatures measured by a microwave radiometer, there is an urgent need to understand the role that breaking waves play in determining scene-averaged microwave brightness temperatures. Knowledge of the microwave emissivity of foam generated by breaking waves can be obtained through near-surface observations of the azimuthal dependence of microwave emission from breaking waves on seawater.

During the Polarimetric Observations of the Emissivity of Whitecaps Experiment (POEWEX) in 2002, radiometric measurements of reproducible breaking waves were performed at 10.8, 18.7 and 37 GHz, along with bore-sighted video measurements of foam coverage. The increase in brightness temperatures due to breaking waves on the open ocean is an aggregate effect of both actively breaking crests and decaying bubble plumes. This experiment demonstrated that brightness temperature increases due to breaking waves vary with respect to the direction of wave breaking.

A second experimental campaign will be conducted during the fall of 2004 to characterize precisely the azimuthal dependence of the microwave emission from reproducible breaking waves. In addition to the WindSat frequencies of 10.8, 18.7 and 37 GHz, a 6.8 GHz radiometer will be included for more complete comparison with WindSat measurements. In-situ measurements of the instantaneous wave field in the radiometers field of view will be used to estimate the effect of long wave slopes on the polarimetric microwave emission. The resulting measurements and models of the azimuthal dependence of the emissivity of breaking waves and foam are expected to improve forward models needed for physically-based wind vector retrieval algorithms, especially at wind speeds of 7 m/s and higher.

Session F/J1, 13:15 – Fri.

**SPECTRUM MANAGEMENT IN
THE 21ST CENTURY**

Co-Chairs: K. St. Germain, M. Davis

NTIA-OSM LONG-RANGE STRATEGIC SPECTRUM PLANNING PROJECT

Barsky, P., Schroeder, N.

Reform Division, Office of Spectrum Management (OSM), NTIA,
Department of Commerce

This presentation will provide an overview of the Office of Spectrum Management, National Telecommunications and Information Administration, U.S. Department of Commerce initiative which supports the Presidential Initiative to improve Spectrum Management in the 21st Century. The background for this project, including the 2003 Presidential Memorandum and subsequent NTIA 2004 reports to the President will be presented as well as an overview of all projects resulting from presidential direction to implement the recommendations presented in the reports. Specifically, the Long-Range Spectrum Planning Project will produce a National Strategic Spectrum Plan which will be a bi-annually updated plan for Spectrum Management tailored to satisfy the future needs of federal government and non-federal government and eventually commercial communication systems. The plan, based upon requirements traceable back to agency missions will address: (1) New technologies or expanded services requiring spectrum, (2) the nature and characteristics of the new radio communications systems required, (3) the nature and characteristics of the spectrum required, and (4) suggested spectrum efficient approaches to meeting the spectrum requirements. The importance of involvement of the USRI community, which as a group is a spectrum user with very special needs, in the long-range planning process, will be emphasized. The methods and processes for clearly identifying and stating the spectrum needs, and the level of detail for the rationale supporting those needs, will be suggested. The international nature of the spectrum needs of the USRI community requires that clear, concise, substantiated spectrum requirements be included in the US National Strategic Spectrum Plan, but also in similar plans of ITU members in which USRI systems will operate.

ITU-R RECOMMENDATION RA.769 AND RADIO ASTRONOMY HARMFUL INTERFERENCE LEVELS IN THE 21ST CENTURY

Tomas E. Gergely
NSF

It is widely known among those interested in radio observatory protection and spectrum managers that the harmful interference levels (HIL) for radio astronomy are given in Recommendation ITU-R RA.769, usually referred to as Rec. 769. Even a summary reading of Rec. 769 reveals however, that while the methodology for the derivation of HILs is clearly described, the values listed in the relevant Tables were derived for single dish telescopes and are based on specific assumptions, e.g. that the maximum observed bandwidth is the width of the radio astronomy band and that a 2000 sec integration time is used in the observation. These standardized assumptions and the HILs in Rec. 769 that are based on them have served radio astronomy very well for over half a century.

Most radio telescopes envisioned for use in the 21st century, some of which are under construction or in various phases of design, are not single dish telescopes and the projected modes of observation are difficult to assimilate to the assumptions in Rec. 769. For example, the Square Kilometer Array (SKA) is envisioned as consisting of a compact core, and a sparse outer component with elements located possibly as far as 3000 km away. Further, the SKA plans to cover a frequency range of 200 MHz to 20 GHz with a large instantaneous bandwidth, and will possibly have multiple beams on the sky. Other instruments, under construction or planned (e.g. ALMA, EVLA, LO-FAR, LWA), are also difficult to assimilate to a single-dish telescope concept, under the assumptions of Rec. 769.

It therefore appears to be timely for the radio astronomy community to consider if: a) the Rec. 769 HIL levels should continue to be used for the next generation of instruments or b) instrument specific levels, that take into account, e.g. the geographical outlay and frequency coverage of the instrument should be calculated on a case-by-case basis. If the first approach is adopted, then a solid justification should be provided why the Rec. 769 levels continue to be valid under the changed circumstances. The second approach will require that the community dedicate substantial resources to carry out the work that will be needed within various national and international regulatory fora. I discuss some of these issues in more detail (but provide no answers to the questions raised)

OBSERVATIONS OF MICROWAVE BRIGHTNESS
TEMPERATURE CONTAMINATION:
A GLOBAL PERSPECTIVE

Kunkee, David
The Aerospace Corporation

Earth observing systems depend on interference-free measurements of the microwave spectrum to support a wide range of critical activities including weather forecasting, climate monitoring, and Earth science investigations. The nature of these measurements is such that they must be global and can not be carried out just on a local or even regional basis. In many instances, space-based measurement of microwave brightness temperature is the only reasonable means of monitoring critical atmospheric and surface parameters in remote areas of the world where in-situ data can not be obtained. Adequate allocation and protection of frequency bands required for these measurements is paramount. Unfortunately, frequency management decisions can not be made with complete knowledge all future implications of proposed rule changes as it is not possible to predict the success, failure, or evolution of proposed systems with certainty. However, significant improvement in our overall insight regarding spectrum utilization is possible with a better understanding of how the RF environment has evolved and how the current RF environment impacts remote sensing products.

To illustrate this perspective, measured brightness temperature data from the Scanning Multi-channel Microwave Radiometer (SMMR) was revisited for the purpose of evaluating Radio Frequency Interference (RFI) during its period of operation from October 1978 until mid-year 1987. This data is compared with data from the currently operating Advanced Microwave Scanning Radiometer (AMSR). Global C-band and X-band images from these sensors provide a perspective on how radio services operating in each spectral region have developed and impacted remote sensing. Many characteristics can be observed in the images, including the disappearance of strong RFI over Germany and the emergence of Fixed Service (FS) terrestrial microwave links in the C-band region. Contamination of AMSR C-band measurements has significantly impacted development of soil moisture retrieval algorithms designed to support hydrology studies. At X-band, increased occurrences of contaminated brightness temperature is apparent over specific countries in Europe and the Far East but is not apparent in general over North America. Reasons for these differences, and potential impacts of the contamination to remote sensing products will be examined.

TECHNICAL RFI MITIGATION AND SPECTRUM MANAGEMENT

Fisher, J. R.

National Radio Astronomy Observatory

Considerable interest and development work on technical solutions to RFI mitigation have been generated in recent years by the radio astronomy community. This adds a new dynamic to the spectrum management process. Radio astronomers have an obligation to employ modern signal processing methods for sharing the spectrum with active services, but everyone must be aware that these methods add to the hardware, software, telescope time, and data analysis effort costs of astronomy research. Also, there are practical limits to which made-made signals can be separated from weak cosmic radiation.

This presentation gives a brief overview of the current state of the art of technical RFI mitigation in radio astronomy. Part of the theoretical framework for unwanted signal cancellation from the electrical and acoustics engineering community is now about 30 years old. Through simulations and a bit of practical prototyping radio astronomers are beginning to understand the weak-signal domain limits of these techniques, and they have extended the mathematical framework into post-correlation signal processing. Pre- and post-correlation canceling methods usually have direct analogs of one another, but there are advantages of signal processing cost and ability to follow rapidly changing interference on both sides of the ledger. Straightforward time blanking techniques work well on low-duty-cycle signals, such as pulsed radar and distance measuring equipment. Foreknowledge of the signal characteristics very often adds to the efficacy of RFI excision, and some types of man-made signals are easier to distinguish from cosmic radiation than others. There is room for negotiations on this point in the spectrum management process.

Because of the added resources required for technical RFI mitigation the new techniques are only very slowly finding their way into practical use. RFI simply makes some types of research too expensive, and this science will be economically out of reach. It is clear that interference-free spectrum allocations for passive radio science are still very much required and will continue to be for the foreseeable future. However, there are a number of interesting opportunities for spectrum sharing to the advantage of both active and passive user of the spectrum that are being opened up by the falling cost of signal processing hardware. Smart radios can use spectrum more efficiently for communications. They can also be aware of radio quiet preserves in the complex time, frequency, and geographic space in an adaptive manner, partly driven by individual observatory spectrum usage patterns.

EESS SPECTRUM ALLOCATIONS AND OPERATIONAL REMOTE SENSING

St. Germain, K.M.

NPOESS Integrated Program Office, Silver Spring, MD

Earth Exploration Satellite Service (EESS) spectrum allocations protect the primary resource used in both civilian and military environmental awareness, including weather prediction, climate change observation and prediction, and basic science exploration. Operational weather observation and prediction have a tremendous, if difficult to quantify, impact on the civilian economy and military effectiveness. In the civilian sector, the economic value is realized in various industries, including fisheries, hydro-electric power, natural gas distribution, electric generation and dispatch, and western agriculture. In addition, warnings such as hurricane forecasts and heat-wave warnings allow the populace to appropriately prepare for severe conditions. In the military sector, battlespace awareness drives tactical decisions such as target and munitions selection as well as logistics management. These positive impacts are supported by a national investment in these capabilities that exceeds one billion dollars annually.

Our continued ability to support these functions depends directly on our ability to protect EESS spectrum allocations, to the necessary levels, over the long term. Initiatives in the spectrum management community, such as the use of interference temperature as an interference metric and development of cognitive radios to make more efficient use of spectrum, pose near term potential threats to operational passive spectrum use. Due to its dependence on spectral phenomena to deduce geophysical parameters, operational passive use of the spectrum is driven by the physics of the earth/atmosphere system. In addition, the ability to adapt to interference threats via mitigation techniques (instrumentation and processing) is severely limited. Active participation in spectrum policy is, in many cases, the only means of defending the ability to operate in the future environment. The ability of the EESS community to influence spectrum policy depends critically on our ability to understand the current environment, quantify harmful interference, and actively participate in analysis of proposed uses of spectrum affecting EESS allocated and neighboring bands.

SUPPRESSION OF SELF-GENERATED RFI EMISSIONS FOR THE EVLA

Robert Ridgeway, Dr. Rick Perley
National Radio Astronomy Observatory, Socorro, NM

When fully operational, the Expanded Very Large Array (EVLA) will be a digital radio telescope with four channels of gigaHertz-speed sampling in each antenna vertex room. The multi-stage, frequency conversion process requires strong, adjacent-band local oscillator (LO) signals in near physical proximity to each feed. Twelve, 10 GHz digital fiber optic data links are used to convey the signals from each of 27 antennas to the correlator. A high-speed correlator is located at the VLA central control building. To ensure that Radio Frequency Interference (RFI) emissions from the digital and LO circuitry located at each antenna and in the central control building do not overwhelm the astronomical signals which the telescope is designed to detect, an extensive program of shielding is being implemented, including an extensive emissions and shielding testing program.

This report describes the efforts by the National Radio Astronomy Observatory (NRAO) in Socorro, New Mexico to characterize the emissions from each module, and describes the design and testing of the RFI shielding used for the EVLA racks, bins, and modules. Sensitivity limits and RFI detrimental levels taken from the ITU-R-RA.769 handbook and established by EVLA program astronomical measurements were used to determine the minimum shielding levels required at critical frequencies for radiating devices located at the antennas. As a result, hierarchical layers of printed circuit board, module, bin, rack, and room shielding are being used to provide the greater than 120 dB of shielding required by these specifications. To reduce Control Building emissions, a high-performance, commercial shielded room is being installed to house the centrally located correlator.

Based on the extensive testing, it is expected that the EVLA will be able to operate free of self-generated interference. This is being done within budget by verifying that in each case the shielding used is slightly greater than that required to prevent corruption of long-integration, astronomical data.

ENSEMBLE SCATTERING AND RFI SPECKLE CAUSED BY
COLLISION AVOIDANCE RADARRuf, C.

University of Michigan

There has been considerable interest and research activity recently concerning automotive collision avoidance radars operating near 24 GHz. In particular, detailed and precise measurements have been made and electromagnetic models have been developed to describe the scattering properties of target automobiles when illuminated by such a device when mounted on an adjacent automobile. The dependence of the scattering on both angular direction and RF frequency have been considered. Knowledge of these scattering properties allows for the estimation of statistical properties governing large ensembles of such targets when arranged in specific configurations such as would be expected in urban centers, freeways or suburbs. The ensemble scattering behavior can, in turn, be used to predict the magnitude of the composite signal that would be observed by a downward looking microwave radiometer that is tuned to the same 24 GHz transmit frequency as the radar.

There are a number of Earth viewing microwave radiometers currently in low Earth orbit that operate near 24 GHz. Their number is expected to increase in the near future. These instruments measure natural thermal emission that is associated with the rotational water vapor absorption line centered at 22.235 GHz. They are able to remotely sense the absolute humidity present in the lower and mid troposphere. Radio Frequency Interference (RFI) at 24 GHz originating from man made sources such as collision avoidance radars can significantly degrade the value of these radiometer measurements for weather forecasting and climate monitoring. This is true even with radars operating at extremely low transmitter power levels.

The aggregate effect of a large ensemble of automotive scattering targets will be addressed in this paper. In particular, a statistical procedure will be presented by which scattering properties of individual targets can be used to estimate the resulting level of RFI to an orbiting microwave radiometer produced by a dense population of cars arranged in typical dense configurations. These results will then be used to determine an allowable level of transmit power by the radar below which RFI should not have a significant effect on the radiometer.

TECHNICAL RFI MITIGATION AND SPECTRUM MANAGEMENT

Fisher, J. R.

National Radio Astronomy Observatory

Considerable interest and development work on technical solutions to RFI mitigation have been generated in recent years by the radio astronomy community. This adds a new dynamic to the spectrum management process. Radio astronomers have an obligation to employ modern signal processing methods for sharing the spectrum with active services, but everyone must be aware that these methods add to the hardware, software, telescope time, and data analysis effort costs of astronomy research. Also, there are practical limits to which man-made signals can be separated from weak cosmic radiation.

This presentation gives a brief overview of the current state of the art of technical RFI mitigation in radio astronomy. Part of the theoretical framework for unwanted signal cancellation from the electrical and acoustics engineering community is now about 30 years old. Through simulations and a bit of practical prototyping radio astronomers are beginning to understand the weak-signal domain limits of these techniques, and they have extended the mathematical framework into post-correlation signal processing. Pre- and post-correlation canceling methods usually have direct analogs of one another, but there are advantages of signal processing cost and ability to follow rapidly changing interference on both sides of the ledger. Straightforward time blanking techniques work well on low-duty-cycle signals, such as pulsed radar and distance measuring equipment. Foreknowledge of the signal characteristics very often adds to the efficacy of RFI excision, and some types of man-made signals are easier to distinguish from cosmic radiation than others. There is room for negotiations on this point in the spectrum management process.

Because of the added resources required for technical RFI mitigation the new techniques are only very slowly finding their way into practical use. RFI simply makes some types of research too expensive, and this science will be economically out of reach. It is clear that interference-free spectrum allocations for passive radio science are still very much required and will continue to be for the foreseeable future. However, there are a number of interesting opportunities for spectrum sharing to the advantage of both active and passive user of the spectrum that are being opened up by the falling cost of signal processing hardware. Smart radios can use spectrum more efficiently for communications. They can also be aware of radio quiet preserves in the complex time, frequency, and geographic space in an adaptive manner, partly driven by individual observatory spectrum usage patterns.

COMPARISON OF RADIO SPECTRUM USAGE IN URBAN
AND RURAL ENVIRONMENTS FOR RADIO ASTRONOMY
AND PASSIVE REMOTE SENSING BANDS

Petrin, A.J., Steffes, P.G.

Georgia Institute of Technology, School of Electrical and Computer Engineering

The increasing usage of radio spectrum in both frequency and power, coupled with the vulnerability of radio astronomy and passive remote sensing systems to interference, necessitates a better understanding of the existing and predicted usage of the spectral environment. The Radio Spectrum Engineering Lab (RSEL) at Georgia Tech has developed a Radio Spectrum Evaluation System (RSES) which provides coverage from 400 MHz to 7.2 GHz and offers the capability to observe and analyze spectral usage in multiple dimensions: frequency, power, location space, azimuth, polarization and time. This system has a demonstrated capability of detecting signals emanating from satellites (GEO, MEO, and LEO), terrestrial radars, and terrestrial communication systems (broadcast, narrow band, spread spectrum, and low duty cycle operation).

Using the RSES system two comprehensive broadband spectrum studies were performed to characterize the spectral environments in an urban area and at a radio astronomy observatory located in rural North Carolina. A measurement site in midtown Atlanta, GA was selected to provide a baseline of spectrum usage in an urban area saturated with spectrum users, to increase the probability of intercepting spurious emissions. The Pisgah Astronomical Research Institute (PARI), located in the Pisgah National Forest was chosen as the comparison spectrum measurement site to analyze spectrum usage in a rural environment. To provide accurate and substantive information on spectrum usage more than five billion data samples were taken. This data was analyzed using an advanced detection algorithm developed at the RSEL to produce information on spectrum usage levels and characteristics.

In this presentation measurements and analysis of spectrum usage in the 608 614 MHz, 1395 1430 MHz, 4950 5000 MHz, and 6425 7200 MHz bands used for radio astronomy and passive sensing will be presented. The urban and rural spectrum measurements will be compared to show the different usage levels and characteristics present in these environments.

COMMERCIAL MOBILE RADIO SERVICES: A PRIMER FOR RADIO ASTRONOMY SPECTRUM MANAGERS

Clegg, A. W.

National Science Foundation, Division of Astronomical Sciences,
4201 Wilson Blvd Suite 1045, Arlington VA 22230

The 21st century will see unprecedented growth in demand for data and information services, with much (or perhaps most) of this growth occurring in the Commercial Mobile Radio Service (CMRS) market. This presentation aims to provide a better understanding of the wireless technologies that have been or will be used to facilitate that growth, and how those technologies will impact spectrum management for radio astronomy.

The presentation will include a primer on cellular and Personal Communications Service (PCS) technologies ("1G" and "2G" systems), concentrating on aspects of the technologies that are relevant to radio astronomy spectrum management. Circuit-switched analog (AMPS) and digital (iDEN, ANSI-136, GSM, and CDMA) technologies will be covered. Physical properties of the air interfaces will be presented, including: frequency bands currently employed for cellular and PCS services; service rules including transmit power limitations and out-of-band emission masks; network topology and cell site characteristics, including antenna characteristics and applications of advanced concepts such as MIMO and smart antenna technologies; temporal signal characteristics, including frame structures for TDMA-based technologies such as ANSI-136 and GSM and spreading methods for CDMA; and spectral signal characteristics including modulation methods, power spectral densities, and "real-world" out-of-band emissions.

Beyond 2G systems, next-generation CMRS services ("2.5G," "3G," "4G," etc.) will play increasingly important roles in spectrum management in the 21st century. Generally, these services are lumped together under the Federal Communications Commission's designation of "Advanced Wireless Services" (AWS), and new spectrum allocations are being developed to accommodate the deployment and predicted growth in demand for AWS. As with 1G and 2G services, a primer on AWS (as embodied by EDGE, WCDMA, and OFDM air interfaces) and characteristics of AWS relevant to radio astronomy spectrum management will be provided.

Because of the ubiquity of CMRS applications, "cellular telephones" (in the general sense) are often perceived by radio astronomers as a major interference threat to passive services. In reality, such technology is providing enormous benefit to all segments of society through the provision of economical, convenient, mobile, and spectrally-efficient communications services, while its impact on radio astronomy is relatively low.

Session G1, 08:55 – Fri.

IONOSPHERIC MODIFICATION

Co-Chairs: P. Bernhardt, M. Sulzer

ELF/VLF WAVES GENERATED BY MODULATED HEATING OF THE AURORAL ELECTROJET WITH THE HAARP HF TRANSMITTER

Robert C. Moore¹, Umran S. Inan¹, Timothy F. Bell¹,
Edward J. Kennedy², Paul A. Kossey³

¹STAR Laboratory, Stanford University, Stanford, California

²Naval Research Laboratory, Washington, District of Columbia

³Air Force Research Laboratory, Hanscom AFB, Massachusetts

ELF/VLF broadband recordings acquired at multiple locations during several recent ELF/VLF generation campaigns conducted with the HAARP HF heater are used to determine the amplitude and phase properties and the occurrence statistics of ELF/VLF waves generated by modulated heating of the auroral electrojet. Extensive, continuous data sets were acquired every night for up to 10 hours during two continuous 14- and 24-day nighttime campaigns. A 24-hour period allowing the investigation of ELF/VLF signal generation under daytime conditions, and a 4-day period including multiple power-step sequences allowing the assessment of the heating characteristics at the wave-generating altitude are also discussed. With the relatively large (4.8 by 4.8 m square) magnetic loop antennas utilized, together with a transformer matched differential preamplifier, system sensitivities of as low as several femtoeslas per root Hz are achieved, depending on the noise environment at the measurement site. A large variety of natural magnetospheric signals, including ELF/VLF chorus, auroral hiss, and lightning-generated whistlers are commonly observed in addition to the ELF/VLF signals produced by HAARP.

Artificially generated ELF/VLF signals at all modulation frequencies were observed every night of operation at receivers within 50 km of the HAARP facility. ELF/VLF signals were robustly produced under varying geomagnetic conditions, although the strongest signal levels were observed during geomagnetically active periods. At the closest receiver site, typical signal levels varied from 1 to 10 picotesla, while on two very geomagnetically active days, intensities of up to 70 picotesla were observed. Observed phase differences between ELF/VLF pulses observed at the same site on two orthogonal magnetic antennas indicate the need to take a laterally as well as vertically distributed source region into account for the modeling of received signal amplitudes at ground distances of up to 150 km. Additional observations show that ELF/VLF signals can be generated well during daytime as well as nighttime and that the signal levels generated depend the location of the electrojet currents rather than on daytime or nighttime ionospheric conditions. While observed signal amplitudes at the modulation frequencies varied linearly with the power transmitted during the power-step sequences, harmonic signal level saturation occurred on a regular basis, consistent with a non-linear heating mechanism.

MAGNETIC RESPONSE OF THE AURORAL ELECTROJET
TO SHORT PULSE HF HEATING

Papadopoulos, K.^{1,2}, Wallace, T.¹, Peter, W.¹
, McCarrick, M.¹, Milikh, G.², Zwi, E.¹

¹BAE Systems-ATI, 1250 Twenty-Fourth St., NW, Washington,
DC 20037, USA

²University of Maryland, Depts. of Physics and Astronomy, Col-
lege Park, MD 20742, USA

It is well known that transient HF heating in ionospheric electrojet regions, such as the polar electrojet, generates a magnetic pulse on the ground due to the transient modification of the local Hall and Pedersen conductivity. Measurements of the magnetic response of the electrojet region as a function of the HF heating pulse length, frequency, polarization and ERP provide important diagnostics of the HF pulse interacting with the ambient plasma. Furthermore they can be used as diagnostics of the ambient plasma properties and to understand puzzles associated with the ionospheric generation of ELF/VLF waves. The results of a comprehensive experimental study of the magnetic response of the auroral electrojet to short pulse and chirped ionospheric HF heating using the HAARP ionospheric heater conducted during the summer of 2005 is presented. The experiments used several HF frequencies in the range of 3.0 to 8.0 MHz and chirped formats. The transient magnetic field on the ground was recorded at a site 12 km away from the heater with EMI BF-6 magnetic sensors. The sensor output was digitized at 24 bit resolution with 96 kHz sampling frequency. GPS time code output simultaneously digitized was used for time reference. A comparison of the results to theoretical models reveals of wealth of saturation, hysteresis and ballistic phenomena that allow us to address fundamental issues, such as harmonic generation, and variation in injection efficiency between the earth-ionosphere waveguide and the magnetosphere. Furthermore they indicate the direction for further experimentation using HAARP and futures expected in short pulse experiments in the equatorial electrojet.

PHYSICS NUANCES CONTROLLING IONOSPHERIC GENERATION OF ELF/VLF WAVES

Papadopoulos, K., Wallace, T., Peter, W.

, McCarrick, M., Milikh, G., Zwi, E., Kennedy, E.

¹BAE Systems-ATI, 1250 Twenty-Fourth St., NW, Washington, DC 20037, USA

²University of Maryland, Depts. of Physics and Astronomy, College Park, MD 20742, USA

³US Naval Research Laboratory, 4555 Overlook Ave., SW, Washington, DC 20375, USA

Generation of ELF/VLF waves by modulating ionospheric currents, such as the auroral electrojet, has been accomplished using a number of ionospheric heating facilities. The observations have generated several physics puzzles¹ predominantly due to the non-linear physics involved in the interaction of modulated HF power with the ionospheric plasma. Critical among the various outstanding issues are:

Scaling of the HF to ELF/VLF conversion efficiency as a function of the HF frequency and ionospheric parameters
The extent and cause of harmonic generation
Near vs. far field propagation

This paper will present experimental results obtained recently by the HAARP ionospheric heater that focus on the non-linear physics. The experiments were conducted at the HAARP facility during the summer of 2005. The North-South and East-West components of the ionosphericly generated magnetic field were recorded at a site 12 km away from the heater with EMI BF-6 magnetic sensors. The sensor output was digitized at 24 bit resolution with 96 kHz sampling frequency. GPS time code output simultaneously digitized was used for time reference. Temporally resolved waveforms of the magnetic signatures observed on the ground obtained with resolution of better than 10⁻⁶ sec will be presented and compared to theoretical models. The observations revealed several critical physics aspects of the ionospheric ELF/VLF generation, including the limits of HF to ELF/VLF conversion efficiency, bandwidth limitations and signal purity. The relevance of the results to the conduct of future experiments using the upgraded HAARP heater will be addressed.

1. K. Papadopoulos, et al., On the Efficiency of ELF/VLF Generation Using HF Heating of the Auroral Electrojet, Plasma Physics Reports, Vol. 29, No. 7, pp 561-565, 2003.

COMPUTER SIMULATION OF ELF/VLF GENERATION USING HIGH POWER HF RADIOWAVES

Keskinen, M.J.

Plasma Physics Division, Naval Research Laboratory, Washington, DC 20375

By modulating the ambient auroral electrojet current in the high latitude ionosphere using ground-based HF transmitters it is possible to generate extremely low frequency (ELF) and very low frequency (VLF) radiation which can enter the earth-ionosphere waveguide and provide a technique for global low frequency communications. This is accomplished by heating the electrons in the lower D region ionosphere with high power HF power modulated at the desired ELF/VLF frequency. With the construction of the new High Frequency Active Auroral Research Program (HAARP) ionospheric research facility in Alaska, many issues remain regarding ELF/VLF generation using HAARP, e.g., what are the ELF/VLF generation efficiencies using high effective radiated powers (ERP) from HAARP and what the ELF/VLF radiation characteristics both in the near and far field. To address these issues we have performed computer simulation studies of the ELF/VLF generation process using a time-dependent 3D full wave code. The code typically simulates a region, centered around the HF heater, extending approximately 3000 km in the horizontal direction and 150 km in the vertical direction. A range of ELF/VLF frequencies can be simulated. For a range of ERPs, we have computed the polarization and field strength in the near field for conditions applicable to HAARP. We have found that the polarization and field strength in the near field can forecast the radiation characteristics and field strength in the far field. We have computed the ELF/VLF amplitude as a function of radial distance and found agreement with that predicted by near and far field radial dependence. We have compared the near field radiation characteristics from the 3D code with experimental observations and found good agreement.

STATISTICS OF EXCITATION OF DUCTED WHISTLER-MODE WAVES VIA MODULATED HEATING WITH HAARP

Gołkowski, M., Inan, U.S., Carpenter, D.L.

STAR Laboratory, Stanford University, Stanford, CA, 94305 USA

Extensive ELF/VLF data collected in both the northern and southern hemispheres during recent HAARP ELF/VLF excitation campaigns are analyzed from the point of view of assessing the occurrence properties of triggered ELF/VLF emissions, both naturally occurring and excited by the HAARP HF heater. Signals in the ELF/VLF frequency range are robustly generated by the HAARP HF heating facility in Alaska. We examine the cases that lead to successful magnetospheric ducting of HAARP generated signals manifested in propagation to the magnetically conjugate hemisphere and back again after reflection from the lower ionospheric boundary. The study focuses on a statistical survey of geomagnetic and ionospheric conditions and HF parameters that show potential correlation with successful ducting and magnetospheric amplification. The survey includes geomagnetic and auroral electrojet indices, magnetic field conditions, and ionospheric profiles. Results suggest the existence of an 'active' and sometimes narrow frequency range in which ducting and magnetospheric amplification occur. Specially formatted ELF/VLF signals in the 1-6 kHz range were transmitted by HAARP and recorded locally as well as at the conjugate point in the South Pacific Ocean. Measurements at the conjugate point were made using a receiver mounted on a buoy designed specifically to detect HAARP induced whistler-mode waves. Signals from both hemispheres are analyzed with attention to the time/frequency format which has shown to be a key factor in successful hemisphere to hemisphere propagation. Relationships between HF carrier frequency, alternated between 3.3 and 5.8 MHz, and signal strength above and below the ionosphere are investigated. The occurrence of HAARP-injected whistler-mode echoes is compared with the occurrence of natural ducted signals (chorus emissions, and lightning-generated whistler echoes), as well as with occurrence rates of ducted whistler-mode signals excited in Siple Station, Antarctica wave-injection experiments.

OBSERVATIONS OF BRIGHT HF-INDUCED AIRGLOW IN THE PRESENCE OF AURORA

Gerken, E.¹, Pedersen, T.², Kelley, M.¹,
Starks, M.², Mishin, E.²

¹Cornell University, School of Electrical and Computer Engineering, Ithaca, NY 14853

²Air Force Research Laboratory, 29 Randolph Road, Hanscom AFB, MA 01731

HF heater-induced artificial airglow observations can be used to diagnose electron energies and distributions in the heated region, illuminate natural and/or artificially-induced ionospheric irregularities, determine ExB plasma drifts, and measure quenching rates by neutral species. At mid-latitudes, in general, only the 630.0 nm oxygen line is bright enough to unambiguously detect with rare cases of detectable 557.7 nm emissions (Bernhardt et al., *J. Geophys. Res.*, **94**, 9071, 1989). However if a sporadic E-layer develops then the heating HF wave is able to interact with a much lower altitude and brighter 557.7 nm emissions (~ 55 R) are observed as patches (Djuth et al., *Geophys. Res. Lett.*, **26**, 1557, 1999; Kagan et al., *Phys. Rev. Lett.*, **85**, 218, 2000). Unlike the mid-latitudes, the nighttime E-layer at high latitudes is typically created by auroral precipitation and associated with strong ionospheric absorption and bright auroral emissions. In the February 2002 HAARP optical campaign, green line emissions were frequently observed simultaneously with red line emissions but these observations were made in the absence of a strong E-layer and the emissions appear to have been generated in the F-layer. In the March 2004 HAARP optical campaign, however, very bright (~ 4 kR) green line airglow emissions were observed in kilometer-scale patches between auroral arcs during blanketing E-layer conditions (Pedersen and Gerken, *submitted*). The single most surprising feature of these airglow patches observed in the presence of aurora is their brightness. At ~ 4 kR total intensity, these patches are above the naked eye threshold and are comparable to dim visible aurora. We present our observations of artificial airglow in the presence of aurora and discuss possible generation mechanisms.

LOW LATITUDE IONOSPHERIC MODIFICATION EXPERIMENTS WITH THE SPACE SHUTTLE

Paul A. Bernhardt, Joseph D. Huba, Carl L. Siefring
Beam Physics Branch, Plasma Physics Division, Naval Research
Laboratory, Washington, DC 20375

The Space Shuttle OMS engines inject 20 kg/s of exhaust vapors that are highly reactive in the F-region ionosphere. Using dedicated engine burns scheduled by the Air Force Space Test Program (STP), the Naval Research Laboratory has conducted OMS burns over the low latitude radars located in Jicamara, Peru and Kwajalein, Marshall Islands. Future OMS burns are scheduled near the equator with observations from ground stations in Hawaii and from space using the Air Force C/NOFS satellite and the Canadian CASSIOPE satellite. The objectives of the low latitude experiments are (1) provide seeds to stimulate the formation of equatorial bubbles and (2) investigate radar scatter for electrostatic waves excited by the high speed exhaust. For the first objective, the OMS burns will occur along an orbit nearly tangent to the magnetic field direction. These burns will reduce the plasma density along the Space Shuttle Trajectory and consequently produce a localized reduction in flux tube integrated Pedersen conductivity. After sunset, this Pedersen conductivity hole will become unstable to form an equatorial bubble. The evolution of the bubble will use the in situ and radio beacon diagnostics on the C/NOFS and CASSIOPE satellites which are in 15 and 80 degree inclinations, respectively. For the second objective, the high speed exhaust vapors will be injected over the Air Force Maui Optical Site (AMOS). The exhaust molecules such as water vapor and carbon dioxide will charge exchange with the ambient oxygen ion to yield 10 eV molecular ions. These ions will stream in spiral orbits to create unstable velocity distributions. The unstable ions will stimulate lower hybrid and ion acoustic waves. Radars located on the west coast of Hawaii will be operated to detect backscatter from these waves. If possible, in situ observations of these waves will be made with plasma wave receivers on satellites.

Session G2, 13:15 – Fri.

DATA ASSIMILATION

Co-Chairs: C. Minter, B. Wilson

IMPACT OF THE BASTILLE DAY SOLAR FLARE ON THE
LOW- TO MID-LATITUDE IONOSPHEREHuba, J.D.¹, Warren, H.¹, Joyce, G.²¹Naval Research Laboratory, Washington, DC²George Mason University, Fairfax, VA

We study the impact of the Bastille Day solar flare radiation on the low- to mid-latitude ionosphere. The methodology is as follows. We develop an EUV irradiance spectrum based upon observations for the Bastille Day flare. Since solar irradiance observations typically do not have the cadence necessary to follow the evolution of a flare, we have developed techniques for computing flare spectra from the available solar data. We then use this spectrum in the NRL three-dimensional ionosphere model SAMI3 to obtain the global impact of the flare on the mid- to low-latitude ionosphere. SAMI3 (Sami3 is Also a Model of the Ionosphere) is the NRL ionosphere code that models the plasma and chemical evolution of seven ion species (H^+ , He^+ , N^+ , O^+ , N_2^+ , NO_2^+ and O_2^+) in the altitude range 85 km – 20,000 km. The complete ion temperature equation is solved for three ion species (H^+ , He^+ and O^+) as well as the electron temperature equation. Ion inertia is included in the ion momentum equation for motion along the geomagnetic field. An offset, tilted dipole geomagnetic field is used and the plasma is modeled from hemisphere to hemisphere. No high altitude boundary conditions are not needed since a complete ionospheric flux tube is modeled. In addition, the $\mathbf{E} \times \mathbf{B}$ drift motion of the plasma is included for both zonal electric fields (vertical drifts) and meridional electric fields (zonal drifts). SAMI3 uses a nonorthogonal, nonuniform, fixed grid. The grid is designed to optimize the numerical mesh so that the spatial resolution decreases with increasing altitude. We assess the flare's impact by comparing simulation results with and without the solar flare enhanced EUV spectrum. A previous study using the NRL two dimensional ionosphere model SAMI2 and a more simplistic EUV spectrum of the Bastille Day storm found that flare radiation can increase the F-region ionosphere density by up to 50% [Meier et al., Geophys. Res. Lett. 29, 10.1029/2001GL013956, 2002].

Research supported by ONR.

UPPER ATMOSPHERIC DRIVER DETERMINATION USING
DATA ASSIMILATION

C. F. Minter, T. J. Fuller-Rowell, M. V. Codrescu
University of Colorado, NOAA Space Environment Center

Work has been conducted recently on developing a data assimilation system for specifying the thermospheric composition and density in near real time. Despite the ability to describe the physics of the upper atmospheric forcing, quantifying the time-dependent drivers still remains difficult during geomagnetic storm conditions. Incorporating the high latitude forcing into the data assimilation system requires knowledge of the spatial and temporal variations of the convection electric field and the auroral precipitation. One of the limitations in data assimilation systems for space weather applications comes from inaccurate knowledge of these drivers. Compared with the solar wind parameters that force the magnetosphere, the drivers of the upper atmosphere, although well understood, remain poorly quantified. At best, the globally averaged Joule heating rate at a given time is only known to within a factor of two. At a given location, this uncertainty can rise to a factor of ten. This research endeavors to better quantify the balance between solar and magnetospheric forcing over the range of solar and geomagnetic activity by observing the response, rather than just the conventional input parameters alone. Since the solar heating at low latitudes and the magnetospheric sources at high latitudes control the magnitude and spatial distribution of the global circulation, these drivers strongly affect the neutral composition and density structure. Observing the change in the neutral density and composition structure can provide an additional information source in specifying the spatial and temporal distribution of the upper atmospheric drivers. The improved driver specification may also improve the composition and density specification in the data assimilation scheme. The results of this research may eventually also improve our knowledge of the fundamental solar and magnetospheric sources in the upper atmosphere.

VALIDATION OF THE USU GAIM DATA ASSIMILATION
MODEL OF THE IONOSPHERE FOR OPERATIONAL USEScherliess, L., Schunk, R. W., Sojka, J. J.

, Thompson, D. C., Zhu, L.

Utah State University, Center for Atmospheric and Space Sciences,
Logan, UT 84322-4405

Physics-based data assimilation models of the ionosphere were developed at Utah State University as the central part of a DoD MURI funded program called GAIM (Global Assimilation of Ionospheric Measurements). Recently, the Air Force Weather Agency (AFWA) has selected one of the USU GAIM models for its operational use and the same model will also be implemented at the Community Coordinated Modeling Center (CCMC) for scientific studies. The selected model is based on a physics-based model of the ionosphere and a Gauss-Markov Kalman Filter (GMKF) as a basis for assimilating a diverse set of real-time (or near real-time) observations. The physics-based model is the Ionospheric Forecast Model (IFM), which accounts of five ion species and covers the E-region, F-region and the topside from 90 to 1400 km altitude. Within the GMKF, the IFM derived ionospheric densities constitute a background density field on which perturbations are superimposed based on the available data and their errors. In the current configuration the GMKF assimilates slant TEC from a variable number of ground GPS sites, bottom-side N_e profiles from a variable number of ionosondes, in situ N_e from four DMSP satellites, and nighttime line-of-sight UV radiances measured by satellites. To test the GMKF for real-time operations and to validate its ionospheric density specifications, we have tested the model performance for a variety of different geophysical conditions. During these model runs various combination of data types and data quantities were assimilated. To simulate real-time operations the model ran continuously and automatically, and produced 3-dimensional global electron density distributions in 15 minute increments. In this paper, we will report on the status of the model development and present the results of our validation study, with an emphasis on a comparison with independent observations.

USC/JPL GAIM: A REAL-TIME GLOBAL IONOSPHERIC DATA ASSIMILATION MODEL

Wilson, B.¹, Hajj, G.¹, Mandrake, L.¹
, Wang, C.², Pi, X.¹, Iijima, B.¹

¹JET PROPULSION LABORATORY, 4800 Oak Grove Dr.,
Pasadena, CA, 91109

²University of Southern California, Dept. of Mathematics, Los
Angeles, CA

We are in the midst of a revolution in ionospheric remote sensing driven by the illuminating powers of ground and space-based GPS receivers, new UV remote sensing satellites, and the advent of data assimilation techniques for space weather. The University of Southern California (USC) and the Jet Propulsion Laboratory (JPL) have jointly developed a Global Assimilative Ionospheric Model (GAIM) to monitor space weather, study storm effects, and provide ionospheric calibration for DoD customers and NASA flight projects. GAIM is a physics-based 3D data assimilation model that uses both 4DVAR and Kalman filter techniques to solve for the ion & electron density state and key drivers such as equatorial electrodynamics, neutral winds, and production terms. GAIM accepts as input ground GPS TEC data from 900+ sites, occultation links from CHAMP, SAC-C, IOX, and the coming COSMIC constellation, UV limb and nadir scans from the TIMED and DMSP satellites, and in situ data from a variety of satellites (C/NOFS & DMSP). GAIM can ingest multiple data sources in real time, updates the 3D electron density grid every 5 minutes, and solves for improved drivers every 1-2 hours.

GAIM density retrievals have been validated by comparisons to vertical TEC measurements from TOPEX & JASON, slant TEC measurements from independent GPS sites, density profiles from ionosondes & incoherent scatter radars, and alternative tomographic retrievals. Daily USC/JPL GAIM runs have been operational since March 2003 using 100-200 ground GPS sites as input and TOPEX/JASON and ionosondes for daily validation. A prototype real-time GAIM system has been running since May 2004. RT GAIM ingests TEC data from 77+ streaming GPS sites every 5 minutes, adds more TEC for better global coverage every hour from hourly GPS sites, and updates the ionospheric state every 5 minutes using the Kalman filter. We plan to add TEC links from COSMIC occultations and UV radiance data from the DMSP satellites, when they become available, to the daily and RT GAIM runs. Our presentation will include results from numerous validation case studies and one year of JASON validation statistics. Customers are currently evaluating the accuracy of USC/JPL GAIM nowcasts for ray tracing applications and trans-ionospheric path delay calibration.

MODELING THE HALLOWEEN IONOSPHERIC STORM IMPACT AT MIDDLE LATITUDES

D. Rice^{1,3}, J. V. Eccles¹, J. J. Sojka¹, R. D. Hunsucker²¹Space Environment Corporation, 221 N Spring Creek Parkway Suite A, Providence, UT 84332 USA²RP Consultants, 7917 Gearhart, Klamath Falls, OR 97601 USA³Dept. of Electrical and Computer Engineering, Utah State University, Logan, UT 84322-4120 USA

Effects of the Halloween Storm of 2004 were observed by a number of instruments at the Utah State University (USU) Bear Lake Observatory (BLO), Utah and at the RP Consultants HF monitoring site in Klamath Falls, Oregon. The HF Investigation of D-Region Ionospheric Variation Experiment (HIDIVE) is a collection of passive HF monitors at BLO and Klamath Falls (KF) measuring signal strengths from WWV and WWVH HF beacons. These observations, described in detail in another paper at this meeting, are used to determine HF absorption characteristics of the D region in real time. These real time data are used to determine ionization drivers within the Data Driven D-Region (DDDR) model to generate weather-sensitive specifications of mid-latitude HF absorption characteristics.

The Data Drive D-Region (DDDR) and the Ionospheric Forecast Model (IFM) are combined to model the ionosphere electron density from 40 to 1600 km altitude for input into HF propagation codes. These models are combined with the HASEL ray-tracing code of C. J. Coleman (*Rep. No. SRL0131TR*, Defence Science and Technology Organisation, Australia, 1993) and HF absorption calculations described in Davies (*Ionospheric Radio*, Peter Peregrinus, Ltd. On behalf of IEE, London, 1990). The ionosphere models and HF propagation codes are combined as described by Eccles et al. (*Space Weather*, in press, 2004) to model the impacts of known drivers of ionization during the Halloween Storm days of 2004. These model results are compared to HIDIVE observations. Discrepancies between model and observations suggest the presence of other drivers such as hard particle precipitation and/or NO transport from high latitudes. This study examines methods of ingesting HF signal strength observations discrepancies to estimate ionization drivers to further enhance the weather-sensitive DDDR model.

SPACE WEATHER MAPS OF THE IONOSPHERIC ELECTRON DENSITY DURING THE 2003 HALLOWEEN STORM

T W Garner, G S Bust, T L Gaussiran II

Center for Ionospheric Research, Applied Research Laboratories,
University of Texas at Austin

The geomagnetic storm that began on October 29 and continued through November 1, 2003 has been called the Halloween storm. It was one of the largest geomagnetic storms yet recorded. The NOAA Space Environment Center rated the storm as severe ($Kp \geq 8$) or extreme ($Kp = 9$) for 18 of the 72 hours of this storm. As with any storm of this magnitude, dramatic changes took place in the ionosphere. To understand these changes, ionospheric observations are processed with the Ionospheric Data Assimilation Three Dimensional (IDA3D) algorithm. IDA3D creates three dimensional space weather maps of the ionospheric electron density. These space weather maps show synoptic and global scale changes in the ionosphere. IDA3D is a 3DVAR objective analysis algorithm. It uses available electron density and electron content measurements and a statistical ionospheric model to make the best estimate of the true ionosphere. IDA3D is a flexible algorithm with several inputs including the model grid and the background climate model. For this study, the maps have been limited to $\pm \sim 60^\circ$ (the maximum latitude of the GPS satellites) in order to concentrate on the behavior of the equatorial ionosphere. In addition, the Riley-ICED-Bent-Gallagher (RIBG) empirical model is used because it models both the ionosphere and the plasmasphere. During the Halloween storm, numerous observations of the ionosphere were made including electron content measurements from GPS receivers, both on the ground and on low altitude spacecraft, and tomography beacon receivers, and electron density measurements from ionosondes and satellite instruments. IDA3D weather maps show the variability of the equatorial anomaly peaks and a significant reduction of the plasmasphere.

THEORETICALLY MODELING THE IONOSPHERIC RESPONSE AT LOW LATITUDES TO LARGE GEOMAGNETIC STORMS

Anderson, D.¹, Anghel, A.¹, Araujo, E.¹,
Eccles, V.², Valladares, C.³, Lin, C.⁴

¹CIRES/Univ of Colorado; NOAA/SEC, 325 Broadway, Boulder, CO 80303

²Space Environment Corp., 221 N. Spring Creek Pky, Suite A, Providence, UT 84332

³Institute for Space Research/Boston College, 140 Commonwealth Ave., Chestnut Hill, MA 02467

⁴NCAR/HAO, 3450 Mitchell Lane, Boulder, CO 80301

In the low latitude, ionospheric F region, the primary transport mechanism that determines the electron and ion density distributions is the magnitude of the daytime, upward ExB drift velocity. During large geomagnetic storms, penetration of high latitude electric fields to low latitudes can often produce daytime, vertical ExB drift velocities in excess of 50 m/sec. Employing a recently-developed technique, we can infer these daytime, upward ExB drift velocities from ground-based magnetometer observations at Jicamarca and Piura, Peru as a function of local time (0700 1700LT). We study the ionospheric response in the Peruvian longitude sector to these large upward drifts by theoretically-calculating electron and ion densities as a function of altitude, latitude and local time using the time-dependent Low-Latitude Ionospheric Sector model (LLIONS). This is a single sector ionosphere model capable of incorporating data-determined drivers, such as ExB drift velocities. For this study, we choose 4 large storms in 2003 May 29, October 29 and 30 and November 20- when daytime ExB drift velocities approached or exceeded 50 m/sec. Initial results indicate that the large, upward ExB drift velocities on Oct. 29 produce equatorial anomaly crests in ionization at +/- 20 dip latitude rather than the usual +/- 16 dip latitude. In addition, crests in electron density at 840 km are observed on either side of the magnetic equator by the DMSP F13 SSIES sensor at 1800 LT for each of the four storm periods. We compare the theoretically-calculated results with a variety of ground-based and satellite observations for these four periods and discuss the implications of these comparisons as they relate to the capabilities of current theoretical models and our ability to infer ionospheric drivers such as ExB drifts.

PRELIMINARY ELECTRON DENSITY RECONSTRUCTIONS
OF THE APRIL 2002 GEOMAGNETIC STORM

Daria Sharman, Trevor Garner, Gary Bust , Tom Gaussarian

Center for Ionospheric Research, Applied Research Laboratories,
The University of Texas at Austin

One of the interesting features of the strong geomagnetic storm that occurred between April 17 and 20, 2002 is the rather smooth recovery, which followed. This storm peaked on April 20 and was followed by a recovery period over April 21-22, 2002. On April 20, the *Dst* index reached a minimum level at -149 nT at 0900 UT. Similarly, the Kp level reached 7.33 between 0300 and 0700 UT, indicating a strong G3 geomagnetic storm. Over the next two days, the *Dst* index recovered to nominal conditions. The Kp index returned to undisturbed values of 2.67 by 2200 UT on April 20, and remained under 3 for most of April 21-22, 2002. These dramatic changes in the geomagnetic conditions drive major changes in the global ionosphere. These changes can be observed by examining space weather maps of the global electron density distribution. This study presents preliminary space weather maps of the electron density demonstrate the global ionospheric behavior during this storm recovery. These maps are generated by the Ionospheric Data Assimilation Three Dimensional (IDA3D). IDA3D is a 3DVAR algorithm for ionospheric electron density. It statistically minimizes the available measurements and a background electron density field. Typically, this electron density field is determined from a climate model of the ionosphere, for this study the RIBG model. IDA3D uses several data sets of electron content and electron density measurements including ground-based GPS electron content, LEO-satellite-based GPS electron content, GPS-occultation electron content, radio beacon tomography electron content, ionosonde electron density, incoherent scatter radar electron density and *in situ* satellite electron density observations.

INVESTIGATIONS OF THE TOPSIDE IONOSPHERE AND PLASMASPHERE DISTRIBUTION OF PLASMA DURING MAGNETIC STORMS

Bust, G.S., Garner, T.W.

Applied Research Laboratories, The University of Texas at Austin
(ARL:UT), 10000 Burnet , Austin Texas, 78758

A relatively new data source is used to probe the topside ionosphere and plasmasphere distribution of plasma during magnetic storms.

The primary observations that will be used in this study are observations of total electron content (TEC) measurements made between a GPS receiver on a low-earth orbiting (LEO) satellite, such as CHAMP, and the GPS satellites. These measurements are different from GPS occultation measurements in that they are for positive elevation angles, that is to say, looking *up* at the satellites. Typically such measurements are made every 10 seconds as the LEO satellite moves in its orbit and anywhere from six to twelve GPS satellites are in view at a given time. Thus, this data set directly probes the topside ionosphere and plasmasphere distribution. Stankov [*J. Geophys. Res.*, 2003] and colleagues in their paper refer to this TEC data source as “over satellite electron content” or OSEC. We will focus on data from four OSEC data sources: CHAMP, SAC-C, and GRACE during this study. By combining this data set with ground GPS TEC, *in-situ* measurements of electron density from DMSP and ionosondes through the ionospheric data assimilation three-dimensional (IDA3D) space-weather mapping algorithm we will be able to relate the high-altitude plasma density near the equator and along field lines to the high-altitude distribution in the polar regions.

This presentation will focus on initial results from the October-November 2003 magnetic storms. The OSEC data will be presented and the variation of the topside and plasmasphere distribution of plasma in space and time will be investigated. Tomographic inversions of the OSEC data will be presented, which allows investigation of the height distribution of the topside and plasmaspheric plasma. Finally, IDA3D space-weather maps, using combined ground and space based data sources, will allow a global interpretation of the OSEC results.

ESTIMATING DAYTIME VERTICAL ExB DRIFT VELOCITIES FROM EQUATORIAL MAGNETOMETER OBSERVATIONS USING A MULTILAYER NEURAL NETWORK

Anghel, A¹, Anderson, D¹, Chau, J.², Veliz, O.²

¹CIRES/Univ. of Colorado, NOAA/SEC, 325 Broadway, Boulder, CO 80303

²Radio Observatorio de Jicamarca, Instituto Geofisico del Peru, Aparatado 13-0207, Lima 33, Peru

A recent study has quantitatively established the relationship between the vertical daytime ExB drift velocity in the ionospheric F region and the DH values measured by two magnetometers in the South American (west coast) longitude sector. Magnetometer H component observations from Jicamarca (0.8 N. dip lat.) and Piura (6.8 N. dip lat.) in Peru and daytime, vertical ExB drift velocities measured by the Jicamarca Unattended Long-term Ionosphere and Atmosphere (JULIA) radar have been used to establish this relationship. The magnetometer observations and the JULIA 150 km echo ExB drift measurements were obtained for the period between August, 2001 and September, 2003. A multilayer feed-forward neural network has been designed and trained in order to estimate the quantitative relationship between the vertical daytime ExB drift velocities in the equatorial F-region and the ground based magnetometer observations. We have found that a neural network approach performs better in capturing the non-linear relationship between the input and the output values than the classical least-squares method. An independent data set of vertical ExB drift velocities obtained from Jicamarca Incoherent Scatter Radar (ISR) observations has been used to validate the neural network approach. The RMS error in ExB drift is approximately 3 m/sec. It is thought that the greatest source of remaining error comes from not knowing the E region, zonal neutral wind velocities on a day-to-day basis. A possible proxy for these winds is the vertical component of the magnetic field (Z), since it is believed that zonal neutral winds will affect the Z component at Piura more than at Jicamarca. For this study we add the DZ observations between the Jicamarca and Piura magnetometers as inputs to the neural network in addition to the inputs previously used. The results of this new study will be presented and discussed with an emphasis on how they can be used to infer the day-to-day variability in zonal neutral wind velocities.

Session G3, 08:15 – Sat.

RADIO AND RADAR

TECHNIQUES I

Co-Chairs: F. Lind, J. Sahr

SPECIFYING ERROR BARS FOR PROFILES DERIVED FROM IONOGRAMS

Leo F. McNamra¹, Terence W. Bullett²

¹Institute for Scientific Research, Boston College, Newton, MA USA

²Space Vehicles Directorate, Air Force Research Laboratory, Hanscom AFB, MA USA

Electron density profiles supplied to Kalman filter based data assimilation models, such as the Utah State University Global Assimilation of Ionospheric Measurements (USU-GAIM) model, must be accompanied by error bars so that they can be weighted appropriately with other data sources. Profiles deduced from ground-based vertical incidence ionograms have fundamental limitations due to the lack of observations below some frequency f_{min} (the starting problem), and the lack of echoes from altitudes within the E-F valley (the valley problem). If the ionograms are scaled automatically, issues of correct echo identification must also be addressed.

Techniques have been developed at AFRL to scan autoscaled ionograms to determine which scaled $h(f)$ traces are acceptable, and then to use the true-height analysis program POLAN to derive the corresponding electron density profiles. Empirical models of the underlying and valley ionization developed by J. E. Titheridge are used to resolve the starting and valley problems.

POLAN is run four times, with upper and lower estimates of the true height at a plasma frequency of 0.5 MHz, and upper and lower estimates of the E-F valley width. In one run, the last scaled frequency is taken to be $foF2$, and in another run the value of $foF2$ is obtained (by POLAN) using a least-squares fit to a Chapman layer

The uncertainties in the plasma frequency at a fixed altitude are found to be largest just above the top of the E-F valley. Large uncertainties also arise at the peak of the layer if the scaled trace does not possess sufficient upwards curvature to define the peak adequately.

THREE-DIMENSIONAL ELECTRON DENSITY INVERSION
FOR THE DYNASONDE: PRINCIPLES AND FIRST RESULTSZabotin N.A.¹, Wright J.W.¹, Zhabankov G.A.²¹CIRES, University of Colorado at Boulder, Box 216, Boulder, CO
80309, USA²Rostov State University, Rostov-on-Don, 344090, Russia

The structure of ionospheric plasma layers often differs significantly from the simplified plane-stratified model that underlies classical one-dimensional algorithms for inversion of ionograms to electron density profiles (e.g., POLAN). Horizontal gradients are always present in the ionosphere, and sometimes these become very significant. Regular examples of this situation are the sunrise/sunset ionospheres. Other important examples are Atmospheric Gravity-Wave signatures, recently recognized storm-enhanced density plumes, and the structures characteristic of equatorial Spread F.

The Dynasonde provides abundant information about the geometry of ionospheric reflections. Each ionogram echo, when accepted by physics-based classification and selection procedures, includes echolocation parameters among its physical attributes. The virtual spatial distribution of echoes often demonstrates very elaborate variations, reflecting actual properties of the three-dimensional plasma distribution. What algorithm may be used to quantify this information?

The dynasonde measures parameters of the reflected echoes at a single point on the ground. This is its main distinction in comparison with tomography and other established inversion methods. It is necessary to have a model for the propagation medium that is sufficiently flexible to represent the varying gradients of electron density, but with the minimum number of parameters suitable for a least-squares procedure applicable to measured values of virtual ranges and angles-of-arrival. We suggest the "Wedge-Stratified Ionosphere" (WSI) for this purpose. The WSI substitutes for the usual plane-stratified assumption: plasma density surfaces are represented locally (at a sequence of ranges) by tilted sections of "frame" planes; the electron density between two frame planes (inside a "wedge") depends only on the corresponding angle between the two planes.

The inversion algorithm shares some generic properties with its one-dimensional counterpart. For example, determination of the WSI model parameters proceeds upward, explicitly in radio frequency, implicitly in slant range, and consecutively from the bottom of the ionosphere. Since the radio propagation is essentially three-dimensional, the inversion problem cannot be reduced to a matrix inversion as is done in some treatments of the one-dimensional case. Numerical ray tracing methods are used instead. First results of application of this approach are demonstrated in this paper.

REAL TIME RAYTRACING THROUGH MEASURED NE
PROFILES IN THE PRESENCE OF IONOSPHERIC TILTS

Reinisch, B. W.¹, Huang, X.¹, McCarthy, K.²

¹Center for Atmospheric Research, 600 Suffolk St, Lowell MA
01854

²Codem Systems, 7 Executive Park Drive, Merrimack, NH 03054

High frequency direction finding systems measure the angles of arrival of signals at selected frequencies. Ray tracing techniques can accurately determine the location of the transmitter if the 3-D electron density distribution between the DF site and the transmitter location is known. A collocated digisonde at the DF site can measure the vertical electron density profile and the local ionospheric tilt in real time providing the inputs for the construction of the 3-D Ne distribution. The vertical profile is obtained from the ARTIST-scaled ionogram, and the local tilt from the skymaps recorded after each ionogram. The characteristics of each layer, e.g., critical frequencies and peak heights, are expressed as function of latitude Λ , and longitude Φ . In the neighborhood of the DF site, (Λ_0, Φ_0) , each characteristic, e.g., f_0F2 , is given as

$$f_0F2(\Lambda, \Phi) = f_0F2(\Lambda_0, \Phi_0)[1 + C_1(\Lambda - \Lambda_0) + C_2(\Phi - \Phi_0)] \\ \times [1 + C_3(\Lambda - \Lambda_0) + C_4(\Phi - \Phi_0)]$$

For a given azimuth measured by the DF sensors, the coefficients C_1 and C_2 are determined with the URSI / CCIR coefficients that are also used by IRI, and calculation of C_3 and C_4 makes use of the measured tilt data. At any time when the measured density profile and tilt data are available, the 3-D density distribution represents the instantaneous ionosphere structure near the site. The calculated distribution reproduces the measured vertical profile and tilt.

The numerical raytracing includes the effects of the magnetic field and properly treats the spitzte effect making the program useful also for small distances. Ray tracing through simulated tilts shows differences of the ground distances for one hop HF propagation to vary from about 1 km to 200 km depending on the assumed tilts and distances. Operational tests have demonstrated very good results in determining the transmitter location for a distance up to ≈ 100 km, and have illustrated the importance of using the current ionospheric profiles and tilts in the ray tracing.

NEW METHODS FOR PULSED RADAR AND IONOSONDES:
ITERATIVE PRECISION SPECTRUM ANALYSIS AND TWO
COHERENT FREQUENCIES FROM SINGLE PULSE

Bibl, K., Cheney, G. P.

Center for Atmospheric Research, 600 Suffolk St., Lowell MA
01854

Using standard spectrum analysis (e.g.: FFT), a simple process determines the exact frequency, amplitude, and phase of the largest spectral line. In the time domain, the accurate sine and cosine functions are subtracted from the data, but stored when the information is useful. By these means not only the spectral line is removed from the spectrum, but also its unwanted wings. This process can be repeated as often as necessary until a sufficient signal-to-noise ratio is established and a sufficient number of wanted signals are detected or interferers are eliminated. Applications are unlimited: precise determination of specific frequencies, including amplitude and phase, in a spectrum; elimination of large interferers in broadband communications; and increase of the dynamic range in special codes and non-linear spectrum analysis.

Even in sophisticated Spectrum Analyzer equipment, processing time for very long spectra significantly limit spectral resolution. But the presented method (which has been patented) can improve the resolution for the larger spectral lines substantially. Thus the amplitudes and phases of harmonics could be measured accurately in respect to the basic frequencies.

Coherent Radars are often affected by narrow-band interference that can be 40 dB above the pulse signal. All the intra-pulse and pulse sequence coding does not help in those cases. Iterative Precision Spectrum Analysis eliminates many spectral lines in real time. In mono-static pulse sounding, measurement of long-range echoes with large Doppler frequencies is often coded pulse sequences cannot be used for pulse compression to reduce noise. Although needed. If, in addition, echoes from short ranges could occur simultaneously, standard phase the method of unevenly spaced pulses, called the Staggered Pulse Code, is a known alternative, it has not been used much because of its limited dynamic range of amplitudes. These limitations are overcome by the proposed method.

For single and sequentially coded pulses, simple half-sine modulation can be used to extract two coherent frequencies for accurate range measurements. In ionosondes this shortens the sounding time by one half.

INTERPRETATION OF HF SOUNDING OBSERVATIONS IN THE EARLY STAGES OF THE FORMATION OF EQUATORIAL BUBBLES

Sales, G.¹, Huang, X.¹, Reinisch, B. W.¹,
, Dozois, C.¹, Abdu, M.²

¹Center for Atmospheric Research, 600 Suffolk St., Lowell MA 01854 USA

²Instituto Nacional de Pesquisas Espaciais (INPE), feAve dos Astronautas 1758 C.P. 515, 12202-970 Sao Jose dos Campos, SP Brazil

During the recent COPEX campaign in South America (Oct. 2002 through Dec. 2002), data taken at the equatorial station near Cachimbo, Brazil often showed, in the early evening, the presence of satellite traces on the vertical ionograms always preceding the appearance of strong equatorial bubbles. These radio soundings, made continuously over the duration of the campaign with a time resolution of five minutes, were previously analyzed to show that these additional ionogram traces appeared, on the average, seven minutes after the vertical velocity in the F-layer reached its peak value and 15 minutes before local spread F began. It is important to note that all of the events occur before the solar terminator, at F-region altitudes, passes over the sounder. F-layer sunset is approximately 60 minutes after ground sunset. The time of occurrence and structure of these satellite traces are interpreted as the initial deformations of the lower region of the F-layer some of which ultimately grow to become eastward drifting equatorial bubbles.

Using a relatively simple model of quasi-periodic perturbations of a realistic F-layer model in conjunction with a new numerical 3-D ray tracing code developed here by one of the authors (Huang), it has been possible to connect these disturbances to the appearance of the extra traces on the vertical ionograms. It is shown here that after sufficient development of the instability, the condition for ray orthogonality with the deformed layer is satisfied over a range of sounding frequencies. These simulations were carried out over the time period for the development of the bubbles from their initial appearance until the instability grows through the peak of the F-layer. These ray tracing results also indicate the trapping of HF waves within the bubble structure, often at frequencies above foF2, resulting in the characteristic extended traces seen on ionograms as equatorial bubbles drift inward from distances of several hundred kilometers from the sounder.

DASI: DISTRIBUTED ARRAYS OF SMALL INSTRUMENTS FOR SPACE SCIENCE RESEARCH

John C. Foster

MIT Haystack Observatory, Atmospheric Sciences Group

Recent ground-based radar and radio-propagation research has revealed space weather storm fronts which sweep across the Americas during strong geomagnetic disturbances. Mesoscale and spatially and temporally localized processes and effects play a significant role in the interconnection between the high-altitude magnetosphere and Earth's ionosphere and lower atmosphere. In order to address the physical causes and characteristics of such space weather phenomena, a means of providing high spatial and temporal resolution observations of Earth's upper atmosphere is needed. In recognition of this need, the NAS Solar and Space Physics Decadal Survey has recommended that the next major ground-based instrumentation initiative for space science research be the deployment of widely-distributed arrays of small instruments. Analogous to the meteorological arrays which support terrestrial weather research, modeling, and predictions, space weather arrays will provide continuous real-time observations of Earthspace with the resolution needed to resolve mesoscale phenomena and their dynamic evolution. Ground-based DASI instrumentation will address the need for observations to support the next generation of space weather data-assimilation models and will push our understanding of the physical processes which interconnect the spheres of Earthspace to a new level. Planning for the deployment of DASI will involve the development of miniaturized and robust instruments and instrument clusters and the ability to communicate with them in real time and to distribute their data to a wide variety of users.

The NAS Committee on Solar and Space Physics (CSSP) is preparing a report on the scientific need for such arrays, the infrastructure needed to support and utilize them, and an implementation plan for their deployment. There are many opportunities for the involvement of the radio science community in DASI - both in its current planning stage, and in its implementation over the coming decade. The current status of the DASI initiative will be reviewed and an outline of the NAS report addressing the compelling science issues to be addressed by small instrument arrays will be presented.

HF BEACON NETWORKS FOR IONOSPHERIC MAPPING

J. J. Sojka², D. Rice¹, J. V. Eccles³, R. D. Hunsucker⁴¹Dept. of Electrical and Computer Engineering, Utah State University, Logan, UT 84322-4120 USA²Center for Atmospheric and Space Sciences, Utah State University, Logan, UT 84322-4405 USA³Space Environment Corporation, 221 N Spring Creek Parkway, Suite A, Providence, UT 84332 USA⁴RP Consultants, 7917 Gearhart, Klamath Falls, OR 97601 USA

The Utah State University (USU) Bear Lake Observatory (BLO) in northern Utah has demonstrated that a relatively low-cost combination of magnetic, optical, and RF instruments can characterize space weather events such as the geomagnetic storm of 31 March 2001 (Sojka et al., *Space Weather*, in press, 2004), but in order to understand the physical processes and their adverse impacts, a network of such magnetic/optical/RF (M/O/RF) instruments is needed.

In addition to the traditional magnetometer, all-sky camera, ionosonde, and the newer GPS TEC system, an HF monitoring system is being developed to provide near-real-time ionospheric diagnostics. While monitoring HF beacons has been used for decades for relatively short-term ionospheric and propagation studies, our approach combines inexpensive automated monitoring of multiple HF beacons with ionospheric models to improve model specification of D-, E-, and F-region ionospheric parameters and to detect the presence of unmodeled phenomena such as sporadic E.

HF beacons and monitors deployed in a continental DASI configuration could map ionospheric responses to space weather phenomena and may be used to infer hard-to-measure D-region chemistry parameters in conjunction with ionospheric models. The system could also map standard ionospheric parameters (critical frequencies, MUFs) with less impact on other spectrum users than traditional sounding approaches.

In this presentation, we describe a prototype monitoring and modeling system (Eccles et al., *Space Weather*, in press, 2004) that has been operating since the end of 2002 and consider the extension of this system to a distributed array of small cognitive beacons (beacons incorporating monitoring and modeling capabilities.) We believe that such a network would be useful for ionospheric weather studies, assimilation models, and for HF communicators who could use the network for real-time channel evaluation (RTCE).

DISTRIBUTED COMPUTING FOR RADIO SCIENCE AT
MILLSTONE HILL

Lind, F.D., Erickson, P.J., Holt, J.M. , Rideout, W.J.
MIT Haystack Observatory, Route 40, Westford, MA 01886 USA

The transition to a Software Radar system at Millstone Hill has resulted in an incoherent scatter radar system where the signal processing and analysis is all performed in software on general purpose computing systems. This architecture uses distributed computing to process RF data from the radar at the voltage level. The distributed computing approach is natural because for most ionospheric radar techniques it is relatively easy to break the signal processing and analysis into individual tasks which can run in parallel. For example processing of different ranges of data or integration periods in time can be handled simultaneously. Additionally it is possible to run multiple types of analysis and processing in parallel on a data stream to exploit more of the scientific information which may be present in the signals. By archiving the voltage level data such analysis may also be done retrospectively.

At Millstone Hill we have recently received hardware support for the Intercepted Signals For Ionospheric Science project (ISIS) as part of the DoD DURIP program. The ISIS Array is a distributed radio science network for studying the mid-latitude ionosphere. The ISIS Array will consist of a series of nodes each of which is a coherent software radio system capable of operating as a flexible multi-role radio science instrument. The nodes will be deployed in the northeast and northwest portions of the continental U.S.A. and will form observational networks in these regions. Operational modes involving active and passive multistatic radar imaging, satellite beacon observations of TEC and scintillation, radio intercept and spectral monitoring, and time difference of arrival (TDOA) applications will be supported over a wide range of operating frequencies

We have combined the cluster computing system associated with the ISIS Array with the one we have constructed for the Incoherent Scatter Radar. By doing this we have created a unified computing system which is powerful enough to handle the signal processing and analysis needs of multiple radio science instruments simultaneously. We will discuss the architecture of the resulting computing system, its capabilities, and discuss its application to radio science data processing for incoherent scatter radar, GPS TEC mapping, and the ISIS Array. We will also discuss the importance of this type of computing architecture in the context of future efforts to develop Distributed Arrays of Small Instruments (DASI) for space science applications.

AMISR-8 AT JICAMARCA

Craig J. Heinselman¹, Todd Valentic¹, John D. Kelly¹
, Rodolfo Cuevas^{1,2}, Jorge L. Chau³

¹SRI International

²Cornell University

³Jicamarca Radio Observatory

The Advanced Modular Incoherent Scatter Radar (AMISR) system has been in the planning and early development stages for several years. The construction of that system was recently funded and it is now in progress. In preparation for the full deployment, a subset of an AMISR face has recently been deployed to Jicamarca, Peru for the first ionospheric measurements with the system. This talk will discuss those measurements and present early results.

The AMISR is the first incoherent scatter radar (ISR) specifically designed to be easily relocated and to allow a flexible physical configuration of the antenna to match specific scientific goals. The smallest building block of the system is called a Panel and consists of a planar array of thirty-two crossed-dipole antennas with associated transmitter, receiver, and control electronics. Each panel is roughly 2m x 3.5m in size and weighs approximately 385 kg. The AMISR-8 sent to Peru consists of eight panels, a 400 Hz power source, Up and Down Converters for the RF drive and reception, two data acquisition systems including digital receiver cards and PC-class computers to support basic data acquisition as well as interferometry, a panel serve computer, a network time server, and calibration electronics.

The capabilities of AMISR are well suited to this deployment. Its ability to change antenna look directions on a pulse-by-pulse basis is especially useful for probing the spatial structure of various coherent echo regions above Jicamarca. Especially when combined with interferometric sampling of the received waveforms, fine scale structures can be probed in detail. The information gathered will furthermore be extrapolated with the idea in mind of extending the array for a possible future deployment.

DETERMINATION OF PRIMARY ELECTRON SPECTRA
FROM INCOHERENT SCATTER RADAR MEASUREMENTS
OF THE AURORAL E-REGIONSemeter, J.¹, Kamalabadi, F.²¹Boston University, Boston, MA²University of Illinois at Urbana-Champaign

A technique is presented for inverting incoherent scatter radar (ISR) measurements of the ionospheric E-region produced by auroral electrons to determine the energy spectrum of primary electron beam. The specific radar mode applied involves simultaneous transmission of a Barker coded pulse and a single 160 μ s on different frequency channels. This scheme allowed us to isolate events wherein total backscatter power provides a reliable estimate of the extreme altitude gradients in the E-region plasma produced by auroral precipitation. These measurements were used to derive ion volume production rate profiles. A linear model was then constructed relating electron differential number flux to our estimates of ion volume production rate. The model was inverted using the Maximum Entropy Method (MEM). A thorough simulation study was performed, demonstrating that this implementation of ISR profile inversion is remarkably robust to the principal sources of model and measurement uncertainty.

The procedure was applied to high resolution measurements (1.2 s X 1 km) by the Sondrestrom ISR during an auroral surge. An analysis of bulk plasma properties extracted from the recovered spectra suggested that the relationship between the characteristic energy (i.e., location of the "bump on tail" in the distribution) and the net number flux (related to current) in the primary auroral electron beam is highly nonlinear during auroral formation. Such a nonlinear current-voltage characteristic is predicted by models of the auroral acceleration region (AAR) involving turbulent transport. This perspective on the temporal behavior of the AAR cannot be accessed through space-borne measurements, which provide a "snapshot" of AAR dynamics compared to timescales involved in auroral arc formation. We, thus, argue that ISR profile inversion is a critical tool for addressing time-dependent coupling of the magnetosphere and ionosphere.

Session G4, 13:35 – Sat.

**RADIO AND RADAR
TECHNIQUES II**

Co-Chairs: F. Lind, J. Sahr

AN INVERSE-THEORETIC APPROACH TO THE OPTIMAL
EXTRACTION OF IONOSPHERIC PARAMETERS FROM IN-
COHERENT SCATTER RADAR MEASUREMENTS

Farzad Kamalabadi, Romina Nikoukar¹, Erhan Kudeki¹
, Michael Sulzer², Sixto Gonzalez²

¹University of Illinois at Urbana-Champaign

²National Astronomy and Ionosphere Center, Arecibo Observa-
tory

The extraction of altitude profiles of ionospheric plasma parameters from the incoherent scatter radar (ISR) measurements requires careful consideration of two aspects of the inversion process. The first is the range smearing effect of the radar pulse on the information from one altitude over a range of altitudes, and the second is due to the nonlinear relationship between the plasma parameters and the measured spectra. The reduction of the range smearing of the ionospheric autocorrelation function has been addressed conventionally by incorporating coding schemes in full-profile analysis whereby initial models of the altitude profiles of the plasma parameters are assumed, the theoretical autocorrelation functions (ACF's) based on these models are calculated upon the proper decoding of the imposed coding schemes, and the result is compared with the data iteratively via non-linear least squares methods to converge to an estimate that is desirably close to the constructed models. The performance of such techniques, however, is limited by the ability to specify accurate initial models for the altitude profiles of the parameters.

In this work, we present a model-free two-step technique for the estimation of ionospheric parameters with improved accuracy and reduced computational complexity. The approach is to remove the range smearing from the measurement in the first step, hence obtaining ionospheric ACF's at each altitude individually. This is accomplished by performing a set of 1-D deconvolutions for each time lag, where regularization techniques are developed and incorporated in order to ensure robustness in the presence of noise. Extraction of the plasma parameters based on the resolved ACF's forms the second step and requires non-linear least squares fitting methods. Toward this goal, simulations were performed to confirm that the transmission of a pair of amplitude modulated (AM) pulses yields more accurate deconvolution results (due to reduction in range smearing effect) and hence more accurate parameter estimation than transmitting a simple long pulse. To evaluate the performance of the method, an F-region experiment was conducted at Arecibo observatory in which two AM pulses and a long pulse were transmitted in 10-second intervals. The new technique was examined on both data sets. The results of applying the new technique to AM data show superior performance over those of the long pulse data, and also over the conventional methods currently used in Arecibo.

L1-NORM AND WAVELET TRANSFORM TECHNIQUES FOR ESTIMATING INCOHERENT SCATTER POWER AND LAG-PROFILES IN THE PRESENCE OF INTERFERENCE OR A RAPIDLY VARYING IONOSPHERE.

Holt, J. M.

MIT Haystack Observatory, Route 40, Westford, MA 01886, USA

Incoherent scatter power and lag-profile measurements must be integrated over many samples in order to reduce the variance of the estimates to a useful level. Typically integration periods on the order of tens of seconds to a few minutes are required to measure ionospheric parameters with sufficient accuracy.

The measurements can be corrupted or rendered useless if they include a non-ionospheric component such as radio frequency interference (RFI) or a satellite in the beam. Little can be done if severe RFI persists throughout the integration, but frequently this type of interference occurs in bursts and lasts only a few seconds. Satellites also remain in the beam for much less than a typical integration period. We have implemented a technique which supplements the usual L2-norm (mean) estimate of the integrated lag-profiles with an L1-norm (median) estimate. Each integration is divided into up to 64 subintegrations and the median of each series of lag-products is computed. Then, either a range-dependent sliding median or L1 cubic spline fit can be computed for each lag-profile, which is particularly useful for alternating-code measurements. In practice, this procedure usually eliminates almost all external interference and sufficiently improves alternating-code measurements that we have been able to eliminate single-pulse measurements in most Millstone Hill combined E-F region experiments.

While it has proven very effective, this technique does not address changes in the ionospheric return which occur on a time scale shorter than the predefined integration period. These changes can be either truly temporal, or the result of antenna motion, as when an azimuth scan moves the beam through an ionospheric feature such as the mid-latitude trough. We have addressed this problem by applying wavelet denoising to long time-series of very short integration periods of, for example, 100 samples. This procedure can isolate changes greater than the inherent accuracy of the short integration (10% for 100 samples of the power profile) with a time resolution equal to the length of the short integration (1 s for 100 samples/s). This effectively amounts to adaptive integration, with the length of each integration period determined by the data instead of being a fixed period of time. A depth 7 wavelet transform of 1 s samples yields integration periods of 1 to 128 s, depending on how rapidly the signal is changing. Very short bursts of interference are also isolated with a resolution equal to the short integration period. Various wavelet transforms can be employed in this technique.

MEASURING F1 REGION ION COMPOSITION AND TEMPERATURES WITH PLASMA AND ION LINE DATA AT ARECIBO

Aponte, N.¹, Sulzer, M. P.¹, Nikoukar, R.²,
Nicolls, M. J.², Gonzalez, S. A.¹

¹Arecibo Observatory, Space and Atmospheric Sciences Group, Arecibo, PR 00612

²University of Illinois at Urbana-Champaign, Department of Electrical and Computer Engineering, Urbana, Illinois 61801

³Cornell University, School of Electrical and Computer Engineering, Ithaca, NY 14853

One particular problem of the incoherent scatter (IS) radar technique since its beginning has been measuring unambiguously the electron and ion temperature (T_e and T_i) plus the molecular ion fraction in the F1 region during the day when T_e is greater than T_i . So far, pretty much all IS radars make some assumptions in order to routinely process IS autocorrelation functions to get at least some values for temperatures or ion composition. In this paper we show one solution to this problem, which is based in the combination of plasma line and ion line portions of the IS spectrum to obtain unambiguous T_e , T_i and molecular ion fraction during the day. While the idea of combining plasma line and ion line information to study the F1 region was initially used in the early 1970s and again tested in the late 1990s, it is only recently that all the technology is in place to develop a technique that can be used routinely (as in World Day observations) to measure both parts of the spectrum with very high accuracy. Thus for this work, we will be using very accurate electron density measurements from the coded long-pulse plasma line experiment to reduce the number of parameters that need to be determined from the least-squares fitting of the F1 region ion line autocorrelation functions obtained from and a new version of the multiple-radar autocorrelation function (MRACF) experiment. The MRACF experiment is the standard mode to determine electron density, electron and ion temperatures, ion composition (above the F peak where there is atomic oxygen and possibly light ions) and ion velocities in the F region at Arecibo.

AN ON-DISH 430 MHZ INTERFEROMETER FOR RADAR METEOR OBSERVATIONS AT ARECIBO.

Mathews, J.D.¹, Briczinski, S.¹, Meisel, D.D.^{1,2}
, Breakall, J.K.¹, Sulzer, M.P.³, Perillat, P.³, Castro, E.I.³

¹Communications Space Sciences Lab, Penn State University,
University Park, PA 16802

²Dept of Physics Astronomy, SUNY-Geneseo, Geneseo, NY 14454

³Arecibo Observatory, NAIC, Arecibo, PR 00612

Radar meteor observations at Arecibo Observatory are characterized by excellent Doppler and range resolution but with only a dynamics-inferred indication of the meteoroid trajectory through the beam. The location of the meteoroid in the beam is in fact the largest unknown for typical events even though the beam is only 300 m in diameter in the meteor zone. The only viable solution to this dilemma is construction of a multi-element interferometer mounted on the carriage house that supports the 96-foot linefeed. The size and layout of the horn-feed in the Gregorian system precludes mounting additional feed horns there. To begin testing an interferometer system, a dual-linear, 4-element Yagi of exceptional mechanical stiffness and pattern appropriate to illuminating the dish with little vignetting was designed, constructed, and mounted near the paraxial surface for validation tests in early September 2004. The mount-point was 5.37 wavelengths up-hill and to the left of the center of the linefeed. The antenna was phased to yield the same circular polarization as the linefeed on receive and low-power was applied to the linefeed determining the isolation between the linefeed and the Yagi to be at least 58 dB. The antenna was then connected to a spare room-temperature receive system with just a limiter as protection against the nominal 2 MW transmitter power. This system yielded a system temperature of 120 K and, when calibrated using multiple scans of point radio source 3C286, was found to have a gain of -18 dB relative to the linefeed—about -10 dB is expected for an optimally situated point source. The nascent interferometer system was used to collect data for nearly 24 hours (11-12 September 2004) at about 0.5 MW peak-power with many coincident meteor events observed. We report on further calibrations of this system, the real-time data processing system that is being prepared, and the first single-axis meteoroid trajectory studies resulting from these recent observations.

FIRST EVIDENCE OF BEAM BROADENING EFFECT DOMINATING DOPPLER SPECTRA OF FIELD-ALIGNED IRREGULARITIES IN SPORADIC E REGION

Chu, Y.H.¹, Wang, C.Y.²¹Institute of Space Science, National Central University²Department of Physics, Chinese Cultural University

With the interferometry technique implemented at the 52 MHz Chung-Li VHF radar, for the first time we present the observational evidence showing that the observed Doppler spectral widths of the field-aligned irregularities in the sporadic E region may be dominated by the beam broadening effect. Statistics indicates that the ratio of the beam broadening spectral width to the observed Doppler spectral width for the data investigated in this research is in the range 0.1–0.6. In a special case, however, the ratio can be as large as more than 0.8. After removing the beam broadening spectral width from observed spectral width, we obtain that the magnitude of the spectral width caused by the random fluctuation of the plasma irregularities is in the range 1–7 m/s comparable to that induced by the neutral turbulences in Es region. We also examine the power law relation between the observed Doppler spectral width and the drift velocity of the irregularities, showing that the estimated power value is only about 0.289 which is much smaller than the value of 4/3 predicted by the theory of non-linear turbulence energy cascade process. This result is in excellent agreement with that obtained by a stochastic model that simulates the observed Doppler spectral width in terms of the combination of the spectral width caused by neutral-induced plasma irregularities and the beam broadening spectral width. Therefore, it appears very likely that the mechanism involved in the generation of the 3-meter field-aligned irregularities for the present case seems to be the neutral turbulences that induce the plasma irregularities responsible for the radar returns, instead of the non-linear turbulence energy cascade process from primary plasma wave associated with the gradient drift instability.

E-REGION ELECTRON DENSITY, AND ZONAL WIND VELOCITY PROFILES INFERRED FROM COHERENT SCATTER RADAR EXPERIMENTS AT JICAMARCA

Shume, E. B.¹, Hysell, D. L.¹, Chau, J.L.²¹Cornell University, Cornell University²Jicamarca Radio Observatory

A series of radar experiments has been conducted since March 2004, utilizing a newly installed bistatic radar system at the Jicamarca Radio Observatory. The radar system is designed to monitor electron density profiles in the equatorial electrojet region using a coherent scatter radar technique that utilizes the Faraday rotation of the scattered signal. Here, we present the resulting E-region electron density profiles. We compare our electron density estimates with: electron density profiles derived from the Chapman production function, electron density profiles measured by rocket experiments, the International Reference Ionosphere (IRI-2001) model predictions, and peak electron density estimates from the Jicamarca Digisonde Portable Sounder (DPS-4). Overall, the radar measured electron density profiles have magnitudes and shapes comparable to the theoretical and experimental electron density estimators mentioned above. However, it is noteworthy that the measured and IRI-2001 model density profiles disagree significantly below the E-region peak.

Next, we present zonal wind velocity profile estimates in the equatorial electrojet region. We combine measured Type II plasma wave phase velocities with a linear wave dispersion relation to retrieve E-region zonal winds. We employ an iterative numerical procedure that retrieves zonal wind profiles whenever the difference between the measured and theoretical Type II phase velocities is tolerable. Type II phase velocities are obtained from the oblique coherent scatter radar observations at the Jicamarca Radio Observatory, and electric fields driving the instabilities are derived from a 3-D electrostatic potential numerical model. We compare our wind estimates with the NCAR TIME-GCM model wind profiles, zonal winds measured with chemical release experiments, and wind profiles measured by the Doppler Interferometer (TIDI) instrument onboard of the TIMED satellite.

DETECTION AND MITIGATION OF POOR SELF AMBIGUITY TO MAINTAIN RESOLUTION IN PASSIVE RADAR.

John Sahr, Andrew Morabito, Melissa G Meyer

University of Washington, Electrical Engineering, Seattle WA
98195-2500

Passive radar systems are completely reliant upon uncooperative source for illumination. Commercial FM broadcasts have proven to be very useful to collect superb interferometric range-Doppler distributions of auroral E region irregularities. However, the range and Doppler resolution is occasionally poor due to features of FM modulation. In particular, speech contains many periods of silence, during which the effective bandwidth of FM modulation is low. During such periods, the range resolution degrades from its typical value of 1 km to as much as 1000 km — effectively ruining the range-Doppler distributions.

Upon detailed examination of the transmitter waveforms we see that the periods of ambiguity are actually quite brief, lasting tens of milliseconds, and rarely occupying more than ten percent of the time series. A variety of mitigation strategies have been considered. One of the more elaborate would involve computing an optimal "mismatched filter" that would at least partially correct the ambiguity. This approach has a number of serious difficulties, not the least of which is the enormous processing which would be needed to determine the filter coefficients. Furthermore, because the matched filter provides optimal SNR (in certain conditions which are approximately relevant here), it is guaranteed that the SNR of the result will be inferior to that of a "better" waveform.

A far simpler approach is to rely upon the fact that the periods of poor ambiguity may be frequent, but are sparse. A simplified "mismatched" filter can then operate by simply discarding the transmitter signal when it has poor ambiguity. If ten percent of the signal is discarded, then the net impact upon the SNR of incoherently detected power is of the order 1 dB — usually quite tolerable.

In this report we provide a statistical study of the occurrence of "bad ambiguity" in real broadcasts. We also describe a very computationally simple technique to dramatically reduce the deleterious effects of poor ambiguity, and illustrate its effect on data taken by observations of electrojet irregularities with the Manastash Ridge Radar.

Session H1, 8:40-Monday

DUSTY PLASMA

Chairperson: Marlene Rosenberg

ACCELERATION AND EXTREME DISTORTION WITHIN
THE VAN ALLEN RADIATION BELTS DURING THE "HAL-
LOWEEN" SOLAR STORMS OF 2003

Baker, D. N.¹, Kanekal, S. G.¹, Li, X.¹
, Monk, S. P.¹, Goldstein, J.², Burch, J. L.²

¹Laboratory for Atmospheric and Space Physics, University of
Colorado, Boulder, CO

²Southwest Research Institute, PO Drawer 28510, San Antonio,
TX

Sunspot group number 484 appeared on the east limb of the Sun's disk on 18 October 2003. As it and concurrent sunspot groups 486 and 488 rotated across the visible solar surface during the subsequent two to three weeks, the Sun produced spectacular enhancements of solar X-rays ('flares'), solar energetic particles, and, ultimately, some of the largest geomagnetic storms on record. The interplanetary shock waves and coronal mass ejections launched by the Sun reached Earth's vicinity in time periods as short as one day. In striking Earth's outer magnetosphere, these high-speed solar disturbances compressed, distorted, and enhanced the Earth's radiation (Van Allen) belts in ways that have not previously been witnessed by in situ measuring devices. We have continuously observed the Van Allen belts for nearly 12 years with the Solar, Anomalous, and Magnetospheric Particle Explorer (SAMPEX) spacecraft. In the SAMPEX lifetime there has not been such an enhancement and significant distortion of the radiation belts as occurred in late 2003. The center of the outer Van Allen belt is usually about 20000 to 25000 km away from Earth's surface (as measured above the equatorial part of the Earth). During the Halloween Storm, the Van Allen radiation belt electron population was powerfully accelerated and was pushed inward toward Earth's surface to a degree not observed before. From November 1 to November 10, the outer belt had its center only about 10000 km from Earth's equatorial surface. This normally is a place where there are almost no energetic electrons at all. Here we show the observational evidence for the powerful and quite profound changes produced in Earth's radiation belts. We also show - through global imaging data - how such changes were related to the highly distorted Earth's plasmaspheric structure. We discuss why these effects persisted for many weeks and months following the geomagnetic storms themselves. We also note the important practical consequences - the "space weather" effects - of such a remarkable solar-terrestrial sequence of events.

RECENT OBSERVATIONS OF RELATIVISTIC ELECTRON
ENERGISATION IN THE EARTH'S MAGNETOSPHERES. G. Kanekal^{1,2}, D. N. Baker¹, J. B. Blake³¹LASP, University of Colorado, Boulder, CO²Catholic University of America, Washington DC³Aerospace Corporation, El Segundo, CA

The energization to relativistic energies of electrons in the Earth's inner magnetosphere is still not fully understood. However, it has long been known that the basic interplanetary drivers are the solarwind and the southward component of the interplanetary magnetic field. Increased solar wind speeds together with the southward turning of the interplanetary field lead to enhanced levels of relativistic electron fluxes in the outer Van Allen radiation belts. Many physical models have been proposed to connect the basic interplanetary causes to the observed increase in the relativistic electron flux levels. Broadly the models rely on particle transport or in-situ acceleration of low energy electron populations. Physical models that have been proposed to explain electron energization invoke physical processes ranging from radial diffusion dominated particle transport to in-situ energization through wave-particle interactions. These models can be discriminated on the basis of pitch angle evolution, flux growth and decay rates.

Observations of the characteristics of electron energization can help identify the dominant physical process(es) causing the energization. Important observational features include pitch angle distributions, electron flux growth and decay rates, spatial extent and electron spectra. Measurements of flux isotropization time-scale which provides information about the time evolution of pitch angle distributions are important in identifying the dominant mechanism.

This paper reviews the recent observations of relativistic electrons made by spacecraft such as SAMPEX, POLAR and GOES and LANL geosynchronous spacecraft. The paper will emphasize observational aspects such as global coherence and spectral characteristics of electron energization. Observations from SAMPEX comprise nearly a solar cycle and POLAR about a decade. Both provide full coverage of the outer zone over the energy range of interest from a few hundred keV to a few MeV.

PHYSICAL PROCESSES LEADING TO HARD ELECTRON FLUXES FROM MAGNETIC STORMS

W. Horton, M. Mithaiwala

The University of Texas at Austin, The Institute for Fusion Studies RLM 11.222, Austin, TX 78712

An integrated picture of the sequence of complex physical processes thought to be responsible for the creation of MeV electrons following the main phase of geomagnetic storms is described. Plasma sawtooth injection events during periods of sustained southward IMF inject energized plasma into the inner magnetosphere from the nightside plasma sheet. The injections are driven by substorms and magnetically characterized as dipolarization events in which low energy (< 300 keV) electrons are convected to the inner magnetosphere. Storms selected by the GEM community for coordinated studies are used to show the characteristics of substorm injections. For example, the 4 October 2000 storm has a eight well diagnosed substorms before the main phase of the ring current signal Dst reaches its minimum of 280nT. Details of electron orbits and their energy gain for ensembles of electrons are shown using the Li et al. model for the dipolarization fronts. The second stage of the process that takes electrons from 100-300 keV to a few MeV is potentially the stochastic heating from the chorus of whistlers measured in a wide range of MLT and L shells during the decaying phase of the storms. We describe the Summers model for the diffusive energization that produces a hard electron flux a few days after the main phase of the storm. The role of the lower frequency EMIC waves in emptying the electron loss cone is noted as an important aspect of the system.

Li, X., M. Temerin, D. N. Baker, G. D. Reeves, and D. Larson, Quantitative prediction of radiation belt electrons at geostationary orbit based on solar wind measurements, *Geophys. Res. Lett.*, 28, 1887, 2001.

D. Summers and C. Ma, A model for generating relativistic electrons in the Earth's inner magnetosphere based on gyroresonant wave particle interactions, *JGR*, 105, 2625, 2000.

M. Mithaiwala and W. Horton, Substorm injections produce sufficient electron energization to account for MeV flux enhancements, submitted to *JGR*, 2004. <http://orion.ph.utexas.edu/windmi>

Work supported by the NSF-ATM grant to the University of Texas at Austin.

MODELING SOLAR ENERGETIC PARTICLE TRAPPING
AND ENHANCED RADIATION BELT FLUXES AT LOW L

M. K. Hudson¹, A. Goodhue¹, B. Kress¹
, K. Perry¹, P. Slocum², J. Blake², H. Hudson³, R. Lin³

¹Physics and Astronomy Dept., Dartmouth College, Hanover NH
03755

²Space Sciences Laboratory, The Aerospace Corporation, Los An-
geles, CA

³Space Sciences Lab, UC, Berkeley, CA 94720

The prompt trapping of Solar Energetic Particles (SEPs) in the inner magnetosphere has been observed at the recent Solar Cycle 23 maximum, including electrons, protons and heavier ions, in association with high speed interplanetary shocks and Storm Sudden Commencements (SSCs). These observations include the Bastille Day 2000 CME-driven storm as well as two in November 2001, and again associated with the Oct-Nov 2003 storm intervals. These events produced a long-lived new proton belt in 2001, trapping of ultra-relativistic electrons in 2003 and trapping of heavy ions up to Fe. A survey of such events around the most recent solar maximum, including high altitude measurements from Polar and HEO satellites along with low altitude measurements from the SAMPEX satellite, indicates similarities to the well-studied March 24, 1991 SSC event. A requirement for such shock-induced acceleration is a high-speed CME-shock at 1 AU, which launches a perturbation with comparable velocity inside the magnetosphere. The CME-shock itself is a source of solar energetic particles, which act as a seed population inside the magnetosphere. Integration of SEP trajectories in electric and magnetic fields taken from the Lyon-Fedder-Mobarry (LFM) global MHD model, using solar wind input parameters from spacecraft measurements upstream from the earth's bow shock, has been carried out for the November, 2001 SEP trapping events, as well as the Bastille storm for heavy ions. The results indicate that an enhancement in solar wind dynamic pressure for these events plays a role in the observed injection of ions to low L-values.

Lifetimes at low altitude where the new belts form $L=2-2.5$ have been investigated with both particle and photon data from the RHESSI spacecraft in low earth orbit, and due to high sensitivity of the Ge detectors provide a window to loss processes to the atmosphere which predominate in the South Atlantic Anomaly. Comparisons with WIND spacecraft measurements during the recent July 2004 interval of recurring high speed streams provides insight into conditions for enhanced trapped fluxes at low L which supplement GOES measurements at geosynchronous.

RADIATION BELT ENERGIZATION VIA INTERACTION WITH ULF WAVES: MHD SIMULATIONS OF MAGNETOSPHERIC ULF ACTIVITY

Scot R. Elkington¹, Michael Wiltberger², Anthony A. Chan³, Daniel N. Baker¹

¹Laboratory for Atmospheric and Space Physics, University of Colorado, Boulder, CO 80303

²NCAR/HAO, Boulder, CO 80301

³Space Physics and Astronomy Dept., Rice University, Houston, TX 77005

The outer zone radiation belts are largely field-aligned structures, with equatorial crossing distances of approximately 3-7 Earth radii. This region of space is of particular significance due to the large number of spacecraft operating at these altitudes, and global society's increasing reliance on space-based platforms for communications, navigation, weather prediction, and a variety of other economic and geopolitical purposes. Energetic electron fluxes in the outer zone can vary orders of magnitude over a variety of time scales, and spacecraft operating here have sometimes been found susceptible to "anomalies" related to changes in the local radiation environment.

Magnetospheric ULF waves, electric and magnetic fluctuations with characteristic frequencies in the mHz range, can efficiently transport and accelerate energetic electrons in the outer zone radiation belts. Magnetohydrodynamic (MHD) simulations of the solar wind/magnetospheric system are capable of modeling ULF waves resulting from a variety of processes, including those resulting from pressure impulses in the solar wind, shear waves along the magnetopause flanks, and large-scale changes in the convective motion of the magnetosphere. In this work, we analyze results from the Lyon-Fedder-Mobarry MHD model, which provides a global, 3d picture of the solar wind's interactions with the Earth's magnetosphere and ionosphere. Using varying solar wind driving conditions, we investigate the spatial and spectral characteristics of ULF waves occurring in the model, including the radial and azimuthal extent of the waves, as well as the wave mode structure and temporal power spectral density. Implications of the model results for energetic particle acceleration in the magnetosphere will be discussed in terms of the range of time scales and regions over which ULF-induced acceleration will occur under various solar wind conditions.

EVOLUTION OF INSTABILITY AND ASSOCIATED PARTICLE LOSS IN THE RADIATION BELTS

G. Ganguli¹, L. Rudakov², D. Papadopoulos³¹Plasma Physics Division, Naval Research Laboratory, Washington DC 20375²Berkeley Scholars Inc., P.O. Box, 852, Springfield VA 22150³University of Maryland, College Park MD 20742

In 1970 Brice [1] noted that it is possible to artificially enhance the energetic particle precipitation rate in the radiation belts by injecting chemicals. Ionization of the released chemicals results in the formation of an ion ring distribution perpendicular to the ambient magnetic field. Such an ion distribution is highly unstable to both electrostatic and electromagnetic instabilities. The objective of this study is to compare the possible electrostatic and electromagnetic instabilities that may be generated by such ion distributions, assess their properties, and quantify the parametric domains and conditions where particular modes dominate. The quasi-stationary instability spectra that result in enhanced loss of ions driven by a fresh supply of ring ions through ionization are analyzed for typical inner radiation belt environments. Conditions under which the electrostatic modes that correspond to the fastest growing modes of the ion ring distribution can be stabilized by Landau damping of the ambient plasma are identified. This allows the electromagnetic modes to dominate since they are not subjected to Landau damping. The threshold density and other parameters that result in predominance of electromagnetic modes and their role in particle loss mechanisms in the radiation belts will also be discussed. * This work is supported by ONR

1. Brice, N., Artificial enhancement of energetic particle precipitation through cold plasma injection, *J. Geophys. Res.*, 75, 4890, 1970.

2. Mikhailovskii, A. B., *Theory of Plasma Instabilities*, (Consultants bureau, New York, 1974), Vol. 1.

3. Vedenov, A. A and R. Z. Sagdeev, Some features of plasma with an anisotropic ion velocity distribution in magnetic field, in *Plasma Physics and the Problem of Controlled Thermonuclear Reactions*, V.3, p.332, Permagon, New York, 1958.

Session H2, 10:15 – Wed.

**PHYSICS OF THE
RADIATION BELT II**

Chair: G. Ganguli

RADIAL DIFFUSION OF RADIATION BELT ELECTRONS

Chan, A.A.¹, Fei, Y.¹, Elkington, S.R.²
, Brizard, A.J.³, Albert, J.M.⁴

¹Dept of Physics and Astronomy, Rice University, 6100 Main Street, Houston, TX 77005

²LASP, University of Colorado, 1234 Innovation Drive, Boulder, CO 80303

³Department of Chemistry and Physics, Saint Michael's College, Colchester, VT 05439

⁴Air Force Research Lab/VSBX, 29 Randolph Rd, Hanscom AFB, MA 01731-3010

Radiation belt particles adversely affect the performance and lifetime of space systems, and they can be a serious health hazard for astronauts. Although much is known about the basic properties of the radiation belts, the physical processes that determine the dynamics of the belts are not well understood.

Radial diffusion is one of the processes which contributes to the overall transport, acceleration and loss of radiation belt electrons. Recent work on radial diffusion has focused on enhanced radial transport during magnetic storms, including drift-resonant interactions with magnetospheric MHD waves in the ULF frequency band.

In this talk analytic calculations of quasilinear radial diffusion coefficients for relativistic electrons in general electromagnetic perturbations will be presented. Beginning with the Vlasov equation and Hamiltonian guiding center theory, we have derived a relativistic Fokker-Planck equation with a 3×3 diffusion tensor (A. J. Brizard and A. A. Chan, *Physics of Plasmas*, **11**, 4220, 2004). The diffusion tensor describes quasilinear transport due to electromagnetic perturbations which can break all three adiabatic invariants, but only the 3-3 element is needed to describe radial diffusion. The resulting radial diffusion coefficient reproduces earlier results in the appropriate limits, but it can be applied to more general perturbations and to off-equatorial particle motion.

Radial diffusion coefficients have also been calculated numerically, using simulations of test particles in model wave fields, and preliminary comparisons (using a dipole magnetic field and purely-electric field perturbations) show good agreement with the quasilinear results. Further work is being carried out to include asymmetric fields and magnetic perturbations and to better understand details of the quasilinear diffusion, including the relative contributions of intrinsic stochasticity (caused by chaotic particle orbits in non-random electromagnetic fields) versus extrinsic stochasticity (caused by random electromagnetic fields).

CALCULATION OF PITCH ANGLE AND ENERGY DIFFUSION COEFFICIENTS WITH THE PADIE CODE WITH APPLICATION TO THE EARTH'S RADIATION BELTS

Horne, R. B., Glauert, S. A.

British Antarctic Survey, Cambridge, England

We present a new computer code (PADIE) that calculates fully relativistic quasi-linear pitch angle and energy diffusion coefficients for resonant wave-particle interactions in a magnetized plasma. Unlike previous codes, the full electromagnetic dispersion relation is used so that interactions involving any linear wave mode in a predominately cold plasma can be addressed for any ratio of the plasma-frequency to the cyclotron frequency $\omega_{pe}/|\Omega_e|$. The code can be applied to problems in astrophysical, magnetospheric and laboratory plasmas. The code is applied here to the Earth's radiation belts to calculate electron diffusion by whistler mode chorus, electromagnetic ion cyclotron (EMIC), and Z mode waves, and to estimate the timescale for electron loss and acceleration during magnetic storms. We show that the high density approximation is remarkably good for electron diffusion by whistler mode chorus for energies $E \geq 100$ keV, even for $\omega_{pe}/|\Omega_e| \approx 2$, but underestimates diffusion by orders of magnitude at low energies (~ 10 keV). The timescale for electron acceleration by whistler mode chorus is calculated from the diffusion rates, and is found to be about 1 day at $L = 4.5$, and compares well with observations. When a realistic angular spread of propagating waves is introduced for EMIC waves, electron diffusion at ~ 0.5 MeV is only slightly reduced compared to the assumption of field aligned propagation, but at ~ 5 MeV electron diffusion at large pitch angles is reduced by a factor of 5, and increased by several orders of magnitude at pitch angles $30^\circ - 80^\circ$. Scattering by EMIC waves should contribute to flattening of the distribution function, in addition to that caused by whistler mode waves. The first results for electron diffusion by Z mode waves are presented. They show that, unlike the whistler and EMIC waves, energy diffusion exceeds pitch angle diffusion over broad range of pitch angles less than 45° . The results suggest that Z mode waves could provide a significant contribution to electron acceleration in the radiation belts during storm times.

NUMERICAL MODELING OF CHORUS PROPAGATION AND
CHORUS-DRIVEN PRECIPITATION MICRO-BURSTSBortnik, J., Thorne, R. M.Department of Atmospheric and Oceanic Sciences, University of
California, Los Angeles, CA. 90095

We obtain realistic wave parameters of individual chorus elements at every point along a specified magnetic field line using a combination of experimental data from the POLAR and CLUSTER satellites, and numerical ray tracing using the Stanford VLF ray tracing code. Following from previous studies, we assume that chorus is generated near the magnetic equatorial plane with the wave normal pointed at the Gendrin angle, and include the effects of Landau damping upon the wave using suprathermal electron distributions from the POLAR/HYDRA instrument. Results of the propagation study show that chorus waves typically propagate to latitudes of $20^\circ - 30^\circ$ before being damped by 10 dB, in agreement with satellite observations that typically show chorus propagating away from the equator. By varying the magnitude of the suprathermal fluxes, we show that chorus waves may be extinguished anywhere from a latitude of 10° for high fluxes, to experiencing a complete magnetospheric reflection for very low fluxes.

We then use the calculated wave characteristics to integrate the non-linear, relativistic equations of motion describing a large number of energetic electrons for gyroresonance modes $m = -5$ to $+5$ resulting in a set of pitch-angle changes describing the scattering of the particles. The set of pitch-angle changes is then combined with typical energetic electron fluxes obtained from the AE8 model to obtain the differential number flux of chorus-driven microburst precipitation. The calculated values are finally cast in a suitable form and compared to experimental observations of chorus-driven microburst events taken aboard the SAMPEX satellite to show good agreement between data and theory.

GROUND-BASED VLF TRANSMITTERS SEEN FROM THE PLASMASPHERE: MODELING AND VALIDATION

Starks, M.J.¹, Small, B.L.¹, Quinn, R.²
, Sales, G.³, Reinisch, B.³

¹Space Vehicles Directorate, Air Force Research Laboratory,
Hanscom AFB, MA

²RADEX Corporation, Bedford, MA

³Center for Atmospheric Research, University of Massachusetts -
Lowell, Lowell, MA

Experiments studying wave-particle interactions involving very low frequency (VLF) radio waves suggest that ground-based transmitters may be useful tools to remediate enhanced radiation belts hazardous to spacecraft. To evaluate this potential, an integrated model has been created to simulate the illumination of the plasmasphere by existing Navy VLF transmitters.

The ground-based Navy transmitters are modeled using the LFCOM code, then projected into the lower ionosphere using a VLF penetration model. These results provide input to the central power tracing system, which propagates individual rays throughout the plasmasphere. The AFRL Space Weather Center of Excellences Next Generation Power Tracing Code tracks the input energy as it expands outward into the plasmasphere, using models of ionospheric and plasmaspheric particle densities and the geomagnetic field. A Volumetric Power Aggregator maps these results into a three-dimensional database of the aggregate power flux at any point in space.

The output of the model has been compared to VLF measurements during 47 benchmark night-time passes by NASA's IMAGE satellite over three Navy transmitters. The results of these comparisons drive model corrections to improve the overall accuracy. The models sensitivity to assumptions is estimated by varying the models and repeating the comparison.

Although the complexity and variability of ionospheric absorption, plasmaspheric dynamics and wave propagation preclude development of an instantaneously perfect model, the resulting simulation provides acceptable fidelity for modeling the illuminated region on average. By exploring variations in transmitter frequency and location, this model helps to gauge the potential effectiveness of ground-based radiation belt remediation efforts versus those conducted from space.

RADIATION BELT LOSS RATES DUE TO GROUND TRANSMITTERS

Albert, J. M., Starks, M. J., Ginet, G. P.
Air Force Research Laboratory

In recent years, it has become appreciated that large ground-based VLF transmitters may have a significant impact on the radiation belts. These transmitters, operated by several countries for military communication purposes, have been in essentially continuous operation for most of the space age. Some amount of wave energy inevitably leaks out of the Earth-ionosphere waveguide and into space, where it couples to relativistic electrons through cyclotron-resonant interactions. It has been estimated [1] that this effect may be as large or larger than the effect of VLF waves generated by lightning or by plasma instabilities from anisotropic particle distributions (whistler hiss).

These estimates are based on a quasi-linear description of the wave-particle interactions, using simple models to parameterize the spatial distribution of wave energy and the wavenormal angle distribution. A large-scale ray-tracing effort underway at AFRL provides a more detailed and realistic model of these quantities [2]. It tracks the ray paths, wavevectors, and wave energy density throughout the plasmasphere from the ionospheric footprint of individual ground transmitters, and is being validated by comparison with dedicated observations from the IMAGE spacecraft.

The aggregated result of these ray computations may be used to provide more realistic wave models for the evaluation of quasi-linear diffusion. Of particular interest are the bounce-averaged pitch angle diffusion coefficient as a function of particle energy, equatorial pitch angle, and drift shell parameter L , and the characteristic lifetime for precipitation (scattering) into the loss cone. The transmitted waves are narrowband in frequency, and for low values of L (~ 1.3 , corresponding to equatorial altitude of about 1900 km), the wavenormal angle distributions are also narrow. This reduces the quasilinear expressions from double integrals to discrete sums over isolated resonances, which greatly aids both evaluation and interpretation.

[1] Bob Abel and Richard M. Thorne, Electron Scattering Loss in Earth's Inner Magnetosphere 1. Dominant Physical Processes, *J. Geophys. Res.*, 103, 2385, 1998.

[2] Michael Starks, Bright Small, Rick Quinn, and Gary Sales, Ground-based VLF Transmitters Seen From the Plasmasphere: Modeling and Validation, this meeting.

Session H3, 15:15 – Wed.

**PHYSICS OF THE
RADIATION BELT III**

Chair: J. Albert

QUASINEUTRAL PARTICLE SIMULATION APPROACH FOR WHISTLERS

Lampe, Martin ¹, Joyce, Glenn ², Manheimer, Wallace ³

¹Naval Research Laboratory - Code 6709, Washington, DC 20375-5346

²School of Computational Sciences, George Mason University, Fairfax, VA 22030

³Icarus Corp., Bethesda, MD

We have developed a new simulation scheme for whistlers which is fully kinetic and fully nonlinear, works in homogeneous or inhomogeneous situations, is not restricted to a single coherent mode, eliminates the speed-of-light time scale and the electron plasma oscillation time scale, and concentrates simulation resources on the parts of the electron distribution that make kinetic contributions to wave growth. The elements of the scheme are as follows. (1) The plasma is represented as a cold fluid component plus a set of simulation particles. At our option, the simulation particles can be chosen to represent any part of the electron velocity distribution that is of kinetic interest, e.g. the complete ensemble of energetic electrons, or only a set of resonant electrons. (2) Quasineutrality (QN) is assumed, i.e. $\text{div } \mathbf{J} = 0$. We emphasize that this does not mean that there are no electrostatic fields, only that $|n_i - n_e| \ll n_e$ and that the electric field \mathbf{E} is determined by QN, rather than by solving Poisson's equation. This assumption is appropriate when the frequencies of interest are slow compared to the plasma frequency, and it eliminates plasma oscillations from the system. In our case, an elliptic equation for \mathbf{E} is derived that combines Faradays and Amperes laws, the cold fluid momentum equation, and a stress tensor constructed from the particle velocities. (3) The displacement current is neglected, since the waves of interest are slow compared to c . This is similar to the Darwin model. However, (1) and (2) allow us to neglect the *full* displacement current, not just the solenoidal part, and thereby avoid all of the complications of the Darwin model. (4) Faradays and Amperes laws, rather than a momentum conservation equation, are used to push the cold fluid velocity. This guarantees QN. (5) The simulation particles are pushed in standard PIC fashion. (6) The magnetic field is determined by Amperes law. In the linear regime, the scheme reproduces the quasi-longitudinal dispersion relation for whistlers, and is accurate for propagation angles up to the resonance cone. A stable and accurate predictor-corrector scheme is used to solve the equations. The code need not resolve spatial scales smaller than the wavelengths of interest, nor time scales shorter than the gyrofrequency. We have used the code to study long-time nonlinear evolution of whistler instabilities; results will be shown for a variety of situations.

MODEL OF IONOSPHERIC DUCTS TO HF-HEATING

Perrine, P.P.¹, Milikh, G.M.¹, Papadopoulos, K.¹
, Huba, J.D.², Joyce, G.²

¹University of Maryland, Depts. Physics and Astronomy, College Park, MD 20742, USA

²Naval Research Lab., Plasma Physics Division, Washington, DC 20375, USA

It is well known that naturally induced field aligned irregularities of the plasma density exhibit enhanced refractive indices and act as ducts that guide waves in the whistler range. The ducting is analogous to light pipes or waveguides that guide those waves that propagate within the critical angle for total internal refraction. There are also indications that echoes observed by satellite sounders of ordinary and extraordinary are the result of ducting by field-aligned irregularities. In this paper we present the results of a theoretical study that addresses the issue of generating and detecting artificial ducts by strong HF heating of F-region using the HAARP ionospheric heater. Such ducts should be capable of ducting whistler waves between the two hemispheres. It is shown by numerical simulations that F-region HF heating creates a depletion of electrons at the heating region, that drives a pressure pulse that propagates along the entire magnetic field line. The paper presents results of simulations using the Sami2 1D ionospheric modeling code, modified to include a flexible source of strong HF heating. Parametric studies involve varying the heating source in strength, location and energy deposition width. A non-linear relationship was determined that relates the source parameters to the maximum amplitude of the pressure, temperature, and density perturbations, their propagation velocity and the characteristic heating and cooling rates of the irradiated region. A steady quasi-steady state is achieved in the duct structure following a transient state. The density profile shows electron depletion at the heated region, surrounded by density increases in the regions just below and above the heated region. The density perturbations then propagate deep inside the plasmasphere to the conjugate F2 point. Utilization of such artificial ducts for injection of ELF/VLF waves generated by HAARP and requirements for proof-of-principle experiments will be presented.

WHISTLER-MODE ILLUMINATION OF THE PLASMASPHERIC CAVITY VIA IN-SITU INJECTION OF ELF/VLF WAVES

Kulkarni, P., Inan, U.S., Bell, T.F.

STARLab, Stanford University, 350 Serra Mall, Stanford, CA 94305

It has recently been suggested by Inan et al. (U.S. Inan et al., Controlled precipitation of radiation belt electrons, *Journal of Geophysical Research-Space Physics*, **108 (A5)**, 1186, doi: 10.1029/2002JA009580, 2003.) that the lifetime of energetic (a few MeV) electrons in the inner radiation belts may be moderated by in situ injection of whistler mode waves at frequencies of a few kHz. The efficacy of this method depends upon the radiation efficiency of electric dipole antennas in the magnetospheric plasma, the propagation of the injected wave energy along raypaths as determined by the magnetic field and cold plasma gradients, and the lifetime of the injected waves as determined by Landau damping. We use the Stanford 2D VLF raytracing program (coupled with an accurate estimation of the path-integrated Landau damping based on measured distributions of suprathermal electrons) to determine the distribution of wave energy throughout the inner radiation belts based on injection location, wave frequency and initial wave normal angle. To determine the total wave power injected and its initial distribution in k-space (i.e., wave-normal angle), we apply the formulation of Wang and Bell (T.N.C. Wang and T.F. Bell, Radiation resistance of a short dipole immersed in a cold magnetoionic medium, *Radio Science*, **4 (2)**, 167-177, February 1969) for a short electric dipole placed at similar locations throughout the inner radiation belts. For a large number of wave frequencies and wave normal angles the data demonstrate that the majority of the radiated power is concentrated near the resonance cone. The combined use of the radiation pattern and efficiency and ray-tracing including Landau damping allows us to make quantitative estimates of the magnetospheric distribution of wave power density for different source injection points. On the basis of our results we estimate the number of individual space-based VLF transmitters necessary to fill the plasmaspheric cavity with enough VLF wave power to significantly affect the lifetimes of energetic electrons in the radiation belts. Specifically, we present data that show how wave energy spreads among the L-shells for an injection source located at a number of different L-shells (from $L = 1.8$ to $L = 3.0$), at a range of latitudes up to 20 degrees from the geomagnetic equator, and for a wide range of wave frequencies and wave normal angles. Initial data indicate that whistler mode waves injected at the magnetic equator at $L = 2$ with a frequency of 2.53 kHz (the local lower hybrid resonance frequency) can project wave power on L-shells of up to $L = 2.4$.

MULTI-HOP WHISTLER-MODE ELF/VLF SIGNALS AND TRIGGERED EMISSIONS EXCITED BY THE HAARP HF HEATER

Inan, U. S., Golkowski, M. , Carpenter, D. L.

, Reddell, N. , Moore, R. C., Bell, T. F.

Space, Telecommunications and Radioscience Laboratory,, Stanford University, Stanford, Ca., 94305

Modulated heating of the lower ionosphere with the HAARP HF heater in Alaska is used to excite 1-2 kHz signals, which are observed on a ship-borne receiver in the geomagnetic conjugate hemisphere after propagating as ducted whistler-mode signals. These so-called 1-hop echoes are believed to be amplified, and are accompanied by triggered emissions. Simultaneous observations near HAARP (~30 km) show 2-hop whistler-mode signals which travel back to the northern hemisphere upon reflection from the sharp lower ionospheric boundary in the south. Multiple reflected hops, up to tenth order (i.e., 10-hop) are detected, with the signal dispersing and evolving in shape, indicative of re-amplification and re-triggering of emissions during successive traversals of the geomagnetic equatorial interaction regions. Whistler-dispersion analysis methods were used to determine the L -shell of propagation of the ducted whistler-mode signals and the equatorial cold plasma density on the field line of propagation. The time delay (at each frequency over the range of observed frequencies of ~1 to ~2 kHz) between the time of origin of the original frequency-time ramp signal and the leading edge of the echo is measured and these data points are extrapolated to determine the 'nose' frequency f_n of minimum time delay and hence f_{Heq} , the equatorial gyrofrequency along the field line, through the relation $f_n \simeq 0.4 f_{\text{Heq}}$, where f_{Heq} is the L -shell of propagation. The measured values are then used together with a diffusive equilibrium model of the cold plasma density distribution along the field line to infer the equatorial electron density N_{eq} . This dispersion analysis revealed values of $L \simeq 4.9$ and $N_{\text{eq}} \simeq 280$ cc, which are consistent with the empirical model of for the outer plasmasphere and with the results of previous wave-injection experiments carried out with the Siple Station VLF transmitter near 2 kHz. With the L -shell of propagation and the cold plasma density determined, the energy of the energetic electrons that would undergo first order cyclotron resonance interactions with the injected waves can be calculated in a straightforward manner. Analysis indicates that the relatively high-pitch-angle electrons which drive the gyroresonance instability and that the therefore likely to be involved in the amplification of the injected waves and the triggering of emissions have energies on the order of a few tens of keV. On the other hand, the energy of gyroresonant electrons in the vicinity of the loss-cone, which would be expected to be pitch angle scattered and precipitated by these waves, is estimated to only be a few keV.

EXPERIMENTAL INVESTIGATION OF THE NONLINEAR
CHARACTERISTICS OF WHISTLER WAVES*

W. E. Amatucci¹, D. D. Blackwell², D. N. Walker¹,
G. Ganguli¹, G. Gatling²

¹Plasma Physics Division, Naval Research Laboratory, Wash-
ington, DC 20375

²SFA, Inc., Largo, MD 20774

Many interesting in situ and laboratory observations of whistler wave propagation and stimulated emissions have been made over the past few decades. In the space environment, observations of artificially stimulated emissions from the magnetosphere triggered by whistler modes launched from VLF transmitters have been reported by *Stiles and Helliwell* [1975]. The emission radiation is assumed to come from the temporary phase bunching of particles by the constant frequency triggering signal. In the laboratory, *Stenzel* [1975] reported on the self-ducting of large-amplitude whistler waves. Those experiments showed that with increasing driving amplitude, the radiation pattern from a small dipole antenna becomes increasingly narrow, and ultimately forms a duct with diameter of the order of the parallel wavelength within which the waves propagate virtually undamped.

Observations such as these have prompted an NRL Space Physics Simulation Chamber investigation of nonlinear whistler wave dynamics in a simulated radiation belt environment. The ultimate goals are to understand and quantify ducting, self-focusing, and amplification of whistler waves, to investigate nonlinear whistler-plasma interactions, and to study the secondary emission of whistler waves. In the initial experiments, transmitting and receiving magnetic loop antennas and crossed electric field dipole receiving antennas have been fabricated and tested. Electromagnetic modes launched in the Space Chamber plasma have been identified as whistler waves due to the correspondence of the wave properties with theoretical predictions. Preliminary investigations into the nonlinear properties of whistler have provided indication of whistler wave ducting.

Space Chamber experiments are also underway to characterize the radiation resistance of different whistler wave antenna geometries, beginning with an investigation of the radiation characteristics of a spherical capacitive probe. Initial results from these experiments confirm the accuracy and performance of the plasma diagnostics by identification of the electron plasma frequency. Simplified plasma models are used to help guide the experimental effort.

*Work supported by the Office of Naval Research and DARPA.

Stiles, G. S. and R. A. Helliwell, *J. Geophys. Res.*, **80**, 608 (1975).
Stenzel, R.L., *Phys. Rev. Lett.*, **35**, 574 (1975).

PRECIPITATION OF TRAPPED ENERGETIC ELECTRONS
IN THE MAGNETOSPHERE BY WHISTLER WAVES: OPTI-
MAL WAVE FREQUENCY AND THRESHOLD CONDITIONKuo, S. P.¹ , Huynh, James T.²¹Polytechnic University²Raytheon Space Airborne Systems

In the magnetosphere, energetic electrons in the radiation belts are trapped by the Earth's dipole magnetic field and undergo bouncing motion about the geomagnetic equator. Those very energetic electrons (in MeV level) have strong impact on passing satellites. The behaviors of the trajectories of these electrons interacting with a large amplitude whistler wave are explored, with the electron energy and wave amplitude and frequency as variable parameters. A surface of section technique is used to examine the chaoticity of the system graphically and the pitch angle time function is also plotted to verify if the electron can be scattered into the loss cone (assuming that the loss cone is around 30 degree) [1]. Once the electron wanders into the loss cone, it precipitates into the ionosphere and/or the upper atmosphere. The bouncing motion of the electron is a key factor to cause chaotic behavior in the interaction. The commencement of chaotic behavior in the electron trajectory for a given electron energy and region (i.e., a L value) requires the whistler wave to have a proper frequency and to exceed a threshold level. The dependency of the optimal wave frequency on the electron energy and L value and the dependence of the threshold condition on the electron energy are determined. The results show that the threshold wave magnetic field is in the range of about 0.001 of the geomagnetic field for precipitating those energetic electrons having kinetic energies larger than 1.5 MeV.

[1] S. P. Kuo, Paul Kossey, James T. Huynh, and Steven S. Kuo, Amplification of Whistler Waves for the Precipitation of Trapped Relativistic Electrons in the Magnetosphere, *IEEE Trans. Plasma Sci.*, 32(2), 362-369, 2004.

Session H4, 13:35 – Thurs.

NUMERICAL SIMULATIONS

Co-Chairs: J. Huba, W. Scales

PHYSICS OF COLLISIONLESS SHOCKS: SOURCES OF THE
FRONT NONSTATIONARITIES FROM MICRO TO MACRO
SCALES .

LEMBEGE, B.

CETP-UVSQ-IPSL-CNRS, 10-12 Avenue de l'Europe, 78140
VELIZY (FRANCE)

Collisionless shocks have intricate dynamics resulting from a balance between nonlinear effects and dispersion/dissipation effects. Both numerical simulations and in-situ satellite observations have largely improved our understanding of this dynamics. Surprisingly, these clearly evidenced that the front of quasi-perpendicular collisionless shocks propagating in supercritical regime presents a strong intrinsic nonstationarity. Many efforts have been performed in order to analyze the features and the sources of these nonstationarities for different sets of plasma parameters and in different Mach regimes. For the purpose of clarity, results issued from 1-D and 2-D PIC (Particle-In-Cell) and hybrid simulations can be classified (i) versus two main spatial directions (respectively along the shock normal and along the shock front) along which nonstationarities develop and (ii) versus characteristic spatial/time plasma scales. The difficulty is coming from the fact that several processes are responsible for these nonstationary effects and lead to a mixing of micro-meso-macro scales within the front. These processes include self-reformation mechanisms of the shock front, nonlinear whistler waves emission due to the unbalance between nonlinear effects and dispersion/dissipation effects, and several types of microinstabilities taking place within the ramp and/or the foot of a supercritical shock. Nonstationarities are shown to have a strong impact on the efficiency of particles energisation at the front which takes place in various types of shocks (in planetary/interplanetary physics, astrophysics, solar physics and heliospheric physics); this motivates the necessity for identifying their source mechanisms. More recently, various and complementary approaches (including both theoretical models and different types of simulations) have been used for these identifications. An overview of these recent works will be presented, in order to raise up a strategy for analysing the recent data issued from the CLUSTER-2 multi-satellites mission.

GLOBAL HYBRID SIMULATIONS OF THE MOON'S WAKE-TAIL

Schriver, D.¹, Travnicek, P.², Hellinger, P.²,
Ashour-Abdalla, M.¹, Bale, S.³

¹Institute of Geophysics and Planetary Physics, UCLA

²Department of Space Physics, Institute of Atmospheric Physics,
Prague, Czech Republic

³Space Science Laboratory, UC Berkeley

We have studied the structure and properties of the Moon's plasma wake-tail by means of a two dimensional global hybrid simulation (particle ions, fluid electrons). Different interplanetary magnetic field (IMF) configurations have been examined for the angle between the direction of the solar wind flow and the IMF between 0 and 45 degrees. The Moon acts as a diamagnetic obstacle removing plasma from the solar wind flow and the tail refilling process on the moon's nightside occurs due to plasma expansion into a vacuum driven by the thermal motion of particles along the IMF magnetic field lines. We have examined the properties of the wake-tail formed behind a Moon-sized obstacle embedded in the solar wind flow for spatial scales up to 50 Moon radii using up to 200 million particles in each simulation run. Results of our study suggest that kinetic processes occur in the Moon's wake-tail that are beyond the ideal MHD description. For example, counterstreaming and anisotropic plasma distributions in the Moon's downstream tail refilling region represent unstable plasma configurations which excites different types of wave modes whose nature depends on the structure of the tail (i.e., on the orientation of the IMF). An initial analysis of these waves for the different cases studied thus far indicate the presence of both electrostatic and electromagnetic emissions. The electrostatic emissions are likely to be ion-acoustic type waves and the electromagnetic emissions are probably whistler waves. The simulation results will be compared with Wind satellite Moon flyby data and Lunar Prospector orbiter data where possible.

COMBINING KINETIC VLASOV AND DISSIPATIVE MOMENT CLOSURE METHODS IN SPACE PLASMA SIMULATIONS

Newman, D. L.¹, Sen, N.¹, Goldman, M. V.¹

, Ergun, R. E.², Andersson, L.²

¹Center for Integrated Plasma Studies and

²Laboratory for Atmospheric and Space Physics, University of Colorado, Boulder, CO 80309

Because of their low noise, kinetic simulations based on direct integration of the Vlasov equations are a valuable tool in the numerical modeling of space plasmas. However, in $D > 1$ spatial dimensions, the computational demand of simulations with a $2 \times D$ (or greater) dimensional phase-space grid of sufficient resolution can be prohibitive. Therefore, alternative simulation schemes in which one or more spatial dimensions can be treated using less than a fully-kinetic approach are always worth pursuing.

One such complementary approach to treating basic plasma kinetic behavior with greater numerical simplicity is known as *dissipative moment closure*. The essence of this method (G. W. Hammett and F. W. Perkins, *Phys. Rev. Lett.*, **64**, 3019-3022, 1990) is to find complex closure coefficients coupling low-order velocity moments of a distribution function that yield a linear susceptibility that approximates the true kinetic susceptibility. Whereas Hammett and Perkins found three and four moment closures that *approximate* the kinetic susceptibility of a *Maxwellian* distribution, we show here that there are closures yielding *exact* agreement with the kinetic susceptibility of a *kappa* distribution [$f(v) \propto (v^2 + w^2)^{-\kappa}$, with $w \propto v_{th}$] for integer values of the parameter κ , provided $\kappa + 1$ moments are retained in the closure. Kappa distributions are of particular interest in the space-physics community because observed distribution typically have power-law rather than Gaussian tails. Although the dissipative closure is linear, dominant nonlinearities such as the ponderomotive force can be incorporated into the numerical algorithms.

We have developed a 2-D simulation code in which the dynamics along the dominant, z , direction (e.g., parallel to a current or external electric field) is modeled using full-Vlasov methods, while the perpendicular, y , dynamics are modeled using a five-moment dissipative closure (corresponding to a distribution with v^{-8} tails). It is important to recognize that this approach goes beyond that of simple fluid closures because a separate set of moments is evolved for each point in z - v_z - y phase space. Simulation results will be presented from a study of the formation and evolution of *double layers* in the auroral ionosphere. In these simulations, electrons were evolved in the strong-magnetization limit, with ions treated as unmagnetized using the five-moment dissipative closure.

SIMULATIONS OF COLLISIONAL IONOSPHERIC PLASMAS
WITH DENSITY GRADIENTS USING ALMOST A BILLION
PARTICLES

Lars Dyrud, Yakov Dimant
Center for Space Physics, Boston University

Plasma density gradients often play an important role in generating instabilities, waves and turbulence within the natural ionosphere. In this talk, we will describe our techniques and the results obtained from simulating gradient driven instabilities in collisional plasmas. These simulators all use parallelized algorithms to model the kinetic physics of the ions and a variety of kinetic and fluid algorithms to model electron dynamics.

We have used these simulators to study the role of plasma density gradients for a number of problems. The first problem we will present is a study of the dynamics of high-density plasma columns created by meteor ionization in the E-region ionosphere. Interaction between the plasma and the overlapping high-density neutral atmosphere require the use of collision algorithms, both kinetic and fluid. We used our kinetic, 2D, hybrid simulator to show that, in 2-D, these plasma columns become unstable. These simulations also allowed us to estimate instability growth rate, the dynamic electric field strengths and the rate of anomalous diffusion. However, before we could learn this, we had to understand the limitations of the simulator and develop a customized electron fluid.

The second problem we will discuss are a set of parallel, hybrid, simulations at various altitudes from 120-200 km, which show a relatively rapid development of gradient-drift type instability waves. For parameters near 200 km altitude and convection velocities of 600 m/s, plasma columns become unstable to waves with a wavelength of about 10-20 m. These results have implications for the interpretation of HF backscatter measurements in such ionospheric regions.

HALL MAGNETOHYDRODYNAMICS: NUMERICAL METHODS AND RESULTS

Huba, J.D

Plasma Physics Division, Naval Research Laboratory, Washington, DC

Over the past fifteen years it has become increasingly clear that Hall magnetohydrodynamics plays a crucial role in many space and laboratory plasma processes: magnetic reconnection, sub-Alfénic plasma expansions, and plasma opening switches to name a few. Hall magnetohydrodynamics is important for plasma dynamics on length scales less than the ion inertial scale length but greater than the electron inertial length. On these scales the ion and electron motions are decoupled; the electrons remain frozen to the magnetic field but the ions are not. In this paper we provide a basic overview of Hall magnetohydrodynamics with an emphasis on numerical methods. We also provide several concrete examples of Hall dynamics: whistler waves, Hall drift waves, and three dimensional magnetic reconnection. For the 3D reconnection simulation study we initialize the system with a magnetic field perturbation localized along the current channel in a reversed field plasma configuration. The perturbation induces a magnetic wave structure that propagates opposite to the current, and leads to the asymmetric thinning of the plasma layer, strong plasma flows in the direction of the current, and rapid magnetic reconnection. The propagating wave structure is a Hall phenomenon associated with magnetic field curvature. We also present results of the reconnection rate as a function of a guide field. It is found that the reconnection rate and plasma energization are reduced for increasing guide field strength. This is caused by a $\mathbf{J} \times \mathbf{B}$ force associated with Hall currents and the guide field that reduce the inflow and outflow velocities. However, the reconnection rate and plasma energization are only reduced by a factor of 2 for $B_{gf} = 5 B_0$. Applications to magnetospheric plasmas are discussed.

Research supported by NASA and ONR.

AN EVENT-DRIVEN APPROACH TO MODELING OF
PLASMAS: OVERCOMING THE COMPUTATIONAL CHAL-
LENGES OF TRADITIONAL TIME-DRIVEN TECHNIQUES

Homa Karimabadi
SciberNet, Inc., UCSD

Computer simulation of many important complex physical systems such as the Earth's magnetosphere has reached a plateau because most conventional techniques are ill equipped to deal with the multi-scale nature of such systems. The traditional approach to modeling spatially distributed physical systems has been based on time-driven (or time-stepped) simulations (TDS) where the whole state of the system is updated synchronously at discrete time intervals. This method has two inherent inefficiencies with severe consequences: (i) the well-known time step restriction imposed by a global CFL condition, (ii) uniform (and unnecessary system update) computational work independent of the level of activity in a given region. We have been working on an entirely different (asynchronous) simulation methodology based on a discrete event-driven approach. Here we report on our progress where we have developed a general parallel infrastructure based on this new technique. We demonstrate the power of this technique through a parallel hybrid simulation of a fast magnetosonic shock as well as the electrostatic simulation of spacecraft charging. We find speed up as large as a factor of 300 compared to the time-driven codes. In our technique, individual parts of the global simulation state are updated on a "need-to-be-done-only" basis and all simulation entities (individual particles/phase space elements/fluid elements, local fields) evolve on their own physically determined time scales. This has immediate implications for all types of plasma simulations. For example, one of the obstacles to the use of Vlasov codes in 2D and 3D is the fact that most of phase space is inactive but still has to be carried in the computation using standard techniques. This inefficiency makes the Vlasov codes almost unusable in 3D where the phase space (consisting of three spatial coordinates and three components of velocity) is very large. In our technique, only the active regions of phase space are updated.

Session H5, 08:15 – Sat.

**PLASMA INSTABILITIES
AND WAVES**

Chair: Y. Dimant

30 MHZ IMAGING RADAR OBSERVATIONS DURING THE
JOULE CAMPAIGN

Bahcivan, H.¹, Hysell, D.L.², Larsen, M.F.³, Pfaff, R.F.⁴

¹Electrical and Computer Engineering, Cornell University

²Earth and Atmospheric Sciences, Cornell University

³Department of Physics, Clemson University

⁴NASA/Goddard Space Flight Center

This paper presents 30Mhz imaging radar observations of the auroral electrojet made during the Joule campaign conducted at Poker Flat in the spring of 2003. The imaging technique allows for measuring fine structure in the auroral convection pattern by sorting radar echoes into compact range and azimuth cells. Radar imaging thereby allows for the unambiguous association of backscatter spectra with in situ electric field measurements made by rockets in a common volume. Both instrumented rocket paths projected along the magnetic field lines to the E region altitudes fell inside the radar imaging volume. Radar backscatter was observed only along the rocket path segments where the electric field was above a threshold. Both uplegs were active and contained type II echoes. Downleg portions were quiet, with the exception of a brief type I region observed by one of the rockets. We find that type I echoes propagate at the ion-acoustic velocity but are confined to small electron flow angles, regardless of the line-of-site electron drift velocity. Type II echoes meanwhile follow the ion acoustic speed times the cosine of the flow angle regardless of the line-of-sight electron drift velocity. The ion acoustic speed is common to both echo types, is a function of the electron drift speed, and is given by well known empirical models. The data interpretation is complicated by the large wind velocity variation in altitude as well as by imprecise knowledge of the scattering altitude. Nevertheless, significant discrepancy with some theoretical expectations suggests a revision of the auroral electrojet theories accounting for the coherent scatter spectra.

WAVE EFFECTS IN THE STORMTIME RING CURRENT-
PLASMASPHERE COUPLINGE.V. Mishin¹, W.J. Burke²¹Boston College Institute for Scientific Research²AFRL, Space Vehicles Directorate

During the magnetic storm of June 5, 1991 Combined Release and Radiation Effects (CRRES) and Defense Meteorological Satellite Program (DMSP) satellites observed a rich variety of wave phenomena. These were simultaneous with enhanced fluxes of low-energy (< 1 keV) electrons and ions in the region of ring current/plasmasphere overlap and the conjugate topside ionosphere. Strong electron cyclotron harmonic waves correlated with the soft electrons at the edge of the plasma sheet. Earthward of the plasma sheet boundary, ULF electromagnetic wave-structures with spatial wave-lengths 500 to 1000 km and magnitudes of 1-3 mV/m dominated. The CRRES plasma wave instrument revealed enhanced lower hybrid and whistler (chorus mode) waves embedded within the ULF wave-structures. The latter seemed to modulate also the plasmaspheric density.

The inner edge of the ring current was located about $2 R_E$ Earthward of the plasma sheet boundary. Near the inner edge, the strongly-structured meridional component of the electric field reached a maximum of 4 mV. Here, the wave activity was dominated by lower hybrid waves, and the electron and ion distributions were dominated by the low-energy particles.

At ionospheric altitudes, the ULF structures produce broad irregular Sub Auroral Polarization Streams (SAPS) with average sunward velocities > 1 km/s. At about the same time DMSP F8, F9, and F10 indeed observed highly-structured SAPS in the topside ionosphere coincident with precipitating ring current ions, enhanced fluxes of suprathermal electrons and ions, elevated electron temperatures, and deep highly-irregular density troughs. Overall, these events represent the so-called strong wave-SAPS phenomenon [Mishin et al., JGR (2003), 108, 1309, 10.1029/2002JA009793; Mishin et al., JGR (2004), to be published].

WHISTLER WAVE INSTABILITY AND GAMMA RAY
FLASHES IN THE ATMOSPHERE

Surja Sharma, Parvez Guzdar, Gennady Milikh
University of Maryland, College Park, Maryland

Whistler waves generated during a lightning play an important role in the generation of energetic electrons and their propagation to higher altitudes. The relativistic electrons produced by cosmic ray showers during a thunderstorm can form the seed population that leads to a runaway discharge at an altitude of about 5 km. In such a discharge the energetic electrons ionize the neutral gas, thus producing thermal electrons which are accelerated to runaway energies by the thunderstorm electric field, and thus generating further ionization. These relativistic electrons drive the whistler waves unstable and lead to the formation of ducts by self-focusing. These ducts in turn facilitate the propagation of the energetic electrons to heights of about 30 km. At these altitudes the gamma rays produced by bremsstrahlung of the relativistic electrons can escape the atmosphere, and are well correlated with the gamma ray flashes detected by spacecraft, e.g., Compton Gamma Ray Observatory. The focus of this paper is on the instability when a beam of hot magnetized electrons interacts with whistler waves in the atmosphere. The drift of the energetic electrons relative to the bulk electrons leads to a negative energy instability of the whistlers. The growth rate of the instability depends on the number density of the energetic electrons and their collision rate, and peaks at about 25 km. The runaway breakdown, which is essential for the whistler instability, develops under conditions similar to those leading to the generation of strong narrow bipolar radio pulses, which have been observed recently. The correlation between these two phenomena is under study.

COMPARISON OF ELECTRIC FIELD MEASUREMENTS OF TWO STREAM WAVES IN THE AURORAL AND EQUATORIAL ELECTROJET

Pfaff, R. F.

NASA/Goddard Space Flight Center

Detailed wavevector electric field and plasma density measurements of plasma instabilities have been carried out on NASA rocket experiments launched into the auroral electrojet from Esrange, Sweden and Poker Flat, Alaska, and from Alcântara, Brazil in the unstable daytime equatorial electrojet. Nearly identical instrumentation on both sets of experiments included multiple boomlength spatial filters and multiple baseline spaced electric field receivers to determine the wavelength and phase velocities of the plasma waves. We utilize these measurements to compare the wavenumber spectrum and phase velocity of the primary two-stream (Farley-Buneman) waves observed in the two electrojet systems. In particular, we compare the observed two-stream waves driven by DC electric fields of 10-15 mV/m at the equator with the auroral two-stream waves driven by DC electric fields that ranged between 30 and 110 mV/m. In general, the rocket measurements reveal phase velocities below the $E \times B$ velocity, peak wave power near 10 m, and 948;E E. In the auroral zone, the observed two stream spectra often display a double-peaked spectrum in the uppermost altitudes of the unstable electrojet region, that may result from ion magnetization effects at the higher altitudes within the unstable region. The data also address the generation of secondary plasma waves including the efficiency of the wave coupling mechanisms to generate non-linear short-scale modes and turbulence. Finally, the data provide limits important to theories of plasma heating by the two stream waves. The data from both experiment groups are interpreted within the framework of current theories of both linear and non-linear two-stream instability physics.

INTERCHANGE INSTABILITY AT THE PLASMA SHEET/LOBE INTERFACE

Golovchanskaya, I.V., Maltsev Y.P.
Polar Geophysical Institute of Apatity, Russia

It has been known for a long time that under certain conditions hot filaments of plasma sheet origin can fill the magnetospheric lobes, while tenuous transients, i.e. bubbles or streams, enter the plasma sheet. These features can be interpreted as due to plasma exchange proceeding in a filamentary manner (the dawn-dusk wave number k_y being dominant) at the plasma sheet/lobe interface (PSLI). We present a description of such a process in terms of interchange mechanism considered in a very low-frequency approximation, which permits to neglect the inertia term in the momentum equation and suggest the perturbed field-aligned currents to close purely by the ionospheric currents. In our treatment the ionosphere is not assumed to be a perfect conductor, thereby the electric field perturbations are suggested to change on a field-aligned scale that exceeds the length of a generation region. For this zeroth harmonic the stabilizing term in the dispersion relation associated with the field-aligned non-uniformity of perturbations is small, and instability develops wherever the magnetic tube is curved and plasma pressure gradient towards the curvature centre is large enough. Though this latter condition is not typically met inside the plasma sheet, it can be satisfied at the PSLI. Specifically, two sites of the PSLI are potentially interchange unstable: the equatorial region of the last closed magnetic field tube and the near-Earth curved segment of a boundary magnetic line. We demonstrate that the interchange, associated with the near-Earth curvature of the boundary plasma sheet, is most likely to be the cause of the above filamentation. The background convection is imposed on the interchange motions. During northward IMF periods the convection favours the extension of plasma sheet filaments into the lobes and their subsequent protrusion toward the dayside. This process is signified in the polar cap ionosphere by midnight arcs or multiple arc events. As opposed, the large-scale convection associated with the southward B_z IMF suppresses hot filament progress into the lobes, while prompting entering of tenuous transients into the plasma sheet.

IDENTIFICATION OF PLASMA SHEET FLAPPING WAVES
OBSERVED BY CLUSTERGolovchanskaya, I.V., Maltsev, Y.P.

Polar Geophysical Institute of Apatity, Russia

Recently it has been reported on the low-frequency oscillations of the plasma sheet generated by some impulsive source in magnetospheric tail center and propagating toward flanks (V. A. Sergeev et al., *Geophys. Res. Lett.*, 31, L05807, 2004). To interpret this finding a number of wave modes have been invoked to and then discarded, for either the group velocities or propagation directions were inconsistent with the observations. In the present study we examine the MHD internal gravitational-type waves, first described in (V.B. Safargaleev and Y.P. Maltsev, *Geomagn. and Aeronomy*, 26, 270 - 274, 1986) as a possible candidate to match the observed flapping motions. The role of gravity is played by the centrifugal force, acting on hot plasma in a curved magnetic field, near-equator magnetic curvature being treated. We present a flapping perturbation to be a standing structure along the magnetic field and a traveling wave in the dawn-dusk direction. The corresponding dispersion relation indicates propagation in the positive/negative yGSM directions with the group velocity of about $fg/3ky$, ky being the dawn-dusk wave number, the frequency fg determined by the background magnetic configuration. Within such a framework the following features of the flapping motions observed in experiment can be readily interpreted: group velocity v_y ranging from 10 km/s to 30 km/s for quiet current sheet and from 30 km/s to 100 km/s for active sheet; a phase shift of $\pi/2$ between BX and VZ oscillations, VZ being the vertical bulk velocity of plasma; a certain dispersion over the wavelengths, that is, longer wavelengths are coming to the flanks first. There is one discrepancy between the predictions of our theory and observations. According to the theory, both kink-like and sausage-like deformations of the current sheet are possible, while only those of the former type have been observed so far.

CONSTRAINTS ON MECHANISMS OF AURORAL ARC FORMATION

Golovchanskaya, I.V., Maltsev Y. P.
Polar Geophysical Institute

Up to now several tens of theories for inverted-V structure and discrete arc formation have been proposed [for survey see (J. E. Borovsky, *J. Geophys. Res.*, 98, 6101 - 6138, 1993)]. In about half of them the source of auroral structuring is supposed to be in the ionosphere (e.g. T. Sato and T. F. Holzer, *J. Geophys. Res.*, 78, 7314 - 7329, 1973), whereas a magnetospheric origin is inferred in others (e.g. L. R. Lyons, *J. Geophys. Res.*, 86, 1 - 8, 1981). In the present study we show that these two classes of mechanisms can be discriminated by the relative orientation of the structured electric E and magnetic B fields, which are closely associated with the auroral features, and which power law spectrum indicates their turbulent character (D. R. Weimer et al., *J. Geophys. Res.*, 90, 7479 - 7494, 1985). Specifically, a downward direction of the cross-product $[E \times B]$ suggests a magnetospheric generator of these fields, while $[E \times B]$ pointing upward indicates an ionospheric mechanism of structuring. Based on the electric and magnetic field measurements of the Dynamic Explorer-2 satellite (altitudes from 300 to 1000 km, spatial resolution of 3.8 km) during the period of one and a half year, we demonstrate that in about 95 per cent of cases the cross product $[E \times B]$ turns out to be downward. This suggests a magnetospheric mechanism at work (at least on the mesoscales that we have considered). Being averaged over the polar cap, the turbulent electromagnetic fields exhibit a steady growth with northward interplanetary magnetic field (IMF) increasing, while averaged over the auroral oval, they grow with increasing the southward B_z IMF. There is a notion that the same mechanism promotes turbulence development in the auroral oval and in the polar cap with increasing, respectively, southward or northward B_z IMF. Another finding about the structured electric and magnetic fields, is their strong connection with the background field-aligned currents (FACs). Interestingly, the amplitude of E and B is determined solely by the density of the FAC and is insensitive to FAC nature. This means that transfer to a turbulent state of the Region 1 FACs, Region 2 FACs, and NBZ currents, which are quite different in their origin, should be described within the same framework.

Session H/G1, 07:55 – Wed.

**USING RADIO BEACONS FOR
ATMOSPHERIC RESEARCH I**

Chair: P. M. Kintner

COMPARISONS OF VHF BROADBAND AND GPS DUAL-FREQUENCY TEC MEASUREMENTS

Huang, Z., Roussel-Dupre, R. A.

Atmospheric, Environmental and Climatic Dynamics Group,
Earth and Environmental Sciences Division, Los Alamos National
Laboratory

In this study we compare the Total Electron Content (TEC) at Los Alamos, New Mexico derived from the FORTE (Fast Onboard Recording of Transient Events) VHF broadband signals and the GPS dual-frequency TEC measurements from two Allen Osborne Associates (AOA) ICS-4000Z GPS receivers mounted at the Physics Building at Los Alamos National Laboratory. Comparisons are made for the diurnal cycle and seasonal change during the solar maximum years (2000-2001). The 27-day solar cycle TEC variations are also examined for the FORTE-derived TECs and the AOA GPS TEC measurements where data are available. Our results show good agreement on average between the GPS TEC measurements and the VHF TECs derived with refractive bending and high-order moments (the quartic effects) included. We address the uncertainties related to the variations of the central frequency and width of the broadband VHF signals used in deriving VHF TECs of a first-order dispersive ionosphere and demonstrate the importance of the frequency-dependent quartic effects at VHF band on TEC estimations. The changes in the magnitude of quartic effects with elevation angle are examined and the critical elevation angles, at which the quartic terms begin to have a significant effect, are evaluated. Beginning at the critical elevation angles of 30-to-40 degrees, the quartic effect increases exponentially from around 10%-to-15% relative contributions to over 60% at the lowest possible elevation angles of about 15 degrees. Point-to-point comparisons are made between the GPS TECs and the VHF TECs to evaluate the effects of fluctuations in the protonospheric TEC contributions and of the approximation of the local F2-region heights. Issues in the GPS TEC measurements related to elevation angle and the use of individual GPS satellites are also examined. Techniques for combining VHF broadband and GPS dual frequency data to improve our TEC determinations will be discussed.

A NEW TOOL FOR ROUTINE ESTIMATION OF GLOBAL TEC MAPS USING 1000+ GROUND-BASED GPS RECEIVER

Komjathy, A., Sparks, L., Mandrake, L.

, Iijima, B., Wilson, B., Mannucci, A.J.

NASA Jet Propulsion Laboratory, 4800 Oak Grove, MS 238-600,
Pasadena, CA 91109 USA

As the number of ground and space-based receivers tracking the Global Positioning System (GPS) steadily increases, it is becoming possible to monitor changes in the ionosphere continuously and on a global scale with unprecedented accuracy and reliability. At the time of writing this abstract (September 2004), there are more than 1000 globally-distributed dual-frequency GPS receivers available using publicly accessible networks including, for example, the International GPS Service (IGS) and Continuously Operating GPS Stations (CORS).

To take advantage of the vast amount of GPS data, researchers use a number of techniques to estimate satellite and receiver interfrequency biases and the total electron content (TEC) of the ionosphere. Most techniques utilize grid methods, spherical harmonic expansion or basis function coefficient sets to separate the hardware-related biases from the ionospheric contribution. These methods often have a limitation of using up to 200 GPS receivers, utilizing a sequential least squares or Kalman filter approach to estimate satellite and receiver interfrequency biases as nuisance parameters. The biases are then later removed from the measurements to obtain unbiased TEC.

In our approach to calibrating GPS receiver and transmitter interfrequency biases, we take advantage of all GPS receivers using a new processing algorithm, based on the Global Ionospheric Mapping (GIM) software developed at the Jet Propulsion Laboratory. This new capability is designed to estimate receiver biases for all stations. In this new approach, we solve for the instrumental biases by modeling the ionospheric delay and removing it from the observation equation using pre-computed GIM maps. The pre-computed GPS maps use about 200 globally-distributed GPS receivers to establish the background used to model the ionosphere at the remaining 800 GPS sites.

In the talk, we will display global maps of GPS ionospheric observations using the 1000 station approach. We will demonstrate this new tool for quiet and storm periods including October 28-31, 2003. We will show point plots that use differential mapping capabilities to highlight the effects of the dramatic storm that severely impacted the US and the equatorial regions. We have made the 900-site global TEC maps freely available to the ionospheric community at <ftp://sideshow.jpl.nasa.gov/pub/axk/allsites/>.

MIT HAYSTACK AUTOMATED PROCESSING OF GPS DATA
TO PRODUCE WORLDWIDE TEC MAPSRideout, W. ¹, Coster, A. ¹, Doherty, P.¹MIT Haystack Observatory, Westford, MA 01886-1299²Institute for Scientific Research, Boston College, Chestnut Hill,
MA 02467-3862

The method in use at the MIT Haystack Observatory for the automated processing of GPS data is described. The processing of GPS data includes applying the satellite biases, determining and applying the receiver biases, and recognizing and removing the bad data points. The final GPS product is used to produce worldwide Total Electron Content (TEC) maps. The satellite biases are downloaded automatically from the web. Receiver biases for over 1000 GPS receivers are determined using a novel approach involving least-squares fitting among sites with coincident data, and minimizing the elevation versus vertical TEC "scallop" effect. It will be shown that incorrect receiver biases cause vertical TEC measurement at low elevations to be systematically either higher or lower than vertical TEC measurements at high elevations, yielding a scalloped look when plotted. Minimizing this scalloping yields an absolute estimate of the receiver bias. For a group of GPS receivers with overlapping data, only one absolute bias measurement is needed after the differential biases are determined via a least squares fit. This one absolute bias can be determined by averaging the receiver biases found via the minimum scallop method for all the receivers in the group. This procedure works well outside of the polar region. Inside the polar region, a separate method is used which assumes that the TEC goes to zero at some point during the day. After biases are determined, another procedure is used to cull the bad data. The effectiveness of any automated processing of GPS data can be determined by measuring the average difference between the vertical TEC measured for all coincident points. Examples of worldwide two-dimensional TEC maps produced via this method will be given.

COMPARISONS OF VHF BROADBAND AND GPS DUAL-FREQUENCY TEC MEASUREMENTS

Huang, Z., Roussel-Dupre, R. A.

Atmospheric, Environmental and Climatic Dynamics Group,
Earth and Environmental Sciences Division, Los Alamos National
Laboratory

In this study we compare the Total Electron Content (TEC) at Los Alamos, New Mexico derived from the FORTE (Fast Onboard Recording of Transient Events) VHF broadband signals and the GPS dual-frequency TEC measurements from two Allen Osborne Associates (AOA) ICS-4000Z GPS receivers mounted at the Physics Building at Los Alamos National Laboratory. Comparisons are made for the diurnal cycle and seasonal change during the solar maximum years (2000-2001). The 27-day solar cycle TEC variations are also examined for the FORTE-derived TECs and the AOA GPS TEC measurements where data are available. Our results show good agreement on average between the GPS TEC measurements and the VHF TECs derived with refractive bending and high-order moments (the quartic effects) included. We address the uncertainties related to the variations of the central frequency and width of the broadband VHF signals used in deriving VHF TECs of a first-order dispersive ionosphere and demonstrate the importance of the frequency-dependent quartic effects at VHF band on TEC estimations. The changes in the magnitude of quartic effects with elevation angle are examined and the critical elevation angles, at which the quartic terms begin to have a significant effect, are evaluated. Beginning at the critical elevation angles of 30-to-40 degrees, the quartic effect increases exponentially from around 10%-to-15% relative contributions to over 60% at the lowest possible elevation angles of about 15 degrees. Point-to-point comparisons are made between the GPS TECs and the VHF TECs to evaluate the effects of fluctuations in the protonospheric TEC contributions and of the approximation of the local F2-region heights. Issues in the GPS TEC measurements related to elevation angle and the use of individual GPS satellites are also examined. Techniques for combining VHF broadband and GPS dual frequency data to improve our TEC determinations will be discussed.

EFFECTS OF STRONG MAGNETIC STORMS OVER GPS SCINTILLATIONS AT EQUATORIAL AND LOW LATITUDE STATIONS

E. R. de Paula¹, P. M. Kintner², B. M. Ledvina²
, F. S. Rodrigues², I.J. Kantor¹, I. S. Batista¹
, L.F.C de Rezende¹, A. Muralikrishna¹, M.S. Canabarro¹
, M. T. A. H. Muella¹, N. Reggiani³

¹National Institute for Space Research

²Cornell University

³Catholic University of Campinas

In collaboration with Cornell University we installed several Global Positioning System (GPS) based scintillation monitors over the Brazilian territory to study L band scintillation. Data from this array of GPS scintillation monitors were used to analyze the effects of strong magnetic storms over the ionospheric scintillations at the equator and under low latitudes, including the southern crest of the Equatorial Ionization Anomaly (EIA). The scintillations are due to the ionospheric irregularities and they can affect the GPS and other satellite based communication systems. The latitudinal scintillation pattern is highly dependent on the background ionization, which is larger over the EIA crests. During strong magnetic storms, eastward magnetospheric electric field can penetrate to the magnetic equator intensifying the EIA, with a consequent shift of the crests to higher latitudes. The latitudinal scintillation pattern changes concomitantly. In this study we observed, during some severe magnetic storms, intensification of the GPS scintillations at the Brazilian stations of So Jos dos Campos (23.21 S, 45.86 W, dip latitude 17.8 S) and So Martinho da Serra (29.28 S, 53.83 W, dip latitude 18.57 S). For the same events, weaker scintillations were observed at the equatorial GPS station in So Lus (2.57 S, 44.00 W, dip latitude 1.3 S) and Cuiab (15.45 S, 56.46 W, dip latitude 6.1 S). The effect of the time of occurrence of the storm sudden commencement over the ionospheric scintillation behavior is analyzed and examples of post-midnight scintillations during magnetic storms are shown. Digisonde and VHF coherent radar data are also used to complement the GPS data.

ASTRONOMICAL AND IONOSPHERIC IMAGING

Lazio, T. J. W.¹, Coker, C.², Makela, J. J.³
, Thonnard, S. E.¹, Loughmiller, P. J.⁴

¹Naval Research Laboratory

²Praxis, Inc.

³National Research Council-Naval Research Laboratory

⁴Cornell University

Radio astronomy was discovered at 20 MHz, and radio astronomers are increasingly looking to observations in the HF and VHF bands as a means of elucidating various astronomical phenomena. High dynamic range, high angular resolution imaging in these bands requires exquisite *differential* compensation of the phase fluctuations induced by the ionosphere; a nominal goal is to maintain uncompensated ionospheric phase fluctuations below a level of 0.1 radian, equivalent to an electron column density of 1 mTECU. Simultaneously, ionospheric scientists are looking to probe the ionosphere at higher spatial and temporal resolutions in order to understand aspects of ionospheric plasma physics, the solar terrestrial relation, and effects on technology systems. We review a series of 74 MHz observations made with the Very Large Array, including a series of joint optical-radio observations utilizing an all-sky optical camera during the summer of 2003. The VLA observations can be used to probe the ionosphere at the milli-TEC unit level, on spatial scales up to roughly 50 km and on time scales as short as 10 s, while the optical camera, combined with additional off-site sensors, was used to identify the dominant, summer nighttime ionospheric phenomena. We find a wide variety of phenomena, even in the mid-latitude location of the VLA. Key to these findings is the identification of specific ionospheric phenomena using the off-site support sensors. We close with a discussion of future VLA campaigns and plans for a larger astronomical/imaging instrument, the Long Wavelength Array (LWA). The latter will be able to probe ionospheric density fluctuations on scales ranging from a few kilometers to potentially as large as 400 km.

Session H/G2, 10:15 – Wed.

**USING RADIO BEACONS FOR
ATMOSPHERIC RESEARCH II**

Chair: A. Komjathy

TOPSIDE ION DENSITY COMPARISONS AND ERROR DISTRIBUTIONS BETWEEN DMSP MEASUREMENTS AND IRI CALCULATIONS

B T Taylor¹, T W Garner¹, G S Bust¹, M R Hairston²¹Center for Ionospheric Research, Applied Research Laboratories, University of Texas at Austin²William B. Hanson Center for Space Sciences, University of Texas at Dallas

The International Reference Ionosphere (IRI) is the most widely used empirical model of the ionosphere. Because transionospheric radio signals are modified by the topside ionosphere, the IRI estimates of the topside ionosphere need to be studied. This study compares the IRI-2000 topside climate with measurements from the SSIES instrument on board Defense Meteorological Satellite Program (DMSP) spacecraft. The SSIES instruments measure the bulk flow of the plasma, the electron density, the concentration of the O^+ , H^+ , and He^+ ions, and the temperatures of the electrons and ions every four seconds along the entire satellite orbit. Since 1995, eight different DMSP satellites flown in polar orbit at an altitude of ~ 840 km with an orbital period of ~ 104 min. Three spacecraft have orbits roughly aligned with the dawn-dusk line. The other five orbits are on roughly the 0930 – 2130 local time line. These data are available through the DMSP database (<http://cindispace.utdallas.edu/DMSP/>). After quality checking, this amounts to roughly tens of millions of data points. The IRI-2000 model is run to predict the ionospheric conditions at each DMSP measurement (roughly every 4 sec along each orbit), and the differences between the DMSP measurements and the IRI-2000 estimates are grouped as a function of magnetic latitude and solar activity. Since the IRI-2000 is a climate model, it is expected to produce Gaussian error distributions with a near-zero mean. This study concentrates on the electron density error distribution function. Occasionally, this distribution of errors is Gaussian. Unfortunately, some error distributions are non-Gaussian. The evidence suggests the shape of the error distribution function is dependent upon magnetic latitude, magnetic local time and solar conditions.

THE ELECTRON DENSITY PROFILE ABOVE THE POLAR IONOSPHERE

Nsumei, Patrick, Reinisch, B., Huang, X. , Song, P. , Tu, J.

Environmental, Earth, and Atmospheric Sciences, Center for Atmospheric Research, University of Massachusetts Lowell, 600 Suffolk Street, Lowell MA 01854.

The plasma density above a few hundred kilometers to a couple of thousands kilometers is important but less known and the International Reference Ionospheric (IRI) model is not reliably predicting densities above 700 km. The radio plasma imager (RPI) onboard the IMAGE spacecraft measures electron density distribution from the satellite location to as low as 2000 km in altitude. The measured density profiles not only provide the density at each height but also the trend, which may be used for extrapolations to lower altitudes. In this preliminary report we show examples of extrapolations of the measured electron density profiles in the polar region down to ionospheric altitudes to connect to the topside electron densities computed with the IRI model. It is found that while the IRI (standard) model might overestimate the density values above 600 km, an α -Chapman function with constant scale height as proposed by Reinisch and Huang [JASR, 2002] underestimates the densities above 700 km, indicating a possible approach for improving the IRI topside models above 600 km. An attempt is made to represent the extrapolated RPI density profiles with a Chapman distribution function. Our study shows that by assuming a linear variation of the scale height with altitude, the extrapolated RPI electron density profiles can well be represented by the Chapman function up to about 1600 km above the F2 peak. The preliminary results are promising, demonstrating the potential of using the RPI measurements, combined with the IRI model, to construct an empirical electron density model that covers the altitude range from the ionosphere to several RE in the polar cap region. A similar method can then be developed for lower latitudes.

A SPACE-BASED INSTRUMENT SUITE TO CHARACTERIZE SMALL SCALE PLASMA TURBULENCE IN THE F REGION IONOSPHERE

Habash Krause, L.¹, Enloe, C. L.¹, Herrero, F. A.²

¹U. S. Air Force Academy, Department of Physics

²NASA Goddard Space Flight Center

It is well-known that spatial irregularities in ionospheric plasma density can disrupt transionospheric propagation of radio waves. To date, investigations of the processes associated with scintillation of this type have primarily focused on length scales relevant to fluid processes. It is postulated that small scale irregularities (on the order of 10s of cm) may be associated with velocity-space instabilities. The Generalized Rayleigh-Taylor (GRT) instability is thought to be the primary mechanism driving density irregularities in the low latitude F region ionosphere. Previous simulation studies of the GRT have shown a greater prevalence of small scale irregularities in the turbulent plasma when it was treated as an ion-kinetic electron-fluid hybrid than if the plasma was treated as a two-species fluid.

A low Earth orbit satellite mission is under development to investigate ionospheric turbulence and its association with non-Maxwellian ionospheric plasmas that may be subject to velocity-space instabilities. Two instruments will be employed: 1) the Plasma Local Anomalous Noise Environment (PLANE) experiment and 2) the Flat Plasma Spectrometer (FLAPS) experiment. PLANE will record power spectra of spatial turbulence in 5 frequency channels, with a dynamic range that allows sensing of irregularities down to 20 cm in size. In addition, the processing electronics are designed to separate local perturbations due to spacecraft-environment interactions from irregularities within the ambient ionosphere. FLAPS is an ion electrostatic analyzer with an energy range from 0.05 eV to 17 eV and a resolution ($\Delta E/E$) of 2%. FLAPS will autonomously focus its energy range to span only the atomic oxygen line upon detection of significant turbulence by the PLANE instrument in order to resolve non-Maxwellian features of the plasma. Results of the initial functional tests of the instruments under vacuum and exposed to a simulated space plasma will be presented.

REFRACTION OF GPS SIGNALS IN DISTURBED IONOSPHERE

Lyakhov, A.N., Pushtarik, V.A., Korsunskaya Yu.A.
Institute of Geospheres Dynamics

We have studied the refraction of dual-frequency GPS signal refraction in the disturbed ionosphere. The following cases have been considered: (a) high-latitude ionosphere disturbed by electron and proton precipitation (computer simulation results and tomographic data from Chatanika ISR); (b) mid-latitude ionosphere under the strong magnetic storm; (c) equatorial ionosphere (both based on the computer simulation). Apparently, the effects of the terminator have been studied. All calculations have been done with the newly developed code for UHF signal propagation for steady-state receiver on the Earth surface as well as for the mobile receiver (1000 km/hr). The results can be summarized as follows:

1. GPS simulation using experimental Chatanika data have shown that refraction causes the error in angle between visible and real satellite positions about $3 \times 10^{-4} \dots 10^{-3}$ rad for 1.6 and 1.2 GHz respectively. The difference between phase and group delay time is as large as 30 nsec for 1.6 GHz and 53 nsec for 1.2 GHz resulting in 10..15 meters error in positioning. The effect of fast growth of the positioning error has been found when the signal propagates under the small angle to large inhomogeneities in the ionosphere. The last is interpreted as a kind of a caustic effect and it can give errors as large as 100 meters.

2. Calculations using simulated ionosphere for low- and mid-latitudes have shown that deviations of the ray are of the same order of magnitude as in the high latitudes. Under terminator passing we observed irregularities in the ray deviations depending on the relative angles of receiver position.

3. In the case of a mobile receiver (airplane) the refraction depends on the direction of relative motion. Counter motion reduces the time interval of minimal positioning error at 1-1.5 hours on the route 6000-10000 km.

Ionosphere corrections based on the model of a multilayered spherical ionosphere or on the TEC can not be considered as successful. Precise ionosphere simulations must be used in order to calculate refractive corrections to GPS.

IMPROVED AMBIGUITY AND RESOLUTION FOR MEASUREMENTS OF TOTAL ELECTRON CONTENT

Paul A. Bernhardt, Carl L. Siefing, Joseph D. Huba
Beam Physics Branch, Plasma Physics Division, Naval Research
Laboratory, Washington, DC 20375

Differential phase at two frequencies for satellite to ground signals passing through the ionosphere provide a measurement of total electron content (TEC). The differential phase technique for VHF, UHF or L-Band signals passing through the ionosphere is limited by phase ambiguities for multiples of one wavelength. The TEC ambiguity is defined as the ionospheric content equivalent to 360 degrees change in the differential phase. If the TEC ambiguity is much smaller than the absolute TEC, then the determination of the absolute TEC is difficult. For the standard NIMS (TRANSIT) or similar beacon signals using 150 and 400 MHz, the TEC ambiguity is 0.1 TECU (1 TECU = 1016 m⁻²). Consequently, absolute TEC for the typical ionosphere in the 10 to 100 TECU range is nearly impossible to determine. A new algorithm using three frequencies has been developed to aid the resolution of absolute TEC. The three frequencies for the CERTO beacons launched on C/NOFS, COSMIC, NPSAT1, CASIOPE, EQUARS and other satellites are 150.012, 400.032 and 1066.752 MHz with an 8/3 ratio between successive frequencies. With the frequencies, the three-frequency TEC algorithm (TFTA) has an ambiguity of 8.3 TECU. The development of the algorithm involves finite number theory applied to integer wavelengths at each frequency. The algorithm has been tested with synthetic TEC derived from the NRL SAMI3 global model of the ionosphere. The addition of noise has been considered in the analysis. The algorithm shows the TEC determination is improved with the TFTA by allowing establishing continuity after a loss of lock for at TEC receiver. In practice, system calibrations will require a one time measurements with incoherent scatter radars to determine fixed phase delays for each transmitters and receiver pair. The technique will not work for three frequency GPS signals at the L1, L2, and L5 bands because the algorithm with the GPS frequency ratios is breaks down from phase noise errors.

Session H/G3, 13:35 – Wed.

**IMPACTS OF THE IONOSPHERE
ON TERRESTRIAL SYSTEMS**

Co-Chairs: A. Coster, P. Doherty

IONOSPHERIC EFFECTS ON LOW-LATITUDE SPACE BASED AUGMENTATION SYSTEMS (SBAS)

Doherty, P.H., Valladares, C.E.

Boston College, Institute for Scientific Research

The ionosphere is a highly dynamic physical phenomenon that presents a variable source of error for Global Positioning System (GPS) signals and GPS based operational systems. The Federal Aviation Administrations (FAA) Wide-Area Augmentation System (WAAS) was designed to enhance the GPS standard positioning service by providing additional accuracy, availability and integrity that is sufficient for use in commercial aviation. It is the first of a number of planned regional Satellite Based Augmentation Systems (SBAS) that include the European EGNOS system, the MSAS system in Japan, the GRAS system in Australia, the GAGAN system in India and the CSTB system in South America.

The WAAS system reached Initial Operational Capability (IOC) in 2003, meeting all performance requirements for Precision Approach (PA) with vertical guidance at many airports located throughout the CONTiguous United States (CONUS). Much of the WAAS ionospheric research and development focused on defining and mitigating ionospheric challenges characteristic of the mid-latitude regions, where the ionosphere is well studied and mostly quiescent. The EGNOS and MSAS systems will primarily operate under a similarly quiescent mid-latitude ionosphere. SBAS system development in South America, India and other low-latitude regions, however, will have to contend with much more extreme conditions. These conditions include strong spatial and temporal gradients, plasma depletions and scintillation. All of these conditions have a potential to limit SBAS performance in the low latitude regions.

In this presentation, we will define the ionospheric phenomena that may challenge SBAS operation and performance in the low latitude regions. This will feature case studies and statistical summaries of plasma depletion activity recorded during the current solar cycle by a chain of dual-frequency GPS receivers extending from 20 degrees South to 16 degrees North Magnetic Latitude along the west coast of South America. Finally, it will illustrate efforts to estimate the ionospheric effects on PA SBAS service capability in the low latitude region.

PERFORMANCE OF NETWORKED HF COMMUNICATION SYSTEMS DURING IONOSPHERIC STORMS

Goodman, J.M.¹, Patterson, J.D.¹RPSI²ARINC

HF communication circuits, on an individual basis, may perform poorly during ionospheric disturbances associated with geomagnetic storms. This is especially true at middle and high latitudes. To achieve a greater degree of reliability, it is necessary to exploit various forms of diversity. The most powerful forms of diversity at HF must exploit multiple communication paths and frequencies. The most reliable communication with an individual entity (e.g., aircraft) will involve a star network involving several independent paths. Moreover, these (redundant) communication paths must have a wide range of communication bands at their disposal. Much of the paper deals with the process by which such diversity systems may provide acceptable communication reliability, even over adverse propagation conditions. A significant portion of the paper will deal with a particular system during a very realistic scenario. The specific system of interest is the GLOBALink/HF system, a unique data communication network.

The GLOBALink/HF system, developed and managed by ARINC, is a global high frequency data link communications network providing service to commercial aviation worldwide. It consists of 14 ground stations located around the globe, and a network control center located in Annapolis. The system was designed to provide reliable aircraft communications through the use of multi-station accessibility, quasi-dynamic frequency management, and a robust time-diversity modem with equalization. Although HF (i.e., 3-30 MHz) signaling has a poor reputation when considering individual circuits, it has been shown that near-real time channel evaluation and/or adaptive frequency management can improve performance considerably. Moreover, multi-station network operation provides an additional form of diversity, which is probably the most valuable design strategy. Our paper briefly describes the system, but the major discussion will be about performance metrics derived during super storms, especially the Halloween storm period of 2003.

STUDYING MID-LATITUDE DENSITY IRREGULARITIES
WITH DISTRIBUTED INSTRUMENT NETWORKSA. Coster¹, F. Lind¹, P. Erickson¹, S. Skone²¹MIT Haystack Observatory, Westford, MA²Department of Geomatics, University of Calgary

Studies have shown an association between scintillation and mid-latitude ionospheric irregularities which are generated by instabilities associated with electron density gradients and strong electric fields [Foster and Aarons, 1998]. To fully understand this association, it is necessary to make observations over wide regions during a variety of geomagnetic activity levels. These investigations can be best accomplished using distributed arrays of instrumentation which have coverage that far exceeds that of any individual instrument. We will describe how data both from the Global Positioning System (GPS) receiver network and from the recently funded Intercepted Signals for Ionospheric Science (ISIS) array has been, and will be, used to study mid-latitude scintillation. For example, the global network of GPS receivers provides near real-time TEC information from many locations around the world. By combining the TEC data from this network, phenomena such as the development of storm enhanced density (SED) can be monitored. A recent study has observed a correlation between SED, which is associated with large gradients in the TEC, and scintillation activity in Canada [Skone, et al. 2003]. In this study, phase scintillation parameters were measured by specially equipped GPS receivers at different sites in Canada. Scintillations were clearly observed in Calgary and other sites during time periods that correspond to presence of SED in Canada. Additional experimental observations are needed to help understand the association of scintillation with SED and the plasmasphere boundary layer (PBL) phenomena.

The ISIS array is based on high performance coherent software radio receivers which can intercept a wide range of signals with extremely precise time and frequency synchronization. The intercepted signals can be used for propagation studies, spectrum monitoring, scintillation observations, passive radar, and multistatic active radar. By using real time data from the ISIS array in the context of GPS TEC maps targeted incoherent scatter observations can be made in regions of the ionosphere where scintillation is observed to occur. This kind of detailed study is needed to fully understand mid-latitude scintillations and their evolution with the development of SED structures. This talk will review our current scintillation observations in the presence of SED and discuss our plans for future measurements.

MIDLATITUDE RADAR OBSERVATIONS OF THE JULY 2004
GEOMAGNETIC STORMMelissa Meyer, John SahrUniversity of Washington, Electrical Engr. Dept., Box 352500,
Seattle, WA 98195-2500

We operate a coherent radar at sub-auroral latitude in Washington State. This "passive radar" takes advantage of existing illumination by commercial FM transmitters, so we are able to observe plasma density irregularities in the E region ionosphere at multiple frequencies (in the FM band) simultaneously. During the geomagnetic storms occurring from 17 July until 27 July 2004, we observed many of these irregularities for long continuous periods (up to 2.5 minutes) every 4 minutes, thus sampling the "storm evolution" completely on both long time scales (several hours) as well as short ones (seconds). Furthermore, we were able to make these observations with two different transmitters simultaneously (at 96.5 MHz and 97.3 MHz), allowing us to study the E region effects of the storms from diverse frequencies, look angles, and waveforms.

Our radar is also capable of fine spatial resolution: 1.5 km in range and approximately 2 km in transverse resolution at a distance of 1000 km (achieved with interferometry). We are able to form rudimentary images and discern velocity shears within scattering volumes with interferometric techniques; we can use antenna pattern, range, and the magnetic aspect angle criterion to roughly locate scatterers in our field of view.

We have found many interesting features in our July 2004 data, including a large-scale wavelike structure with a period that suggests a gravity wave, or TID, and irregularities whose speed sharply increases over a few kilometers in range. We will present some of these storm-time observations, along with any analyses we are able to perform on the data, and corroborating observations from other instruments (satellite and GPS data). We will discuss our observations with respect to storm-time magnetosphere-ionosphere coupling, storm evolution at midlatitude, and the plasma physics of E region density irregularities.

SOME EFFECTS OF THE HALLOWEEN IONOSPHERIC STORM ON MIDLATITUDE HF SYSTEMS

R. D. Hunsucker², D. Rice^{1,3}, J. J. Sojka¹, J. V. Eccles¹

¹Space Environment Corporation, 221 N Spring Creek Parkway, Suite A, Providence, UT 84332 USA

²RP Consultants, 7917 Gearhart, Klamath Falls, OR 97601 USA

³Dept. of Electrical and Computer Engineering, Utah State University, Logan, UT 84322-4120 USA

The HF spectrum (nominally 3-30 MHz) supports a variety of legacy analog long-distance communications, as well as modern digital point-to-point services used by military, government, and civilian agencies for backup and sometimes primary communications. In addition, the HF spectrum is used for ground-based ionospheric diagnostics such as sounding and riometry. The Halloween Storm of 2004 produced long duration, large magnitude disruptions of midlatitude HF systems.

HF paths from WWV (Fort Collins, CO) and WWVH (Kauai, HI) have been monitored for the HF Investigation of D-Region Ionospheric Variation Experiment (HIDIVE) since December 2002 (Eccles et al., *Space Weather*, in press, 2004). These results, together with observations from the Utah State University (USU) Bear Lake Observatory (BLO), demonstrate the impact of the storm on the midlatitude ionosphere and on HF communications based on the 1400 km path between WWV and the RP Consultants monitoring site in Klamath Falls, OR. BLO is near the midpoint of the WWV-to-Klamath Falls path.

In addition to deep HF signal fades due to x-ray flare absorption, WWV signal levels were severely disturbed for much of November, and the low-power CADI sounder at BLO revealed periods of strong absorption (trace dropouts), sporadic-E, and spread-F. Other intense short-term effects were also observed, including substantial GPS scintillations and four-hour position errors at BLO associated with CME impacts on 29 and 30 October 2003.

Taken together, these results provide insight into the response of the ionosphere above northern Utah to certain space weather events during a major geomagnetic storm. We describe these storm responses and impacts on HF and GPS systems; modeling results for this period are presented in a companion paper. A more extensive observational network would be needed to infer the spatial development of the storm response on a continental scale.

LARGE VARIATIONS OF THE LOW LATITUDE IONOSPHERE DURING THE OCTOBER-NOVEMBER, 2003 SUPERSTORM: RESULTS FROM OBSERVATIONS AND MODEL

Lin, C. H.¹, Richmond, A. D.¹, Bailey, G. J.²

, Lu, G.¹, Yeh, H. C.³, Paxton, L. J.⁴

, Liu, J. Y.³, Tsai, H. F.⁵, Su, S. Y.³

¹High Altitude Observatory, NCAR

²Department of Applied Mathematics, University of Sheffield, UK

³Institute of Space Science, National Central University, Taiwan

⁴Space Department, Applied Physics Laboratory, Johns Hopkins University

⁵National Space Program Office, Taiwan

The GPS derived total electron content (TEC), drift measurements from the ROCSAT-I at 600 km, and far ultraviolet airglow measured by the Global Ultraviolet Imager (GUVI) carried aboard the NASA TIMED satellite are utilized for studying the large disturbance of the low latitude ionosphere during the Oct.-Nov., 2003 superstorm period. It is found from GPS-TEC that the equatorial ionization anomaly (EIA) expanded to much higher latitudes compared with their locations during magnetic quiet times. Following the expansion of the EIA, the suppression lasted at least for a day. The derived ExB drifts measured from the Ionospheric Plasma and Electrodynamics Instrument (IPEI) onboard the ROCSAT-I showed strong upward drifts during the expansion of the EIA. These upward drifts imply the penetration of the eastward electric field from high latitude to low latitude and lifted the low latitude ionosphere to very high altitude resulting in strong plasma fountain effect. The IPEI measurements also indicated downward ion drifts in some locations, in good agreement with the suppression of the EIA. These drift measurements have been input to the Sheffield University Plasmasphere Ionosphere Model (SUPIM). The model results show good qualitative agreement on both expansion and suppression of the EIA. We also analyze the 135.6 nm and LBH emissions from the GUVI to monitor the O/N_2 variations during the entire storm period. The large extended areas of the negative storm during the recovery phase are observed by GPS-TEC and are in good agreement with the global O/N_2 variations inferred from GUVI emission measurements. We also present the TEC enhancements observed during the storm recovery phase.

THE CLIMATE OF MID-LATITUDE IONOSPHERIC IRREGULARITIES ACCORDING TO DYNASONDE OBSERVATIONS AT BEAR LAKE, UTAH

Wright, J.W.¹, Zobotin, N.A.¹, Berkey, F.T.²

¹CIRES, University of Colorado at Boulder, Box 216, Boulder, CO 80309, USA

²Utah State University, Logan, Utah, USA

A time series (11 Feb. 2003 to present) of mid-latitude dynasonde observations supports a climatological study of small-scale (0.1-10 km) irregularity parameters by the "Phase Structure Function" and "Anomalous Attenuation" methods. The Phase Structure function method is based on precision measurements of short-period phase variations in totally-reflected radio echoes, as statistically summarized in the temporal structure function, SFp. We relate parameters of the SFp to the irregularity spectrum parameters ($\Delta N/N(1000\text{m})$, and spectral index ν) by means of diffraction theory. The ionospheric E and F regions are treated separately. Another diagnostic approach, based on the theory of multiple scattering, predicts a significant level of anomalous attenuation (tens of decibels) of totally-reflected echoes arising from a specific mode of radiowave interaction with ionospheric irregularities. This is, we believe, the first synoptic study of small-scale ionospheric irregularities.

Study of about one years data yields the following results:

a) Characteristic (and different) average diurnal variations are found for E and F regions, and for the seasons. There is an evident cause and effect relation between, for example, the sunrise/sunset processes in the ionosphere and irregularity amplitude.

b) There is evidence that the electron density irregularity absolute amplitude, ΔN , is of more fundamental significance than the relative amplitude $\Delta N/N$ for small scales. Clearly, ΔN should be less dependent on diurnal variations of average electron density, and we find that it has a distinct tendency to preserve its value (on the average) along a magnetic tube, between E and F regions.

c) There is an evident correlation between irregularity amplitude and plasma gradient, in both E and F regions.

d) Irregularity amplitude is correlated with the local magnetic K index at higher latitudes, but not at Bear Lake.

e) On the other hand, we observed indications of a significant increase of the anomalous attenuation during some stages of the record Halloween 2003 magnetic storm days, probably signifying an increase in the relative importance of the small-scale (sub-kilometer) end of the irregularity spectrum compared to quiet days.

MID-LATITUDE COHERENCE BANDWIDTH ESTIMATIONS
FROM TRANSIONOSPHERIC VHF SIGNALS

Roussel-Dupre, R. A. , Huang, Z.

Atmospheric, Environmental and Climatic Dynamics Group,
Earth and Environmental Sciences Division, Los Alamos National
Laboratory

Broadband radio signals with spectral content in the VHF can experience significant temporal and spatial distortion as a result of propagation through electron density perturbations in the ionosphere. While the most intense effects are observed in the equatorial and polar regions, an understanding of such effects at mid-latitude is crucial in view of our increased reliance on space-based communication and navigation systems which are vulnerable to mid-latitude ionospheric scintillations. The coherence frequency bandwidth is an important parameter that describes the characteristics of the signal distortion in time and represents the primary method for characterizing ionospheric structure by means of transient signals measured at a single satellite. This study examines the likely occurrence of ionospheric scintillations of the broadband VHF signals (30-100MHz) from the Los Alamos Portable Pulser (LAPP) received by the FORTE (Fast Onboard Recording of Transient Events) satellite during the period of 1997-2002. The scintillation characteristics, the mean time delay and its standard deviation of the transionospheric signals, are analyzed and the coherence frequency bandwidths are calculated using the thin phase-screen approximation in which the thick scattering layer is simplified by an equivalent thin phase-screen with infinitesimal thickness and the same overall phase variance. The variations of coherence bandwidth at Los Alamos with the changes in local time, season, solar activity, and geomagnetic conditions are described. The results are compared with the values estimated from a wideband scintillation model (WBMOD) and those from other mid-latitude coherence bandwidth studies. Selected case studies are conducted to demonstrate the 4th power relationship between the signal frequency and the coherence bandwidth. The uncertainties related to the FFT spectrogram based algorithm are discussed for a range of FFT windowing sizes and the appropriate values are validated through an independent wavelet-based algorithm. Preliminary case studies on the coherence bandwidth at equatorial regions are presented using FORTE lightning data to illustrate the reasonable differences in the coherence bandwidth between the mid-latitude and the equatorial region as indicated in previous literatures.

NOWCASTING AND DELIVERY SYSTEM FOR IONOSPHERIC ELECTRON DENSITIES AND SCINTILLATION GROWTH RATES

Boris Khattatov¹, Marianna Gnedin¹, Michael Murphy¹
, Jason Boisvert¹, Jeff Sheffel¹, Vijay Jayaraman¹
, Valery Yudin³, Tim Fuller-Rowell²

¹Fusion Numerics Inc

²NOAA/CIRES

³NCAR

This paper describes an operational system sponsored by the US Air Force for generating and distributing near real-time three-dimensional ionospheric electron densities and corresponding GPS propagation delays. The system adapts technologies developed and routinely used for operational weather forecasting in order to nowcast and forecast ionospheric conditions. It consists of two parts: a first-principles numerical model of the ionosphere and a data assimilation component.

The core ionospheric model solves plasma dynamics and composition equations governing evolution of density, velocity and temperature for 7 ion species on a fixed global three-dimensional grid. It uses a realistic model of the Earth's magnetic field and solar indices obtained in real time from the NOAA Space Environment Center. While the core model is capable of delivering realistic results, its accuracy can be significantly improved by employing a special set of numerical techniques known as data assimilation. These techniques originated in and are currently used for numerical weather forecasting. The core ionospheric model is continuously fed real-time observational data from a network of reference GPS ground stations. This improves both the nowcast and the forecast.

We believe that given advances in computing power and increases in the number of real-time ionospheric measurements, forecasting ionospheric conditions with systems similar to the one described here will become routine in the very near future. This article aims to give a high-level overview of system principles, design, and operations as well as present current data delivery mechanisms based on SOAP/XML web services. Additionally, we describe extensions of the model to scintillation growth rates forecasting and the impact of intense solar activities. Web-based access to the system is provided to early users for validation and exploration purposes at <http://www.fusionnumerics.com/ionosphere>

Session H/G4, 13:15 – Thurs.

**DUSTY PLASMAS AND
LABORATORY EXPERIMENTS I:
PMSE**

Co-Chairs: L. Gelinas, M. Horanyi

IN SITU OBSERVATIONS OF THE CHARGED PARTICLE ENVIRONMENT ASSOCIATED WITH PMSES AND NLCS

Croskey, C.L., Mitchell, J.D.

Penn State University, 303 Electrical Engineering East, University Park, PA 16802 U.S.A.

Through a combination of electrodynamic measurements made by sounding rocket payloads, we have observed both positively and negatively charged particles in regions of PMSE or NLC activity. These rocket flights included the NASA-sponsored MaCWAVE Program during July 2002 and the DROPPS Program during July 1999, both from the Andya Rocket Range, Norway. Our investigations were coordinated with the European MIDAS Campaign, which involved additional rocket flights and ground-based measurements by the ALOMAR Observatory and the EISCAT Radar Facility.

The instrument suite for each payload included Langmuir probes which observed deep depressions in the electron concentrations associated with PMSE/NLC regions. Simultaneous measurements of ram and wake Langmuir probes have shown that these bite outs are not an artifact of electron collection in a wake nor are they an artifact due to ram collision with charged positive particles. The bite outs were also observed when the applied collection voltage was adjusted to compensate for shifts in the spacecraft potential, thereby demonstrating that such bite outs are not the result of spacecraft charging.

In addition, high-time/altitude resolution measurements of charged particles were made with screened blunt probes. This flat-plate Langmuir probe configuration was used in the ram to identify the net polarity of charged particle regions. The blunt probes were configured in pairs; one had a fixed bias voltage of +2.5 volts and the other had a -2.5 volts bias voltage. The current signatures obtained during the flights are indicative of the existence of both positively and negatively charged particle regions. On some occasions both polarities were observed during the same flight. A direct correlation between the largest particle effects and the electron bite out regions was observed.

For the DROPPS payloads, a Gerdien condenser provided a third probe technique for investigating the vertical structure of ion constituents—both more mobile molecular species and low-mobility particulate species—in the vicinity of PMSE/NLC regions. A detailed, high-time resolution display of the Gerdien condenser currents showed a direct correlation of the positive-ion and charged-particle fine structure.

In all of the charged species data, sharp layers or edges in the concentration profiles were seen. Layer structures down to one-meter thickness, with random occurrences on the order of a few meters, suggest that these charge structures are related to the observation of PMSE events. In this paper we describe and interpret the data from a number of these sounding rocket flights.

MESOSPHERIC CHARGED DUST LAYER: IMPLICATIONS
FOR NEUTRAL CHEMISTRY

Gelinas, L.J.¹, Lynch, K.A.², Collins, R.L.³, Kelley, M.C.¹

¹Cornell University, Ithaca, NY

²Dartmouth College, Hanover, NH

³University of Alaska Fairbanks, Fairbanks, AK

The presence of a dust layer in the Earth's mesosphere is generally accepted on theoretical grounds [Hunten et al., 1980], but its experimental verification has been difficult and its influence on mesospheric dynamics and chemistry is not yet understood. Four sounding rockets carrying detectors designed to measure nanometer-sized charged dust particles were flown from Poker Flat in March 2002. In-situ measurements of charged dust and plasma densities were compared to the ground-based lidar data. Ground-based lidars were used to measure neutral sodium and iron densities during the launches in an effort to determine whether dust has an influence on mesospheric chemistry, specifically, as related to atomic sodium and iron. Strong correlations between the charged dust and neutral iron profiles were observed on all four flights.

The observed correlations between charged dust and iron indicate that dust does influence mesospheric chemistry, possibly serving as a metal reservoir for atomic iron at low altitudes, and may also be a sink for atomic sodium. Models of mesospheric atomic metals have shown that sodium and iron are good tracers of neutral wind motions above about 85 km, but that chemical enhancements can affect metal densities at lower altitudes [Plane et al., 1999]. The similarity of the iron and dust profiles may also indicate that gas-phase chemical enhancements are less efficient in shaping the iron layer than dust-related chemistry. In this paper we describe the ground-based and in-situ measurements investigating the link between meteoric dust particles and atomic metals in the mesosphere, and discuss the charged dust measurements in the context of the Hunten et al. (1980) mesospheric dust model.

ROCKET-BORNE INSTRUMENT TO DETECT CHARGED
SMOKE AND CLOUD PARTICLES IN THE MESOSPHERE

Robertson, S., Horanyi, M., Sternovsky, Z.

Dept. of Physics, University of Colorado, Boulder, CO 80309,
USA

A rocket-borne instrument has been developed to detect charged, sub-visible aerosol particles in the polar mesosphere. The instrument is designed to fly on a sounding rocket and has a 30 square centimeter entrance slit. Venting ports are placed lower on the detector in order to let the air out and reduce pressure buildup inside the detector. The air sample flows between four pairs of graphite electrodes biased symmetrically with increasing bias potentials. Electrons, light ions (less than 200 amu), cluster ions (200 amu - 1,500 amu) and heavy charged aerosol particles (1,500 - 200,000 amu corresponding to 0.85 - 2 nm radius) of both polarities are collected mass-selectively on the electrodes that are connected to sensitive electrometers. Direct Simulation Monte Carlo (DSMC) codes have been used to optimize the supersonic airflow around the instrument. The design of the entrance slit reduces the effect of the shock on the motion of the aerosols. A separate code is used to model the motion of charged particles within the detector. The effect of collisions with the residual gas is modeled using Monte Carlo techniques and collection efficiency is calculated. A laboratory prototype of the instrument has been fabricated and is currently under testing and calibration using ion beams. The instrument is designed to return data on the mass distribution of PMSE particles in the polar summer mesosphere, and data on meteoritic smoke particles in the polar winter mesosphere. Data from a summer 2007 flight will allow comparisons with remote sensing data from the Aeronomy of Ice in the Mesosphere (AIM) satellite.

POTENTIAL DISTRIBUTION AROUND SOUNDING ROCKETS IN MESOSPHERIC LAYERS WITH CHARGED AEROSOL PARTICLES

Sternovsky, Z.¹, Holzworth, R. H.², Horanyi, M.¹,
Robertson, S.¹

¹Physics Department, University of Colorado, Boulder, CO 80309-0390

²Earth and Space Sciences, University of Washington, Seattle, WA 98195-1650

It is shown that large potential variations can exist inside the wake of sounding rockets moving with supersonic velocity through the summertime mesopause region. The potential distribution is driven by charge separation induced by the shock wave of the rocket. The low conductivity conditions due to the attachment of free electrons to aerosol particles allow large electric fields, of the order of V/m, to be maintained. Large potential variations were observed within the wake of the two DROPPS payloads while studying the electrical structure of the narrow layers of aerosol particles present in the summertime mesosphere. We have used a DSMC (Direct Simulation Monte Carlo) code to calculate the neutral flowfield around a 3 m long, 43 cm diameter cylinder resembling the DROPPS payload. The calculation is done for 85 km altitude that is where a deep reduction of the free electron density (bite-out) due to the electron attachment to aerosol particles has been observed by the DROPPS-1 payload. For the conditions studied, the light positive ions are embedded in the neutral flow and thus ions have the same compression factor as the neutral gas. This is because the neutral drag force dominates over the electrostatic force for electric field on the order of 1 V/m. On the other hand, the heavy aerosol particles are only weakly affected by the shock and their distribution remains homogeneous. This assumption is valid for particles larger than 1 nm. The photometer data onboard the DROPPS-1 payload indicated aerosol particles up to 20 nm in size somewhat below the bite-out. Assuming that only light positive ions and heavy aerosol particles are present within the bite-out region, Poisson's equation is solved for the potential distribution. The results show that the shock of the rocket has a positive few volts potential. The numerical results are in good qualitative as well as quantitative agreement with the DROPPS observations.

MODELLING THE AEROSOL-PLASMA INTERACTION

Lie-Svendsen, Ø., Blix, T.A., Brattli, A. , Hoppe, U.-P.
Norwegian Defence Research, Establishment

We discuss how aerosol (dust) particles interact with the ambient mesospheric plasma, and in particular how small-scale aerosol density fluctuations impact the plasma and can cause Polar Mesospheric Summer Echoes (PMSE).

The high mobility of electrons, and the much lower mobility of ions, lead to rapid negative charging of aerosol particles. This charging has two effects on the ambient plasma: It modifies reaction rates and thus the ionization equilibrium of the plasma, and, secondly, small-scale charged aerosol density fluctuations induce ambipolar flow in the plasma which leads to density fluctuations in the ambient ions and electrons.

We have used a one-dimensional, time-dependent numerical model to study this interaction. The model solves the continuity and momentum equations for neutral and charged aerosols, positive ions, and electrons, and include attachment of electrons and ions by aerosols, diffusion of aerosols, ions and electrons, and gravitational settling. The model therefore encompasses the huge range of time scales involved, from the (sub-) second time scale of electron attachment, to the aerosol diffusion time scale which can be of order hours or days. On the length scales most relevant to PMSE, of order a few meters, electron and ion ambipolar flow in response to aerosol density gradients is usually the dominant process.

The main result is that small-scale aerosol density fluctuations induce small-scale electron density fluctuations of the same magnitude, which can cause PMSE. The lifetime of the electron density fluctuations is equal to the aerosol diffusion lifetime, of order hours or more. Moreover, the lifetime is independent of the aerosol density, which explains the observed fact that most PMSE are detected when the aerosol density is much smaller than the ambient electron density. The ambipolar flow in the presence of aerosol fluctuations also causes an anticorrelation between electron and ion density perturbations, in agreement with most in situ rocket observations. We therefore believe we now have a good understanding of how aerosol particles in the mesosphere affect the ambient plasma. In order to explain PMSE, the main issues remaining are therefore to understand how aerosols are formed, and how small-scale aerosol fluctuations are created in the first place.

ELECTRON TEMPERATURE EFFECTS ON PLASMA IR-
REGULARITIES ASSOCIATED WITH CHARGED DUST IN
THE EARTH'S MESOSPHERE

Scales, W.A., Chen C.

Bradley Department of Electrical and Computer Engineering, Vir-
ginia Tech

Polar mesospheric summer echoes PMSEs are strong radar echoes in the 50 MHz to 1.3 GHz frequency range produced by scattering from electron irregularities in the earth's mesosphere. The electron irregularities believed to produce PMSEs result from electron charging on subvisible dust that exists in the mesosphere. The study of PMSEs is a forefront issue in near earth space science because of the tremendous remote sensing diagnostic possibilities that exist for studying the earth's middle atmosphere. Recently, experimental results have shown that PMSEs may be modulated by radio wave heating the irregularity source region with a ground-based ionospheric heating facility. The strength of the PMSEs is reduced within second time-scales upon turning on the radio wave heating and there is a similar time-scale for recovery of the PMSEs upon turning the radio wave heating off. Also, it has been recently predicted and observed that an overshoot effect may occur during the recovery period. The modification behavior of PMSE obviously shows great promise as a diagnostic of mesospheric dust. A numerical model is used to investigate the time evolution of the effects of radio wave heating on the irregularities believed to produce PMSEs. The effects of dust charging and chemistry as well as diffusion is included in the model. The results indicate that diffusion of electrons and ions are of primary importance at early times after turn on or turn off of the radio wave heating while dust charging may have important effects at later times. Also, the scale-size of the irregularities has important effects on the reduction and recovery behavior of the irregularities.

THE GENERATION OF POLAR MESOSPHERE SUMMER ECHOES (PMSE)

Hoppe, U.-P.¹, Blix, T.A.¹, Brattli, A.¹
, Lie-Svendsen, O.¹, Rapp, M.²

¹Norwegian Defence Research Establishment (FFI), N-2027
Kjeller, Norway

²Leibniz-Institute of Atmospheric Physics, D-18225, Kuehlungs-
born, Germany

We have found that six ingredients are necessary to create PMSE: (1) sufficiently cold temperatures, (2) water vapor, and (3) suitable condensation nuclei to create aerosol particles; (4) a pre-existing gradient in aerosol particle number density and (5) episodes of turbulence to create small-scale fluctuation structures in the aerosol; and finally (6) a sufficient density of free electrons to (a) charge the aerosol particles at least partially and (b) a sufficient number of remaining free electrons to "mediate" the charged aerosol fluctuating structure to the electromagnetic wave of the (VHF) radar. At times and places where any of these six conditions is lacking, no PMSE are observed.

We will refer to existing work regarding the first two conditions, and briefly discuss why we consider "smoke particles" (Hunten et al., 1980) to be better candidates for the condensation nuclei than cluster ions. The process of turbulent episodes acting upon a pre-existing gradient of aerosol particle number density to create small-scale structures in the aerosol will be treated in greater detail. We hope to quantify the necessary minimum for the pre-existing gradient as well as why turbulence creates fine-scale structures instead of erasing them. We will use radar and rocket observations as well as simulations to shed light on this process. Observed relationships between PMSE spectral width and PMSE power and the degree of specularity (aspect sensitivity) or isotropy of the radar echoes are interpreted in relation to the generation and removal of the fluctuations.

These authors and others have modelled or simulated by slightly different methods and with slightly differing boundary conditions how observed (by rocket) or assumed charged aerosol number density fluctuations create the electron density fluctuations necessary for PMSE, when and where there are free electrons. The fact that all these simulations give similar results indicates that our present understanding is robust. The physics of the different boundary conditions and modelling methods will be explained and compared.

Session H/G5, 15:55 – Thurs.

**DUSTY PLASMAS AND
LABORATORY EXPERIMENTS II:
LABORATORY EXPERIMENTS**

Chair: S. Robertson

EXPERIMENTAL STUDY OF THE EFFECT OF ION FLOW SHEAR ON ELECTROSTATIC ION CYCLOTRON WAVES

Merlino, R. L.¹, Kim, S.¹, Agrimson, E. A.¹,
D'Angelo, N.¹, Miller, M. J.¹, Ganguli, G. I.²

¹Department of Physics and Astronomy, The University of Iowa,
Iowa City, IA 52242

²Plasma Physics Division, Naval Research Laboratory, Washing-
ton, D. C. 20375

Magnetic field-aligned currents have traditionally been invoked to explain satellite observations of plasma waves near the ion gyrofrequency in the Earth's auroral region. EIC waves provided an explanation for the transverse (to the geomagnetic field) energization of cold ionospheric ions, which eventually are driven upward by the magnetic mirror force, forming ion beams and conics. These ions ultimately find their way into the magnetosphere, where they account for a significant population of hot magnetospheric ions. One problem with this scenario has been that often the waves were observed in association with currents that were subcritical. Also, while the wave spectrum was expected to be narrowband and structured around cyclotron harmonics, a broadband frequency spectrum was often reported. The need for alternate or additional excitation mechanisms seemed obvious. Ganguli and his associates (Phys. Plasmas 9, 2321, 2002) suggested that transverse gradients in the ion flow along the magnetic field (for simplicity, ion flow shear) could provide a mechanism for EIC wave generation, either in addition to the field-aligned currents, or in the absence of field-aligned currents. They showed further, that since the critical shear required to excite EIC waves was approximately independent of the cyclotron wave harmonic number, ion flow shear could generate higher cyclotron harmonics, a common signature of the auroral observations.

In this work, the effect of ion flow shear on the excitation of electrostatic ion cyclotron (EIC) waves was studied experimentally in a double-ended Q-machine. An annular region of ion flow shear was produced by using a ring + disk configuration, as described by Kim et al. (Phys. Plasmas 11, 4501, 2004). Waves with frequencies near the ion gyrofrequency and multiple harmonics were launched from an antenna into a plasma with no field-aligned electron current. As the EIC waves propagated across the magnetic field through a region with ion flow shear, the waves were observed to grow in amplitude. The simultaneous excitation of a multi-harmonic EIC spectrum was also observed when a broadband signal from a white noise source was applied to the antenna.

This work was supported by NSF and DOE.

EVOLUTION OF THE ION VELOCITY DISTRIBUTION IN
PULSED THRUSTER-LIKE PLASMASEarl Scime*

West Virginia University

A number of groups have been exploring the potential use of expanding helicon source plasmas as plasma thrusters [1-3]. The substantial ion acceleration observed in these experiments is believed to result from the formation of a current-free, electric double layer (DL) at the end of the source (where the magnetic field begins to rapidly diverge). Recent measurements suggest that the DL forms within 100 microsecond of plasma initiation [4]. Here we present detailed measurements of the ion velocity distribution in both steady-state and pulsed helicon plasmas that exhibit high-speed ion flows. The measurements were obtained with laser induced fluorescence on helicon source experiments at West Virginia University, Princeton Plasma Physics Laboratory, and the Australian National University. Detailed measurements of bulk ion flow towards the DL from the upstream side will be presented as well as measurements of ion flow speed downstream of the DL for a wide range of plasma conditions. For pulsed helicon plasmas, we will present time resolved measurements of the parallel ion velocity distribution that suggest the formation of the DL occurs well after the initiation of the plasma. The time resolved measurements also suggest that the DL can be unstable, therefore it only exists for part of the plasma pulse. Details of the experimental apparatus used to make the measurements will also be presented. [1] C. Charles and R. Boswell, *Applied Phys. Letters* 82, 1356 (2003) [2] Cohen, S.A., N.S. Siefert, S. Stange, E.E. Scime, R. F. Boivin, and F. Levinton, *Phys. Plasmas* 10, 2593 (2003) [3] Sun, X., C. Biloiu, and E. Scime, 13, 359 (2004). [4] C. Charles and R. Boswell, *Phys. Plasmas* 11, 3803 (2004) *In collaboration with X. Sun, A. Keesece, S. Cohen, C. Charles, and R. Boswell

APPLICATION OF THE PHYSICS OF THE AURORAL CURRENT REGION IN THE VASIMR ROCKET

Bruskardt M.S.¹, Bering, E.A.¹, Chang-Daz, F.R.²,
Squire, J.P.², Jacobson, V.², Glover, T.W.²,
Eckberg, J.T.¹, Castro-Nieto, J.²

¹University of Houston, Department of Physics, Houston TX
77204-5005

²Advanced Space Propulsion Laboratory, JSC/NASA, 13000
Space Center Blvd, Houston TX 77059

The greater scope of space exploration is making increasing demands on spacecraft capabilities. Solar radiation and long flight times make manned interplanetary flight quite dangerous. The limitations of chemical rockets is making electric propulsion systems more important to space exploration. One of these electric propulsion systems is the variable specific impulse magnetoplasma rocket (VASIMR). The VASIMR uses a helicon discharge as an ion source using lower hybrid heating then has a separate downstream stage that uses ion cyclotron resonance heating (ICRH) to provide the bulk of the ion energy. The selective partitioning of input power to the helicon and ICRH systems will provide thrust/ specific impulse ratio control to the VASIMR. The VASIMR applies and simulates several important physical processes occurring in the magnetosphere. These processes include the mechanisms involved in the ion heating and acceleration that occur in the Birkeland currents of an auroral arc system. Several auroral current region processes, such as lower hybrid heating, parallel electric field acceleration, and ion cyclotron acceleration are also simulated in the VASIMR. This paper will summarize the physics in the VASIMR engine. The helicon discharge uses lower hybrid heating as the physical mechanism of the ionization source of the VASIMR. Ion exit energy measurements show a substantial parallel field due to ambipolar charge separation in the axial magnetic field of the VASIMR engine. Ion cyclotron heating during a single pass through the resonance region has been achieved. Perpendicular ion cyclotron heating in the VASIMR is shown in ion velocity phase space distribution data.

Session H/G6, 08:35 – Fri.

METEOR PHYSICS I

Chair: S. Close

REDUCING THE METEOROID RISK TO SPACECRAFT:
THE NEED FOR NEW RADAR METEOR OBSERVATIONS.Cooke, W.J.¹, Suggs, R.M.²¹UNITEs Contract, Space Environments Team, Marshall Space
Flight Center²Space Environments Team, Marshall Space Flight Center

The recent loss of the orbiter Columbia and its crew, while not caused by a meteoroid strike, has resulted in re-evaluations of the current meteoroid models used by NASA and other agencies. The most prevalent of these, that published by Grun et al. in 1985, assumes an isotropic meteoroid background in which all meteors travel at speeds of 20 km s⁻¹, and is clearly oversimplified. The standard Divine NASA interplanetary model, currently called METEM, is a set of empirical fits to data using distributions that have little or no resemblance to reality; consequently, the models environment directionality and velocity distributions are in error. The recommendation of the Columbia Accident Investigation Boards (CAIB) report that meteoroid risk to Space Shuttle missions be evaluated in a manner similar to that used for the International Space Station, combined with the insistence that these environment assessments be accompanied by confidence levels or uncertainties, is a driving force behind the development of new, physics-based meteoroid environment models for near-Earth space and elsewhere.

Such models, of course, must be calibrated. In-situ measurements by spacecraft would be ideal, as they can sample throughout the Solar System. However, the small collecting area of current detectors renders them useless for detecting particles with sizes capable of causing spacecraft damage, which is greater than 100 microns. Fortunately, ground-based sensors, such as radar, can, at least in principle, measure the fluxes of particles in the threat regime, thereby providing the necessary calibration points. This paper will discuss the role classical meteor radars and High Power Large Aperture (HPLA) systems can play in helping to mitigate the meteoroid threat to spacecraft and highlight specific areas, such as velocity measurements, where such data are urgently needed.

METEOROID BULK DENSITY FROM HIGH POWER LARGE APERTURE RADAR HEAD ECHO OBSERVATIONS

Drew, K.¹, Brown, P.¹, Close, S.², Durand, D.²¹University of Western Ontario, London Ont., Canada²MIT Lincoln Labs, Boston, USA

The bulk density of meteoroids is an important physical quantity from both an engineering and a planetary science point of view. The bulk density of meteoroids is a proxy measure for the porosity and density of their parent bodies, providing details of the physical structure of asteroids and comets at scales of order microns. Knowing the essential building blocks of these larger bodies can help distinguish between processing effects (such as thermal metamorphism) on evolved bodies from pristine material, such as dust from interstellar clouds incorporated into cometary nuclei. Meteoroids near the Earth can pose a threat to orbiting satellites. One critical parameter needed to understand the impact effects of meteoroids on spacecraft are their bulk density. Previously, the density of microgram mass meteoroids has been assumed or extrapolated from data gathered for larger bodies; direct measurements have been lacking. Changes in the assumed bulk density of impacting meteoroids will influence future satellite and spacecraft design. Here we use head echo observations of meteoroids to carefully measure their mass and deceleration simultaneously and independently to uniquely determine their instantaneous bulk density. Large aperture radar observations are well suited to this task as they are able to make very precise spatial and temporal measurements of meteoroids moving across the radar beam. Observations were made using the ARPA Long-Range Tracking and Instrumentation Radar (ALTAIR). ALTAIR is a high power large aperture radar which can operate simultaneously at 158 and 422 MHz. Data was collected on Aug. 12, 1998, Nov. 17, 1998 and Nov. 17, 1999 and consists of approximately 80 minutes of observation time. During the observation periods, the ALTAIR beam was pointed mainly at the north apex sporadic source of meteors, which is populated with high inclination meteoroids, believed to be associated with long-period comets. Thus our sampling is biased toward this source and cannot be taken as broadly representative of the entire meteoroid background. Meteoroid masses are obtained by applying a new full wave scattering theory to the observed radar cross section. The observed meteoroids are in the mass range of 10^{-10} to 10^{-6} kg. Meteoroid densities are calculated using the equations of the classical physical theory of meteors and are found to have a median value of approximately 1000 kg/m^3 . This is somewhat lower than has previously been assumed for meteoroids in this size range and is lower than the average found for stratospheric interplanetary dust particles. In addition to densities, meteoroid orbits are calculated and found to be largely retrograde. Both the calculated densities and orbits are consistent with a cometary origin for this observed population of meteoroids.

UNDERSTANDING THE NEAR-EARTH MICROMETEOR ENVIRONMENT USING RADAR MEASUREMENTS

Janches, D.¹, Chau, J.L.², Palo, S.E.³
, Avery, S.K.¹, Avery, J.P.⁴, Lau, E.M.¹

¹CIRES, University of Colorado, USA

²Jicamarca Radio Observatory, Lima, Peru

³Dept. of Aerospace Engineering, University of Colorado, USA

⁴Dept. of Electrical Engineering, University of Colorado, USA

We discuss results of meteor head-echo observations conducted using the 430 MHz dual-beam Arecibo (AO) radar in Puerto Rico and the 50 MHz Jicamarca (JRO) radar in Peru. The seasonal behavior that is reflected in the fast component of the micrometeor velocity distribution measured at AO is explained by a micrometeor radiant distribution centered at the Earth's apex. This proposed radiant distribution is derived from meteor measurements using JRO in interferometric mode. We conclude that these and probably every other high power/large aperture radar, only detect this Apex-centered dust population. No evidence of other meteoroid sources becomes apparent from these observations. Additionally we present specular meteor trail measurements from the quasi-all-sky meteor radar system. This system was installed in 2001 to measure the horizontal wind field in the mesosphere and lower thermosphere (MLT) region. The diurnal and seasonal variability of the meteor flux observed over the South Pole indicate that most of the activity occurs during the Antarctic summer around a very concentrated region of the sky in elevation and azimuth. These results agree with previous Arctic meteor observations and suggest that most of the flux is concentrated around the ecliptic plane. This also is in agreement with the Apex-centered dust distribution detected by the HPLA radars. We also show that in order to explain the diurnal and seasonal variability of the meteor rate detected at AO and JRO an atmospheric filtering effect must exist produced by the early and higher ablation of micrometeors, which enter the atmosphere at low elevation angles. These particles probably reach high temperature at higher altitudes and deposit some or all their material before they penetrate deep into the MLT region.

UNDERSTANDING RADAR METEOR BIASES VIA COMPARISONS OF SPECULAR, NON-SPECULAR TRAILS AND HEAD ECHOS

Dyrud, L.¹, Jances, D.², Urbina, J.³
, Oppenheim, M¹, Denney, K.¹

¹Boston University

²University of Colorado

³University of Arkansas

We used radar observations from the Coqui II 50 MHz radar, located near Salinas, Puerto Rico, to measure observed counts of both specular and non-specular meteor trails, and observations Arecibo to measure head echos in the E-region ionosphere. The Coqui II observations were made during local times between 18:00 to 08:00 on various days in 1998 and 1999. The Coqui II radar has two sub-arrays, both pointed to the north in the magnetic meridian plane, perpendicular to the magnetic field, at an elevation angle of approximately 41 degrees. Traditional meteor radars require trail specularity (trail perpendicular to radar beam) for a reflection, but over the past decade, two new types of radar meteor reflections, known as meteor head echoes and non-specular trails, have become known or widely used. Many estimates for determining global meteor mass flux have used these traditional meteor radars counting only specular meteor trails. To determine the extent that various trail detections represent a non-biased, full spectrum observation of the meteor flux, we examine the diurnal and seasonal variability of specular trails, non-specular trails, and head echos. We use observations of these three types of meteor reflections from the same location to show that the diurnal variability of specular trails, non-specular trails, and head echos are not equivalent. A revealing comparison comes from comparing the maximum count rate in the morning to the minimum at dusk. Specular meteor trails showed a max/min ratio of 8, that is 8 times more frequent trail observations at maximum than minimum. Non-specular trails show greater increase near 30, while head echos observation have a max/min of many hundred times more meteors at maximum (dawn) then minimum (dusk). We shall examine some of the possible causes of this discrepancy, and discuss what it may teach us about the filtering effects of various radar systems and meteor reflection mechanisms.

DETERMINING THE SELECTION EFFECTS IN HPLA METEOR HEAD ECHO DATA

Close, S.¹, Brown, P.², Oppenheim, M.³
, Drew, K.², Durand, D.¹, Cooke, B.⁴

¹M.I.T. Lincoln Laboratory

²University of Western Ontario

³Boston University

⁴Marshall Space Flight Center

High-power large-aperture (HPLA) radars provide a unique capability for characterizing the meteoroid population. HPLA radars are best-suited for detecting the meteor head echo, which is the radar return from the plasma immediately surrounding the meteoroid and moving at approximately the meteoroid velocity. Classical meteor radars, in comparison, are best suited for characterizing the specular trail, which is the reflection from the quasi-stationary plasma behind the meteoroid. The meteoroid population detected by HPLA radars differs from meteoroids detected using classical radars. For example, HPLA radars primarily detect sporadic meteoroids, even during shower periods, and the particles tend to be smaller and less massive than those seen by classical radars. Most notably, HPLA radar data show a higher velocity distribution, near 55 km/s, relative to classical data. One possible explanation for this difference lies in the radar selection effect. Specifically, it has been posed that HPLA radars are more sensitive to the high-velocity meteoroid population and are therefore less likely to see low-velocity meteoroids. This presentation addresses this possibility in order to characterize the true meteoroid velocity distribution, and hence the HPLA radar selection effect. First, we review the dependence of head echo signal-to-noise (SNR) and radar-cross-section (RCS) on meteoroid mass and velocity. Second, we identify and model this radar selection effect and apply it to our data, which were collected using the ALTAIR HPLA radar system. Finally, we determine the limiting velocity distribution as a function of radar sensitivity and apply this to HPLA radar systems in order to characterize the selection effect.

DIFFUSION OF METEOR TRAILS IN THE E-REGION IONOSPHERE: IMPLICATIONS FOR RADAR MEASUREMENTS

Dimant, Y. S., Oppenheim, M. M., Dyrud, L.
Center for Space Physics, Boston University

A meteoroid penetrating the Earth's ionosphere leaves behind a trail of dense plasma observed by radars. Obtaining accurate quantitative predictions for the diffusive evolution and fields generated by these trails within the magnetized ionosphere has proven difficult. In this talk we will present a new model of the fields and evolution which fully accounts for the magnetic fields and the background plasma. This model has important implications for radar measurements of meteors. Low-power, small-aperture radars detect localized specular echoes which occur only when trail lies perpendicular to the radar line-of-sight. Upper atmospheric scientists use these radars to monitor winds between 85 and 105 km altitude and solar system scientists use them to estimate the population of small particles in the solar system. High-power, large-aperture (HPLA) VHF and UHF radars observe both head echoes, short duration signals traveling with the ablating meteoroids, and non-specular echoes, long duration signals persisting for a relatively long time in a broad altitude range within the *E*-region ionosphere. We have argued that non-specular echoes result from radar signals scattered from turbulent electron density irregularities generated by plasma instabilities (M. Oppenheim et al., *J. Geophys. Res.*, **108**, 1064, 10.1029/2002JA009549, 2003) and that head echoes result from scattering from the front edge of a meteoroid ionization path (S. Close et al., *Icarus*, **168**, 43-52, 2004). Modeling of specular radar echoes requires knowledge of spatial/temporal distribution of the trail plasma density, while modeling of non-specular trails requires knowledge of evolution and structure of the polarization electric field which drives instabilities. Earlier papers on this topic (e.g., T. R. Kaiser et al., *Planet. Space Sci.*, **17**, 519-552, 1969); W. M. Pickering and D. W. Windle, *Planet. Space Sci.*, **18**, 1153-1161, 1970; W. Jones, *Planet. Space Sci.*, **39**, 1283-1295, 1991; A. M. Lyatskaya and M. P. Klimov, *J. Atm. Terr. Phys.*, **50**, 1007-1014, 1988; R. E. Robson, *Phys. Rev. E*, **63**, 026404, 2001) did not provide accurate predictions for the plasma trail density and the polarization electric field because they did not properly treat interaction between the trail and the background ionospheric plasma. We will present results of our recent 2-D analytical theory and numerical computations which treat such interaction for a range of trail configurations. This study provides a quantitative estimate of the plasma density and electric field spatial distribution and dynamics. We will show that during trail evolution the polarization electric field may drop below the level necessary to drive instabilities while significant plasma density perturbations of the meteor trail may still exist. Combining our theory with radar observations of specular and non-specular echoes should yield useful information about meteor trails and the surrounding atmosphere.

ACTIVITY AND DEVELOPMENT OF THE
GEMINID/SEXTANTID METEOR STREAM COMPLEX

Webster, A.R., Wiegert, P., Jones, J.

The University of Western Ontario, London, Ontario. N6A5B9,
CANADA

Based on their orbital elements and similarities in activity, the origins of the December night-time Geminid and September day-time Sextantid meteor streams are believed to be related to the asteroid 3200 Phaethon which in turn is believed to be the remnants of a small comet.

In this presentation, the orbital evolution of Phaethon is studied by numerically integrating its equations of motion into the past. Using a symplectic integrator that can handle close encounters with planets correctly and a suite of clones, the past behaviour of Phaethon can be investigated to the limits that current knowledge of its orbit and the obscuring effects of chaos allow. From this, changes in the orbital elements of the parent body, and in particular potential intersections of its orbit with that of the Earth, can be investigated.

The activity of the two meteor showers has been monitored in recent years using the Canadian Meteor Orbit Radar (CMOR) located at a site near London, Ontario. This system is capable of locating accurately the position in space of a given meteor, and from an accumulation of such measurements a statistical estimate of the shower radiant is accessible. Recent addition of two outlying stations allows a good estimate of the orbital elements of the individual meteors that are observed on all three stations, about 25 percent of the total meteors seen at the main site. Using this system, the activity of the two showers in recent times is investigated and evidence is presented showing similarities in the behaviour of the two streams consistent with a common origin from Phaethon.

CHARACTERISTICS OF THE METEOR DISTRIBUTION
AND WIND FIELD OVER THE GEOGRAPHIC SOUTH POLE
USING AN INTERFEROMETRIC METEOR RADAR

Lau, E.M.¹, Avery, S.K.¹, Avery, J.P.²
, Janches, D.¹, Palo, S.E.³, Makarov, N.A.⁴

¹University of Colorado, Cooperative Institute for Research in Environmental Sciences (CIRES), U. S. A.

²University of Colorado, Department of Electrical and Computer Engineering, U. S. A.

³University of Colorado, Department of Aerospace Engineering, U. S. A.

⁴Institute for Experimental Meteorology, Scientific Production Association TYPHOON, Russia

Meteor radars have been routinely used to estimate atmospheric winds in the mesosphere-lower thermosphere (MLT) region by measuring the Doppler signature of the diffusing meteor trails. These trails are ionization columns created by the ablation of meteoroids that enter our upper atmosphere and drift with the wind.

A meteor radar system was installed at the South Pole in 2001 to measure the horizontal wind field in the MLT region. It uses four 6-element yagi antennas pointing in orthogonal directions for transmission. For reception two independent systems are used: the same yagi antennas used for transmission (COBRA data acquisition system) and an interferometric array of five crossed-dipole antennas (MEDAC data acquisition system). Such a system is capable of locating the meteor trail as well as provide information on a number of atmospheric parameters.

We will present the results obtained using the interferometric receive antenna array. The main characteristics of the meteor distribution over the geographic South Pole will be shown and discussed. Time, altitude, angular, and seasonal distributions show that the bulk of the meteor activity takes place around a concentrated region around the ecliptic plane and is more pronounced during the Antarctic summer. Additionally, we will present the preliminary features of the observed wind field. We notice that the main tidal components during the Antarctic summer are the westward-propagating diurnal and semidiurnal tide (both having wavenumber $s = 1$). More importantly, these interferometric observations allow us to take a first look into the altitudinal structure of the atmospheric waves in the MLT region. We will compare these observational results to previous observations and theoretical expectations.

ESTIMATION OF METEOR RADAR PARAMETERS

Palo, S.E., Kang, C.

University of Colorado, Department of Aerospace Engineering

Low power all-sky meteor radar systems provide a method for estimating the neutral horizontal wind field and possibly the temperature field. Accurate determination of the horizontal wind field depends upon the estimation of the received Doppler frequency while temperature measurements are dependent upon estimation of the damping coefficient. Typically only underdense meteor echoes are used for wind determination and these signals can be accurately modeled as a single complex damped sinusoid in additive white Gaussian noise. This damped sinusoid can be represented using four parameters. These are frequency, damping rate, amplitude and phase. Once the frequency and damping rate of the signal have been estimated the amplitude and phase can be estimated using standard least squares techniques. While meteor radars have been utilized to determine the horizontal wind field for many years, little work has been presented regarding the parameter estimation techniques that have been utilized. One basic technique that has been historically used is to fit the complex phase of the signal to a linear model and the power of the signal to an exponential model using a least squares technique. A second method is maximum likelihood technique that utilizes a fast fourier transform (FFT). We will compare these estimators with a global search method, fast maximum likelihood (FML), a generalized version of Rifes estimator and an FFT augmented with a Newton-Raphson search. The results for both the estimator of frequency and damping coefficient will be compared with the Cramer-Rao lower bound (CRLB), a measure of the minimum variance that an unbiased estimator can obtain. Our results show that all of the estimators except the linear phase estimator achieve the CRLB for high signal to noise ratios. However the performance is variable for moderate signal to noise ratios and all of estimators diverge from the CRLB for signal to noise ratios below 0dB. Given our results we can choose the lowest variance and hence best estimator for Doppler frequency and damping coefficient. Additionally, as we have determined the statistical performance of the estimators we can determine a confidence estimate for every determination of Doppler frequency and damping coefficient. Accurate knowledge of confidence intervals associated with the estimated parameters will help to separate the natural atmospheric variability in the measurements from inherent instrumental variability.

Session H/G7, 08:35 – Fri.

**LIGHTNING-IONOSPHERE
INTERACTION I**

Chair: E. Gerken

INITIAL RESULTS FROM THE ISUAL EXPERIMENT ON-BOARD THE ROCSAT-2 SATELLITE

Han-Tzong Su¹, Rue-Ron Hsu¹, Alfred B. Chen¹,
Stephen B. Mende², Harald U. Frey², Hiroshi Fukunishi³,
Yukihiro Takahashi³, Toru Adachi³, Lou-Chuang Lee¹⁴

¹Department of Physics, National Cheng Kung University, Tainan 70148, Taiwan

²Space Sciences Laboratory, University of California, Berkeley 94720, USA

³Department of Geophysics, Tohoku University, Sendai 980-8578, Japan

⁴National Applied Research Laboratories, Taipei 10636, Taiwan

Imager of Sprites and Upper Atmospheric Lightning (ISUAL) and its platform ROCSAT-2 satellite were successfully launched on 20 May 2004 from Vandenberg Air Force Base in California. The ISUAL payload consists of an ICCD imager, a spectrophotometer (SP) and an array photometer (AP). Goals of ISUAL project are to determine the location and timing of upper atmospheric transient events above thunderstorms, to investigate their spatial, temporal and spectral properties, to obtain a global survey of upper atmospheric flashes, and to perform additional global surveys of auroras, airglows and gravity waves. The ISUAL imager is bore-sighted with the two photometers, and the field of view of imager is 20 degrees horizontal and 5 degrees vertical. The imager is equipped with a filter wheel and it can be operated in a number of wavelength regions uninhibited by atmospheric absorption. The band-pass selection of ISUAL-SP covers the spectral ranges of sprite N21P band at 623-750 nm and the lightning signature at 777.4 nm. In addition, the SP also has two photometers covering the far-UV (150-280 nm) and near-UV (250-390 nm) bands. The ISUAL-AP can capture spatial and temporal evolution of TLEs at 370-450 (blue) and 530-650 nm (red) bands. An array photometer band consists of a 16-channel PMT-array stacking in the vertical direction, and each channel has a field of view of 0.23 degrees (vertical) by 22.5 degrees (horizontal). ISUAL views the Earth's limb across the track toward the mid-night region. The targeted region is at 1500km to 3373km away and the center of FOV is at 70 km above the tangent point. ISUAL/ROCSAT-2 circles the Earth in a sun-synchronous track, with 14 daily revisiting orbits. After passed early orbit checks, ISUAL has started its long term survey of sprites and other transient luminous phenomena above thunderstorms from space since 1 July 2001. As of mid-September 2004, ISUAL has recorded over 150 TLEs and some exploratory aurora and gravity images from orbit. In this talk, the ISUAL payload, the key parameters of ROCSAT-2, the observation strategy of the experiment, and the initial findings will be presented. *Works performed at National Cheng Kung University were supported in part by grants from NSPO (93-NSPO(B)-ISUAL-FA09-01) and NSC (NSC93-2112-M-006-007, NSC93-2111-M-006-001) in Taiwan.

CHARACTERISTICS OF LIGHTNING ASSOCIATED WITH
ISUAL-DETECTED TLES

Steven A. Cummer¹, Rue-Ron Hsu², Han-Tzong Su²
, Alfred B. Chen², Stephen B. Mende³, Harald U. Frey³
, Hiroshi Fukunishi⁴, Yukihiko Takahashi⁴

¹Electrical and Computer Engineering Department, Duke University, Durham, USA

²Physics Department, National Cheng Kung University, Tainan, Taiwan

³Space Sciences Laboratory, University of California, Berkeley, USA

⁴Department of Geophysics, Tohoku University, Sendai, Japan

Much of what is known about the characteristics of lightning that produces transient luminous emissions (TLEs) in the mesosphere comes from measurements made over many years in the U.S. High Plains. Some measurements in other regions suggest that these characteristics may be different in different geographic regions. For example, the MEIDEX space shuttle experiment recorded video observations of a number of sprites and elves that occurred with a surprising lack of extremely low frequency (ELF) transients (C. Price and Y. Yair, personal communication) that are typically associated with large cloud to ground lightning strokes. The ISUAL instrument on ROCSAT-2 is steadily recording TLEs over much of the globe and offers a unique opportunity to systematically investigate with a reasonably large database whether TLEs are produced by the same kind of lightning independent of location. Two sets of magnetic field sensors spanning the entire <1 Hz to 30 kHz frequency range have been operating at Duke University continuously since March 2004 and thus cover the initial months of ISUAL operations. Focusing primarily on TLEs observed in the Americas and Africa, which are close enough to the sensors that direct VLF signals are usually detectable from large lightning strokes, we estimate and analyze lightning parameters such as charge moment change, peak current moment, and current moment rise time in an effort to determine whether the TLE-lightning relationship is geographically variable. In particular, these parameters will be compared to those derived for U.S. High Plains TLEs from magnetic field observations using the same set of sensors.

WHAT IS A BIG LIGHTNING STROKE?

Lyons, W.A.¹, Cummer, S.A.², Rodger, C.J.³, Huffines, G.H.⁴

¹FMA Research, Inc., Fort Collins, CO

²Duke University, Durham, NC

³University of Otago, Dunedin, New Zealand

⁴University of Northern Colorado, Greeley, CO

This may seem a strange question to pose. However, in our exploration of the interactions between tropospheric electrical discharges and stratospheric/mesospheric transient luminous events (TLEs) such as sprites, elves, blue jets, etc., the attention has often been focused on lightning events in the tails of the distribution of an increasing number of parameters. Advances in remote sensing over the past decade now provide us with a number of means to characterize the bigness of a flash. Lightning detection networks, such as the U.S. NLDN, have long provided an estimate of the peak current (kA) of initially, the first stroke in a flash, and now all detected strokes in a flash. The peak current has been found to be poorly correlated to the likelihood of sprite production, though there appears a stronger correlation to halo and/or elve occurrences. Results of an extensive climatology of peak current/TLE relationships during the 2000 STEPS program will be presented. Stroke multiplicity, now determined better than before, and for some purposes, large numbers of strokes in flash may be an appropriate measure of bigness, especially for positive polarity CGs. The most relevant lightning metric for sprite production is charge moment change (CMC), now relatively easy to retrieve from ELF/VLF signal. A CMC threshold on any given night appears to discriminate with considerable skill those +CG strokes which do and do not produce sprites. The CMC is composed of the product of the charge lowered to ground and the height from which it is lowered (Z_q). New 3-D Lightning Mapping Arrays provide additional characterizations of the size of discharge: Z_q , the area and volume from which the charge is drawn, the discharge duration, and the dimensions of the electrically active portions of the parent storm. Z_q , the vertical extent of CGs, which may vary by a factor of 4 or more, is a key parameter in TLE modeling studies. Continuing currents, which have highly variable durations and magnitudes, accompany both positive and negative CGs. Remote sensing in the ULF now provides additional means to distinguish these lightning features which likely play a key role in triggering long delayed sprites. High speed cameras also provide optical confirmation of bright and long lasting discharges, both in cloud and cloud-to-ground. Field research programs designed to investigate the impacts of urbanization or land use on lightning must now recognize there exist multiple means whereby lightning may be characterized beyond the traditional metrics of flash density, polarity and peak current. In addition, analyses of four years of data from the New Zealand Lightning Detection Network reveal some unusual patterns in large peak current CGs due to impacts of both land/salt water boundaries and terrain.

FDTD STUDIES OF THE DIURNAL AND SEASONAL VARIATIONS IN SCHUMANN RESONANCE PARAMETERS

Heng Yang, Victor Pasko

Electrical Engineering Department, The Pennsylvania State University

Observations of Schumann resonances (SR) in the Earth-ionosphere cavity [Schumann, *Z. Naturforsch.*, 7a, 149, 1952] represent a powerful tool for variety of remote sensing applications [e.g., Williams, *Science*, 256, 1184, 1992; Cummer, *IEEE Trans. Antennas Propagat.*, 48, 1420, 2000; Roldugin et al., *JGR*, 109, A01216, 2004], which in recent years included studies of thunderstorm related transient luminous events in the middle atmosphere and related lightning discharges [e.g., Sato and Fukunishi, *GRL*, 30, 1859, 2003; Su et al., *Nature*, 423, 974, 2003]. The observed SR parameters are strongly related to the distributions of the conductivity and global lightning activity in the Earth-ionosphere cavity. In the realistic cavity, the conductivity distribution is not laterally uniform, but varies with the local time and seasons. Additionally, the lightning activity in the three main areas (Africa, South-East Asia, and South America) exhibits strong diurnal and seasonal variation patterns. The resultant diurnal and seasonal variability of the SR parameters has been well documented in the existing literature [e.g., Sentman and Fraser, *JGR*, 96, 15973, 1991; Satori, *JATP*, 58, 1483, 1996; Price and Melnikov, *JASTP*, 66, 1179, 2004]. In this talk we report results from a 3D FDTD model of the Earth-ionosphere cavity with realistic conductivity profile and realistic distribution of lightning sources, which is designed to account for the observed diurnal and seasonal variations of the SR parameters. The employed model was first introduced in [Yang and Pasko, *EOS Trans. AGU*, 84, Fall Meet. Suppl., AE42A-0796, 2003] and has recently been extensively validated [e.g., Yang and Pasko, *EOS Trans. AGU*, 85, Fall Meet. Suppl., 2004] by comparisons of eigenfrequency and quality factor solutions derived from the model with a set of classical results available in the literature for the laterally uniform spherically symmetric Earth-ionosphere cavity [Sentman, *JATP*, 45, 55, 1983; *JATP*, 52, 35, 1990; *JGR*, 101, 9479, 1996; Greifinger and Greifinger, *Radio Sci.*, 13, 831, 1978; Mushtak and Williams, *JASTP*, 64, 1989, 2002] and with the recent observations of SR during solar proton events and X-ray bursts [Roldugin et al., *JGR*, 106, 18555, 2001; *JGR*, 108, 1103, 2003; 2004]. Specifically in this talk, we will report comparisons of the FDTD model results with the diurnal and seasonal variability of SR parameters reported recently by Price and Melnikov [JASTP, 66, 1179, 2004]. We will also discuss variability of SR power at different locations on the Earth surface as a function of the local and universal time and provide comparisons with related experimental measurements by Sentman and Fraser [JGR, 96, 15973, 1991].

SPACE-BORNE OBSERVATIONS OF INTENSE GAMMA-RAY
FLASHESFishman, G.J. ¹²¹NASA-Marshall Space Flight Center, Huntsville, AL, USA²National Space Science and Technology Center (NSSTC),
Huntsville, AL, USA

Intense millisecond flashes of MeV photons were discovered with the space-borne detectors of the Burst and Transient Source Experiment (BATSE) aboard the Compton Gamma-Ray Observatory (CGRO). These flashes originate at altitudes above at least 30 km, in order to be observable by the orbiting detectors. Over the entire CGRO mission, from 1991 until 2000, about 70 of these events were observed. Nearly all TGFs had short (millisecond) durations and sub-ms rise-times and fall-times, however a small fraction of them had longer timescales associated with them. Most were single pulses, but about a dozen had double pulses and a few had more than two pulses.

The TGFs are observed in a photon-by-photon recording mode, with each photon from eight independent detectors being tagged to the nearest two microseconds in four energy channels. The TGFs show very hard spectra, in most cases there are more photons recorded above 300 keV than below. Several of the TGFs were also recorded by the thicker (but smaller area) spectroscopy detectors that provided improved spectral resolution than the large area detectors. The temporal and spectral characteristics of the events and the capabilities of the detectors will be described in more detail than the in the original paper.

The association of TGFs with thunderstorms is primarily statistical; the TGFs show a strong correlation with the global distribution of lightning, as observed with recent satellites. There has also been an association based upon coincidences with spheric events, however, this association is debatable due to the high spherics rate and the non-directionality of the detectors. This talk gives an update of the BATSE observations of TGFs were published by the BATSE instrument team over ten years ago.

DETECTION OF TERRESTRIAL GAMMA-RAY FLASHES
WITH THE RHESSI SPACECRAFT

Lopez, L.I.¹, Smith, D.M.², Lin, R.P.¹
, Barrington-Leigh, C.P.³

¹Physics Department and Space Sciences Laboratory, University of California, Berkeley, 7 Gauss Way, Berkeley, Ca. 94720

²Physics Department and Santa Cruz Institute for Particle Physics, University of California, Santa Cruz, 1156 High Street, Santa Cruz, Ca. 95060

³University of British Columbia, 2329 West Mall, Vancouver, BC V6T1Z4, Canada

We report the detection of Terrestrial Gamma-ray Flashes (millisecond bursts of gamma-rays seen from space, dubbed TGFs) with the Reuven Ramaty High Energy Solar Spectroscopic Imager (RHESSI) satellite, the second instrument ever to observe this phenomenon. The first instrument to detect these events was the Burst and Transient Source Experiment (BATSE), launched on board the Compton Gamma-Ray Observatory (CGRO) in 1991. RHESSI has been in orbit since February 2002. BATSE detected over 75 TGF events during its 9-year lifetime, here, we present 38 TGFs from 3 months of observations. RHESSI records every interaction in 1 microsecond time bins and into one of 9 germanium detectors. TGFs synthesize 30 single photon events, on average. We find over ten times as many events per month as BATSE, and find that single photon energies extend to greater than 10 MeV, a factor of 30 higher in energy than BATSE was capable of distinguishing, since its highest energy channel included everything from 300 keV and up. Duration for these events ranges from 195 to 3515 microseconds. The RHESSI TGFs, like BATSE's, are found to be concentrated above regions of high thunderstorm activity worldwide. Collaborations have been established with research groups worldwide to directly correlate TGF events with radio signatures of lightning storms, individual strokes, sferics, and optical phenomena, namely red sprites and blue jets. An exact TGFs production mechanism is yet unknown, however, they may be caused by electrical discharges in the upper atmosphere related to large lightning storms; there have been alternate models proposed. A relationship between TGFs and high-altitude optical phenomena has been considered due to the common correlation with thunderstorms.

HIGH-SPEED TELESCOPIC IMAGING OF SPRITES

Marshall, R. A. , Inan, U. S.
Stanford University

Telescopic images of sprite streamers and beads at high frame rates reveal evolution and propagation of these structures on decameter scale at millisecond resolution and higher. In July and August 2004, sprites were observed from Langmuir Laboratory using a 1000+ frames-per-second CCD imager mounted on a Dobsonian telescope. This data is presented along with photometric data of sprites and sprite halos, taken with the Wide-angle Array for Sprite Photometry (WASP), and ELF and VLF observations at nearby sites. Results show a variety of structure, including bead formation and propagation and streamer evolution. As an example, one captured sprite shows a series of seven 1-ms resolution images, in the first of which four bead-like structures are seen to appear. In the second frame, two of these beads have evolved into streamers propagating upwards and downwards as far as the beads below, but do not coalesce with those beads. The streamer structures fade in 1-2 ms, while the beads persist for 7 ms. In another example, a tapered streamer-like structure appears in the first frame, with a 300 m width at the edge of the frame and a 10 m width at the tip, constrained by the resolution of the imager. In subsequent frames more streamers appear on either side of the first structure. All of these structures fade in 5-6 ms. In most cases, structures do not appear to propagate, meaning they either appear as stationary structures or propagate at speeds which cover the field-of-view in under 1 ms. The latter possibility does not require velocities far beyond those predicted for streamers at this altitude.

HIGH SPEED SPECTRAL SPRITE MEASUREMENTS

McHarg, M.G.¹, Stenbaek-Nielsen, H.C.²

¹United States Air Force Academy

²University of Alaska, Fairbanks

The physical processes involved in sprites develop on very fast time scales, and high speed spectroscopy may be the key to unraveling them. For this purpose we conducted a field campaign at the Langmuir Laboratory in Socorro, NM, during the New Moon period in August, 2004. High speed spectra were recorded by two instruments designed to make complimentary high speed measurements. The first instrument is a large aperture imaging spectrograph with the 1000 fps imager previously used by Stenbaek-Nielsen et al. (2002) to image sprites. The recordings were made over two wavelength ranges, 550-730 nm, and 620-800 nm, covering the brightest molecular nitrogen bands in the optical/near infrared emissions previously reported by Hampton et al. (1996). The second instrument is a hyper-spectral photometer based on the multi-anode photometer used by McHarg et al. (2002) to measure sprite propagation speeds. The hyper-spectral photometer measures colors in 32 wavelength bands from 400-800 nm at 25 kHz per channel. Preliminary analysis of the ms imaging spectra show the band structures to be well resolved, but at the time of this writing it is uncertain if any ionized lines were present. During the evening of 11 August 2004, a large meso-scale thunderstorm was observed. At 08:05:34 UT a series of three positive cloud to ground lightning strokes were observed on the National Lightning Detection Network (NLDN)18. The peak current observed in these three strikes were 146, 88 and 40 kilo amps. There were several smaller positive cloud to ground lightning strikes in the same vicinity during the same time. Three sprites were observed in a narrow field low light level TV camera from the Langmuir Labs site at 08:05:34 UT. These three sprites were within the field of view of the hyper-spectral photometer. Details of analysis for both data sets are ongoing, and will be reported in this paper.

Session H/G8, 13:35 – Fri.

METEOR PHYSICS II

Chair: D. Janches

A NOVEL TECHNIQUE FOR MEASURING IONOSPHERIC ELECTRIC FIELDS IN ELECTROJET REGIONS

Papadopoulos, K.^{1,2}, Milikh, G.¹, Wallace, Y.²,
Dimant, Y.³, Oppenheim, M.³

¹University of Maryland, Depts. of Physics and Astronomy, College Park, MD 20742, USA

²BAE Systems-ATI, 1250 Twenty-Fourth St., NW, Washington, DC 20037, USA

³Boston University, CAS Astronomy, 725 Commonwealth Ave., Boston, Mass 20201, USA

Electric fields in the auroral and equatorial ionospheric regions are a critical input to ionospheric and overall global space weather models. Such measurements are extremely difficult and most models rely on the few results acquired by rockets. Backscatter radar measurements operate only for significant values of the electric field and are difficult to interpret since they require measurements of the ambient ionospheric parameters. In this paper we discuss a novel technique for measuring D and E region electric fields in electrojet regions. The technique relies on coincident radar measurements of meteors entering the D and E regions and of the magnetic signature observed by ground magnetometers and electric field sensors. When meteors enter the D and E region ablate generating columns of ionized particles. The interaction of the ionized particles with D and E region electric fields generates transient currents whose electromagnetic signature can be measured by ground based electric and magnetic sensors synchronously with the radar detection of the ablating meteor. Theoretical modeling of these signatures indicates that the electromagnetic signature depends only on the meteor mass and velocity and the ambient electric field, and is independent of the ambient plasma parameters. As a result measurements of the electromagnetic signatures on the ground can be used to determine ambient electric fields in auroral and equatorial regions. In addition to the physics issues the paper will discuss signal to noise and signal processing aspects of the measurements as well as the requirements and predictions for proof-of-principle experiments at equatorial and auroral electrojet regions.

INTERFEROMETRIC CALIBRATION TECHNIQUES FOR
THE PLATTEVILLE, CO MEDAC METEOR RADARSde la Pena, S¹², Avery, S.K.¹, Avery, J.P.², Lau, E.M.¹²¹Cooperative Insitute for Research in Environmental Sciences²Department of Electrical and Computer Engineering

Meteors falling into the earth atmosphere, at the rate of several thousands per day, leave a trail of ions that reflects electromagnetic waves. In the presence of a wind field, this trail drifts and causes a Doppler shift in the frequency of electromagnetic wave reflecting from it. This frequency shift, can be used to estimate the winds in the mesosphere and lower thermosphere (MLT) region. The Meteor Detection and Collection (MEDAC) systems at the Platteville Atmospheric Observatory in Colorado currently uses an improved five receiver interferometer in order to estimate the location of the trail, and record its Doppler frequency. An accurate measurement of the phase of the signal recorded at each receiver is needed for the correct estimation of the angle of arrival of the signal. Errors in antenna placement, differences in transmission lines length, and instrumental phase differences in the system produce error in the phase that may result in erroneous spatial location estimates of the trail, which is needed for the correct estimation of the wind field, since the radars usually operate under a quasi all-sky mode, which requieres the location of the source of the reflected signal. Different techniques are used to reduce these errors and improve estimations. We present and discuss a tecnhique previously used with the MEDAC system radars, which involves the use of beacons at known locations. We will talk of other techniques used with different meteor radars, which uses meteors for the calibration, and we will present advances in recent attempts to obtain better results where other techniques have failed.

RECENT AUTOMATED-SEARCH METEOR RESULTS FROM
ARECIBO 430 MHZ RADAR OBSERVATIONS

Briczinski, S.J., Wen, C.-H., Mathews, J.D.

The Pennsylvania State University, Communications and Space
Sciences Laboratory

The automated micrometeor search algorithm has now cataloged over 33,000 separate sporadic meteor events seen with the 430 MHz Arecibo Observatory radar over 30 hours of observation time. The results of the new automated technique are compared with previous results, indicating that our current technique is able to detect over 95% of all possible events in the absence of strong sources of radio interference, an improvement over previous techniques (Janches et al. 2000; Mathews et al. 2003). A significant percentage (approximately 15%) of meteor events are observed to (apparently) catastrophically destruct within the beam the terminal event in less than 1 ms. This non-ablative mass deposition process may play an important role in the aeronomy of the upper atmosphere as it apparently produces sub-micron sized particles. We present the meteor parameters obtained from an automatic FFT meteor searching routine and consider the terminal-event destruction of meteoroids and resultant mass deposition as an important factor in the aeronomy of the meteor zone. We also present results on the altitude, speed, and mass distributions of terminal event meteoroids yielding some clues on the physics of the terminal-event including meteoroid interaction with the near 100-km atmosphere and ionosphere.

Janches, D., J. D. Mathews, D. D. Meisel and Q. H. Zhou (2000). "Micrometeor observations using the Arecibo 430 MHz radar." *Icarus* **145**: 53-63.

Mathews, J. D., C. H. Wen, J. F. Doherty, S. J. Briczinski, D. Janches and D. D. Meisel (2003). "An update on UHF radar meteor observations and associated signal processing techniques at Arecibo Observatory." *J. Atmos. Solar Terrestrial Phys.* **65**: 1139-1149.

A REPORT ON CURRENT RESEARCH REGARDING THE
METEOR TRAIL ECHO AND HYPER-SPEED METEOR
EVENTS USING THE ARECIBO 430 MHZ RADAR

Wen, C.-H., Doherty, J. F., Mathews, J. D.²

Communications and Space Sciences Laboratory,, The Pennsylvania
State University,, University Park, PA 16802-2707, USA

The meteor return signature (MRS) and the filterbank algorithms for meteor detection (C.-H. Wen et al., Geoscience and Remote Sensing, IEEE Trans., 42, 501-510, 2004) are used for the usual meteor searching process as applied to Arecibo 430 MHz meteor observation data. This approach is used to automatically find and process thousands of meteor events. Currently we use (in slightly modified form) the same algorithms to search for the meteor trail-echo and to search for the hyper-speed (≥ 72 km/sec) meteor events. We use the filterbank algorithm to estimate the Doppler frequency (velocity) and the altitude of each meteor event. For some meteor events we have found significant power at low Doppler frequency (near DC) that correlates with the altitude of the head-echo event. This result suggests that the Arecibo 430 MHz radar can detect the meteor trail-echo in some cases thus suggesting additional clues as to the meteor processes. Observational trail-echo results will be shown in this paper.

We also modified the meteor search algorithm for enhanced sensitivity to short (one or two radar pulse returns only) hyper-speed meteor events. In this algorithm we combine two inter-pulse period (IPP) signals together on a FIFO basis and find the Doppler spectrum. If a meteor event is present in both IPPs, there is a corresponding signature in the frequency spectrum. We then apply the MRS correlator and set a threshold (determined by the noise level) to detect the presence of an event signature. Observational results analyzed in this manner suggests the existence of hyper speed meteoroids. We give examples.

Session H/G9, 13:35 – Fri.

**LIGHTNING-IONOSPHERE
INTERACTION II**

Chair: S. Cummer

IN-SITU AND GROUND-BASED INVESTIGATIONS OF
SPRITE ENERGETICS OVER SOUTHERN BRAZIL

R. H. Holzworth¹, J. N. Thomas¹, M. C. McCarthy¹
, M. J. Taylor², P.-D. Pautet², S. A. Cummer³ , O. Pinto Jr⁴

¹University of Washington, Seattle, WA, USA

²Utah State University, Logan, UT, USA

³Duke University, Durham, NC, USA

⁴INPE, Sao Jose dos Campos, SP, Brazil

In November, 2002, and March, 2003, two campaigns were conducted over southeastern Brazil to investigate the presence and characteristics of transient luminous events (TLE), which are associated with positive lightning discharges. Two stratospheric balloons were flown directly over large, active thunderstorms and we recorded EM data on the largest electric field transients from positive lightning ever obtained over thunderstorms above 30 km. Optical measurements, using intensified CCD video cameras equipped with GPS timing, were also made from a field station at Cachoeira Paulista (23S, 45W), and from an Embraer aircraft (both operated by the Instituto Nacional de Pesquisas Espaciais; INPE). These observations provided the first quantitative measurements of sprites over Brazil, nevertheless, the weather conditions prevented simultaneous in-situ and optical observations. In order to continue our investigations, a new balloon campaign will be conducted in February-March, 2005, from Santa Maria (29.7S, 53.8W), Rio Grande do Sul, in order to fly over some of the largest storms in the world (over southern Brazil and northern Argentina). In addition to the previous electronic and optical capabilities, two major improvements have been developed: video imaging from the balloon itself, and the addition of a down-range telemetry receiving station for accessing more distant sprite-active thunderstorms. Charge moment changes and related lightning parameters will be measured using local ground based extremely- and very low frequency electric and magnetic field sensors (from Duke University), and lightning timing and location will be provided by the Brazilian lightning detection network. This talk will summarize the previous campaign measurements and will discuss the planned new observations.

LIGHTNING-INDUCED HEATING OF THE LOWER IONOSPHERE

Gerken, E., Kelley, M., Vlasov, M.

School of Electrical and Computer Engineering, Cornell University, Ithaca NY 14853

One of the most fascinating developments in near earth space science in the last decade is the detection of upper atmospheric lightning-related electrical discharges commonly known as "sprites", "elves", and "blue jets". While much recent work has focused on studying the impact of lightning on the D-region of the ionosphere and below, little is known about the effects in the higher ionospheric regions. Cornell University has launched four rockets over thunderstorms from Wallops Island (Kelley et al., *Geophys. Res. Lett.*, **24**, 1111, 1997; Kelley et al., *Geophys. Res. Lett.*, **17**, 2221, 1990; Siefring and Kelley, *J. Geophys. Res.*, **96**, 17,813, 1991; Baker et al., *J. Spacecraft and Rockets*, **33**, 92, 1996). One of the most intriguing, and as yet not understood, features observed in these launches is the parallel electric field accompanying each strike. One of the Cornell rocket experiments, named "Thunderstorm II", was carried out at the Wallops Island Flight Facility in July 1988. It involved the simultaneous launch over a thunderstorm of two high-flying rockets (apogees over 300 km) with electric field and particle detectors. Parallel electric field pulses accompanying nearly every detected lightning strike were observed during this flight. A second Cornell rocket experiment, "Thunderstorm III", was launched from Wallops Island Flight Facility in September 1995 to further study electromagnetic pulses above thunderstorms. Complete waveform information was obtained for this sounding rocket using a specially designed 4-M sample/sec triggered burst memory (Baker et al., *J. Spacecraft and Rockets*, **33**, 92, 1996). This rocket launch produced the first ionospheric observations of the spectrum of lightning-induced electromagnetic waves from ELF through MF bands. These data were obtained on a near vertical path over a very active thunderstorm cell using a double-probe electric field sensor. The payload was magnetically aligned so the two detectors perpendicular to B saw a dispersed circularly polarized whistler mode wave. Similar to data obtained by the Thunderstorm II experiment, parallel electric field components observed during Thunderstorm III took the form of pulses lasting several ms and the features were similar for each strike. The average value of these fields was found to be ~ 1.5 mV/m during 13 s of the upleg of the rocket flight. Using the thermal balance equation with this data set, it is determined that the electron temperature should be greatly enhanced within a few seconds. Modeling of the height distributed 630 nm oxygen airglow emission shows the lightning strikes should produce airglow enhancements which may be detectable from the ground, depending on the efficiency of the molecular nitrogen vibrational barrier.

HIGH FREQUENCY MEASUREMENTS OF PARALLEL ELECTRIC FIELDS AND WAVES IN THE IONOSPHERE OVER AN ACTIVE THUNDERSTORM

Douglas Rowland¹, John R. Wygant², Keith Goetz²,
Steve Monson², Robert Holzworth³, Michael McCarthy³

¹Laboratory for Extraterrestrial Physics, NASA / GSFC, Greenbelt, MD 20771

²School of Physics and Astronomy, University of Minnesota, Minneapolis, MN 55455

³Earth and Space Sciences, University of Washington, Seattle, WA 98195

Sounding rockets launched by the Cornell group demonstrated the existence of transient (1 ms) electric fields associated with lightning strikes at high altitudes above active thunderstorms. These electric fields had a component parallel to the Earth's magnetic field, and were unipolar and large in amplitude. They were thought to be strong enough to energize electrons and generate strong turbulence as the beams thermalized. The parallel electric fields were observed on multiple flights, but high time resolution measurements were not made within 100 km horizontal distance of lightning strokes, where the electric fields are largest. In 2000 the "Lightning Bolt" sounding rocket (NASA 27.143) was launched directly over an active thunderstorm to an apogee near 300 km. The sounding rocket was equipped with sensitive electric and magnetic field instruments as well as a photometer and electrostatic analyser for measuring accelerated electrons. The electric and magnetic fields were sampled at 10 million samples per second, letting us resolve the structure of the parallel electric field pulse up to and beyond the plasma frequency. In addition, many lightning strokes within 100 km horizontal distance of the rocket were observed.

We will present results from the Lightning Bolt mission, concentrating on the parallel electric field pulses that arrive before the whistler wave modes. We observe pulses with peak electric fields of a few mV/m lasting for a substantial fraction of a millisecond. Superimposed on this is a high-frequency signature, comparable in amplitude to the pulse itself. Parallel fields of both polarities were observed, and there was a strong decrease in parallel field strength both with increasing altitude and increasing horizontal distance from the lightning stroke. In addition, there is suggestive evidence of a reversal of the parallel electric field polarity with increasing altitude. These are the first direct observations of this structure in the parallel electric field, within 100 km horizontal distance of the lightning stroke. We will present evidence for the method of generation of these parallel fields, including evidence for the probable wave mode, and will discuss their probable effect on ionospheric electrons.

CORONA DISCHARGE WAVES IN THUNDERCLOUDS AND
THE FORMATION OF IONIC CHANNELS

Losseva, T.V., Fomenko, A.S., Nemtchinov, I.V.
Institute of Geospheres Dynamics, , Russian Academy of Sciences,
, Leninsky pr. 38-1, Moscow 119334, Russia

Measurements of the electric field strength in thunderclouds persistently give values by an order of magnitude lower than the breakdown threshold of the pure air. Models of the lightning propagation through the thundercloud usually start with the existing highly conductive channel in the cloud of rather large length and rather thin, at the end of which the field is already enhanced due to the charge redistribution along the channel and thus the channel may increase its length due to streamers and the leader formation. It is not clear how such the long highly conductive channel may be formed.

It is well known that the droplets, ice particles, hailstones or snowflakes may enhance the electric field and produce the corona discharge. We assume that in a small part of the thundercloud an exceptionally high concentration of large hailstones or (and) water drops is formed and the onset-strength of the corona discharge becomes smaller than the background electric field. Polarization of this hot spot (high conductivity and high ionization rates) produces charges at opposite sides of this volume. The increased electric field initiates the corona discharge in other parts of the cloud with normal sizes of hailstones and water droplets. The high conductivity channel increases its length. The corona discharge front moves as a wave.

We describe this non-stationary problem by Poisson equation which is solved simultaneously with a simplified set of kinetic equations for ions, small charged particles and (at high electric fields) electrons, including ionization due to electronic impact, attachment and formation of positive ions, and charging of small particles in addition to their normal charging in the thundercloud due to non-inductive charging mechanisms. A simple analytical model of such a wave is developed. 3D numerical simulations are fulfilled.

MOLECULAR NITROGEN LBH BAND SYSTEM FAR-UV
EMISSIONS OF SPRITE STREAMERS

Liu, N., Pasko, V. P.

CSSL Laboratory, Department of Electrical Engineering, Penn
State University

Optical and near-UV emissions have been detected in transient luminous events (TLEs) above thunderstorms during observations from the ground and aircraft [e.g., Sentman et al., GRL, 22, 1205, 1995; Mende et al., GRL, 22, 2633, 1995; Hampton et al., GRL, 23, 89, 1996; Armstrong et al., JASTP, 70, 787, 1998; Suszcynsky et al., JASTP, 70, 801, 1998; Armstrong et al., GRL, 27, 653, 2000; Morrill et al., GRL, 29, 1462, 2002]. The recent successful launch of the ISUAL instrument [Chern et al., JASTP, 65, 647, 2003] on ROCSAT-2 satellite provides new opportunities for studies of far-UV (FUV) emissions of TLEs, which are not observable by the ground and aircraft based instruments due to the strong absorption by atmospheric molecular oxygen. The ISUAL instrument includes a spectrophotometer with bandpass 150-280 nm, which is well overlapping with the emissions spectrum 100-260 nm of N₂ Lyman-Birge-Hopfield (LBH) band system [e.g., Chern et al., JASTP, 65, 647, 2003, and references therein]. The first successful observations of FUV emissions by the ISUAL have been recently reported [Mende et al., NATO ASI on Sprites, Corte in Corsica, July 24-31, 2004; Frey et al., Eos. Trans. AGU, 85, Fall Meet Suppl., 2004], and theoretical understanding of FUV emissions arising from different types of TLEs, and from sprite streamers in particular, represent an important component of related studies needed for interpretation of the experimental data. In this talk, we report results on application of time dependent optical emission model developed in [Liu and Pasko, JGR, 109, A04301, 2004] to studies of sprite streamers under different applied electric fields representative of conditions at sprite altitudes with particular emphasis on FUV emissions from the N₂ LBH band system. Our modeling results indicate, in particular, that for streamers propagating in low electric fields characteristic of lower parts of sprites (i.e., below the initiation altitude) the LBH emissions originate mostly from the streamer tips with the integral intensity a factor of 20 lower than that of red emissions of the first positive band system of N₂, while a factor of 2 stronger than the blue and near-UV emissions of the first negative of N₂⁺. The results for streamers propagating in low electric fields also demonstrate that the streamer channel is dark, and most of the optical luminosity of streamers in this case arises from tips of streamers, in agreement with recent time resolved (~1 ns) imaging of laboratory streamers in point-to-wire or point-to-plane discharge geometry conducted at ground and near ground pressures [van Veldhuizen et al., IEEE Trans. Plasma Sci., 30, 162, 2002; Yi and Williams, J. Phys. D. Appl. Phys., 35, 205, 2002].

A FRAMEWORK FOR UNDERSTANDING THE PHYSICS OF SPRITES

Triplett, L.A.¹, Gerken, E.A.², Roussel-Dupre, R.A.¹
, Symbalisky, E.M.D.³

¹Los Alamos National Laboratory, EES-2, MS F665, Los Alamos, NM 87545

²Cornell University, 320 Rhodes Hall, Ithaca NY 14853

³AFTAC/TTAD, 1030 S. Highway A1A, Patrick AFB, FL 32925-3002

The breakdown processes that lead to sprite formation are still being debated. Are sprites formed through conventional breakdown, runaway breakdown, or a combination of both? If it is a combination of both, can one predict when each process will dominate based on the parent lightning characteristics, the upper atmospheric conductivity profile, the geometry of the discharge, the measured brightness and spectrum of the sprite, or some other metric? The purpose of this study is to provide a framework for discussing what underlying physics is revealed, or not revealed, by current measurements and to stimulate discussion in the sprite community, both on how to refine this framework and what future measurements would be useful.

We will start with a brief overview of conventional and runaway breakdown processes. Next, we will take a two-pronged approach to understanding the underlying physics. First, we will discuss photometer and parent lightning measurements as a function of morphology of the sprite. We will then present what underlying physics may or may not be discerned from these measurements. The measurements will be separated into three bins: those that can be explained by conventional only, those that can be explained by runaway only, and those that could be explained by either (i.e. either both present or the measurements are not yet to the point where we can differentiate). Time will not permit an exhaustive discussion of all measurements and all physics; therefore, the goal of this talk will be to provide a framework for continuing the discussion.

Our second approach will be to show results from a fully 2-D electromagnetic model (UNIMAX) and optical model (POEM) for both conventional and runaway breakdown processes. We will compare two runs with different parent lightning characteristics and show that different measurements are predicted. We will then present two runs in which runaway is turned off and show how this affects the results. We will compare the model results to measurements and separate out the results into the three bins discussed above. We will also discuss the effects of spatial and temporal averaging on the comparison of modeling results to measurements. We will conclude with our suggestions for future measurements and solicit input from the community on how to refine this framework and refine future measurements.

AIR HEATING ASSOCIATED WITH SPRITE DISCHARGES

Victor P. Pasko

CSSL Laboratory, The Pennsylvania State University, University Park, PA 16802, USA

The understanding of ambient gas heating processes initiated by needle-shaped filaments of ionization, called streamers, embedded in originally cold (near room temperature) air represent a long standing problem, which is of interest for studies of long laboratory sparks and natural lightning discharges [e.g., Gallimberti et al., *C. R. Physique*, 3, 1335, 2002]. The visual appearance of a subset of the recently observed transient luminous events in the middle atmosphere, which originate from thundercloud tops [Wescott et al., *JGR*, 106, 21549, 2001; Pasko et al., *Nature*, 416, 152, 2002; Su et al., *Nature*, 423, 974, 2003], indicate that these events may be related to conventional lightning leader processes and therefore are associated with significant heating of the air in the regions of atmosphere through which they propagate [Pasko and George, *JGR*, 107, 1458, 2002]. Many of the small-scale features observed in sprites at higher altitudes [e.g., Gerken and Inan, *JASTP*, 65, 567, 2003] can be interpreted in terms of corona streamers, which, after appropriate scaling with air density, are fully analogous to those, which initiate spark discharges in relatively short (several cm) gaps at near ground pressure [Liu and Pasko, *JGR*, 109, A04301, 2004, and references therein] and which constitute building blocks of streamer zones of conventional lightning leaders in long gaps [Gallimberti et al., 2002]. The recent reports of infrasound bursts originating from 60-80 km altitudes in sprites, with durations consistent with the optical widths of the sprites [e.g., Farges et al., *Eos. Trans. AGU*, 85, Fall Meet Suppl., 2004], provide an additional motivation for studies of the heating of the ambient air and associated chemical effects caused by streamers in transient luminous events. In this talk we will discuss scaling properties of physical processes involved in the air heating in streamer channels as a function of air pressure and will report the most recent results from a model, which was originally introduced in [Pasko, *Eos. Trans. AGU*, 84(46), Fall Meet. Suppl., AE41B-05, 2003] for investigation of effective time scales of air heating in streamer channels. The model has been upgraded to explicitly include energy input in vibrational ($v=1-8$) excitation of nitrogen molecules, the time dynamics of the vibrational temperature and the vibrational-translational relaxation processes, and to account for the effects of gains in electron energy in collisions with vibrationally excited nitrogen molecules on the rate constants of ionization and dissociative attachment processes [Belinov and Naidis, *J. Phys. D: Appl. Phys.*, 36, 1834, 2003, and references therein].

OCCURRENCE RATES OF VLF SIGNATURES OF LEP
EVENTS MEASURED BY THE HAIL ARRAYW. B. Peter, U.S. InanSTARLab, Stanford University, 350 Serra Mall, Stanford, CA
94305

Subionospherically propagating Very Low Frequency (VLF) signals have long been used to detect localized disturbances of the lower ionosphere. A distributed set of VLF observing sites, known as the Holographic Array for Ionospheric and Lightning Research (HAIL), captures the occurrence of lightning-induced electron precipitation (LEP) events over the Central United States. Quantitative understanding of the occurrence properties of LEP events is needed for accurate quantification of the role of lightning discharges in radiation belt losses at mid-to-low latitudes.

In particular, we examine the effects of several geomagnetic storms, including the Halloween storm (late October of 2003), on the occurrence rates of LEP events. The occurrence rate is found to be highly variable with geomagnetic activity. Comparison of LEP event occurrence rates with measurements of energetic electron flux levels from the NOAA-POES satellite supports the notion that this variability in the number of LEP events detected by the HAIL array is largely due to increases in the energetic electron population in the slot region with the advent of geomagnetic activity.

We also examine the occurrence of LEP events associated with highly localized and long lasting thunderstorms, such as that which occurs in lightning associated with hurricanes. In mid-September of 2003, Hurricane Isabel passed through the Great Circle Path (GCP) of a sub-ionospherically propagating LF signal between the NAU transmitter in Puerto Rico and a VLF/LF receiver located outside Boston. Cloud-to-ground lightning flashes detected by the Long-Range Lightning Detection Network (LRLDN) and located in the outer rainbands of the hurricane were associated with perturbations in the received LF signal consistent with LEP events. The number of perturbations detected on the LF signal consistent with lightning-induced electron precipitation events tended to increase with the occurrence of hurricane-associated lightning near the GCP.

Session J1, 08:15 – Wed.

**OPTICS FOR WIDE FIELD
IMAGING**

Chair: N. Halverson

BOLOCAM OPTICAL DESIGN AND PERFORMANCE

J. Glenn¹, J.E. Aguirre¹, P.A.R. Ade²
, J.J. Bock³, S.F. Edgington⁴, A. Goldin³
, S.R. Golwala⁴, D. Haig², A.E. Lange⁴
, G.T. Laurent¹, P.D. Mauskopf², H. Nguyen³
, P. Rossinot⁴, J. Sayers⁴, P. Stover¹

¹University of Colorado

²Cardiff University

³Jet Propulsion Lab

⁴California Institute of Technology

Bolocam is a millimeter-wave (1.1 mm and 2.1 mm) camera with a monolithic array of one hundred and forty-four 300-mK bolometers. Bolocam is used on the 10.4-m Caltech Submillimeter Observatory (CSO) for observations of submillimeter galaxies, galaxy clusters, secondary anisotropies in the cosmic microwave background radiation, and Galactic star formation regions. Bolocam has a hexagonal field-of-view of 8 arcminutes. The neutron transmutation doped Ge bolometers with silicon nitride micromesh absorbers reside between an array of close-packed, straight-walled, conical feedhorns and a reflecting backshort, optimized for each waveband. The feedhorns are coupled to the telescope by a double-parabolic cryogenic lens and a room-temperature ellipsoidal mirror. The mirror reimages the CSO primary mirror onto a cryogenic cold stop, which apodizes the beams. The bandpasses are formed by the waveguides and a stack of metal-mesh filters. Bolocam has been fully characterized and commissioned at the CSO.

I will describe the optical design, simulations, and results of laboratory and telescope optical characterization, including: beam maps over the bolometer array, diffraction by the cold stop, and optical loading. Good agreement is found between the optical performance and beam parameters, as predicted using Zemax EE (trademark), and the measured performance, including diffraction in the near field of the cold stop. The system exhibits mild distortion, which is corrected for in software when pointing corrections are applied. The optical performance is good over the entire field-of-view and the design serves as the baseline for Bolocam II, which is being built for use on the 50-m Large Millimeter Telescope in Mexico.

THE CAPMAP FOCAL PLANE ON THE CRAWFORD HILL
7-M ANTENNAJeff McMahon

Princeton University, dept. of Physics

CAPMAP is an ongoing experiment to characterize the small scale polarization of the cosmic microwave background radiation (CMB). CAPMAP is comprised of an array of 16 correlation polarimeters with 4 operating at 40GHz and 12 operating at 90GHz. This array is fielded on the Crawford Hill antenna which is an off-axis cassegrain telescope with a 7 meter diameter primary mirror and large focal plane which has Strehl ratios greater than 0.97 over a 1.4° diameter field of view. In this talk I will describe how we designed the CAPMAP focal plane to take advantage of the many attractive features of the Crawford Hill antenna, and also to mitigate aspects of the design which are not optimal for our purposes. The discussion will include measurements of the performance of the CAPMAP system, which is currently acquiring data for its third season.

The CAPMAP focal plane uses individual horn plus lens feed assemblies for each receiver. The 7-meter telescope achieves its large focal plane and excellent optical quality through its long focal ratio $f = 5.6$. This means the primary mirror is only 10° wide as viewed from the focal plane. Thus the feeds must produce tightly collimated beam patterns. Additionally for CMB observations the side-lobes of the feeds must be minimized since those which fall outside this 10° cone pass beyond the edge of the primary and can hit the ground which could lead to spurious non-cosmological signals. The corrugated feed horn and microwave lens systems are carefully optimized to produce narrow beams with low side-lobes (-40dB) and low cross-polarization (-35dB).

The fact that each receiver has an independent feed allows for significant freedom in the arrangement of the feeds in the focal plane and equivalently, the pattern of beams on the sky. We exploit this freedom to introduce 4-fold and 8-fold symmetries into the focal plane which when combined with our scan strategy produces a uniform polarization coverage over a 2.2° diameter disk on the sky, with built in systematic checks between different receivers.

WIDE FIELD OPTICAL DESIGN FOR SCUBA-2

Duncan, W. D.¹, Atad, E.², Peacock, T.²
, Harris, J.², Holland, W. S.², Audley, M. D.²

¹NIST, 325 Broadway, Boulder, CO 80305, USA

²UKATC, Royal Observatory, Blackford Hill, Edinburgh, EH9
3HJ, UK

We outline the design approach for the SCUBA-2 optical design and suggest it as a practical method for designing other wide-field instruments in the mm to few THz range. The field of view of the James Clerk Maxwell is 600mm in diameter at the Cassegrain focus. An optical system is required to image this focal plane onto the detector arrays which are operated at 100 mK and are manufactured at the 3" Si wafer size scale. In addition, the SCUBA-2 instrument is too large and heavy to consider co-rotating it with both axes of the telescope. It will be located at the Naysmyth focus which inevitably leads to a complex optical system. To avoid dielectric losses an all reflecting design is used. This means that the system is all off-axis. Simple calculations show that the Strehl ratio of the relay optics has to be very high to avoid increasing the losses associated with the telescope surface. This high performance must be established across the field of view by the optics and maintained as the telescope changes elevation. It is also highly desirable to have low field distortion to greatly simplify image construction. The optical design has to have a good image of the telescope aperture close to the array in order to limit the field of view of the pixels and control stray light. The optical design must also predict the detailed surface shape of the mirrors for manufacture and using time reverse diffraction calculations predict the field at each mirror and stop so they can be sized correctly. The large number of optical elements requires that the surface accuracy of each element must be 1 micron rms to avoid significant throughput losses due to surface scattering. The SCUBA-2 optical system consists of 10 off-axis mirrors of general aspheric shape with some mirrors being greater than 1 m sq. This level of optical design and ability to manufacture such mirrors has only become possible in the last few years using commercial codes and 5-axis machining and polishing.

MILLIMETER WAVE OPTICS FOR THE GBT AND ACT TELESCOPES.

Dicker S.R.¹, The ACT collaboration¹²⁴⁵⁶, The GBT collaboration

¹University of Pennsylvania, Philadelphia, Pennsylvania, USA

²Princeton University, Princeton, New Jersey, USA

³National Radio astronomy Observatory, Green Bank, West Virginia, USA

⁴Goddard Space Flight Center, Greenbelt, Maryland, USA

⁵National Institute of Standards and Technology, Boulder, Colorado, USA

⁶Cardiff University, Cardiff, UK

In recent years it has become possible to construct large arrays of bolometric detectors. Even at millimeter wavelengths detector noise has dropped below the statistical noise due to the random arrival of photons. Consequently to make the best use of these detectors it is important to collect as many photons as possible. This requires wide-field optics.

This talk will describe two sets of optics designed for millimeter-wave receivers. The first are the cold optics of a 90 GHz camera being built for the Green Bank Telescope (GBT), a 100 m diameter off-axis Gregorian telescope located in West Virginia USA. The camera has an eight by eight array of transition edge sensor (TES) bolometers. The detectors are used without feeds so the cold optics define the illumination of the telescope and keep the incident power per detector below 7pW. Each detector is separated by 4.2 arcseconds (half a beamwidth) on the sky so that a fully sampled map can be made with a single pointing.

Experience from the GBT design has facilitated the design of optics for the Atacama Cosmology Telescope (ACT). This instrument will measure anisotropy in the Cosmic Microwave Background (CMB) on 1.7 arcminute scales. It has three frequency bands at 145, 225, and 265 GHz with a 32 by 32 array of TES bolometers in each band. The ACT telescope will have a 6 m primary mirror and an off-axis design. Requirements for the cold optics include a 0.366 degree square field of view (in each band), extremely low spillover, and control of loading on the detectors. A lens based system which meets these requirements has been chosen.

SUBMILLIMETER-WAVE OPTICAL CONFIGURATIONS
FOR THE SOUTH POLE TELESCOPE

Stark, A. A.

Harvard-Smithsonian Center for Astrophysics

The South Pole Telescope is a 10-m diameter millimeter- and submillimeter-wave astronomical telescope currently under development for deployment in 2007 to Amundsen-Scott South Pole Station in Antarctica (J. Ruhl et al., *Proc. SPIE International Symposium on Astronomical Telescopes* 2004). The atmosphere over the South Pole site has exceptionally high millimeter-wave transparency and stability. The telescope design provides a large field of view ($> 1^\circ$ diameter), to feed a new generation of detector arrays that have thousands of elements. The detector packages and their ancillary optics are placed near the prime focus, in order to reduce the effective focal length of the optical system compared to a conventional Cassegrain design. The telescope has a bilaterally symmetric, off-axis paraboloidal primary mirror, with an unobstructed aperture. The telescope structure can support a variety of optical configurations in a receiver cabin located below the prime focus.

The configuration currently being developed by the SPT consortium has no optical chopper; a field lens and the detector array will simply be located at the focus of a low-magnification ($M = -1.37$) Gregorian secondary which satisfies the Dragone relation. The detectors will be scanned across the sky by driving the entire telescope. The secondary mirror will be cooled to cryogenic temperatures (~ 10 K), and the edge of the secondary serves as the only optical stop in the system; all other apertures are oversized. There will be a foam vacuum window and infrared blocking filters near the prime focus. The secondary mirror and detector system will be enclosed in a single large (2 m diameter \times 3 m long) vacuum chamber. This configuration has exceptionally low spillover, background temperatures, and detector offsets.

Other optical configurations that do include a chopper mirror are possible for future detector systems. A warm Gregorian secondary is then followed by a tilting chopper mirror located near the image of the aperture formed by that secondary. A field mirror at the Gregorian focus flattens the image, followed by a focal reducer providing a relatively small (165 mm diameter) image of the aperture at a Lyot stop just inside the detector dewar window. The stop is reimaged onto the detector by a cold lens. This allows for a relatively small detector dewar (< 1 m³), dewar window (< 220 mm diameter), and infrared blocking filter (< 180 mm diameter). The 200 mm diameter focal plane could accommodate tens of thousands of detectors at $\lambda 200 \mu\text{m}$. Compared to the chopperless configuration, the additional six warm reflecting surfaces will result in a higher noise background, but at submillimeter wavelengths where the temperature of the sky is high and variable, this may be a desirable trade.

C - CONTRIBUTED PAPER

Huan T. Tran, Adrian T. Lee

University of California Berkeley, Dept of Physics

The Polarbear telescope is one of the next generation wide field polarimeters. It will be used to study the polarization of the Cosmic Microwave Background. It is specifically designed to have both the sensitivity and resolution to characterize the faint B-Mode signature of gravitational waves created during inflation. The goals of the optical design are to support 1000 resolution elements at 150 GHz and achieve a 4 arcmin beam. The large number of elements is required to achieve high enough sensitivity to measure B-mode polarization and the size of the beam is chosen to resolve a contaminant induced by gravitational lensing by intervening galaxy clusters. The telescope will feed a two dimensional array of antenna-coupled bolometers. This detector technology imposes additional constraints on the design. The planar nature of the array requires a flat field, with the chief rays of each element perpendicular to the plane. Antenna-coupled bolometers typically have large sidelobes, which must be intercepted by a cold aperture stop, or a Lyot stop. The design generically consists of a traditional 3-meter Dragone- Mizuguchi reflector with 3 reimaging lenses. The offset nature of the Dragone-Mizuguchi combined with the use of lenses leads to an unblocked aperture. The lenses form the cold stop and produce a telecentric focal plane. Special consideration must also be given to polarization performance, both in cross polarization and instrumental polarization. This design was chosen after considering many other designs, including on-axis designs like traditional Cassegrains. The need for a wide field, however, leads more naturally to offset designs. The reflector and three lens combination is generic enough to support many thousands of elements, and is suitable for future CMB polarization experiments.

RF OPTICS DESIGN FOR THE Q/U IMAGING EXPERIMENT

Imbriale, W. A.
JPL, Pasadena, CA 91109

This paper describes the RF optics design of the Q/U Imaging Experiment (QUIET) intended to image the polarization of the cosmic microwave background (CMB) with detectors at two frequencies with unprecedented sensitivity. Observing the polarization of the CMB demands exquisite sensitivity to both Q and U Stokes parameters and freedom from systematic errors. QUIET makes use of recent breakthroughs in millimeter-wave circuit packaging to enable large arrays of radiometers or polarimeters for modest cost. Modules based on IC-style packaging with waveguide inputs provide fully functional pseudo correlation polarimeters capable of detecting Q and U simultaneously. The feeds themselves are corrugated horns built up from stacked platelets, each with an array of holes, defining one groove in each feed.

The optical design of the array is critical to the ultimate systematic performance as a polarimeter. Structures with asymmetric cross-polarization patterns create instrumental polarization (IP), the partial polarization of an otherwise unpolarized signal. Since the polarized E-mode CMB signal is at least a factor of 10 smaller than the unpolarized intensity fluctuations, minimizing IP is a prime concern for QUIET.

Only corrugated feed structures have demonstrated cross-polarization symmetry at the -35dB level over the required bandwidth of 80 to 105 GHz at W-band and 38 to 46 GHz at Q-band. For this reason, corrugated feed horns with the closest spacing allowable given the module size were chosen. The resulting outer feed diameter of 1.4 inches yields a beam size of 8 degrees at 90 GHz. Similarly, the 40 GHz feed with an outer diameter of 3 inches also yields a beam size of 8 degrees.

For the 1 and 2-meter class telescopes, a side fed Cassegrainian design was selected because of its excellent cross-polarization and wide angle scan performance. For either the one or two-meter design, an extremely large and flat field of view is realized with an angular extent of 12 on the sky. The 1-meter design can accommodate 91 feeds at W-band and 37 feeds at Q-band. At W-band the beam size is 0.31 degrees and at Q-band the beam size is 0.69 degrees. A two-meter design can accommodate 400 feeds at W-band and 91 feeds at Q-band. In fact, a three meter scale of the one-meter design would be capable of 1000 feeds at W-band.

FIELD OF VIEW OF RADIO INTERFEROMETERS

Timbie, P.T.¹, Tucker, G.S.²¹Department of Physics, University of Wisconsin, Madison, WI 53706²Department of Physics, Brown University, Providence, RI 02906

We are studying the feasibility of measuring faint polarization signals in the 2.7 K Cosmic Microwave Background (CMB) radiation using a close-packed interferometer array. The use of an interferometer instead of an imaging system is motivated by the need to control systematic effects. A filled array is chosen to achieve the high sensitivity levels required for these measurements. Under the assumption that background-limited detectors are employed, the sensitivity of imaging and interferometer systems is determined by the total throughput ($A\Omega = n\lambda^2$) of the optical system. We are studying interferometers in which corrugated horn antennas view the sky directly. The field-of-view of the interferometer is determined by the beamwidth of the horn antennas and in principle can be very large (i.e greater than 7 degrees FWHM). A large field-of-view is important for making instantaneous maps of large sections of the sky without scanning. The optical throughput of the interferometer is determined then by the number of horns in the array. Of course, one must keep in mind that the diameter of the array (the longest baseline) constrains the maximum RF bandwidth of each spectral channel of the interferometer. As a demonstration, we are constructing an instrument called the Millimeter-wave Bolometric Interferometer (MBI) that will operate from the ground at 90 GHz. MBI is an adding interferometer: RF amplitudes from the horn antennas are combined in waveguide structures and the interference signals are measured using cooled bolometers as detectors. These efforts are part of a study of the Einstein Polarization Interferometer for Cosmology (EPIC), a mission concept study for NASA's Einstein Inflation Probe.

THE LARGE ADAPTIVE REFLECTOR, A WIDE-FIELD OPTICAL DESIGN FOR LARGE RADIO TELESCOPES

Dewdney, Peter E., Veidt, Bruce G., Gray, Andrew D.
National Research Council of Canada, Herzberg Institute of Astrophysics, Dom. Radio Astrophysical Observatory

The Large Adaptive Reflector (LAR) is an "optics" design for a radio-reflector telescope that mechanically decouples the two main components, a deformable reflector and a moveable, focal-plane antenna-array. This combination enables the construction of larger reflectors (diameter > 150 m) than possible with traditional designs, while maintaining a field-of-view similar to that possible only with much smaller reflectors. Since the concept could find applications at other wavelengths and in other situations, it is presented as generally as possible, while the application as the Large Adaptive Reflector is explained in more detail.

The LAR reflector is designed with a nominal 2.5 focal ratio (f/D), much larger than the 0.3-0.4 range, typical of traditional reflectors. The result is a nearly "flat" parabolic profile, which can be implemented as interconnected panels that form a "faceted" approximation to an offset parabolic surface. The panels are supported on vertical actuators that support the surface uniformly over the entire reflector area. The actuators, which permit deformation of the reflector, can change the position of the focal point in 3-D space. This simultaneously changes the offset and the focal length so that the telescope can effectively be pointed to any Azimuth and all Zenith Angles up to about 60° . This technique avoids the limitation of traditional, mechanically tilted, fixed focal-length reflectors, which concentrates the structural loads into a small area, making diameters much greater than 100 m impossible.

For a 200-m diameter reflector, the focal distance is about 500 m, a problem for mounting the focal apparatus, which must "follow" the pointing direction. Somewhat arbitrarily we have chosen a semi-hemispheric surface centered on the reflector as a focal-point trajectory-surface. We have selected a system involving a stabilized platform supported by an aerostat, from which a focal plane array (FPA) can illuminate the reflector.

Off-axis aberrations are small compared with those suffered by antennas with small focal ratios. The FPA is an adding interferometer array placed in the focal plane. The FPA uses simple, wide-band elements that can be spaced at $\sim \lambda/10$ at the lowest frequency in the band. This critical property permits full Nyquist sampling of the focal-plane fields over large bandwidths. By combining the weighted outputs of an array of simple elements in a beam-forming network, multiple adjustable feed patterns are available. This meets the fundamental need for an adjustable feed pattern to compensate for angular foreshortening of the reflector with Zenith Angle. It also decouples aperture size from the field-of-view by forming multiple beams. It is possible to "receive signal" from an area of sky that is limited only by off-axis aberrations.

CORRUGATED PLATELET FEED ARRAYS FOR MILLIMETER WAVE IMAGING

Wollack, E.J., Moseley, H.S.
NASA/GSFC

Millimeter and submillimeter wave imaging systems for radio astronomy and remote sensing require high efficiency coupling structures. The realization of such antenna elements in large focal plane arrays can potentially enable reductions in observing time and improvements in calibration accuracy while maintaining desirable imaging properties. Low-loss transitions from free-space to high performance sensors require a conversion in the impedance level, electromagnetic modal symmetry, and the detectors thermal environment, while achieving the desired image sampling and maintaining the radiometers angular, polarization, and frequency selectivity. The conical corrugated horn is a commonly used element due to its symmetrical (scalar) Gaussian beam, low-side lobe levels, and cross-polarization response. These properties are achieved over a large fractional bandwidth by transitioning from the dominant TE_{11} mode in circular waveguide with half-wavelength slots to quarter-wavelength slots in order to produce HE_{11} illumination at the aperture.

The conventional technique for manufacturing a corrugated feed in the high frequency limit is by precision electro-forming on a non-reusable machined mandrel which is subsequently removed by chemical etching. We investigate means of fabricating large arrays for these structures by sandwiching precision chemical-milled thin metal sheets which are then mechanically bonded. To explore the feasibility of this approach and the achievable tolerances, we have manufactured and characterized a pair of ~ 1000 element arrays with input guide cutoff and hybrid frequencies of 264 and 391 GHz respectively. Our alignment design rules are guided by the observation that tolerances relative to wavelength more critical than absolute placement for this class of adiabatic structures.

Post-fabrication mechanical and electrical survey of a subset of array elements indicates that this goal was maintained across this ~ 1 mm waveband array. The match for feed elements was observed to be better than 20dB with a vector network analyzer outfitted with millimeter wave heads. The measured co- and cross-polar response for elements are uniform and in agreement with the theoretical performance computed from the feed geometry (E and H-planes FWHM are 28.4 and 28.0 degrees respectively). To explore the potential influences of the various bonding processes on the transmission efficiency, diffusion welded and thin film epoxy laminate platelet waveguide samples in WR28.0, WR10.0 and WR5.1 were fabricated, characterized and sectioned. The observed loss was observed to be within a factor of two of the theoretical estimate computed from the bulk metal resistivity. We conclude that it is feasible to realize arrays with this construction up to ~ 1 THz.

HIGH DIRECTIVITY PLANAR SLOT ANTENNA ARRAYS
FOR MILLIMETER AND SUB-MILLIMETER IMAGINGA. Vayonakis¹, A. Goldin¹, JJ. Bock²
, HG. Leduc², J. Zmuidzinas¹¹Caltech²JPL

We are developing a new family of planar antennas which are of great interest for use in future millimeter and submillimeter direct-detection focal-plane architectures, such as CMB polarimetry using antenna-coupled bolometer arrays. Such architecture promises a lot of advantages compared to existing systems. Compared to bolometers with extended area radiation absorbers, antenna-coupled bolometers provide greatly reduced thermally active area, allowing for gains in sensitivity and response speed. Furthermore, the large sub-K feedhorn optics currently required by missions such as Herschel and Planck which comprise more than 95% of the sub-K focal plane mass and volume, would be eliminated. Such highly integrated architectures would allow for a very large number of pixels.

Each antenna consists of an array of N long slot antennas which are fed along their length at M points. The resulting $N \times M$ feed points are combined using a binary summing tree made of low-loss superconducting microstrip lines. The amplitude and phase of the electric field at each element of the array control the pointing and far-field beam pattern. By passively adding the electric fields of each antenna in a phase-coherent manner, we can synthesize the diffraction-limited beam. Due to its large size, the resulting array antenna produces a narrow beam pattern, around 15 degrees FWHM for the device demonstrated here, and can therefore be used without additional coupling elements such as hyperhemispherical lenses or feedhorns. The radiation and impedance characteristics of the antenna were obtained from a moment method calculation. We have measured the beam pattern of a singlepixel 110 GHz device coupled to an SIS detector, and find good agreement with the calculated response.

Session J2, 13:15 – Wed.

**NEW DEVELOPMENTS IN
BOLOMETERS FOR RADIO
ASTRONOMY**

Chair: J. Zmuidzinas

APEX-SZ: EXPERIMENTAL DESIGN AND INSTRUMENT STATUS

Halverson, N. W.¹, for the APEX-SZ collaboration¹²³

¹University of California, Berkeley

²Lawrence Berkeley National Laboratory

³Max Planck Institute for Radio Astronomy

The APEX-SZ experiment is a survey instrument designed to conduct a mass-limited survey of galaxy clusters via the Sunyaev-Zel'dovich effect at millimeter wavelengths. The instrument consists of a 320 element Transition Edge Sensor (TES) bolometer array camera operating initially at 2 mm wavelength. It will be deployed on the Atacama pathfinder experiment (APEX) telescope, a 12-m submm telescope currently undergoing commissioning tests on the Atacama plateau in Chile. The APEX-SZ survey instrument is scheduled to see first light in early 2005. In roughly five months of observation spread over several years, we will be able to image 100–200 square degrees of sky to $\sim 10\mu\text{K}$ with one arcminute resolution.

The survey will achieve this unprecedented sensitivity by utilizing the full 0.38 degree diameter field of view of APEX telescope. The tertiary optics for the APEX-SZ system have been designed to couple the large throughput to a small 13-cm diameter focal plane. The APEX-SZ focal plane detectors are Si_3N_4 spiderweb TES bolometers with backshort reflectors, monolithically fabricated in six pie-shaped wedges, and optically coupled via an array of conical horn feeds. The focal plane will be cooled to an operating temperature of 250 mK with a mechanical pulse tube cooler coupled with a three stage $^4\text{He}/^3\text{He}/^3\text{He}$ sorption refrigerator. We are also developing a shunt feedback SQUID amplifier to read out the voltage-biased bolometers. The bolometers are AC biased at frequencies up to several hundred kHz, well above the frequency of dewar microphonics. APEX-SZ will use individual readouts for every bolometer, although the hardware is upgradeable to the frequency domain multiplexing currently under development at Berkeley.

Both experimental design and instrument status will be discussed.

SCUBA-2 TES ARRAYS

Duncan, W. D.¹, Hilton, G.¹, Irwin, K.¹
 , Reintsema, C. J.¹, Vale, L.¹, Ullom, J.¹
 , Xu, Y.¹, Holland, W. S.², Audley, M. D.²
 , MacIntosh, M.², Gostick, D.², MacGregor, H.²
 , Ade, P. A. R.⁴, Bintley, D.⁴, Gannaway, F.⁴
 , Hunt, C.⁴, Sudiwalla, R.⁴, Woodcraft, A.⁴

¹NIST, 325 Broadway, Boulder, CO 80305 USA

²UKATC, Royal Observatory, Blackford Hill, Edinburgh, EH9 3HJ, UK

³SMC, University of Edinburgh, The Kings Buildings, West Mains Road, , Edinburgh EH9 3JF, UK

⁴Cardiff University, Department of Physics and Astronomy, P. O. Box 913, Cardiff CF24 3YB, UK

We describe the fabrication and performance of the 40 by 32 pixel SCUBA-2 prototype. SCUBA-2 is expected to use 8 of the two-side buttable arrays, with 4 being operated at 450 microns and the remainder at 850 microns. At these wavelengths the SCUBA-2 instrument will increase the mapping speed of the James Clerk Maxwell Telescope in Hawaii by factors of several hundred.

The dilution refrigerator test facility at Cardiff University has been used to measure the first SCUBA-2 prototype array using multiplexer electronics supplied by NIST. The array has been deployed in the focal plane assembly and uses the cold electronics and wiring expected to be used in the SCUBA-2 instrument.

We report the performance of the focal plane engineering; in particular the thermal isolation results and the temperature of the multiplexer and array versus the power dissipated in the focal plane. We also report the test results from measuring the NEP, response speed, and intrinsic and optical responsivity of the large portions of the array. The intrinsic and optical responsivity are used to estimate the pixel absorption efficiency. We also estimate nearest neighbour and distant pixel electrical cross talk. The performance of the multiplexer and the day to day reproducibility of the SQUID tuning and array biasing are presented. The optical responsivity is compared with models of the expected optical absorption efficiency.

We compare the results with the need for the science grade arrays for SCUBA-2 and compare the operational needs of the instrument with the experience of operating the prototype. The impact of the measurements on the fabrication of the science grade arrays is also outlined.

A FULLY-SAMPLED PLANAR SUPERCONDUCTING BOLOMETER ARRAY FOR THE GREEN BANK TELESCOPE

Dominic J. Benford¹, Simon R. Dicker², Mark J. Devlin², Mark P. Supanich², James A. Chervenak¹, Tina C. Chen¹, Johannes G. Staguhn¹, S. Harvey Moseley¹, Edward J. Wollack¹, Kent D. Irwin³

¹Infrared Astrophysics Branch, NASA / GSFC, Greenbelt, MD 20771 USA

²Department of Physics Astronomy, University of Pennsylvania, Philadelphia, PA 19104 USA

³Electromagnetic Technology Division, NIST-Boulder, Boulder, CO 80305 USA

We describe a close-packed, two-dimensional imaging detector system for operation at 90 GHz (3.3 mm) for the 100 m Green Bank Telescope (GBT), being built by the University of Pennsylvania, NASA/GSFC, and NRAO. This system will provide high sensitivity ($\sim 500 \mu\text{Jy}$ in 1s) rapid imaging ($15' \times 15'$ to $250 \mu\text{Jy}$ in 1 hr) at the world's largest steerable telescope. The heart of this camera is an 8×8 close-packed, Nyquist-sampled array of superconducting transition edge sensor (TES) bolometers. We have designed and are producing a functional superconducting bolometer array system using a monolithic planar architecture and high-speed multiplexed readout electronics. With an NEP of $\sim 2 \times 10^{-17} \text{ W}/\sqrt{\text{Hz}}$, the TES bolometers will provide fast, linear, sensitive response for high performance imaging. The detectors are read out by an 8×8 time domain SQUID multiplexer, including dark SQUID channels for drift signal reduction. A digital/analog electronics system has been designed to enable high speed control and readout of the SQUID multiplexer. The detector and first stages of SQUID amplification are cooled to $\sim 300 \text{ mK}$ by means of a compact $^3\text{He}/^4\text{He}$ two-stage sorption refrigerator coupled to a pulse tube cooler, for a cryogen-free cooling system. The cryogenic system has been demonstrated to be robust, and is capable of cycling autonomously, providing $15 \mu\text{W}$ of cooling below 286 mK with a hold time over 70 h. Although modest in size, a combination of the collecting area of the GBT and the low noise of the TES detectors will make this receiver one of the most sensitive of its kind. First light for this instrument on the GBT is expected in the coming winter.

ATMOSPHERIC NOISE REMOVAL FOR BOLOCAM

Sayers, J.¹, Ade, P.A.R.², Aguirre, J.E.³
 , Bock, J.J.¹⁴, Edgington, S.F.¹, Glenn, J.³
 , Goldin, A.⁴, Golwala, S.R.¹, Haig, D.²
 , Lange, A.E.¹, Laurent, G.T.³, Maloney, P.R.³
 , Mauskopf, P.D.², Nguyen, H.⁴, Rossinot, P.¹ , Stover, P.³
¹California Institute of Technology, Pasadena, CA 91125
²Physics and Astronomy, Cardiff University, 5 The Parade, P.O.
 Box 913, Cardiff CF24 3YB, Wales, UK
³University of Colorado, 389-UCB, Boulder, CO 80309
⁴Jet Propulsion Laboratory, 4800 Oak Grove Dr, Pasadena, CA
 91109

Bolocam is a millimeter-wave (1.1 and 2.1 mm) camera with an array of 115 working bolometers. The instrument has been commissioned at the Caltech Submillimeter Observatory in Hawaii, and is now in routine operation. Mapping blank fields ($\approx 1 \text{ deg}^2$) is the primary use of Bolocam, but it has also been utilized to observe galactic objects. Atmospheric emission from water vapor is the dominant source of noise in Bolocam data, producing a signal 1-2 orders of magnitude larger than the irreducible photon and detector noise.

The beams of individual bolometers coincide at the primary mirror of the telescope, and overlap through the majority of the atmosphere; so most of the sky noise is common to all bolometers. Removal of this common mode signal can then be accomplished by subtracting the average bolometer signal from each bolometer's data. Alternatively, a more advanced common mode subtraction algorithm, Principal Component Analysis (PCA), can be used to subtract the sky noise (see e.g. R. C. Gonzalez, R. E. Woods, *Digital Image Processing*, Addison Wesley, US, 1992). It should be noted that the sky noise remaining in the data after either common mode subtraction is still comparable to the photon and detector noise, even in the best weather.

Attempts are now being made to use the atmospheric model described by Lay and Halverson (*The Astrophysical Journal*, **543**, 787, 2000) to remove more sky noise from the Bolocam data. This model assumes that all temporal fluctuations in the atmosphere are due to wind. This assumption, along with the slight separation of the bolocam beams, means that the sky signal seen in any given bolometer will be seen in other bolometers, but at different times (t_i). Determining the t_i , which depend on the wind vector and geometry of the beams, will allow the common mode subtraction to remove more sky noise.

Additionally, we now have access to data from the phase monitor near the James Clerk Maxwell Telescope. This phase monitor measures the difference in water vapor for two columns through the atmosphere, separated by 100 m. Correlations between Bolocam data and the phase monitor data will help us determine some of the spatial characteristics of the atmosphere.

ESTIMATOR BASED ITERATIVE DATA REDUCTION FOR
LARGE FORMAT SUBMILLIMETER ARRAYS - THE VIEW
OF THE WORLD THROUGH SHARC-2

Kovacs, A, Dowell, C.D., Phillips, T.G.
CalTech MC 320-47, Pasadena, CA 91125

The arrival of a new generation of large format bolometer detector arrays in submillimeter astronomy has brought with it new possibilities as well as new challenges in the field of data reduction. A key aspect of successful data reduction at submillimeter wavelengths is the proper rejection of the rapidly varying and bright atmospheric emission that often dwarfs the typical astronomical signal by several orders of magnitude in power. The large number of pixels, now available in new instruments like SHARC-2, all simultaneously collecting information on the atmospheric background, enable novel approaches of sky subtraction without the traditional differencing via position-switch or chop, thus promising to overcome a range of problems associated with chopped images.

The elimination of differencing, however, makes one more exposed to other sources of slowly varying signals in the data stream, such as instrumental drifts, and require instrumental stability on longer time-scales, lower 1/f detector noise properties, as well as a more in-depth understanding of the instrument itself. However, the experience of SHARC-2 has demonstrated that the right combination of carefully chosen observing modes together with an iterative data reduction approach, modeling all relevant signals via a series of maximum-likelihood estimators, can achieve images with unprecedented clarity and fidelity.

While its relative simplicity cannot match singular value decomposition (SVD) algorithms in rigour, the estimator based approach can readily deal with model non-linearities, like those arising from internal detector gain fitting, while the sequential solving of the various models provides more intuitive insight into the workings of the data reduction and allows for easier fine tuning for any particular data set. Meanwhile, the processing time requirement of an estimator based reduction algorithm is relatively modest and is expected to scale linearly with the size of the incoming data stream, making it an attractive choice for future instruments boasting ever larger pixel counts and/or increased sampling rates.

NOISE PERFORMANCE OF TES BOLOMETERS FOR FAR
INFRARED ASTRONOMYStaguhn, J.G., Benford, D.J., Moseley, S.H.

, Allen, C.A., Chervenak, J.A., Stevenson, T.R. , Hsieh, W.-T.

NASA/GSFC, Greenbelt, MD 20771, USA

The development of large format (> 1000 elements) cryogenic bolometer arrays is a requirement for future astronomical imaging and low resolution spectroscopy in the far-infrared and submillimeter. Recent research has led to a new approach to building arrays of many bolometers. Instead of a semiconducting thermistor, a superconducting transition edge sensor (TES) is used to read out the detector temperature. A TES bolometer has a faster response time than an identically-designed, same-sensitivity semiconducting bolometer (or a more sensitive bolometer for the same response time) due to the strong negative electrothermal feedback intrinsic in a voltage-biased TES. TES bolometers are inherently low impedance devices, so they are well matched to being read out by DC SQUID amplifiers. These amplifiers have a large noise margin over the TES Johnson noise and bolometer phonon noise. This permits the bolometer to be read out in a multiplexed fashion by a suitable SQUID multiplexer, potentially vastly reducing the amplifier size and the wire count. In light of these advantages, we have been developing the technologies for fabricating multiplexed superconducting TES bolometer arrays. Recently we have investigated the noise performance of Mo/Au-bilayer TES bolometers. These detectors use normal metal regions for the suppression of excess noise. These regions can be oriented either parallel to ("bars") or transverse to ("stripes") the direction of current flow. Detectors with stripes and/or with bars were fabricated at the NASA/GSFC detector development facility. The lowest noise detectors are found to have normal metal regions oriented transversely. We compare the noise measurement and quantitative analysis of the noise level in each device as a function of the detector parameters with focus on the properties of the most recently produced devices, which we have successfully used for astronomical observations in the submillimeter broadband spectrometer FIBRE at the Caltech Submillimeter Observatory.

SQUID-
 BASED FREQUENCY-DOMAIN MULTIPLEXED READOUT
 FOR TRANSITION-EDGE SENSOR ARRAYS

Hsiao-Mei Cho¹, John Clarke^{1,2}, Matt. A. Dobbs³
 , Trevor M. Lanting¹, Adrian T. Lee^{1,3}, Martin Lueker¹
 , P. L. Richards^{1,3,4}, H. G. Spieler³, A. Smith⁵

¹Physics Department, University of California, Berkeley, CA 94720

²Materials Sciences Division, Lawrence Berkeley Laboratory, Berkeley, CA 94720

³Physics Division, Lawrence Berkeley Laboratory, Berkeley, CA 94720

⁴Space Sciences Laboratory, University of California, Berkeley, CA 94720

⁵TRW-Northrup Grumman, One Space Park, Redondo Beach, CA 90278

The new generation of Cosmic Microwave Background Radiation observations requires large-format superconducting transition edge (TES) sensor arrays to increase their sensitivity. This approach has been made possible by the development of microfabrication techniques for the production of arrays of a thousand or more sensors. However, readout of these large-scale arrays remains a major instrumental challenge. We address this challenge using frequency-domain multiplexing of signals from an array of TES sensors. Our present readout system involves an 8-detector module. Each TES sensor is connected in series with an LC tuned circuit and biased with an alternating current at a selected frequency, ranging from 380 kHz to 1 MHz. The signal from each sensor amplitude-modulates its respective bias current. The implementation of the LC filter on each channel largely reduces the Johnson noise generated in the remaining sensors. The signals are combined at a current summing node and measured with a single superconducting quantum interference device (SQUID) array. The 100-SQUID array is operated with custom, directly-coupled electronics, the output of which is fed back to the summing point as a current to null the signals from the sensors. The measured slew rate is $1.2 \times 10^7 \Phi_0/\text{sec}$ at 1MHz. The resulting output voltage produced by each sensor is lock-in detected and encoded as a digital signal. Previously, we showed the characteristic of a TES with alternating current bias, and demonstrated a two-channel multiplexer. In this talk, we present the sensor noise of our 8-channel multiplexed system. Demodulated noise spectra show white noise down to 100 mHz. In addition, we report the crosstalk measurement on adjacent channels.

ANTENNA-COUPLED BOLOMETER ARRAYS USING TRANSITION-EDGE SENSORS

Michael J. Myers¹, Peter Ade², Greg Engargiola³
, William Holzapfel¹, Adrian T. Lee¹, Roger O'Brient¹
, P. L. Richards¹, Andy Smith⁴, Helmuth Spieler⁵
, Huan T. Tran¹

¹Department of Physics, University of California, Berkeley, California, 94720

²School of Physics and Astronomy, Cardiff University, Cardiff, Wales, UK

³Department of Astronomy, University of California, Berkeley, California, 94720

⁴Northrop Grumman, Redondo Beach, California, 90278

⁵Lawrence Berkeley National Laboratory, Berkeley, California, 94720

Bolometers are the most sensitive photometric detectors of millimeter wavelength light. Absorber-coupled bolometers have been used successfully in several cosmological applications, including the characterization of the Cosmic Microwave Background (CMB) and galaxy cluster surveys. Antenna-coupled bolometers use an integral planar antenna to couple radiation into a planar transmission line, which is then terminated in a load resistor. This approach has several advantages for large bolometer array construction. The antenna defines the beam, removing the need for bulky and expensive feed horns. Filters can be integrated into the transmission line and signals from a broadband antenna can be split into several bands. This would allow multicolor pixels on a single chip without the conventional off-chip quasioptical elements. As bolometer arrays approach the size limits set by millimeter wave telescope design, multicolor pixels will become increasingly important to fully use the available focal plane space. The inherent polarization sensitivity of a planar antenna is also advantageous when polarization information is useful.

We have developed an antenna-coupled bolometer for use in a CMB polarization experiment. Our design uses a double-slot dipole antenna which feeds superconducting niobium microstrip. Microstrip filters are used to define the frequency band to which the bolometer is sensitive. The microstrip is then terminated with a load resistor and the dissipated power is measured with a superconducting Transition Edge Sensor (TES). The load resistor and TES are in good thermal contact on a silicon nitride substrate. The substrate is leg isolated to achieve the required sensitivity. We will present results from electrical and optical testing of antenna-coupled bolometer prototype pixels with and without microstrip filters. We will also discuss progress in the design and construction of a bolometer array based on the single pixels.

TES ANTENNA COUPLED POLARIMETER

Kuo, C.-L.^{1,2}, Bock, J.J.^{1,2}, Day, P.¹
, Goldin, A.^{1,2}, Gowala, S.², Kenyon, M.¹
, Lange, A.E.², Le Duc, H.G.¹, Rossinot, P.²
, Vayonakis, A.², Yun, M.¹, Zmuidzinas, J.^{1,2}

¹Jet Propulsion Laboratory

²California Institute of Technology

We describe the design of an antenna coupled bolometer array operating at 150 GHz optimized for the measurements of the Cosmic Microwave Background polarization. The array consists of 8×8 pixels, with 4 TES bolometers per pixel. At each pixel, the Mm-wave radiation is detected by the 16×16 planar dipole array, added up coherently with a series of binary summing trees to form a $2f\lambda$ beam, and sent to 4 TES bolometers through superconducting microstrips. The other key components between the antenna and the TES are a band-defining lumped-element filter, a microstrip 180° hybrid, and a polarization switch that uses SIS junctions. The difference between the first bolometer pair gives the Stokes Q parameter, and the difference between the second pair gives the Stokes U parameter. The modulation can be done at a frequency up to a few Hz with the SIS switch to avoid $1/f$ noise. The entire focal plane array can be fabricated on a 4 inch silicon wafer using photolithographic techniques. It can be scaled up easily by joining sub-arrays. We have fabricated several test devices to assess the performance of various components in the system. The Molybdenum-Gold bi-layers bolometers are shown to have stable T_c and appropriate resistance for SQUID multiplexers (MUX). We demonstrated the read-out of an 8 element Mo/Au bolometer array with the MUX system developed by the NIST group, and showed that the read-out noise is not significant. The angular response of the phase array is measured with SIS junctions and found to be consistent with the theoretical calculations. We also present the latest progress in the testing of the filter, the switch, and the 180° hybrid.

MEASUREMENT AND EVALUATION OF SOME CANDIDATE SUPERCONDUCTING DETECTOR TECHNOLOGIES FOR ASTRONOMICAL IMAGING AND SPECTROSCOPY

Day P.K.¹, Leduc H.G.¹, Mazin B.A.², Zmuidzinas J.²¹Jet Propulsion Laboratory, 4800 Oak Grove Dr., Pasadena, CA²California Institute of Technology, 1200 E. California Blvd., Pasadena CA

Several types of superconducting detectors are presently being considered for application in astronomical instruments. The microwave kinetic inductance detector (MKID) is a relatively new detector technology that provides a possible path to the large arrays that are needed for cameras, because of a straightforward approach to array readout. These detectors are based on planar high Q superconducting resonators which allows for multiplexing in the frequency domain at microwave frequencies. Measurements have been made which identify the limiting noise source of the MKID and which elucidate the sensitivity degradation under input power loading. Progress has been made toward reducing the noise of these detectors to the photon noise limit. Transition edge sensor bolometers, isolated with suspended silicon nitride structures, have demonstrated adequate sensitivity for background limited imaging at millimeter through FIR wavelengths and are compatible with SQUID multiplexing techniques. For space-borne medium resolution spectroscopy where the photon background is greatly reduced, NEP on the order of $2 \times 10^{-20} \text{W}/\text{Hz}^{1/2}$ is needed. To achieve that sensitivity, the thermal conductance of the supporting silicon nitride beams must be decreased by a factor of 100 - 1000 as compared with the current state-of-the-art devices. The description energy transport through such structures is falls well within the quantum regime, with only the lowest few vibrational modes contributing to the conductance. Measurements demonstrating the crossover to quasi-1D thermal transport in silicon nitride beams will be presented. Antenna coupled hot electron bolometers are an alternative technology for both imaging and spectroscopy in the submillimeter and FIR. New data on the achievable electron-phonon thermal conductance and possible detector designs will be discussed.

NORMAL-INSULATOR-SUPERCONDUCTOR JUNCTIONS
WITH MICROWAVE READOUT FOR LARGE ARRAYS OF
ULTRALOW NEP BOLOMETERS

J. N. Ullom¹, D. Schmidt², A. M. Clark³
, W. D. Duncan¹, K. D. Irwin¹, N. Miller¹
, G. Chattopadhyay⁴, K. Lehnert²

¹NIST, 325 Broadway, Boulder CO, 80305

²JILA, NIST, and Department of Physics, University of Colorado,
Boulder CO, 80309

³Ball Aerospace, Boulder CO, 80301, formerly at NIST

⁴California Institute of Technology, Jet Propulsion Laboratory,
Pasadena CA, 91125

We are developing antenna-coupled hot-electron bolometers based on normal-insulator-superconductor (NIS) tunnel junctions. These junctions make electrical contact to a small normal metal island while preserving its thermal isolation. Their current-voltage curves are used to monitor the response of the island temperature to incident power. We have recently measured a NET of $0.6 \mu\text{K}/\text{rt Hz}$ at 270 mK in a prototype device with a normal volume of $4.5 \mu\text{m}^3$ and infer an NEP of $7 \cdot 10^{-17} \text{ W}/\text{rt Hz}$. Our devices incorporate two recent advances: 1) improved designs for NIS structures in which the application of a bias refrigerates the normal metal, thus providing lower effective operating temperatures and increased resistance to saturation, and 2) microwave readout in which the device is imbedded in an impedance transforming resonant circuit that reflects a microwave drive signal into a HEMT amplifier. This readout technique is compatible with multiplexing tens to hundreds of sensors per HEMT. It is also compatible with high bandwidth measurements such as far-infrared photon counting. To achieve lower NEPs, we are now building devices with smaller volumes, lower operating temperatures, and integrated heaters for exact power calibration. The anticipated limits on NEP and array size will be discussed. Since our sensing elements are made with a robust, wafer-scale photolithographic process, large arrays are straightforward to fabricate. Electromagnetic simulations indicate that it is possible to integrate these bolometers into dual slot antenna structures with high coupling efficiencies near 1 THz. These devices will be suitable for a number of applications in far-infrared and submillimeter astronomy.

SMALL SILICON THERMISTORS AS HOT-ELECTRON BOLOMETERS

Stevenson, T. R.¹, Cao, N. T.¹⁵, Henry, R. M.²
 , Hsieh, W.-T.¹⁴, Isenberg, H. D.¹, Mitchell, R. R.¹
 , Moseley, S. H.³, Schneider, G.¹⁴, Stahle, C. M.¹
 , Travers, D. E.¹⁴, Wollack, E. J.³

¹NASA Goddard Space Flight Center, Detector Systems Branch,
 Code 553, Greenbelt, Maryland, USA 20771

²NASA Goddard Space Flight Center, Optics Branch, Code 551,
 Greenbelt, Maryland, USA 20771

³NASA Goddard Space Flight Center, Infrared Astrophysics
 Branch, Code 685, Greenbelt, Maryland, USA 20771

⁴Raytheon ITSS, Upper Marlboro, Maryland, USA 20774

⁵Ball Aerospace Technologies Corp., P. O. Box 1062, Boulder,
 Colorado, USA 80306

We discuss a new type of direct detector, a silicon hot-electron bolometer, for measurements in the far-infrared and submillimeter spectral ranges. Semiconductors with partially compensated doping levels just below a metal-insulator transition can make highly sensitive thermistors at sub-kelvin temperatures. Silicon thermistors have been used successfully as the thermometer element in x-ray microcalorimeters and FIR bolometer arrays. In such arrays, the weak thermal conductance is engineered by supporting the radiation absorber and thermometer on a thin membrane or bridge. However, the electron-phonon thermal conductance in doped silicon can be made the dominant thermal isolation from the cryogenic bath, potentially allowing a smaller thermal conductance and a more sensitive bolometer for low-background photometric and spectroscopic applications. Another key feature is that, while the dc resistance of a silicon thermistor film is very high, its surface impedance at terahertz frequencies is conveniently low, making feasible efficient antenna coupling of radiation into the hot electron system. The temperature independent high dielectric constant predicted by theory is observed by us directly in fourier transform spectrometer measurements, and its frequency dependent loss fits a relaxation time model with physically reasonable parameters. To test for deviations from simple scaling of the electron-phonon conductance with volume, we made small silicon thermistors with linear dimensions 1-10 μm approaching the typical variable range hopping distance responsible for electrical conduction at temperatures of order 100 mK. While deviations were observed, a hot-electron model still works well with a conductance that is only a few percent of typical values for ordinary metals. In a 10 $\mu\text{m} \times 10 \mu\text{m} \times 1.4 \mu\text{m}$ device, we measured a thermal conductance as small as 0.4 pW/K at 100 mK (still decreasing with temperature), which corresponds to a thermal fluctuation limited Noise Equivalent Power (NEP) of $5 \times 10^{-19} \text{ W}/\text{Hz}^{0.5}$.

Session J3, 12:55 – Thurs.

**MIRROR FABRICATION,
ALIGNMENTS AND METROLOGY
FOR RADIO TELESCOPES**

Chair: S. Padin

NEAR-FIELD HOLOGRAPHY TECHNIQUES FOR LARGE RADIO ANTENNAS

Tirupati K SridharanHarvard-Smithsonian Center for Astrophysics, 60 garden Street,
Cambridge, MA 02138, USA

The ever increasing operating frequencies of radio antennas have approached the Tera Hertz bands, placing stringent demands on antenna performance and characterization. Near-field radio holography is the method of choice for characterizing the optics of large millimeter/sub-millimeter/THz wavelength antennas. In this presentation, near-field techniques to measure and align the components of such antenna systems will be reviewed. In particular, studying and setting the figures of the primary reflectors of sub-millimeter wavelength antennas will be discussed. Experience with the antennas of the 8 element Submillimeter Array, some of which have been set to an rms surface accuracy of 12 micron, will be used to illustrate the techniques. High signal to noise ratios are easily achieved in near-field measurements leading to maps of the aperture phase at high spatial resolution. This allows measurement and correction of flexures of individual panels of primary reflectors. The aperture amplitude maps measure the illumination achieved and can be used to validate the feed and beam wave-guide systems often used. The main limitation of the technique is the low elevations typical of such measurements. It is necessary have a good understanding of the gravitational deformation of the antennas in order to achieve good performance at operational elevations. Holographic measurements on astronomical sources can provide the complimentary information needed in addition to models of the deformations. Astronomical measurements typically have poorer signal to noise due the weakness of the radiation sources and high spatial resolutions are difficult to achieve. However, gravitational deformations occur on large spatial scales. Therefore, a combination of near-field and astronomical holographic measurements can completely characterize the primary reflector of an antenna system. Near-field techniques are also being used to align components of beam-waveguide systems and the current status of such measurements will also be discussed.

USE OF PHOTOGRAMMETRY AT THE ATA

DeBoer, D.R.¹, Fleming, M.C.²

¹SETI Institute, 515 N. Whisman, Mountain View, CA 94043

²Radio Astronomy Laboratory, University of California, Berkeley, CA 94720

For rigged and outfitted antennas, photogrammetry is a good complementary tool to microwave holography measurements to determine the figure of the optics. However, in developing the process to mass produce antennas (for example the tool used to hydroform dishes) holography is not an option and photogrammetry is the preferred technique over other surveying methods. At the Allen Telescope Array, we have used photogrammetry in both ways. Our photogrammetric system uses a specially modified Nikon D1 digital camera and proprietary software from Geodetic Services Inc. (Melbourne, FL) along with reference-length bars (scale bars), a reference-origin bar (autobar) and retro-reflective dots. Our own software then analyzes the photogrammetric output data to determine the topological profile of the dish and aggregate surface roughness. These data are then used to provide feedback to the tuning of the hydroforming tool, done at Andersen Manufacturing (Idaho Falls, ID), as well as to verify the rigging of our offset Gregorian optical system.

The data are acquired by taking many (on the order of 40) pictures of the antenna from a variety of positions and orientation. The software then iteratively solves for the position of the retro-reflective dots, as well as the position and orientation of the camera for each picture. An arbitrary number of dots may be placed (we typically have between 200 and 400, depending on the specific goal). The centroid of each dot is located in three dimensions to an accuracy to about 1 part in 80,000 over the field of view of the pictures, which equates to an absolute accuracy of about 50 microns for our application. Results from the Allen Telescope Array will be presented.

A MECHANICAL ALIGNMENT METHODOLOGY FOR SUBMILLIMETER-WAVE OPTICS

Stark, A. A.

Harvard-Smithsonian Center for Astrophysics, 60 Garden St.
MS12;, Cambridge, MA 02138

Millimeter- and submillimeter-wave detector systems often contain many optical elements which must be accurately aligned to function correctly. For the AST/RO project (A. A. Stark et al., *PASP*, **113**, 567), an alignment method was developed which worked well and has potential application to other systems where the optical elements are separated by distances of no more than a few meters.

AST/RO is a 1.7-m diameter offset Gregorian. Both the primary and secondary mirrors were fabricated with four polished and hardened steel reference balls, 5 mm diameter, mounted with roughly equal spacing around the edge of each mirror, several centimeters outside the active optical surface. The positions of the balls with respect to the mirror surface were measured together with the mirror surface during post-fabrication verification. The positions of the centers of the balls are therefore accurately known with respect to the best-fit curve for each mirror surface. Consider each pair of balls consisting of one ball on the primary and one ball on the secondary; there are 16 such pairs. For each pair, there is a well-determined minimum distance between the surfaces of the two balls. From the optical design and the shop measurements, it is possible to calculate what these distances would be if the two mirrors were accurately aligned. The mirrors are placed on their mounts in rough alignment. A large inside micrometer is then used to measure the actual separation between each pair of balls. Inside micrometers capable of measuring with a precision of $10\ \mu\text{m}$ over distances of a few meters are commercially available. These values are input to a computer program which solves for the current position of the two mirrors and calculates the adjustment to their mounts needed to bring them into alignment. Usually, one mirror is left fixed (from some prior alignment) and the other is moved in order to improve the alignment. The program uses a nonlinear least-squares method to fit for the 3 rotations and 3 translations of the non-fixed mirror which connect its current position to its aligned position. These 6 motions are overdetermined by the 16 measurements, allowing an estimate of the errors. Not all 16 measurements are needed; any subset of 6 or more will determine a solution. The cycle of measurement and adjustment is iterated, until all measurements are correct within the measurement errors. In practice, this method has proven very robust. Only 3 or 4 iterations are needed. The geometric model of the mirror mounts can be crude—it is enough to be able to calculate the direction and approximate magnitude of each adjustment. On AST/RO, the residual rms errors after alignment are less than $200\ \mu\text{m}$.

FABRICATION, ALIGNMENT, AND MEASUREMENT OF THE SZA REFLECTOR SURFACE

Hennessy, R.M.^{1,2}, Woody, D.P.³, Forcier, J.⁴¹Department of Astronomy and Astrophysics,, University of Chicago, , Chicago, IL 60637²Kavli Institute for Cosmological Physics,, University of Chicago,, Chicago, IL 60637³Owens Valley Radio Observatory,, California Institute of Technology,, Pasadena, CA 91125⁴Forcier Machine Design, 123 Marshall Ave, Petaluma, CA 94952

We describe the techniques required to provide the eight telescopes of the Sunyaev Zeldovich Array (SZA) with a 3.5m reflecting surface capable of precision measurements of the Cosmic Microwave Background. The SZA operates at 1 cm and 3 mm wavelengths, with a planned expansion for 1 mm observations. The design goal is a surface accuracy of 25 microns. The surface consists of 27 panels machined from custom castings. The average RMS surface error for the machined panels is 8 microns. We describe the fabrication process and quality control measures. To preserve this high level of surface accuracy during telescope mounting, we implemented a series of leveling fixtures which permitted the alignment of panels to better than 2 arcseconds. By aligning each panel individually and then assuring that the continuity between adjacent panel heights is better than 25 micron, we infer a global surface roughness better than 50 micron. To ascertain the validity of this assumption, a rigorous assessment of the SZAs aperture and beam efficiencies will be performed using the holographic method. Observations at 1 cm wavelengths will be made during the 2004 winter using an astronomical source to probe the far-field radiation pattern and custom software to back-transform to the aperture electric field distribution. This technique will be used to produce amplitude and phase maps of the primary reflector surface. Amplitude maps will be used to optimize the alignment of the tertiary and subreflector surfaces. Phase maps will be used to fit a physical model of the 9 three-point mount and 18 four-point mount panels used on each telescope. Successive iterations of panel adjustments and the resultant phase maps will be used to produce primary mirrors with surface roughness better than 50 micron RMS. We discuss the unique challenges of the holographic technique for small-aperture, close-packed interferometric arrays.

A CRYOGENICALLY COOLED SECONDARY MIRROR FOR THE SOUTH POLE TELESCOPE

Joy, M. K.

National Space Science and Technology Center

An off axis ellipsoidal secondary mirror is being built for the *South Pole Telescope* (SPT), a large diameter (8 meter) telescope which will be used to perform deep, wide field astronomical survey observations at millimeter wavelengths. The telescope optics are of Gregorian design; to minimize spillover effects and noise the secondary mirror will be located at the exit pupil of the SPT optical system and the secondary will be cryogenically cooled to ~ 10 K, providing a highly effective cold stop. The ellipsoidal secondary is 1.02 by 1.05 meters in size, and the goal is to achieve a surface accuracy of ~ 10 microns RMS under cryogenic operating conditions.

A prototype SPT secondary mirror is being fabricated, and the following results will be discussed: (i) mirror fabrication techniques, including the use of indexing and alignment fixtures to permit fabrication of a large off axis ellipsoidal mirror on a standard CNC milling machine; (ii) metrology of a smaller scale optic, establishing that the desired $\sim 10\mu\text{m}$ RMS surface accuracy can be achieved on a size scale of 35 cm using a standard CNC milling machine; (iii) lightweighting of the mirror to reduce the thermal mass that must be cryogenically cooled; (iv) metrology of the prototype ellipsoidal mirror, obtained using a Zeiss coordinate measuring machine which has a measurement accuracy of $\sim 1\mu\text{m}$; and (v) stress relief methods to minimize the distortion of the mirror when it is cooled from room temperature to ~ 10 K.

TESTS OF THE EMISSIVITY AND SNOW ACCUMULATION
ON SOUTH POLE TELESCOPE (SPT) PRIMARY MIRROR
TEST PANELS

S. S. Meyer¹²³⁴, S. Hansen¹², C. Pryke¹²³
, J. Ruhl⁵, M. Runyan¹², M. Sharp²⁴

¹Department of Astronomy and Astrophysics, University of
Chicago, Chicago, IL 60637, USA

²Kavli Institute of Cosmological Physics, University of Chicago,
Chicago, IL 60637, USA

³Enrico Fermi Institute, University of Chicago, Chicago, IL 60637,
USA

⁴Department of Physics, University of Chicago, Chicago, ILO
60637, USA

⁵Department of Physics, Case Western Reserve University, Cleve-
land, OH 44106, USA

Test panels with a variety of surface treatments have been placed in a test setup at the South Pole Station to characterize the surfaces for use in the primary mirror of the South Pole Telescope (SPT). Tests carried out at the South Pole include power required to raise the panel temperature and observations of the effect of snow buildup and snow clearing with panel temperature and heating. The test panels are manufactured of milled aluminum, similar to the planned SPT panels and have various candidate mirror surface preparations. The tests show that heating requires on average about $55 \text{ W K}^{-1} \text{ m}^{-2}$ under average wind conditions. Photographs of the panels also show that heating the panels by 1K significantly reduces the accumulation of snow on the panels and speeds the clearing after a snow storm. For the SPT a waste heat input of 15 KW into the primary mirror will keep the primary clear except for intervals of a day or so after heavy snow accumulation conditions.

The test panels were exposed to the sun for part of the testing both before and after the 2004 austral winter. The temperature rise from solar heating depends on the surface treatment and is important for setting the panel gaps to prevent panel interference.

A second set of test panels with the same surface treatments have been tested in the lab to determine the mm and sub-mm emissivity of the surface treatments. The panel thermal emission is compared to that of a bare milled aluminum surface in 30% wide bands from 90 to 450 GHz.

ARRAY ANTENNA DESIGN CONCEPTS

Schultz, R.T.

Schultz Associates, 1214 Awalt Drive, Mountain View CA 94040

Radio astronomy arrays with very large numbers of antennas are being planned, and the development of advanced design concepts can achieve significant total cost savings for these programs. The new arrays have large surface areas, so new methods of manufacture and production-line type assembly must be considered. A blend of past antenna construction technology, creativity, and new technology is needed to provide the best possible telescope for the proposed science goals. Development costs are significantly diluted by the great quantity of antennas required. Key concepts for antennas for large arrays will be presented as follows:

SHELL REFLECTORS: Traditional large microwave reflectors (mirrors) have been made up of many panels. More cost effective designs result when the surface is a continuous shell that can significantly contribute to the structural integrity of the reflector. Both stretch formed and hydroformed reflectors provide a continuous structural shell.

ADVANCED CONCEPTS FOR REFLECTOR AND MOUNT GEOMETRY: New geometry materially reduces initial and operating cost. Traditional geometry is contrasted to advanced geometry. Placing the elevation axis near the reflective surface reduces axis wind torque. Such reduction reduces initial cost and operating expenses for the axis drives. Such placement is allowed by innovative "throated" reflector back structure designs. A short pedestal is allowed by axis eccentricities.

Progress in the development of these concepts for the S. K. A. program will be reported. Pictures of structural arrangements, results of structural stress and deflection analysis and resultant surface error, resonant frequency and pointing error will be reported. Manufacturing, shipping and alignment concepts for shell antennas will be discussed.

ACCURATE GAIN CALIBRATION OF LARGE ANTENNAS AT 86 GHz

Gibson, J.L., Welch, Wm. J., Forster, J.R.

Astronomy Department, University of California, Berkeley

The effective aperture of one of the BIMA (now CARMA) 6m mm-wave interferometer antenna elements has been measured at 86 GHz with an accuracy of about 10% aperture only a few square centimeters. It was possible to compare signals from these, which differ in power by 10^5 , with an accuracy of 1% as an element of the interferometer. The horn and the large antenna to be calibrated were alternated into the array and the visibility amplitudes compared. The correlator is able to measure a voltage ratio of 300 with the requisite accuracy. Interferometry eliminates traditional problems such as ground pickup in sidelobes since only correlated signals are recorded. With a 1 GHz bandwidth, the correlation length is small, and so inaccuracy due to multipath and reflection is greatly reduced. A bright celestial target (Venus) was used as the signal source. Antenna surface figure and pointing were stable to within the required tolerance. The gain-calibrated large antenna was then used in a single dish experiment to measure the flux of Venus and Jupiter at 86 GHz, also to an accuracy of about 1%

An ambient temperature receiver incorporating a waveguide transfer switch was used to alternate the signals from the reference horn and the large antenna. Since such switches are not available for higher frequencies, as for example most of the ALMA bands, it is desired to find a method that doesn't require them. Accordingly, a method to determine the source flux directly by means of an visibility amplitude closure relationship was tested and compared with our first method. No mechanical switches are required for this technique, although knowledge of atmospheric opacity is required continuously over a period of hours. Methods, difficulties, results will be presented.

LOWMASS MEMBRANE TELESCOPES

Mark Dragovan
Jet Propulsion Laboratory

Progress in observational astrophysics parallels the development of telescope technology and the associated instrumentation. The problem of constructing telescopes using polished metal mirrors has a long history tracing back to Gregory(1663), Newton(1672), and Cassegrain. The first successful mirrors with silver reflecting surfaces on a glass substrate were constructed in the late 1850's by von Steinheil and Foucault. Current state-of-the-art reflectors can trace their roots back to this technology.

The function of the substrate is to support the thin layer of high reflectivity material; the glass or metal substrate is formable into a shape that has useful optical properties. In current state-of-the-art telescopes the mass of the substrate is $10^3 - 10^6$ times the mass of the reflecting layer. Clearly, new perspectives on telescope systems are necessary to reduce the cost and mass of the primary element.

The technology described achieves a significant reduction in mass by minimizing the thickness of the substrate. The telescope systems described use reflectors whose three dimensional shapes and curvatures are formed by the elastic bending or plastic stretching of a membrane over an appropriate boundary. The membrane is deformed by this process, with the result that the surface assumes a shape that concentrates electromagnetic radiation. If the field of view needs to be larger than can be afforded by a single primary reflector, subsequent optics can correct the aberrations intrinsic to the primary. In either case, a diffraction limited system will result. By using suitable materials for the membrane and other structures, systems with very low areal mass density ($\sim 1\text{kg/m}^2$) that are scalable to large apertures (~ 10 to 20 meters) are constructable.

Almost all telescope systems are on-axis, where the secondary and tertiary optics obstruct the primary reflector. Scattering and diffraction of the incident electromagnetic radiation by the secondary optics and its support structure reduces the performance of the overall system. This is particularly problematic for observations of low-contrast objects, or in communications systems where cross-talk between nearby antennas is undesirable. The solution is to use an unobstructed, off-axis design. The systems described are naturally suited for off-axis construction.

A CSO SUBMILLIMETER ACTIVE OPTICS SYSTEM

Leong, M.M.

Caltech Submillimeter Observatory

Active surface correction of the Caltech Submillimeter Observatory (CSO) primary mirror has been accomplished. The Dish Surface Optimization System (DSOS) has been designed and built to operate at the CSO, on Mauna Kea, Hawaii. The telescope consists, in part, of an 84-hexagonal paneled 10.4-meter primary dish designed by Robert Leighton. The DSOS corrects the dish surface figure for imperfections and gravitational deformations, as the dish moves in elevation during observations. This improvement in the telescope's aperture efficiency aids observations at the shorter wavelengths, specifically in the 350- μm -wavelength range.

There are 99 steel rod standoffs that interface the dish panels to its backing structure. Each standoff is now fitted with a heating/cooling assembly. Applying a controlled potential to each of the 99 assemblies adjusts the surface of the dish. Heating elongates and cooling shortens the standoffs, providing the push or pull on the primary's panel surface. The needed correction for each standoff, for a given elevation, is determined from stored holography maps of the dish surface.

The CSO's telescope, before corrections, has an optimum aperture efficiency of 33% at 350 μm . With a correctly adjusted DSOS, the telescope could have an improved efficiency of up to 66%. This improvement of a factor of 2 is the predicted limit determined by individual panel imperfections and other errors not accessible to the DSOS.

From holography, the latest measured optimum surface accuracy of the telescope is about 13 μm RMS, with the DSOS on. The decrease from 25 μm RMS (without the DSOS) to 13 μm RMS, translates to an improvement in aperture efficiency from 33% to 62% at the 350- μm -wavelength range. Further system improvements have been performed since these measurements.

The DSOS has been in operation on the CSO since February 2003. Observers using the SHARCII (a 384 pixel submillimeter high angular resolution camera) and the 850 GHz heterodyne receiver, have been able to detect new weak and/or distant objects with the help of this active optics system.

POINTING AND FOCUSING THE GBT

Constantikes, K. T., Prestage, R. M., Balsler, D. S.
, Condon, J. J.
National Radio Astronomy Observatory

The Green Bank Telescope (GBT) is a offset-Gregorian design 100 meter aperture telescope with design goal of operation at 115GHz. Achieving the required pointing, focus, and efficiency for such a large instrument at these frequencies is a non-trivial task, made even more challenging by our desire to achieve these goals over most operating environments, e.g., all times of day. The Green Bank Precision Telescope Control System (PTCS) project has made significant improvement in GBT beyond the as-delivered performance. Improvements in hand include order-of-magnitude improvement in blind focus and pointing. Improvements to collimation and wavefront error are underway.

This presentation will address our interim approach to improving pointing and focus. We will present information on the instrumentation systems, algorithmic approaches, fundamental mechanisms causing degradations, modeling software, the operational software infrastructure, and performance statistics. Another presentation will outline our updated approach to a metrology system that will provide additional improvements using a more direct approach than the one discussed herein. We will spend little time reviewing the GBT design itself, so interested parties should visit our web site (www.gb.nrao.edu) to get an overview of the GBT.

The fundamental approach we have taken is semi-empirical: Known drivers of degradations (e.g., thermal gradients) are measured and then combined with astronomical observations of the true pointing and focus. Then simple models of the effect on pointing and focus (e.g., superposition and linearity) are used to robustly estimate model coefficients. The majority of the model coefficients are estimated simultaneously: thus, we derive both a thermally neutral gravity model and a thermal model. Our most sophisticated model takes into account gravity, thermal, wind, and azimuth track irregularity. Models are developed using a dataset that spans approximately 9 months of observations, which additionally demonstrates the stability and repeatability of the corrections.

AN UPDATE ON THE GBT METROLOGY SYSTEM

Constantikes, K. T.National Radio Astronomy Observatory

The Green Bank Telescope (GBT) is a offset-Gregorian design 100 meter aperture telescope with design goal of operation at 115GHz. Achieving the required pointing, focus, and efficiency for such a large instrument at these frequencies is a non-trivial task, made even more challenging by our desire to achieve these goals over most operating environments, e.g., all times of day. The Green Bank Precision Telescope Control System (PTCS) project has made significant improvement in GBT beyond the as-delivered performance. Improvements in hand include order-of-magnitude improvement in blind focus and pointing. Improvements to collimation and wavefront error are underway.

Current approaches are semi-empirical, using astronomical data and models driven by information about the pose of the GBT and environmental data. While the value of this approach is manifest (see our other presentation: Pointing and Focusing the GBT), we also are pursuing a direct metrological approach. Direct measurement of parameters associated with structural distortions may be needed to achieve the GBT design goals. For example, while collimation can be improved via observations, there are benefits to a direct measurement of the position and pose of the subreflector in a coordinate system tied to the primary reflector.

GBT development has from its inception included a metrology program based upon laser ranging and trilateration position measurements. As a result of these prior efforts in instrument development and actual experience, we are updating our approach. Changes being considered include major modifications to the laser rangefinder design, inclusion of angle measuring instruments (including autocollimation), a new approach to the system geometry, and addition of some other specialized instruments.

We will present our notional system design and details about the new instruments. We are currently proceeding with prototype instrument fabrication and test as well as system studies to determine if the notional system will plausibly meet overall system requirements. Data regarding error budgets, system sensitivities, and instrument performance will be included if possible.

Session J4, 08:35 – Fri.

**LARGE LOW-FREQUENCY ARRAYS
FOR RADIO ASTRONOMY I**

Chair: R. Perley

VERY LOW NOISE AMPLIFIERS AT 300K FOR 0.7 TO 1.4 GHz

Gawande R. S.¹, Wadefalk N.¹, Weinreb S.^{1,2}

¹California Institute of Technology, 1200 E California Blvd. MSC 136-93, Pasadena, CA 91125, USA

²Jet Propulsion Laboratory

The Square Kilometer Array (SKA) is a next generation radio telescope for astronomy which utilizes a large number of array elements. For this large number of receivers a significant reduction in cost and complexity can be achieved by using room temperature very low noise amplifiers instead of the cryogenically cooled amplifiers usually used in radio astronomy.

This paper investigates the different possibilities of achieving a very low noise figure (0.14dB or 10K) at room temperature for the frequency band of 0.7 - 1.4 GHz. High electron mobility transistor (HEMT) and Hetrojunction bipolar transistor (HBT) are studied as the possible active element for the LNA. Theoretical limits on transistor noise temperature will be discussed. In order to achieve a noise figure of 0.14dB the loss introduced by matching network must be very small and this leads to design of special matching networks for the LNA.

In the low microwave frequency band under consideration the key HBT device parameter is the current gain β . The noise temperature at any temperature is limited by base and collector shot noise to $290K/\sqrt{\beta}$. The latest SiGe HBTs exhibit β as high as 800 at 300K and this value increases with cooling; thus noise temperature of the order of 10K appear feasible if circuit losses can be kept very low. Microwave Office simulation results using IBM 8HP generation transistors will be presented.

A noise temperature of 31 K is reported using InP HEMTs for the frequency band 4-8 GHz (N. Wadefalk etc, *IEEE transactions on MTT*, vol. 51, 1705-1711, June 2003). The minimum noise in HEMTs drops monotonically with frequency except 1/f noise limits performance below a few GHz. The 1/f limits may vary greatly from one transistor manufacturing process to another and has not been accurately measured in the frequency range of 0.7 to 1.4 GHz. We are investigating this problem and will report our results.

THERMOELECTRIC COOLING OF LNAs TO 200 K

Jones, G., Weinreb, S.

Caltech, 1200 E. California Blvd., Pasadena, CA 91125

As the performance of room temperature low noise amplifiers (LNAs) continues to improve, very low noise systems can be built without the use of traditional cryogenic coolers. Instead, modern thermoelectric coolers (TECs) can be used to attain a physical temperature of around 200K without the cost and complexity of other refrigeration methods.

TECs have been widely used for cooling infrared and visible imaging devices, but so far they have not been used extensively for cooling LNAs. Cooling to 200K is particularly convenient for emerging LNAs built around SiGe hetero-junction bipolar transistors (HBTs), because the intrinsic gain (β) is greatly increased from room temperature. Intrinsic gain is a dominant factor in determining the noise performance of HBTs. Traditional high electron mobility transistor (HEMT) technology LNAs also benefit from thermoelectric cooling.

To achieve such low temperatures with TECs, it is necessary to make a multistage stack of thermoelectric modules. Compact, multistage TECs are commercially available which are capable of pumping 300mW or more at 200K while dissipating about 20W of waste heat. Such inefficiency requires that special consideration be given to insulation. A vacuum better than 10 microrr provides the best insulation, but other options may yield satisfactory results without the complexities of a vacuum.

An experimental module will be described that is designed to be inexpensive, compact, and extremely reliable, while providing exceptional noise performance. A module with these characteristics is especially desirable for radio astronomy arrays employing a large number of antennas. Results and analysis of this module will be presented. Additionally, advantages and disadvantages of thermoelectric cooling versus other methods will be discussed.

A WIDEBAND MMIC LNA FOR THE 11 TO 34 GHZ BAND

Morgan, M. A.National Radio Astronomy Observatory

The concept proposed by the United States for the Square Kilometer Array consists of a large number of small diameter paraboloidal dishes. Among the many advantages of this so-called Large-N/Small-D (LNSD) array over other proposed designs is the ability to reach higher frequencies. However, a key element to the success of any large-N architecture is minimizing the replication cost of the electronics.

The combined requirements of extending the SKA frequency coverage up to the low millimeter-wave band and minimizing the global cost of the array lead us to two immediate conclusions. First we must reduce the number of independent receivers needed by developing very wideband receivers, and second we must optimize the tradeoff between cost and performance by selecting a MMIC approach for as many elements of the receiver as possible. Efforts are underway to develop MMIC components for many key areas, but potentially the most beneficial receiver component to be realized in MMIC form is the LNA. It determines the ultimate sensitivity of the array elements, and could be the linchpin of an all-MMIC solution to the analog portion of the receivers.

This paper reports on progress in the design of a wideband cryogenic low-noise amplifier for the US SKA concept. The MMIC amplifier is targeted for the upper frequency band of 11 to 34 GHz. It is to have a flat small-signal gain of 34 dB with equivalent noise temperature of 12 K over the entire frequency range. The chip has been fabricated by Northrop Grumman in their proven cryogenic low-noise InP pHEMT MMIC process. If successful, this design would represent a significant head start on the challenging electronics development task for the SKA.

CRYOGENIC, LOW NOISE, 0.5-11 GHZ ACTIVE BALUN MMIC

Niklas Wade Falk, Sander Weinreb
California Institute of Technology, Pasadena, CA 91125

Background

Recent development in ultra wideband log-periodic antenna feeds [1, 2] for radio astronomy applications calls for a wideband balun. Common for these feeds is that they all have a balanced output. The balanced signal from the feed can be transformed to an unbalanced signal using a passive balun and then amplified with a conventional single-ended amplifier. Alternatively, an amplifier with differential input can be connected directly to the feed, and if the output is also differential, it would be followed by a passive balun. We have developed an amplifier with a balanced input and an unbalanced output that covers the frequency range of 0.5-11 GHz. This active balun replaces both the passive balun and the single-ended LNA in a receiver.

Circuit design

The active balun MMIC uses a differential pair input stage, very similar to those used in operational amplifiers. The output stage is a regular common source stage. The design and theoretical values for gain and noise is discussed and compared to regular single-ended amplifiers. The external input matching network allows the differential input impedance to be chosen between approximately 100 and 300 ohms, which makes it ideal for integration with wideband antenna feeds whose impedance usually falls within this range. A suggested way of integrating the active balun with such a feed is presented.

Measurements

The amplifier can be used as a regular single-ended LNA with two separate inputs referenced to ground and with a single output. Measurement result in this single-ended mode using co-planar waveguide probes is presented and discussed. To be able to measure the amplifier's differential mode performance, a new measurement system had to be developed. The system is a 200 ohm Differential Variable Temperature Load (DVTL), which allows us to measure the gain and noise of the active balun at different ambient temperatures. The design of the DVTL is discussed in detail and measurement result is presented at 300, 77 and 12 Kelvin ambient temperature.

[1] G.Engargiola, Non-planar log-periodic antenna feed for integration with a cryogenic microwave amplifier, IEEE Antennas and propagation society international symposium and USNC/URSI national science meetings, page 140-143, 2002

[2] Olsson R, Kildal P-S, Weinreb S, A novel low-profile log-periodic ultra wideband feed for the dual-reflector antenna of us-ska, Antennas and Propagation Society Symposium, 2004. IEEE , Volume: 3, Pages:3035 3038

CONTROL OF SITE RFI EMISSIONS AT THE ALLEN TELESCOPE ARRAY

Robert W. Ridgeway, David R. DeBoer, Geoff Bower
National Radio Astronomy Observatory, SETI Institute, University of California in Berkeley

URSI-BOULDER, Co. 2005

Control of Site RFI emissions at the Allen Telescope Array

ABSTRACT: The Allen Telescope Array (ATA), located at Hat Creek, California will consist of 350 offset parabolic antennae. Radio frequency interference (RFI) levels that are undetectable in typical radio communications will cause interference to the ATA. This is especially true if the RFI is present during a significant portion of the total observation time and over a large part of the bandwidth, as is the case with a digital signal Processor. Potential RFI emissions from the ATA correlator and other digital equipment would have all of these undesired qualities and must be prevented.

Cryogenic, low noise amplifiers directly modulating a laser beam provide for a very special quality. Ultra wideband analog fiber optic transmission systems can now quietly convey signals from each antenna to the RF converters, IF Digitizers, and correlator. A very high level of shielding must be implemented here to ensure that (RFI) emissions from these high-speed circuitry do not overwhelm potential extraterrestrial emissions which the telescope is designed to detect. The ITU harmful level standards for phased array radio astronomy can be applied in this case, where the band-width of 1Hz would not be unusual. The array factor for the ATA will greatly improve the resistance to any RFI not in the main beam.

The harmful levels are converted to effective isotropic radiated power (EIRP) dBW at the average distance to the nearest neighboring antenna. The loop back loss from each antennas electronics to its feed is measured and used to specify the minimum required shielding for this means of propagation. The EIRP, and average distance of digital equipment RFI coming from the central building must also be considered. The emissions of key components are measured in a reverberation chamber. Super shielded boxes that can provide the needed shielding (≥ 150 db) for various levels of PCB radiation have been designed to fit the requirements. These boxes can provide this extraordinary shielding with off the shelf filters and connectors. Due to the interleaved perimeter design there is no need for expensive gaskets. These extreme levels of shielding will be useful to only a few other specialized RF facilities like planetary radar, encryption device enclosures, and shielding against directed energy weapons. Because of careful RFI planning and extensive level measurement and shielding, it is expected that the ATA will be able to operate free of site-generated RFI.

A LOW FREQUENCY ARRAY DESIGNED TO SEARCH FOR THE 327 MHz LINE OF DEUTERIUM

Rogers, A.E.E., Dudevoir, K.A., Carter, J.C.C.,
 , Fanous, B.J., Kratzenberg, E.
 MIT Haystack Observatory, Westford, MA 01886

An array has been constructed to search for the 327 MHz line of deuterium. The array, which is located near the Haystack Observatory, Westford, Massachusetts, consists of 24 stations covering about 1 hectare. Each station is an array of 24 active crossed Yagi antennas mounted on a 4.4 x 4.4 m ground plane. A 48 channel receiver, consisting of analog downconversion followed by A/D conversion, digital downconversion and filtering is mounted below the ground plane of each station. Multiple station beams are formed in software and the spectra from the stations are periodically transferred via fiber optic ethernet to a central processor. The array design is optimized for the expected diffuse nature of the deuterium line emission so that the signals at each station are uncorrelated and the multiple stations provide a means of acquiring the same amount of station data in one year that would take 24 years with a single station. Special care has been taken to limit the self-generated RFI by enclosing the receivers in well shielded boxes and double filtering the A.C. power lines entering each receiver. The effects of external RFI have been minimized by adding resonant directors which make Yagi elements that have 10 dB less gain near the horizon than dipole elements. In addition the software at the central processor performs excision of RFI transients and suppression of discrete RFI carriers.

The array characteristics are:

Number of dual polarization elements per station	24
Number of stations	24
Receiver noise temperature	40 K
Station beamwidth	14 degrees
Number of simultaneous beams processed	4
Receiver bandwidth	250 kHz
Receiver resolution	244 Hz

The estimate of the D/H abundance in the interstellar medium of about 15 ppm from the Lyman- α observations of the FUSE satellite results in an expected opacity of the 327 MHz line of only about 8 ppm. The expected signal strength, accounting for receiver noise, beam efficiency and scan loss is about 4 ppm in a 10 kHz bandwidth. This should result in a 6 sigma detection in 1 year observing the anti-center with the 24 station array for 4 hours per day.

LOW FREQUENCY OBSERVING WITH THE ALLEN TELESCOPE ARRAY (ATA)

Welch, Wm. J.¹, DeBoer, D.², Bower, G.¹
 , Dreher, J.², Lugton, J.¹, Flemming, M.¹
 , Davis, M.², Harp, G.², Ackermann, R.²
 , Urry, Lynn¹, Thornton, D.¹, Weinreb, S.³
 , Wadefalk, N.⁴, D'Addario, L.³

¹UC Berkeley Radio Astronomy Lab

²SETI Institute

³Jet Propulsion Laboratory

⁴Cal Tech

When it is complete, the ATA will consist of 350 6.1 m diameter antennas in a two dimensional array of 800 m diameter. The distribution is irregular in appearance but is designed to have a nearly Gaussian distribution of baseline lengths to achieve a Gaussian snapshot beam. Maximum central sidelobes have peaks less than one percent. The field of view, corresponding to the 6.1 m beam is about three degrees at 1000 MHz, and the synthesized beam is about 1.5 arc minutes at this same frequency. The Array is expected to operate over a span of frequencies covering the range 500 MHz to 11.2 GHz with a single broadband receiver. Because potential interference from low frequency radio broadcast stations at low elevation angles is especially serious, an optical design has been chosen for the antennas that has minimal ground pick-up. This design also minimizes receiver noise pick-up from the ground. Low ground pick-up is characteristic of dual mirror systems, and an offset Gregorian was chosen accordingly. The offset choice is dictated by the need to operate at long wavelengths without too much blockage from a secondary mirror that is 2.4 m in diameter (four wavelengths at 500 MHz). The secondary is large compared to the 6.1 m primary. A further feature is a metal shroud, approximately cylindrical in shape that partially surrounds the feed, mounted between the primary and secondary at the bottom of the optical system. We describe the measured properties of one antenna in this array and the expected synthesized beam. We also discuss the excellent RFI characteristics of the Hat Creek site at low frequencies.

Session J5, 08:15 – Sat.

**LARGE LOW-FREQUENCY ARRAYS
FOR RADIO ASTRONOMY II**

Chair: R. Perley

THE PRIMEVAL STRUCTURE TELESCOPE

Jeffrey B Peterson¹, Ue Li Pen², Xiang Ping Wu³¹Department of Physics, Carnegie Mellon University, Pittsburgh, PA²Canadian Institute for Theoretical Astrophysics, University of Toronto, Toronto, Ontario, Canada³National Astronomical Observatories, Chinese Academy of Sciences, Beijing, China

The Primeval Structure Telescope (PaST) will be used to study early ionization of the universe. The telescope will image and spectrally resolve hyperfine emission of neutral hydrogen at redshifts from about 6 to 20.

Recently released data, obtained with the WMAP satellite, indicate that the universe was ionized very early, at around redshift 15. Right now, there is very little information on this ionization, since the WMAP data do not tell us the ionization history or the energy source. If the energy source was emission from collapsed objects, perhaps ultraviolet radiation from the first stars, the ionization did not occur homogenously. Earlier star formation in high-density regions causes these to be ionized first. Just when the ionization was half complete, the large-scale structure of the universe became visible in the ionization pattern. We will use redshifted 21 cm brightness to image the largest of the ionized bubbles in three dimensions, allowing us to determine the redshift of the early ionization. In addition, we will be able to study the evolution and merging of the ionized bubbles.

PAST will be a sparse array telescope consisting of 10,000 log periodic antennas, providing over 50,000 square meters of effective collecting area. These antennas will be grouped into 80 phased arrays of 127 antennas. Current plans have these phased arrays fixed, pointed at the North Celestial Pole. Later, we can add electronic beam steering. Signals from the 80 phased arrays will be processed using a correlator built from a network of about 100 PC computers.

The telescope will occupy ten square kilometers in the Ulaistai Valley, Xin Jiang, China. The telescope will be built almost entirely of inexpensive commercially available off-the-shelf components.

A series of tests of prototypes, made on-site, have allowed us to study the performance of the telescope and its components. We will present these results and show sky images obtained with the prototypes.

We anticipate that one quarter of the array will be assembled by the time of the meeting and we will present an up to date progress report.

THE MILEURA WIDEFIELD ARRAY DEMONSTRATOR

Hewitt, J. N., Cappallo, R. J., Kasper, J. C.
, Lonsdale, C. J., Morales, M. F., Salah, J. E.
Massachusetts Institute of Technology

The Mileura Widefield Array (MWA) Demonstrator, to be built in the radio-quiet environment of Western Australia, has several primary science goals. First, we seek to detect and characterize the redshifted HI signals from the cosmological Epoch of Reionization (EOR). The array will be capable of measuring the power spectrum of fluctuations, as well as imaging structures created by the ionizing radiation from quasars at a redshift of about 6.5. These investigations will shed light on the processes that led to the formation of the first galaxies and quasars. Second, the wide field capabilities of the array will be exploited to perform blind searches for transient sources of radio emission, a class of astronomical radio source that to date is largely unexplored. Third, the array will be used to probe the magnetoionic medium of the heliosphere with unprecedented precision by measuring propagation effects on the signals of background radio sources. Both interplanetary scintillation and Faraday rotation will be simultaneously monitored in order to constrain the magnetic field orientation in coronal mass ejection (CME) events, with the goal of better predicting the coupling of CME energy to the terrestrial magnetosphere.

The MWA Demonstrator will consist of 500 phased-array antennas optimized for the 80-300 MHz frequency range. It will have very high spectral and temporal resolution, electronic pointing agility and multibeaming capability. Most importantly, it will feature an inherently wide 20 to 30-degree field of view. We report on the status of the 500-element array MWA Demonstrator and detail the aspects of the design that uniquely address the science goals.

EQUIPPING THE VLA FOR VHF OPERATION TO MAP HI STRUCTURES PRESENT DURING THE EPOCH OF REIONIZATION

Lincoln Greenhill¹, Ray Blundell¹, Rick Perley², Chris Carilli², Avi Loeb¹, Matias Zaldarriaga¹, Steve Furlanetto³

¹Center for Astrophysics

²National Radio Astronomy Observatory

³California Institute of Technology

We report on a program proposed by the SAO to equip the NRAO Very Large Array with VHF receivers (170-200 MHz) to enable detection of neutral Hydrogen at the end of the cosmological epoch of reionization (EOR).

The structure and evolution of the universe during the EOR are essentially unknown. Analyses of Cosmic Microwave Background (CMB) temperature and polarization fluctuations detected with WMAP have been used to infer reionization began between redshifts 11 and 30 (Kogut et al., *ApJS*, **148**, 161, 2003), while Ly α absorption in the optical spectra of quasars have been used to argue reionization was largely complete at redshift $z \sim 6.2$. What occurred in between is uncertain, and the history of reionization may have been complex, with multiple peaks (e.g., Wyithe Loeb *Nature*, **427**, 815, 2004).

With VLA VHF receivers, it may be possible to detect and image HI emission from shells of warm material surrounding the many-Mpc-scale HII bubbles ionized by quasars. There are three quasars known from the Sloan sky survey that are believed to lie "within" the EOR ($z \sim 6.2 - 6.4$). Detection would enable estimation of fundamental quantities, e.g., the neutral fraction of the universe, state of the IGM - warm or cold, anisotropy of emission, and quasar ages or formation time after cosmological recombination. Overall, hard estimates would provide much needed constraint for cosmological theory. In addition to direct imaging of structure, the deep integrations used to detect cosmological HII bubbles may also be used to describe the statistics of weak HI brightness fluctuations, much as has done in experiments to measure CMB fluctuations once foreground sources have been subtracted, and to further constrain theory.

The planned SAO VHF system leverages past investments in VLA hardware and software to achieve "first science" in short order (2005) and at lower cost than the other, larger facilities that are in the works (e.g., MWA, PAST). Little is known about the EOR from observations. First detection of an EOR signal with the VLA will have a high (scientific) impact, and it will be helpful in guiding development and operation of the later facilities.

THE 74 MHZ SYSTEM ON THE VLA AND THE BREAK-
THROUGH TO SUB-ARCMINUTE RESOLUTION IMAGING
AT LOW FREQUENCIES.

Kassim, N.E.¹, Lazio, T.J.L.¹, Peters, W.¹
, Cohen, A.¹, Ray, P.¹, Hicks, B.¹
, Stewart, K.¹, Crane, P.¹, Perley, R.A.² , Erickson, W.C.³

¹Naval Research Laboratory

²National Radio Astronomy Observatory

³University of Tasmania

High red-shift radio galaxies, galaxy clusters and relics, pulsars, supernova remnants, and even planets (and possibly exoplanets) emit strongly at frequencies below 100 MHz. Low frequency radio observations also offer unique access into diverse astrophysical phenomena due to intrinsic (e.g. synchrotron self-absorption) and extrinsic (e.g. thermal absorption) propagation effects that cannot be measured by other means. This great potential of low frequency radio imaging remains mostly untapped due largely to the poor sensitivity and angular resolution of the previous generations of low-frequency telescopes. Those limitations are the consequence of ionospheric phase perturbations that have prevented the development of connected-element low frequency (≤ 100 MHz) interferometers with baselines greater than 5 km. The 74 MHz system on the VLA is the first to overcome this ionospheric limitation on baseline length and break through to a new regime of resolution and sensitivity. Its success is driving a quiet renaissance in long wavelength radio astronomy and serves as both a scientific and technical pathfinder towards an emerging suite of next generation instruments with even greater capabilities, such as the Long Wavelength Array (LWA) and the Low Frequency Array (LOFAR). In this talk I will describe the 74 MHz VLA system which is currently the most powerful imaging interferometer operating below 100 MHz, and show how its unique capabilities are being used to investigate a wide variety of astrophysical problems. I will also describe the technical challenges and fundamental limitations that restrict the system but at the same time illuminate the path forward for developing the next generation low frequency instruments.

THE VLA LOW-FREQUENCY SKY SURVEY

Cohen, A.S.¹, Lane, W.M.¹, Kassim, N.E.¹
, Lazio, T.J.W.¹, Cotton, W.D.², Perley, R.A.²
, Condon, J.J.², Erickson, W.C.³

¹Naval Research Laboratory

²National Radio Astronomy Observatory

³University of Tasmania

We present an overview of the ongoing VLA Low-frequency Sky Survey (VLSS, formerly known as 4MASS). The VLSS will map an area of 9.1 sr covering the entire sky above a declination of -30 degrees, at a frequency of 74 MHz or 4 meter wavelength, with an unprecedented combination of sensitivity and resolution at this low frequency. The observational challenges at this wavelength include radio frequency interference (RFI), ionospheric phase distortions and a large field of view filled with sources. These challenges have been surmounted by a variety of new algorithms. The principle data products from the survey will be a set of publicly available images along with a source catalog of approximately 80,000 objects. Thus we will create an on-line virtual observatory at this previously unexplored frequency which will complement other major surveys at higher frequencies such as the NVSS. From these data, statistically useful samples of extra-galactic and Galactic objects, such as high redshift radio galaxies, galaxy clusters, supernova remnants and pulsars can be assembled for further study. In addition to the many scientific benefits of this survey, creating a sky model at this low frequency will help in the use and design of the planned next-generation of large low frequency telescopes such as LWA and LOFAR. The observations are now roughly 50% complete, and we expect to observe the majority of the remaining fields by spring 2005 with an anticipated public data release in the latter half of 2005. Data products and more information are available on our website (URL:<http://lwa.nrl.navy.mil/VLSS/>).

LOW FREQUENCY SOLAR PHYSICS WITH THE FREQUENCY AGILE SOLAR RADIOTELESCOPE

T. S. Bastian¹, R. Fisher¹, R. Bradley¹,
D. Gary², G. Hurford³, S. White⁴, A. Kerdraon⁵, C. Ruf⁶

¹National Radio Astronomy Observatory

²New Jersey Institute of Technology

³Berkeley

⁴University of Maryland

⁵Paris Observatory

⁶University of Michigan

The Frequency Agile Solar Radiotelescope (FASR) is an instrument designed to perform broadband imaging spectroscopy of the Sun over a frequency range of roughly 30 MHz to 30 GHz. It will do so with angular, spectral, and temporal resolutions commensurate with physical processes that occur on the Sun. As such, FASR will address an extremely broad program of solar physics. The key science goals of FASR include 1) coronal magnetic fields; 2) energy release in flares; 3) drivers of space weather; 4) the thermal Sun. In this talk, low frequency radiophysics and its relevance to drivers of space weather will be emphasized, which includes radio diagnostics of the nature and origin of coronal mass ejections, formation and propagation of coronal shocks, and the origin of solar energetic particles.

FASR will comprise three antenna arrays, each designed to cover roughly a decade in bandwidth. FASR A will observe in centimeter wavelengths, FASR B in decimeter wavelengths, and FASR C in meter wavelengths. Antennas in FASR A and B will be steerable paraboloids while FASR C will be composed of fixed broadband elements. The antenna configuration in each array will be optimised to produce high fidelity snapshot imaging over the entire frequency range.

This talk will summarize the specifications of each array and the design approach to the instrument. The fact that FASR is a solar-dedicated instrument eliminates the need for large antennas, cooled front ends, and a large correlator. Yet FASR nevertheless raises interesting design challenges, including the need for low-cost, robust antennas, operations in the presence of a variety of RFI sources, and the need for an extremely stable instrument.

SOLAR IMAGING RADIO ARRAY (SIRA): IMAGING SOLAR,
MAGNETOSPHERIC, AND ASTROPHYSICAL SOURCES
BELOW 15 MHz

S. D. Bale¹, R. J. MacDowall², N. Gopalswamy²
, M. L. Kaiser², M. Reiner², D. Jones³, J. Kasper⁴, K. Weiler⁵

¹Dept of Physics and Space Sciences Laboratory, University of
California, Berkeley

²Laboratory for Extraterrestrial Physics,, NASA, Goddard Space
Flight Center

³NASA, Jet Propulsion Laboratory

⁴Center for Space Research, MIT

⁵Naval Research Laboratory

The Solar Imaging Radio Array (SIRA) is a space mission to perform aperture synthesis imaging of low frequency solar, magnetospheric, and astrophysical radio sources. The primary science goal is to image radio sources from coronal mass ejection (CME) - driven shock waves in the solar corona and interplanetary plasma. To achieve this, a space-based interferometer is required, because plasma emission frequencies in the solar wind are below the ionospheric cutoff and are, therefore, shielded by the ionosphere. As such, the SIRA mission serves as a lower frequency counterpart to LWA, LOFAR, and similar ground-based radio imaging arrays. SIRA will require 12 to 16 microsatellites to establish a sufficient number of baselines with separations on the order of kilometers. The constellation consists of microsats located quasi-randomly on a spherical shell, initially of radius 5 km or less. Reasonable mission designs can achieve 1 arcmin angular resolution at 15 MHz and 90 dB of dynamic range. We explore the options of both 3-axis stabilized and spinning spacecraft with body-mounted solar arrays and earth pointing high gain antennas. A retrograde orbit at 500,000 km from Earth was selected as the preferred orbit because it reduces the downlink requirement while keeping the microsats sufficiently distant from terrestrial radio interference. Also, the retrograde orbit permits imaging of terrestrial magnetospheric radio sources from varied perspectives. We also consider the possibility of an L1-based constellation. The SIRA mission serves as a pathfinder for space-based satellite constellations and for spacecraft interferometry at shorter wavelengths. SIRA will be proposed to the NASA MIDEX proposal opportunity in mid-2005.

DESIGN AND PROPERTIES OF THE LONG WAVELENGTH ARRAY (LWA)

Gaussiran, T.L.¹, Kerkoff, A.J.¹, York, J.A.¹
 , Slack, C.M.¹, Ray, P.S.², Ellingson, S.W.⁴
 , Price, R.M.³, Crane, P.², Hicks, B.²
 , Stewart, K.P.², Polisensky, E.², Kassim, N.²

¹Applied Research Laboratories, The University of Texas at Austin

²Naval Research Laboratory

³University of New Mexico

⁴Virginia Polytechnic Institute State University

The Long Wavelength Array (LWA) is a sensitive, high-resolution synthesis array operating in the 10-90 MHz regime that has been proposed by the South West Consortium (SWC). The SWC consists of two main universities (University of New Mexico and The University of Texas at Austin) as well as two national laboratories (Naval Research Laboratory and Los Alamos National Laboratory). The SWC is working closely with the National Radio Astronomy Observatory in both the design and siting of the LWA. New discoveries in science often come about by investigating new regions, with its low frequencies, high sensitivities and high resolutions the LWA will open a new window on the universe. The LWA will be a multi-beamed (8 independent beams) fully digital telescope that will be capable of covering a total of 32 MHz of bandwidth. The design currently calls for ≈ 50 stations with each station having 256 dual polarization dipoles. The current design employs a direct sampling receiver that helps to keep the overall cost of the LWA low.

We will review the current design for LWA. We will cover the overall design parameters of the LWA. This will emphasize the current vision of the LWA but will also point out how this design differs from the Long Wavelength Demonstration Array (LWDA). We will cover several of the design choices that are being considered as well as the implications of those choices. The review will start from the point of view of the array as a whole. We will then begin to look at the various components in greater detail. This will hopefully provide the audience with an overall view of the telescope and its capabilities.

THE DESIGN OF THE LONG WAVLENGTH ARRAY, A
LONG-BASELINE RADIOTELESCOPE FOR 10-90 MHZWilliam Junor¹, Thomas L. Gaussiran, II², Namir Kassim³¹Los Alamos National Laboratory²Applied Research Laboratories, University of Texas at Austin³Naval Research Laboratories

We will describe the scientific motivations for a long wavelength radio telescope operating between 10 and 90 MHz with baselines up to 450 km. The need for such an instrument was recognized in the NAS decadal report, Astronomy and Astrophysics in the New Millennium. A consortium of universities and national laboratories has been formed to promote the design, implementation and operation of this instrument, the Long Wavelength Array (LWA). The principal members of this consortium are the University of New Mexico, the University of Texas, the Naval Research Laboratory and Los Alamos National Laboratory. The LWA will operate in the last poorly explored part of the electromagnetic spectrum. The instrument will address scientific questions in astronomy and astrophysics, cosmology, solar and planetary science, and ionospheric physics. An important part of the LWA's mission is to educate students in hardware and software design and in signal and image processing.

The consortium plans to site the radio telescope in New Mexico, in order to exploit synergies with the EVLA and other regional facilities and initiatives. The implications of the science drivers for the design of the Long Wavelength Array will be presented. The talk will examine the trade space for scientific goals and instrumental complexity and cost. Particular emphasis will be placed on our ability to perform ionospheric calibration over the whole array. We will also address possible approaches to the excision of radio frequency interference in the instrument's operating range. In addition, we will discuss the software requirements for what is essentially a "software telescope".

We will also present results from prototyping activities funded by the Naval Research Laboratory. These activities are part of our 4 stage plan to develop, construct and operate the LWA, while performing useful and interesting science at each stage.

SITE SELECTION FOR THE LONG WAVE ARRAY

Price, R.M.,

Department of Physics and Astronomy, University in New Mexico

The Long Wave Array (LWA) will consist of approximately fifty stations arranged geographically so as to optimize u-v coverage and to allow baselines of up to hundreds of kilometers. Each station will consist of an array of 256 crossed dipoles within a diameter of approximately fifty meters. The LWA will have a core of 25 dishes in a five-kilometer diameter circle. The inner kilometer will be densely populated enough with stations and equipment so as to require its own (non shared) land. Other stations each will be contained within a 70-meter diameter fenced area (approximately one acre). Observational frequencies will be 30 to 90 MHz.

From an economic and construction point of view station sites must be available, or obtainable at reasonable cost and/or effort, accessible by road, and close to power and fiber. The economics of each of these points must be considered. Concerns and needs of residents in the area of the station must also be taken into account.

From a technical point of view, the radio spectrum usage environment (generally called RFI by radio astronomers) must be well understood. The LWA and the SKA both require an extensive set of RF measurements at typical station locations. Typically RFI is measured as received power vs. frequency and percent channel occupancy vs. frequency. These measurements should be taken for typical 24-hour periods during both workdays and weekends. Additional measurements will measure diffraction propagation over mountain ranges separating the array stations from major transmitters. Effects of weather and vegetation are also being measured.

Since the ionosphere will contribute considerably to observational data at such low frequencies, it is necessary to know the structure of the ionospheric total electron content and variations on a scale of tens of kilometers. This will be accomplished by careful reduction of existing 300 MHz and 74 MHz VLA observations to obtain optimum imaging. The calibration data obtained from the observations will relate to the ionospheric conditions at the time of the observations.

THE SQUARE KILOMETER ARRAY: MEETING THE DEMANDS OF LOW-FREQUENCY SCIENCE

James Cordes

Cornell University

The current science case for the international Square Kilometer Array project includes five key science areas: (1) Galaxy Evolution and Large-Scale Structure, including Dark Energy; (2) Probing the Dark Ages through studies of highly redshifted atomic hydrogen and carbon monoxide; (3) Cosmic Magnetism; (4) Probing Gravity with Pulsars and Black Holes; and (5) The Cradle of Life, including studies of protoplanetary disks, organic molecules, and the search for extraterrestrial intelligence.

The technical specifications that follow from the science requirements include very challenging constraints on the configuration, frequency range, field of view, polarization purity, real-time processing throughput, post-processing algorithms, modes of operation, and other aspects of the design. The current plan is to configure antennas in a centrally condensed array out to distances of at least 3000 km. The project is in the process of identifying the best antenna or concentrator that will be based on work being done around the world on small parabolic reflectors; cylindrical reflectors; large adaptive reflectors with aerostat-suspended feed arrays; Arecibo-like reflectors; and aperture arrays. Some of the challenges for the SKA will be addressed by the construction and operation of low-frequency arrays that are now being planned. However, others are explicit to the SKA, including (a) how to cover the 0.1 to 25 GHz frequency range: can it be accomplished with a single antenna type or is a hybrid-array or multiple-array solution inevitable? (b) how can the proposed wide field of view ($> 1 \text{ deg}^2$ at 1.4 GHz) be utilized for wide-field spectroscopic and time-domain surveys and for wide-field imaging?

I will discuss the SKA concept with these issues in mind. For specificity, I will often but not exclusively refer to the Large-N, Small-diameter paraboloid concept for the SKA being pursued in the US.

Session K1, 08:35 – Wed.

**ELECTROMAGNETICS IN
BIOLOGY AND MEDICINE**

Co-Chairs: S. Hagness, K. Ito

BIOLOGICALLY INSPIRED SENSING AND IMAGING OF POLARIZATION INFORMATION IN NATURE

Engheta, N., Pugh, Jr., E.N., Lin, S.S. , Yemelyanov, K.M.

University of Pennsylvania, Department of Electrical and Systems Engineering, Philadelphia, Pennsylvania 19104, U.S.A.

When we view the world with unaided eyes, two of the characteristics of image-forming visible light from the scene, namely, the intensity and the wavelength, are detected by our visual system, and then are encoded into perceptual qualities of brightness and color. Our eyes, however, cannot gather and use the information about the third physical characteristic of light, its polarization, and are thus blind to this important component of optical signals. It is well known, however, that several species of animals have visual systems capable of detecting lights polarization and using the information so extracted (see e.g., R. Wehner, Matched filters neural models of the external world, *J. Comp. Physiol. A*, Vol. 161, pp. 511-531, 1987). These species typically use this ability for navigation. However, it is believed that some species may also use polarization information to enhance in detecting predators and prey and in breaking camouflage.

We believe that much can be learned from polarization vision in nature, and indeed we have introduced and developed various imaging algorithms, sensing schemes and visualization and display methodologies inspired and informed by biological consideration (see e.g., K. M. Yemelyanov, S.-S. Lin, W. Q. Luis, E. N. Pugh, Jr., and N. Engheta, *Bio-Inspired Display of Polarization Information Using Selected Visual Cues*, the 2003 SPIE-The International Society for Optical Engineering, Volume 5158 (the Polarization Science and Remote Sensing), San Diego, California, August 3-8, 2003, pp. 71-84). Our ongoing research efforts demonstrate that these bio-inspired polarization sensing and imaging techniques facilitate better target detection, enhanced visibility in otherwise low-contrast conditions, longer detection range in optically scattering media, man-made polarization-sensing adaptation based on changing environments, surface deformation/variation detection (e.g., detection of finger prints on a smooth surface using polarization-based vision), shadow removal by displaying polarization information instead of conventional intensity information, and many more novel outcomes. These results show the numerous possibilities and potential applications of these bio-inspired methods in various sensing, imaging, and display technologies. In this talk, we will present an overview of some of the various aspects of our research efforts in this area.

A 3-DIMENSIONAL NON-UNIFORM MULTI-RESOLUTION
MESH CLUSTERING AND ELECTRIC NETWORK GENERATION
SCHEME FOR BIOELECTROMAGNETIC SIMULATIONS

Cela, C.J., Brown, P.K., Lazzi, G.L.
North Carolina State University

As the detail of the available biological computational models for bioelectromagnetic simulations increase, new schemes are needed for the efficient solution of larger discretized models. In this work, a scheme to model low frequency bioelectric interactions by means of non-uniform, multi-resolution, 3-dimensional network of impedances is introduced, and its application to the computation of current spread in the human retina stimulated by an array of electrodes to restore partial vision to the blind is presented.

The core method is based on the impedance method. However, while typical impedance method algorithms utilize uniform sized voxels, our proposed algorithm allows to apply different clustering strategies to different portions of the model, resulting in the generation of different voxel sizes and geometries in different areas. This strategy results in significant memory and computational time savings. This article presents a 3-dimensional generalization of the clustering methods previously used by our group on 2-dimensional models, as well as a scheme for generating SPICE compatible files describing the model properties in terms of electric circuit elements.

In addition, our scheme allows defining model areas having different levels of detail, keeping adequate spatial resolution in the parts of interest while reducing overall system size. Spatial coordinates of the mesh model are preserved on the resulting SPICE file, allowing for cross referencing between the physical model and the resulting electric circuit model.

Results related to the utilization of the proposed method for electrical stimulation of the human retina in a retinal prosthesis system to restore partial vision to the blind will be presented.

A MATCHED-FILTER FDTD-BASED TIME REVERSAL APPROACH FOR MICROWAVE BREAST CANCER DETECTION

Kosmas, P., Rappaport, C.

Center for Subsurface Sensing and Imaging Systems, Northeastern University, ECE Department

The feasibility of microwave breast cancer detection with a time reversal algorithm is examined. This algorithm is based on the finite difference time domain (FDTD) method, and compensates for the wave decay and therefore is suitable for lossy media. In the present work, we consider a two-dimensional (2-D) breast model based on magnetic resonance imaging (MRI) data, and examine the focusing abilities of a time reversal mirror (TRM), comprised of an array of receivers with a single, ultra-wideband pulse excitation. Without special considerations, resolving small (3 mm diameter) tumor-like scatterers requires very short duration pulses. This requirement demands hardware with unusually high performance. We propose a way to overcome this difficulty based on the observation that the amplitude and phase information of the tumor response is sufficient to achieve focusing.

We first assume that the tumor/scatterer response is known exactly, and show that the time reversal process is robust to background uncertainties. In particular, focusing is achieved even when the time-reversed model ignores a priori information such as breast tissue inhomogeneities or skin layer thickness and dielectric properties. We then examine the much more challenging realistic situation where the target response is not known and can only be estimated from the total (clutter-dominated) signal. The detection and localization problem is divided into two distinct processes: 1) a method that can identify and estimate the tumor response from the data is required; 2) this estimated tumor response at each receiver is backpropagated through the medium, and the wave is focused to the tumor/scatterer location. A matched filter approach to solve the signal-processing problem of the first process is proposed and applied to the TRM data, and FDTD time reversal is used to backpropagate the output of the matched filter algorithm. Detection and localization is achieved for different target locations, and the ability of the time reversal algorithm to avoid false alarms is demonstrated. The overall good performance of the method suggests that it is a promising new technique for microwave breast cancer detection.

EXTREMELY COMPACT WIRE ANTENNAS FOR WIRE-
LESS DATA TELEMETRY IN A RETINAL PROSTHESIS

Keyoor Gosalia, Gianluca Lazzi
NC State University, Raleigh, NC 27695-7914

In this work, compact planar wire dipole antenna geometries' impedance matching properties and compression efficiencies are compared with respect to their use as intraocular (embedded) elements in a retinal prosthesis. A novel method of matching a specific planar meander line dipole antenna at its higher order mode (full wave resonance) will be discussed and compared with the conventional technique of matching the fundamental mode. For this planar meander wire antenna a minor offset in the feed point—introduced by shortening one of the dipole arms can induce a current phase reversal and provide an impedance match while retaining the feed point at the structure's symmetrical center. It will be demonstrated that phase reversal on wire antenna configurations possessing a high degree of current vector alignment among adjacent wire lengths can improve the broadside directivity, albeit at a deterioration in the bandwidth.

An edge fed planar meander line dipole antenna measuring $5.25 \times 5.25 \times 1.5$ mm is implemented to operate at 1.4 GHz for its use as an intraocular element in a retinal prosthesis. This wire dipole antenna is impedance matched using the current phase reversal technique. Coupling measurements (between an external patch antenna and the compact wire dipole antenna) were performed both in free space and with the wire dipole antenna embedded in an eye model. These measured results were compared with corresponding results obtained using an embedded compact microstrip patch antenna. At a fixed separation of 25 mm, the coupling in free space and in the presence of the eye model using the planar meander wire dipole (as the intraocular element) is higher than that observed with the compact microstrip patch antenna. Comprehensive measurement results comparing the performance of such a data telemetry link using both (patch and wire) types of antennas will be presented.

SOLVING BIOELECTROMAGNETIC PROBLEMS USING THE ADI FDTD METHOD

Schmidt, S., Lazzi, G.

North Carolina State University, Dept. of Electrical and Computer Engineering, Raleigh, NC 27695-7914, USA

As more applications of wireless devices in the personal space are emerging, the interaction between electromagnetic energy and the human body has become increasingly important. Due to the risk that health damage may be caused by the use of wireless devices, it is important to minimize their electromagnetic interaction with biological objects. Our research addresses the need to develop efficient numerical methods for the computation and minimization of the specific absorption rate (SAR) associated with wireless devices as an alternative to repetitive design prototyping and measurements.

Bioelectromagnetic problems involving inhomogeneous dispersive media are easily solved using the finite-difference time-domain (FDTD) method. In this class of problems, the spatial discretization is often dominated by very fine geometric details rather than the smallest wavelength of interest. For an explicit FDTD scheme, these fine details dictate a small time-step due to the Courant-Friedrichs-Lewy (CFL) stability bound, which in turn leads to a large number of computational steps. The alternating-direction-implicit (ADI) method eliminates the CFL stability bound. For large time steps, the ADI method has larger dispersion and phase errors than the explicit FDTD method, but it is still useful for the computation of SAR where those errors are tolerable.

Further, it is often necessary to truncate the model and therefore extend a dielectric material into the absorbing boundary conditions (ABC). We use the D-H-formulation, which allows easy implementation of perfectly-matched-layer (PML) ABC with unsplit field components, independent of the materials modeled in the FDTD space. We present numerical results for the reflection errors of our PML ABC implementation with truncated material models.

The ADI method, as previously proposed for the simulation of bioelectromagnetic problems, does not converge as quickly as the explicit FDTD methods with resistive source implementation. Thus, we extend the ADI method with a new resistive source condition to achieve convergence rates that are similar to those of the explicit FDTD method. We compute the SAR in spherical geometries and models of the human head using the ADI method. We show that the ADI method with resistive source converges faster than without resistive source and at a rate comparable to the explicit FDTD method with resistive source. We also show that for spherical geometries, the SAR computed using the ADI method, with and without a resistive source, is in good agreement with experimental results and the explicit FDTD method.

A SIMPLE ABDOMEN PHANTOM OF PREGNANT WOMEN AT VHF BAND

Ito, K.¹, Kawai, H.², Takahashi, M.¹
, Saito, K.¹, Ueda, T.³, Saito, M.³
, Ito, H.³, Osada, H.⁴, Koyanagi, Y.⁵, Ogawa, K.⁶

¹Research Center for Frontier Medical Engineering, Chiba University

²Graduate School of Science and Technology, Chiba University

³Department of Radiology, Graduate School of Medicine, Chiba University

⁴Department of Obstetrics and Gynecology, Chiba University Hospital

⁵R & D Center, Panasonic Mobile Communications Co., Ltd.

⁶Communication Devices Development Center, Matsushita Electric Industrial Co., Ltd.

Recent years, radiofrequency devices, which are usually placed in the vicinity of the human body, have been widely used. Pregnant women may be exposed to the electromagnetic (EM) waves radiated from these devices, e.g., portable radio terminals, induction heating cookers, etc. It is therefore necessary to evaluate the EM exposure to a fetus inside pregnant women.

To the authors' knowledge, several papers on the evaluation of the EM exposure to the fetus have been published. However, in those papers, the structure of the pregnant women was inaccurate. In addition, little is known about the dielectric constants of the amniotic fluid and fetus, because the measurement of such values is quite difficult. Therefore, an accurate structure of the model and the dielectric constants of the fetus are indispensable to evaluate the precision EM exposure to the fetus.

In this paper, firstly, the dielectric constants of the amniotic fluid and fetus of rabbits are measured, because the electrical properties of mammals are almost equal to those of the human. As a result, it has been confirmed that the conductivity of the amniotic fluid and fetus is 1.8 and 1.3 times larger than that of the muscle of an adult at 150 MHz. Next, a simple abdomen model of pregnant women, which is composed of three different types of tissues, based on measurements of magnetic resonance imaging (MRI) tomograms is introduced. Finally, the SAR inside the abdomen model close to a short dipole antenna, which has the same axial length of the normal mode helical antenna (NHA), is calculated by the FDTD method at 150 MHz. As a consequence, the local 10-g SAR in the fetus is less than 34 % of that in the mother's body. From these investigations, the abdomen model including the amniotic fluid is necessary to evaluate the SAR in the fetus.

TISSUE-MIMICKING PHANTOM MATERIALS FOR NARROWBAND AND ULTRAWIDEBAND MICROWAVE APPLICATIONS

Lazebnik, M.¹, Madsen, E. L.², Frank, G. R.², Hagness, S. C.¹

¹Department of Electrical and Computer Engineering, University of Wisconsin, Madison, WI 53706

²Department of Medical Physics, University of Wisconsin, Madison, WI 53706

Over the past several decades, growing interest and research on the effects of electromagnetic energy on biological tissues as well as on the development of diagnostic or therapeutic applications has resulted in an increased need for biological phantoms that mimic the electromagnetic properties of tissues, particularly at radio and microwave frequencies. Although a variety of tissue-mimicking (TM) material recipes have been published to date that simulate the properties of biological tissues at discrete frequencies, there is currently a need for TM materials for ultrawideband (UWB) applications that enable production of heterogeneous and anthropomorphic phantoms.

We propose a solid gelatin-based TM phantom recipe that simulates the dispersive dielectric properties of a variety of biological tissues at a wide frequency range (500 MHz to 20 GHz). The TM muscle is created from primarily gelatin and water. The TM fat is made using the same gelatin material, except that, prior to congealing, it is combined with safflower oil and a surfactant in a volume ratio of 1:4 (resulting in an 80% oil-in-gelatin dispersion). The dielectric properties of the materials are controlled by varying the volume percent of the oil. Since the TM muscle and the gel matrix surrounding the oil droplets of the TM fat have the same composition, these materials can be placed in direct contact with no risk of diffusion of the solvent or solute. Thus, a critical property of this recipe is the ability to create heterogeneous configurations with long-term stability of mechanical and electromagnetic properties.

Our results indicate that the phantom compositions with very little oil (0-10%) are appropriate materials for mimicking high-water-content tissue, such as muscle or malignant breast tumors, below about 8 GHz. Above 8 GHz, however, the permittivity of the TM material will be somewhat lower than desired. Compositions with a high percentage of oil (70-80%) are appropriate materials for mimicking low-water content tissue, such as fat, over the entire frequency range reported. By decreasing the volume percent of the oil, we can create materials with intermediate dielectric properties spanning these two bounds. This recipe is also very well suited for a narrowband application, since the dielectric properties of the materials can be tuned precisely by appropriate choice of the volume percent of oil.

BIOLOGICAL TISSUE-EQUIVALENT AGAR-BASED SOLID PHANTOMS FOR 3 TO 6 GHZ AND SAR ESTIMATION USING THE THERMOGRAPHIC METHOD

T. Onishi^{1,2}, R. Ishido², T. Takimoto²,
K. Saito³, S. Uebayashi¹, M. Takahashi³, K. Ito³

¹NTT DoCoMo, Inc., Japan

²Graduate School of Science and Technology, Chiba University, Japan

³Research Center for Frontier Medical Engineering, Chiba University, Japan

Recently, wireless systems used at high frequency, such as wireless LAN devices have become popular and the Ultra Wide Band (UWB) system was developed. In addition, the standardization of measurement method for Specific Absorption Rate (SAR) 30 MHz - 6 GHz is now in progress. In this paper, the biological tissue-equivalent agar-based solid phantoms from 3.0 to 6.0 GHz are described. The solid phantom composes of agar, deionized water, polyethylene powder, sodium chloride, TX-151 and sodium dehydroacetate. The phantoms can maintain its shape by itself. Another feature of the phantom is that arbitrary shapes can be fabricated easily using a mold. The developed phantoms can reproduce the electrical constants of biological tissues, e.g. the human head and body, within 5%, and it is not necessary to change the phantom for each frequency band in the range of 3.0 to 6.0 GHz during the measurements. The constants of this phantom can be adjusted mainly by using polyethylene powder and sodium chloride. The phantoms can be used to evaluate the Specific Absorption Rate (SAR) as well as antenna characteristics in the range of 3.0 to 6.0 GHz.

The investigation of SAR measurements is performed on the phantom at 5.2 GHz using the thermographic method. Calculations using the FD-TD method and the heat transfer equation are carried out in order to evaluate the thermal diffusion in the measurements using the thermographic method. The measured and calculated temperature distributions are in good agreement. There is evidence that the thermal diffusion influences the SAR estimation at 5.2 GHz more than a lower frequency range even though this method basically does not depend on the frequency.

THE EFFECTS OF ELECTROMAGNETIC FIELDS ON VIBRIO VULNIFICUS/PARAHAEMOLYTICUS IN OYSTERS

Jose Pvallalta, Erdem Topsakal
Mississippi State University

Vibrio vulnificus, commonly found in coastal waters, is a bacterium responsible for 149 serious illnesses resulting in 75 deaths between 1989 and 1996 according to the Centers for Disease Control and Prevention (CDC). Each year in the United States, *Vibrio* also causes an estimated 8000 infections. *Vibrio* bacteria are found naturally in coastal waters and are not related to pollution. Although one can get infected in the water through open cuts or wounds, generally fatal cases are related to raw oysters, clams or other shellfish consumption. Oysters filter *Vibrios* from seawater, where they are ubiquitous, although not always in high abundance, nor always a pathogenic strain. As a result, the bacteria will appear in the pallial cavity and are directed to the mouth and then into the gut where they will typically reach their highest concentrations. Thoroughly cooking will kill the bacteria but will also compromise the oyster. The goal of this study is to investigate the effects of electromagnetic fields on *Vibrio vulnificus* and *Vibrio parahaemolyticus* in oysters.

The analysis was performed using Finite Element Boundary Integral Method (FE-BI). Finite elements have been extensively used to model open- and closed- domain electromagnetic problems in scalar form in two and three dimensions. The derivation of the FE-BI equations begins with the vector wave equation. This second-order partial differential equation is solved by employing the Galerkin method to form a residual. The goal is to minimize this residual or equivalently to minimize the difference between the solution of the FE-BI discrete approximation and physical reality.

Through simulations, a 3-D volumetric field distribution map of the oyster was derived. The analysis was done using different sources for a wide range of frequencies. The results obtained during this study were aimed to help to determine the appropriate source, source location and frequency that will destroy the bacteria without compromising the oyster itself.

INDEX

A

Abdelnasser, A.E. 54, 102
 Abidi, M. 130
 Abdu, M. 247
 Ackermann, R. 438
 Adachi, T. 363
 Adams, R.J. 41, 42
 Ade, P. 389, 404, 406, 410
 Agrimson, E.A. 345
 Aguirre, J. 389, 406
 Akbarpour, R. 198
 Akhavan, M. 64
 Al Sharkawy, M. 85
 Albert, J.M. 273, 277
 Alexeff, I. 121
 Aliakbarian, H. 11, 64, 133
 Allen, C.A. 408
 Altgilbers, L.L. 138
 Alu, A. 31
 Amatucci, W.E. 285
 Anagnostou, E.N. 183
 Anagnostou, M.N. 183
 Anderson, D. 237, 240
 Anderson, D.Z. 53
 Anderson, K.D. 191
 Andersson, L. 291
 Andrade, T. 34
 Anghel, A. 237, 240
 Antar, Y.M.M. 101
 Aponte, N. 257
 Araujo, E. 237
 Asher, W.E. 205
 Ashour-Abdalla, M. 290
 Asmar, S. 115
 Atad, E. 391
 Atchley, L.M. 138, 140
 Audley, M.D. 391, 404
 Avery, J.P. 353, 358, 374
 Avery, S.K. 358, 374

B

Bagri, D. 431
 Bahadori, K. 105
 Bahar, E. 71
 Bahcivan, H. 297
 Bailey, G.J. 328
 Baker, D.N. 265, 266, 269
 Baker-Jarvis J. 5
 Baktur, R. 22
 Bale, S. 290, 447
 Ballato, J.M. 22
 Balsler, D.S. 427
 Banai, A. 118
 Bardin, J.C. 431
 Barott, W.C. 59

Barrington-Leigh, C.P. 368
 Barsky, P. 209
 Bastian, T.S. 446
 Batista, I.S. 311
 Baum, C.E. 17, 137, 139,
 140
 Baum, C.W. 129
 Baylor, M. 53
 Bayram, Y. 149
 Bekheit, M.Z.I. 101
 Bell, P. 112
 Bell, T.F. 221, 283, 284
 Benford, D.J. 405, 408
 Bering, E.A. 347
 Berkey, F.T. 329
 Bernhard, J.T. 52, 110
 Bernhardt, P.A. 227, 319
 Best, S. 51
 Bhattacharjee, S. 122
 Bibl, K. 246
 Bintley, D. 404
 Blackwell, D.D. 285
 Blake, J. 266, 268
 Blix, T.A. 339, 341
 Blundell, R. 443
 Bock, J.J. 389, 399, 406,
 411
 Boisvert, J. 331
 Boksiner, J. 145
 Booske, J.H. 122
 Bopp III, C.L. 43, 44
 Bortnik, J. 275
 Bowen, L.J. 138
 Bower, G. 436, 438
 Bradley, R. 446
 Brady, D. 199
 Brattli, A. 339, 341
 Breakall, J.K. 258
 Briczinski, S. 258, 375
 Bringi, V.N. 185
 Brizard, A.J. 273
 Brown, G.S. 192
 Brown, P. 352, 355
 Brown, P.K. 456
 Brukardt, M.S. 347
 Bullett, T.W. 243
 Burch, J.L. 265
 Burgess, E.H. 153, 162
 Burk, S.D. 155
 Burke, W.J. 298
 Bushyager, N. 67
 Bust, G.S. 236, 238, 239,
 315
 Butler, C.M. 43, 44, 77

C

Caloz, C. 35
 Canabarro, M.S. 311
 Canning, F. 42
 Cao, N.T. 414
 Cappallo, R.J. 442
 Carilli, C. 443
 Carpenter, D.L. 225, 284
 Carter, J.C.C. 437
 Casciato, M.D. 165
 Castro, E.I. 258
 Castro-Nieto, J. 347
 Cela, C.J. 456
 Cha, J. 60
 Chan, A.A. 269, 273
 Chandrasekar, V. 184, 185
 Chang-Daz, FR. 347
 Chappell, I. 141
 Charnotskii, M.I. 90
 Chattopadhyay, G. 413
 Chau, J. 240, 251, 260, 353
 Chen, A.B. 363, 364
 Chen, C. 340
 Chen, T.C. 405
 Cheney, G.P. 246
 Cheong, B.L. 182, 203
 Chervenak, J.A. 405, 408
 Cho, H.M. 409
 Chrysanthou, C. 145
 Chu, Y.H. 259
 Cimini, D. 173, 174, 176
 Clark, A.M. 413
 Clarke, J. 409
 Clegg, A.W. 218
 Close, S. 352, 355
 Codrescu, M.V. 232
 Cohen, A. 444, 445
 Coker, C. 312
 Collins, R.L. 336
 Condon, J.J. 427, 445
 Constantikes, K.T. 427, 428
 Cooke, B. 355
 Cooke, W.J. 351
 Cordes, J. 451
 Coster, A. 309, 325
 Cotton, W.D. 445
 Cotts, B. 202
 Crane, P. 444, 448
 Croskey, C.L. 335
 Crowe, T.W. 126
 Cuevas, R. 251
 Cummer, S.A. 36, 364,
 365, 379

D

D'Addario, L. 438
 D'Angelo, N. 345
 Davis, M. 438
 Davis, W.A. 15, 16, 18, 21, 23
 Day, P. 411, 412
 de la Pena, S. 374
 de Paula, E.R. 311
 de Rezende, L.E.C. 311
 DeBoer, D.R. 418, 436, 438
 DeGroot, D.C. 4
 DeMinco, N. 106
 Demir, V. 85
 Denney, K. 354
 Devlin, M.J. 405
 Dewdney, P.E. 397
 Dicker, S.R. 392, 405
 Dimant, Y. 292, 356, 373
 Dobbs, M.A. 409
 Dockery, G.D. 158
 Doherty, J.F. 376
 Doherty, P. 309, 323
 Dowell, C.D. 407
 Dowlatsshahi, S.G. 174, 176
 Dozois, C. 247
 Dragovan, M. 425
 Dreher, J. 438
 Drew, K. 352, 355
 Dudevoir, K.A. 437
 Duncan, W.D. 391, 404, 413
 Durand, D. 352, 355
 Dvorak, S.L. 197
 Dwyer, D. 87
 Dyrud, L. 292, 354, 356

E

Eccles, J.V. 235, 237, 249, 327
 Eckberg, J.T. 347
 Edgington, S.F. 389, 406
 El-Ghazaly, S.M. 104
 Eldek, A.A. 54, 102
 Eleftheriades, G.V. 34, 38
 Elkington, S.R. 269, 273
 Ellingson, S.W. 448
 Elnour, B. 86
 Elsherbeni, A.Z. 54, 85, 102
 Engargiola, G. 410
 Engheta, N. x, 31, 455
 Enloe, C.L. 317
 Erentok, A. 32
 Ergun, R.E. 291
 Erickson, K. 53
 Erickson, P. 250, 325
 Erickson, W.C. 444, 445
 Erricolo, D. 86, 94
 Eshrah, I.A. 24

Etheridge III, C.R. 159, 160
 Etheridge IV, C.R. 159

F

Fanouf, B.J. 437
 Faraji-Dana, R. 133
 Farr, E.G. 138, 140
 Fast, S.A. 161
 Fathy, A.E. 104, 130
 Fazi, C. 27, 146
 Fei, Y. 273
 Fisher, J.R. 212, 216
 Fisher, R. 446
 Fishman, G.J. 367
 Fleming, M.C. 418
 Flemming, M. 438
 Fomenko, A.S. 382
 Forcier, J. 420
 Forster, J.R. 424
 Foster, J.C. 248
 Francis, M. 7
 Frank, G.R. 461
 Frasier, S.J. 182, 201, 203
 Freundorfer, A.P. 101
 Frey, H.U. 363, 364
 Fuegen, T. 166
 Fuks, I.M. 90
 Fukunishi, H. 363, 364
 Fuller-Rowell, T.J. 232, 331
 Fung, A.K. 193
 Furlanetto, S. 443

G

Ganguli, G. 270, 285, 345
 Gannaway, F. 404
 Garner, T.W. 236, 238, 239, 315
 Gary, D. 446
 Gasiewski, A.J. 89, 173, 174, 176, 177
 Gatling, G. 285
 Gaussiran, T.L. 236, 238, 448, 449
 Gawande, R.S. 432
 Gehman, J.Z. 158
 Gelinas, L.J. 336
 Genack, M. 122
 Gergely, T.E. 210
 Gerken, E. 226, 380, 384
 Gerstoft, P. 154, 157
 Gibson, J.L. 424
 Ginot, G.P. 277
 Ginley, R.A. 3
 Glauert, S.A. 274
 Glenn, J. 389, 406
 Glisson, A.W. 24
 Glover, T.W. 347
 Gnedin, M. 331
 Godin, O.A. 90

Goetz, K. 381
 Goldin, A. 389, 399, 406, 411
 Goldman, M.V. 291
 Goldstein, J. 265
 Golkowski, M. 225, 284
 Golliday, C.L. 147
 Golovchanskaya, I.V. 301, 302, 303
 Golwala, S.R. 389, 406, 411
 Gonzalez, S. 255, 257
 Goodhue, A. 268
 Goodman, J.M. 324
 Gopalswamy, N. 447
 Gosalia, K. 458
 Goshi, D.S. 109
 Gostick, D. 404
 Goyal, A. 189
 Gray, A.D. 397
 Grbic, A. 34, 38
 Green III, E. 159, 160
 Greenhill, L. 443
 Guerrieri, J. 7
 Guzdar, P. 299

H

Haack, T. 155
 Habash Krause, L. 317
 Hagness, S.C. 461
 Haider, S.A. 92
 Haig, D. 389, 406
 Hairston, M.R. 315
 Hajj, G. 234
 Halverson, N.W. 403
 Hamilton, J. 9
 Hansen, S. 422
 Harp, G. 438
 Harris, J. 391
 Harriss, J.E. 75
 Hastriter, M. 87
 Havrilla, M. 87
 Heinselman, C.J. 251
 Hellinger, P. 290
 Hennessy, R.M. 420
 Henry, R.M. 414
 Herczfeld, P.R. 124
 Herman, B. 197
 Herrero, F.A. 317
 Hewitt, J.N. 442
 Hicks, B. 444, 448
 Hilton, G. 404
 Hobbs, S.L. 156
 Hodgkiss, W.S. 154
 Hoffman, M.W. 182, 203
 Hojjat, N. 11, 133
 Holland, W.S. 391, 404
 Holloway, C.L. 68
 Holt, B. 91
 Holt, J.M. 250, 256

Index

- Holzappel, W. 410
 Holzworth, R. 338, 379, 381
 Hood, A.Z. 70
 Hoppe, U.-P. 339, 341
 Horanyi, M. 337, 338
 Horne, R.B. 274
 Horton, W. 267
 Hristov, T.S. 191
 Hsieh, W.-T. 408, 414
 Hsu, R.-R. 363, 364
 Huang, J. 103
 Huang, W. 24
 Huang, X. 245, 247, 316
 Huang, Z. 307, 310, 330
 Huba, J.D. 227, 231, 282, 293, 319
 Hudson, H. 268
 Hudson, M.K. 268
 Huff, G.H. 52, 110
 Huffines, G.H. 365
 Hughes, B.L. 55
 Hunsucker, R.D. 235, 249, 327
 Hunt, C. 404
 Hurford, G. 446
 Hussein, Z.A. 91, 103
 Huynh, J.T. 286
 Hysell, D.L. 260, 297
- I**
 Iijima, B. 234, 308
 Imbriale, W.A. 395
 Inan, U.S. 116, 202, 221, 225, 283, 284, 369, 386
 Irisov, V.G. 89, 177
 Irwin, K. 404, 405, 413
 Isenberg, H.D. 414
 Ishido, R. 462
 Ishimaru, A. 91
 Ito, H. 460
 Ito, K. 460, 462
 Itoh, T. 35, 109
 Iturbide-Sanchez, F. 175, 204
 Ives, R.L. 122
- J**
 Jablecki, M.C. 156, 157
 Jackson, D.R. 45, 94
 Jackson, R.W. 204
 Jacobson, V. 347
 Jances, D. 354
 Janches, D. 353, 358
 Janezic, M.D. 5
 Jaruwatanadilok, S. 91
 Jayaraman, V. 331
 Jiang, H. 122
 Jin, N. 100
 John, S. 150
 Johnston, D. 115
 Jones, D. 447
 Jones, G. 433
 Jones, J. 357
 Joy, M.K. 421
 Joyce, G. 231, 281, 282
 Junor, W. 449
- K**
 Kabos, P. 8, 68
 Kaiser, M.L. 447
 Kamalabadi, F. 252, 255
 Kanekal, S.G. 265, 266
 Kang, C. 359
 Kantor, I.J. 311
 Karacolak, T. 47
 Karimabadi, H. 294
 Kasper, J. 442, 447
 Kassim, N. 444, 445, 448, 449
 Kawai, H. 460
 Kelley, M. 226, 336, 380
 Kelly, J.D. 251
 Kenyon, M. 411
 Kerdraon, A. 446
 Kerkoff, A.J. 448
 Keskinen, M.J. 224
 Khan, Z.A. 149
 Khattatov, B. 331
 Kim, E.M. 132
 Kim, S. 345
 Kimura, M. 80
 Kintner, P.M. 311
 Kirby, P.L. 78
 Kishk, A.A. 24
 Klein, M. 173, 174, 176, 177
 Kletzing, C.A.
 Klopff, E.K. 175
 Klopff, E.M. 205
 Knoerzer, S. 166
 Kochhar, A.K. 158
 Kohlberg, I. 27, 141
 Kollman, R. 95
 Komjathy, A. 308
 Konanur, A.S. 55
 Korsunskaya, Y.A. 318
 Kory, C.L. 122
 Kosmas, P. 457
 Kossey, P.A. 221
 Kovacs, A. 407
 Koyanagi, Y. 460
 Kratzenberg, E. 437
 Kress, B. 268
 Krishnamurthy, S.H. 55
 Kudeki, E. 255
 Kuester, E.F. 68
 Kuga, Y. 60, 91
 Kulkarni, P. 283
 Kunkee, D. 211
- Kuo, C.-L. 411
 Kuo, N.C. 193
 Kuo, S.P. 286
 Kuroki, F. 79, 80, 81
 Kurum, M. 181
 Kwon, H.M. 150, 189
- L**
 Lahart, M.J. 27
 Lalezari, F. 99
 Lampe, M. 281
 Lane, W.M. 445
 Lang, R.H. 181, 200
 Lange, A.E. 389, 406
 Lanting, T.M. 409
 Larsen, M.F. 297
 Lau, E.M. 353, 358, 374
 Laurent, G. 389, 406
 Lawry, D.I. 140
 Lazebnik, M. 461
 Lazio, T.J.L. 444
 Lazio, T.J.W. 312, 445
 Lazzi, G. 55, 456, 458, 459
 Leduc, H.G. 399, 411, 412
 Ledvina, B.M. 311
 Lee, A.T. 394, 409, 410
 Lee, J.-F. 37
 Lee, L.C. 363
 Lee, S. 8
 Lee, S.-C. 37
 Lee, S. 60
 Lee, S.W. 91, 104
 Lehnert, K. 413
 Lembege, B. 289
 Leong, K.M.K.H. 35
 Leong, M.M. 426
 Lertsirimit, C. 94
 Leuski, V. 173, 176, 177
 Li, S. 88
 Li, X. 265
 Li, Y. 124
 Liao, D. 190
 Lichtenberger, A.W. 126
 Licul, S. 15, 16
 Lie-Svendsen, O. 339, 341
 Lim, S. 35
 Limbach, S. 122
 Lin, C. 237, 328
 Lin, R. 268, 368
 Lin, S.S. 455
 Lind, F. 250, 325
 Linnehan, R. 199
 Liu, J.Y. 328
 Liu, N. 383
 Liu, Y. 185
 Liu, Z. 126
 Lockard, M.D. 77
 Loeb, A. 443
 Lonsdale, C.J. 442
 Lopez, L.I. 368

Index

Lopez-Dekker, F.J. 182, 203
 Losseva, T.V. 382
 Loughmiller, P.J. 312
 Love, D.C. 46
 Lu, G. 328
 Luebbers, R.J. 168
 Lueker, M. 409
 Lugton, J. 438
 Lumori, M.L.D. 132
 Lyakhov, A.N. 318
 Lynch, K.A. 336
 Lyons, W.A. 365

M

MacDowall, R.J. 447
 MacGregor, H. 404
 MacIntosh, M. 404
 MacReynolds, K. 7
 Madsen, E.L. 461
 Makarov, N.A. 358
 Makela, J.J. 312
 Maksimovic, D. 112
 Maloney, P.R. 406
 Maltsev, Y.P. 301, 302, 303
 Mandrake, L. 234, 308
 Manheimer, W. 281
 Mannucci, A.J. 308
 Marengo, E.A. 169
 Marshall, R.A. 369
 Marshall, R.E. 153, 162
 Masteron, K.D. 9
 Mathews, J.D. 258, 375, 376
 Mattioli, V. 173
 Maurer, J. 166
 Mauskopf, P.D. 389, 406
 Mazin, B.A. 412
 McCarrick, M. 222, 223
 McCarthy, K. 245
 McCarthy, M. 379, 381
 McDonald, J.L. 99
 McDonald, K. 91
 McHarg, M.G. 370
 McIntyre, E.M. 177
 McMahan, J. 390
 McNamra, L.F. 243
 Meisel, D.D. 258
 Mende, S.B. 363, 364
 Meneghini, R. 181
 Merlino, R.L. 345
 Mev, F. 42
 Meyer, M. 261, 326
 Meyer, S.S. 422
 Milikh, G. 222, 223, 282, 299, 373
 Miller, J.R. 75
 Miller, M.J. 345
 Miller, N. 413
 Minter, C.F. 232
 Mishin, E. 226, 298

Mitchell, J.D. 335
 Mitchell, R.R. 414
 Mithaiwala, M. 267
 Miyamoto, K. 81
 Mohamadi-Baghaee, R. 10
 Mohammadi-Baghaee, R. 133
 Monk, S.P. 265
 Monson, S. 381
 Moore, H. 141
 Moore, R.C. 116, 221, 284
 Morabito, A. 261
 Morales, M.F. 442
 Moreland, J. 8
 Morgan, M.A. 434
 Mosallaei, H. 69
 Moseley, H.S. 398
 Moseley, S.H. 405, 408, 414
 Muella, M.T.A.H. 311
 Mumcu, G. 33
 Muralikrishna, A. 311
 Murphy, M. 331
 Myers, M.J. 410

N

Natzke, J.R. 48
 Nemtchinov, I.V. 382
 Newman, D.L. 291
 Nguyen, H. 389, 406
 Nicolls, M.J. 257
 Nikoukar, R. 255, 257
 Nsumei, P. 316

O

O'Brient, R. 410
 O'Neill, K. 92
 Ogawa, K. 460
 Onishi, T. 462
 Oppenheim, M. 354, 355, 356, 373
 Oroskar, S. 45
 Osada, H. 460

P

Padmanabhan, S. 205
 Pajic, S. 112
 Pak, K. 91
 Palmer, R.D. 182, 203
 Palo, S.E. 353, 358, 359
 Papadopoulos, D. 270
 Papadopoulos, K. 222, 223, 282, 373
 Papapolymerou, J. 78
 Parvez, G. 299
 Pasko, V.P. 202, 366, 383, 385
 Patterson, J.D. 324
 Patterson, M.S. 146

Pautet, P.-D. 379
 Paxton, L.J. 328
 Peacock, T. 391
 Pearson, L.W. 22, 75, 129, 131
 Pedersen, T. 226
 Pen, U.L. 441
 Perillat, P. 258
 Perley, R. 214, 443, 444, 445
 Perlovsky, L. 199
 Perrine, P.P. 282
 Perry, K. 268
 Peter, W. 222, 223
 Peter, W.B. 386
 Peters, W. 444
 Peterson, J.B. 441
 Petrin, A.J. 217
 Pfaff, R.F. 297, 300
 Phillips, T.G. 407
 Pi, X. 234
 Pincenti, J.C. 28
 Pinto, O. Jr. 379
 Pogorzelski, R.J. 61, 131
 Polisensky, E. 448
 Popa, B.-I. 36
 Popovic, Z. 53, 112
 Prestage, R.M. 427
 Price, R.M. 448, 450
 Pryke, C. 422
 Pugh, Jr., E.N. 455
 Pushtarik, V.A. 318
 Pvilalta, J. 463

Q

Quinn, R. 276

R

Rahman, S. 86
 Rahmat-Samii, Y. 100, 105
 Randa, J. 6
 Rangaswamy, M. 199
 Rapp, M. 341
 Rappaport, C. 457
 Rappaport, T.S. 93
 Rashed-Mohassel, J. 10, 11
 Ray, P. 444, 448
 Read, M.E. 122
 Reddell, N. 284
 Reeder, M. 110
 Reggiani, N. 311
 Reiner, M. 447
 Reinisch, B. 245, 247, 276, 316
 Reintsema, C.J. 404
 Reising, S.C. 175, 204, 205
 Rengarajan, S.R. 62
 Rice, D. 235, 249, 327
 Richards, P.L. 409, 410

- Richmond, A.D. 328
 Rideout, W. 250, 309
 Ridgeway, R. 214, 436
 Riley, T.J. 117
 Rincon, R.F. 181
 Roach, T.L. 52
 Robertson, S. 337, 338
 Rodeffer, G. 104
 Rodger, C.J. 365
 Rodrigues, F.S. 311
 Rogers, A.E.E. 437
 Rogers, L.T. 156, 157
 Rose, L.A. 205
 Rosker, M.J. 123
 Rossinot, P. 389, 406, 411
 Rothwell, E.J. 46, 87
 Rottier, J.R. 153, 159, 160, 162
 Roussel-Dupre, R.A. 307, 310, 330, 384
 Rowland, D. 381
 Rudakov, L. 270
 Ruf, C. 215, 446
 Ruhl, J. 422
 Runyan, M. 422
 Rusyn, T.L. 117
- S**
 Sahr, J. 261, 326
 Saito, K. 460, 462
 Saito, M. 460
 Salah, J.E. 442
 Sales, G. 247, 276
 Sarabandi, K. 69, 165, 190
 Satyapal, S. 147
 Saunders, K.E. 161
 Sayers, J. 389, 406
 Scales, W.A. 340
 Scharstein, R.W. 63, 88
 Scherliess, L. 233
 Schindler, J. 199
 Schmidt, D. 413
 Schmidt, S. 459
 Schmieder, L. 104
 Schneider, G. 414
 Schriver, D. 290
 Schroeder, N. 209
 Schultz, R.T. 423
 Schunk, R.W. 233
 Schuster, J.W. 168
 Scime, E. 346
 Scott, W.R. 76
 Seetharam, V. 129
 Semeter, J. 252
 Sen, N. 291
 Sengele, S. 122
 Sertel, K. 33
 Sharma, S. 299
 Sharman, D. 238
 Sharp, M. 422
- Sheffel, J. 331
 Shume, E.B. 260
 Siddiqui, O. 34
 Siefring, C.L. 227, 319
 Siegel, P.H. 125
 Sihvola, A. 25
 Simpson, J.J. 167
 Singh, H. 141
 Skone, S. 325
 Slack, C.M. 448
 Slocum, P. 268
 Small, B.L. 276
 Smith, A. 409, 410
 Smith, C.E. 54, 102
 Smith, D.M. 368
 Smith, P. 53
 Sojka, J.J. 233, 235, 249, 327
 Song, P. 316
 Sparks, L. 308
 Spieler, H.G. 409, 410
 Squire, J.P. 347
 Sridharan, T.L. 417
 St.Germain, K.M. 213
 Staguahn, J.G. 405, 408
 Stahle, C.M. 414
 Stark, A.A. 393, 419
 Starks, M. 226, 276, 277
 Steffes, P.G. 59, 217
 Stenbaek-Nielsen, H.C. 370
 Sternovsky, Z. 337, 338
 Stevenson, T.R. 408, 414
 Stewart, K. 444
 Stewart, K.P. 448
 Stover, P. 389, 406
 Stuchly, M.A. ix
 Su, H.T. 363, 364
 Su, S.Y. 328
 Sudiwalla, R. 404
 Suggs, R.M. 351
 Sulzer, M. 255, 257, 258
 Supanich, M.P. 405
 Symbalisty, E.M.D. 384
- T**
 Taflove, A. 167
 Takahashi, M. 460, 462
 Takahashi, Y. 363, 364
 Takimoto, T. 462
 Taylor, B.T. 315
 Taylor, M.J. 379
 Tentzeris, M. 67
 Terzuoli, A. 87
 Tesche, F.M. 44
 The ACT Collaboration 392
 The GBT Collaboration 392
 Thiel, M. 165
 Thiel, W. 165
- Thomas, J.N. 379
 Thompson, D.C. 233
 Thonnard, S.E. 312
 Thorne, R.M. 275
 Thornton, D. 438
 Timbie, P.T. 396
 Tompkins, C.M. 131
 Topsakal, E. 47, 70, 463
 Tran, H. 394, 410
 Travers, D.E. 414
 Travnicek, P. 290
 Triplett, L.A. 384
 Tsai, H.F. 328
 Tu, J. 316
 Tucker, G.S. 396
 Tulu, Z.C. 201
- U**
 Uebayashi, S. 462
 Ueda, T. 460
 Ulker, S. 126
 Ullom, J. 404, 413
 Urbina, J. 354
 Urry, L. 438
 Uslenghi, P.L.E. 26, 28, 86
 Utku, C. 200
- V**
 Vale, L. 404
 Valentic, T. 251
 Valentine, C.G. 161
 Valladares, C. 237, 323
 van der Weide, D.W. 122
 Vayonakis, A. 399, 411
 Veidt, B.G. 397
 Veliz, O. 240
 Venermo, J. 25
 Venkatesan, J. 76
 Vivekanandan, J. 183
 Vlasov, M. 380
 Volakis, J.L. 33, 149
 Voronovich, A.G. 89
 Vouvakis, M.N. 37
- W**
 Wadefalk, N. 432, 435, 438
 Walker, D.N. 285
 Wallace, C.B. 148
 Wallace, T. 222, 223
 Wallace, Y. 373
 Wallis, T.M. 8
 Wang, C. 234
 Wang, C.Y. 259
 Wang, G. 41
 Wang, H. 93
 Wang, N. 112
 Wang, Y. 109
 Wang, Y. 184
 Warren, H. 231

Index

- Weber B.L. 177
Webster, A.R. 198, 357
Wei, L. 132
Weikle, II, R.M. 126
Weiler, K. 447
Weinreb, S. 431, 432, 433,
435, 438
Welch, W.J. 424, 438
Welter, J.D. 122
Wen, C.-H. 375, 376
Westwater, E. 173, 174, 176
White, S. 446
Wiegert, P. 357
Wiesbeck, W. 166
Wilson, B. 234, 308
Wiltberger, M. 269
Wilton, D.R. 45, 94
Wittmann, R. 7
Wollack, E.J. 398, 405, 414
Woodcraft, A. 404
- Woody, D.P. 420
Wright, J.W. 244, 329
Wu, K. 168
Wu, X.P. 441
Wygant, J.R. 381
- X**
Xu, Y. 404
- Y**
Yakovlev, A.B. 24
Yamaoka, K. 79
Yang, H. 366
Yang, H.Y.D. 95
Yang, T. 18
Yang, Y. 130
Yardim, C. 154
Ye, X. 197
Yeh, H.C. 328
- Yemelyanov, K.M. 455
Yoneyama, T. 79
York, J.A. 448
Yousefi, L. 118
Youzefzadeh, V. 112
Yudin, V. 331
Yun, M. 411
- Z**
Zabotin, N.A. 244, 329
Zaldarriaga, M. 443
Zhang, Y. 24
Zhbakov, G.A. 244
Zhu, L. 233
Zihlman, B. 104
Ziolkowski, R.W. 32
Zmuidzinas, J. 399, 411,
412
Zwi, E. 222, 223



